Hexacyanometallate as an Effective Building Unit: Soft Supramolecular Networks to 3D Functional Porous Coordination Frameworks

A thesis submitted
in partial fulfillment for the degree of

Master of Science

as a part of the

Integrated Ph.D. Programme
(Materials Science)

by

Arpan Hazra

Molecular Materials Laboratory
Chemistry and Physics of Materials Unit
Jawaharlal Nehru Centre for Advanced Scientific Research
(A Deemed University)
Bangalore, India.

Dedicated
to my Family

DECLARATION

I hereby declare that the matter embodied in the thesis entitled "**Hexacyanometallate as an Effective Building Unit: Soft Supramolecular Networks to 3D Functional Porous Coordination Frameworks**" is the result of investigations carried out by me at the Chemistry and Physics of Materials Unit, Jawaharlal Nehru Centre for Advanced Scientific Research, India under the supervision of Dr. Tapas Kumar Maji and that it has not been submitted elsewhere for the award of any degree or diploma.

In keeping with the general practice in reporting the scientific observations, due acknowledgement has been made whenever the work described is based on the findings of other investigators. Any omission that might have occurred due to oversight or error in judgement is regretted.

Arpan Hazra

CERTIFICATE

I hereby certify that the work described in this thesis entitled "**Hexacyanometallate as an Effective Building Unit: Soft Supramolecular Networks to 3D Functional Porous Coordination Frameworks**" has been carried out by Mr. Arpan Hazra under my supervision at the Chemistry and Physics of Materials Unit, Jawaharlal Nehru Centre for Advanced Scientific Research, India and that it has not been submitted elsewhere for the award of any degree or diploma.

Dr. Tapas Kumar Maji

(Research Supervisor)

ACKNOWLEDGEMENT

I am very pleased to thank my research supervisor Dr. Tapas Kumar Maji who gave an opportunity to work on the fascinating field of Porous Coordination Framework. His simple way of thinking about a problem always inspires me a lot. I shall remain ever thankful to him for giving me enough freedom to work on my own area of interests.

Words fail me when I start to thank Prof. C. N. R. Rao for being a constant source of inspiration to me. He has been a motivation for me whenever I have faced any hurdles. His enthusiasm and energy are what have kept me going in difficult times. It is indeed an honour being in the same institute and watching him every day.

I am very grateful to my labmates, Prakash, Ritesh, Sudip, Anindita, Jaya Ram, Krishna Kumar, Suresh and Dr. Nagaraja for providing a healthy environment in the lab. It is a pleasure working in their company. I have been privileged to work with a wonderful person like Prakash, who has taught me a lot during the various experiments we have done together. I have indeed learnt a lot from him, for which I will be eternally grateful to him.

It is with great joy that I thank my batchmates, Chidambar, Dileep, Gayatri, Pandu, Rana, Sharma, Sudeshna and Varun for the wonderful times we have had in the past 3 years. It was a pleasure knowing such nice people. I have learnt a lot from all of them and I am very grateful to each one for their company.

My friends mean the world to me, and it is with the utmost pride that I acknowledge each one of them for the wonderful moments spent so far: Debabrata, Barun, Pralok, Bharath, Dibyajyoti, Partha, Varun, Babhru, Sabyasachi, Jia, Amrit, Ritesh, Arup, Gautam, Laxmi.

I have learnt a lot from my seniors, and I am grateful to them for sharing their knowledge with me: Leela, Jithesh, Neenu, Pranab, Soumik, Bivas, Abhay, Nitesh, Piyush, Urmi, Vini, Nisha and Ritu.

My friends from bachelor's days have given me some of my most memorable times, and it would not be just for me to omit anyone's name in acknowledging my near and dear ones: Arnab, Debanjan, Babul, Shawon and Sudip.

Thanks are also to the various CPMU and TSU professors for the courses provided by them. It was a great learning curve for me and I am very much thankful to the course coordinators,

Prof. S. Balasubramanian, Prof. G. U. Kulkarni, and later Dr.T. K. Maji for giving me the opportunity to learn so much in such little time.

I would also like to thank Anil for the PXRD measurements; Vasu for TGA, IR, DTA; Murthi for the various small but significant requirements in the day to day jobs and Srinivas for helping in single crystal XRD measurements.

My parents deserve the most special mention when I complete the acknowledgements. They are the people who have moulded me into whatever I am today. The support I have got from them during any trouble cannot ever be compensated. My family has always been there for me, and it is with the greatest pleasure that I thank all of them for being there whenever I have needed them the most.

Last but not the least; I thank God almighty for providing me with such a successful life in more ways than one.

PREFACE

This thesis consists of five chapters describing hexcyanometallate as an effective building unit for the construction of supramolecular network as well as 3D functional porous coordination frameworks. The studies on structure determination, magnetic property and interesting adsorption property are recorded in a systematic way.

Chapter 1 gives a general overview about soft porous crystal, porous coordination framework and their fascinating properties. Effect of unsaturated metal sites (UMS) and aromatic π cloud on the adsorption profile have been also studied.

Chapter 2 discusses about the supramolecular isomerism in soft porous crystal. Selective adsorption of co-crystal as well as the effects of external stimuli on these porous crystals has been also studied.

Chapter 3 talks about the multifunctional material where magnetism and adsorption are nicely combined in a single framework. This chapter also discuss about the guest induced magnetic modulation of a biporous host. The effect for UMS on hydrogen storage is also elaborated here.

Chapter 4 shows how MOF can be decoded as selective adsorbent of greenhouse gas like CO_2. This chapter also discuss the effect of metal ions (which act as UMS) on adsorption behaviour.

Chapter 5 discuss about a MOF which is isostructural with previously described coordination framework. But the interesting feature is in changing the metal ion causes an abrupt increase in adsorption amount. The magnetic property of the as-synthesised framework has also been studied.

Table of Contents

CHAPTER: 3

High heat of hydrogen adsorption and guest-responsive magnetic modulation in a 3D porous pillared-layer coordination framework.

CHAPTER: 4

Highly Selective CO_2 uptake in 3D Porous Frameworks of $[M(CN)_6]^{3-}$ (M = Fe, Cr) and Zn(II): Effect of Change in Pillar Modules and it's Ratio.

CHAPTER: 5

Synthesis, Structural Characterization, Gas Storage and Magnetic Study of a 3D Framework of Co(II) Bridged by $[Cr(CN)_6]^{3-}$ and 4,4′-bipy.

Chapter-1

Introduction: A General Overview of Coordination Polymers

1.1: *Soft Porous Crystals*

Modular synthesis of soft materials, e.g. block copolymers, organic thin films and molecular inclusion compounds, promise precession engineering of specific properties and functions. Amongst them, the class of molecular compounds (also termed as inclusion compounds) is of particular interest because of their widespread applications in the field of magnetism,[1] ferroelasticity,[2] non-linear optical effects,[3] chemical storage[4] and catalysis.[5] Moreover, extended networks sustained solely by non-covalent interactions exhibit a greater degree of flexibility resulting in selectivity in terms of guest accommodation.[6] The flexible structure could be compared to a human hand as it is very easy to recognize forms and shapes which is also having multifunctional characters. Crystalline solids have intrinsic advantages where crystallinity allows an efficient collection of guests because of the large number of same repeating porous units, whereas flexibility produces a highly selective capture of guests. Designing new class of functional host materials based on the art of host–guest systems, one could easily extrapolate the attributes of both crystallinity and flexibility in such type of materials. Such modular nature of a host framework would provide not only rigid properties, but also enzyme-like soft specificity, producing intelligent host materials that are responsive to guests under the appropriate conditions.

Introducing these features in a single-entity host material, we have focused on the synthesis of porous supramolecular frameworks which are constructed by metal ions and organic ligands.[7] Compare to other molecular crystals, (e.g. organic compounds,[8] discrete metal complexes[9] etc.) porous supramolecular frameworks are the most appropriate material for combining regularity and softness. It is very clear that high crystallinity and diverse structural topologies with porous architectures make them most adorable material for the preparation of smart soft materials. Moreover the molecular interactions used to assemble the components have a wide range from non-covalent interactions to coordination bonds which has a great control in producing soft materials having a porous scaffold.[10]

Soft porous crystals are the porous solids which possess both a highly ordered network and structural transformability. They can exhibit themselves as bistable or multistable crystalline materials with long-range structural ordering, reversible transformability between the different states, and permanent porosity. The term permanent porosity refers to the fact that,

at least one crystal phase possesses space that can be occupied by guest molecules, so that the framework exhibits reproducible guest adsorption.

It is a well-known fact that strong non-covalent interactions viz., H-bonding (Fig. 1) and π-π interactions are prerequisite for the stability of functional supramolecular networks.

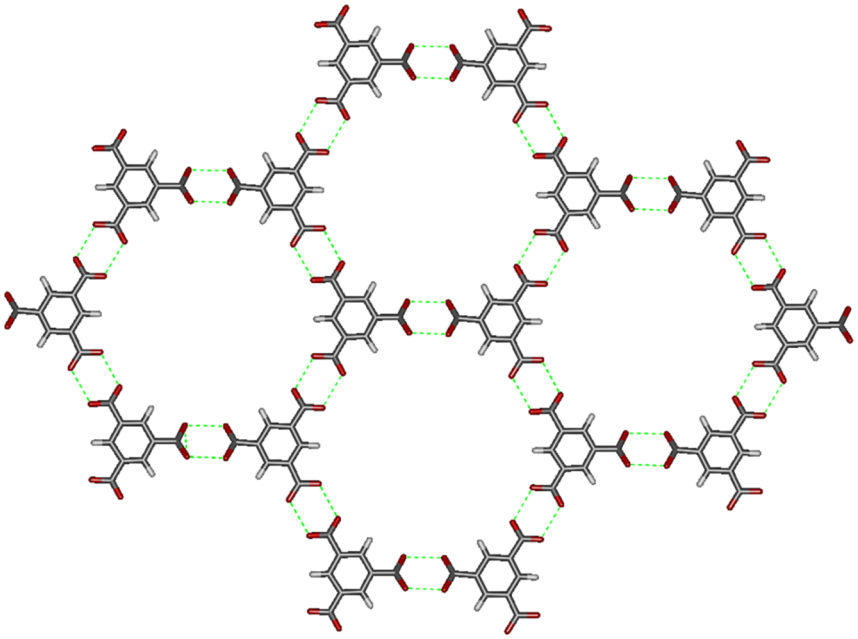

Fig. 1: Honeycomb structure. The power of H-bonding is clearly reflecting from this.

Therefore, it is very crucial to choose of molecular subunits whose structure and functions can be tuned using appropriate strategies with the help of crystal engineering. For this purpose, we have deliberately chosen hexacyanometallate as one of the building unit of supramolecular architecture.

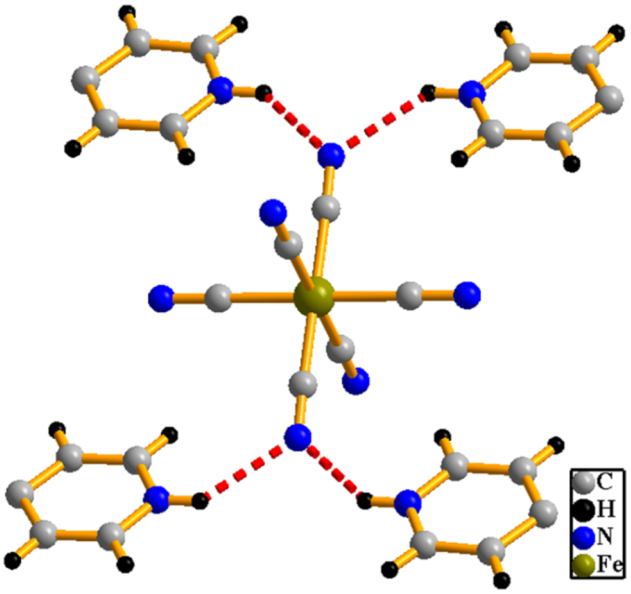

Fig. 2: Figure shows H-bonding interaction with $[Fe(CN)_6]^{3-}$ and heterocyclic aromatic molecules.

The nitrogen end of cyanide ligands can play the role of good acceptor to form H-bonding with other donor atoms. As for example, it can be easily connected with protonated heterocyclic aromatic molecules through H-bonding which leads to 1D, 2D or 3D supramolecular structure (Fig. 2). Except this, small molecules like H_2O, CH_3CN can also easily form H-bonding with hexacyanometallate leading to 1D or 2D array which has an immense importance in forming supramolecular structure based on non-covalent interactions.

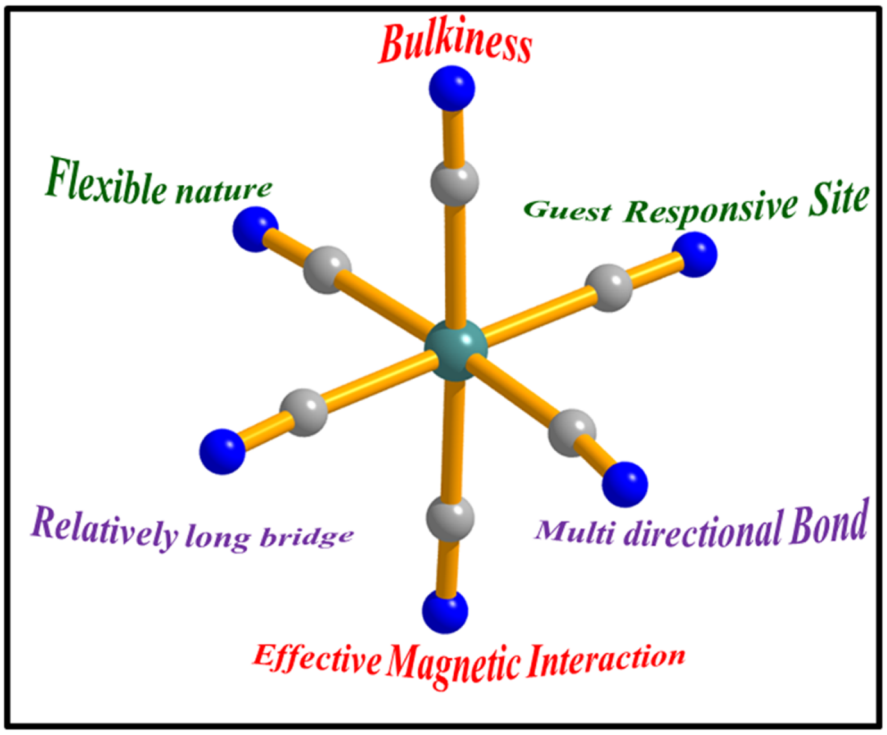

Fig. 3: Characteristics of the polycyanometallate anion.

Not only the non-covalent interactions but also other enormous facilities like bulkiness, guest responsive site, multidirectional bond, magnetic hub etc. (Fig. 3) drag the immense interest of the material scientists.

1.2: ***Porous Coordination Polymers (PCPs)***

Recently progress in the arena of molecular inorganic–organic hybrid polymers has reached a remarkable height. The synthesis and characterization of infinite one-, two-, and three dimensional (1D, 2D, and 3D) networks, sustained by coordination bond, has been an area of rapid growth in the field of material science.

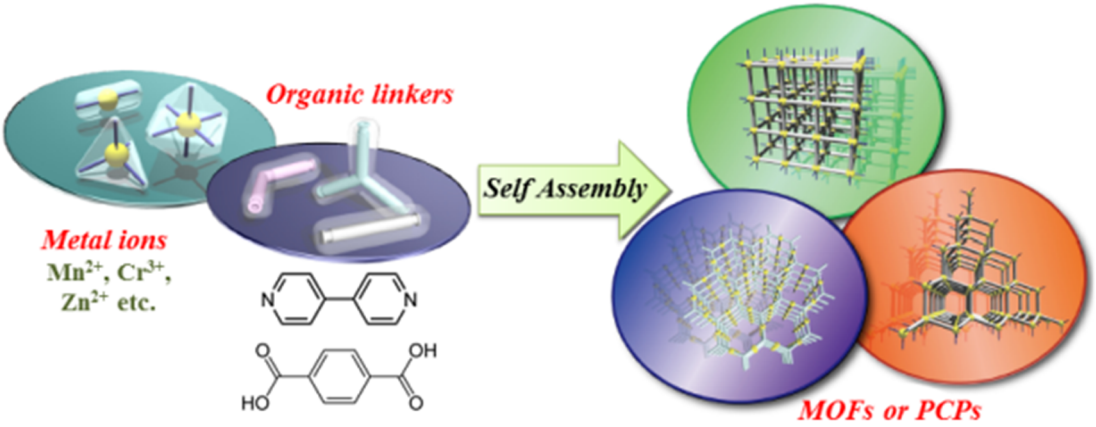

Fig. 4: Figure explains the judicious choice, metals and linkers for the construction of MOFs.

Coordination compounds with infinite structures have been intensively studied, in particular where the compounds constructed from the backbones of metal ions as connectors and ligands as linkers (Fig. 4). The so-called "coordination polymers" were reviewed in the early 1960s and since then versatile synthetic approaches for the assembly of target structures from molecular building blocks have been developed.

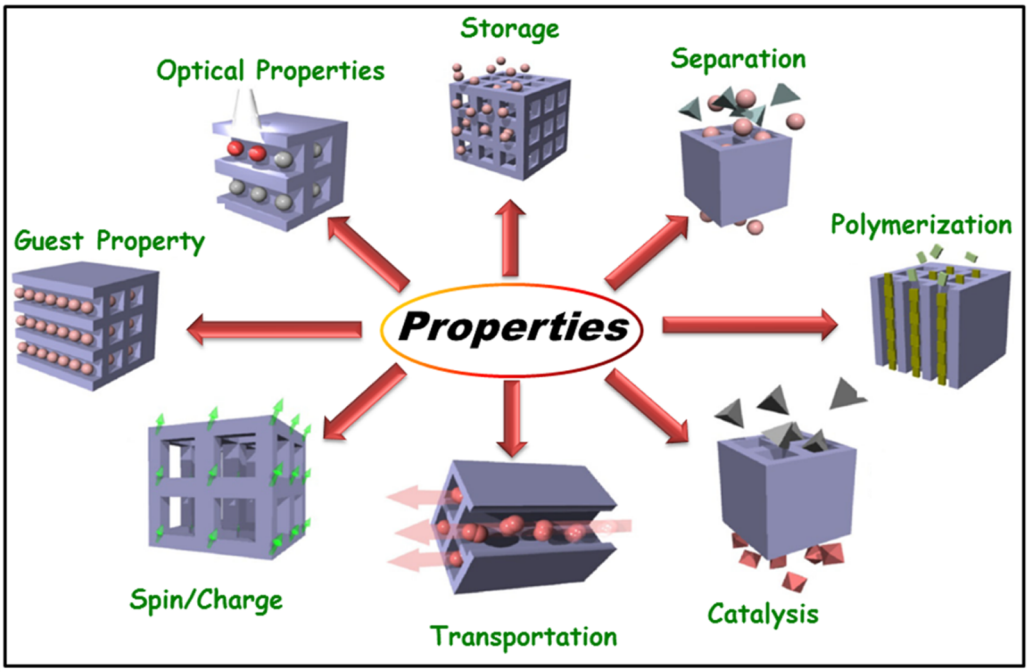

Fig. 5: Various properties PCPs.

The emerging application of MOF in various fields makes them in the list of highly sought after material. Porous coordination framework or metal–organic frameworks (MOFs), which have emerged as new zeolite alternative, have attracted considerable research interest in the past decades (Fig. 5).[11] A combination of almost all metal ions in the periodic table with

variety of organic linkers can afford a wide range of crystal structures as well as in chemical compositions (Fig. 4). The properties can be easily tuned by altering the metal and of course by modifying the length and/or the functionalization of the organic linkers.

1.3: ***Hydrogen Storage Properties***

1.3.1: ***Porous Coordination Polymers (PCPs) as Hydrogen Storage Materials***

Contributing to their exceptional structural and chemical tunability, sensing, catalysis, magnetism and drug delivery, metal-organic framework have recently come under intensive study for use as solid-state sorbents in gas storage application.[12] The immense employment of hydrogen as a clean energy substituting for hydrocarbons is still bounded due to the lack of a convenient, safe and cost-effective storage system.[13] In this respect the porous property of MOFs is gaining increased attention with time and the framework materials have emerged as an excellent storage alternative to high pressure and liquefied hydrogen tanks.[14]

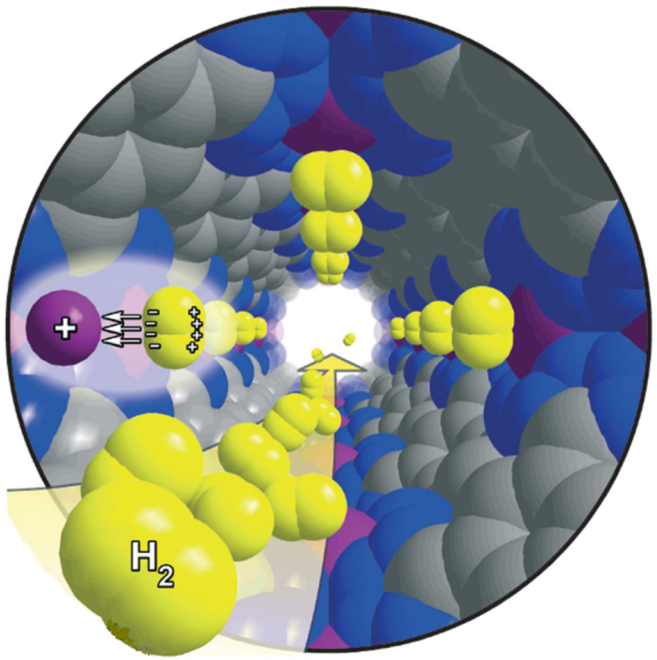

Fig. 6: Schematic diagram shows the adsorption of hydrogen by unsaturated metal centre.[15]

But regrettably the performance of these materials is greatly decreased at ambient temperature due to weak, physisorptive interactions between the internal pore surface and the hydrogen molecules. In fact, the isosteric heat of H_2 adsorption of these materials typically lies in the range of -5 to -7 kJ mol^{-1}, which is far below from the optimal value of -15 kJ mol^{-1}

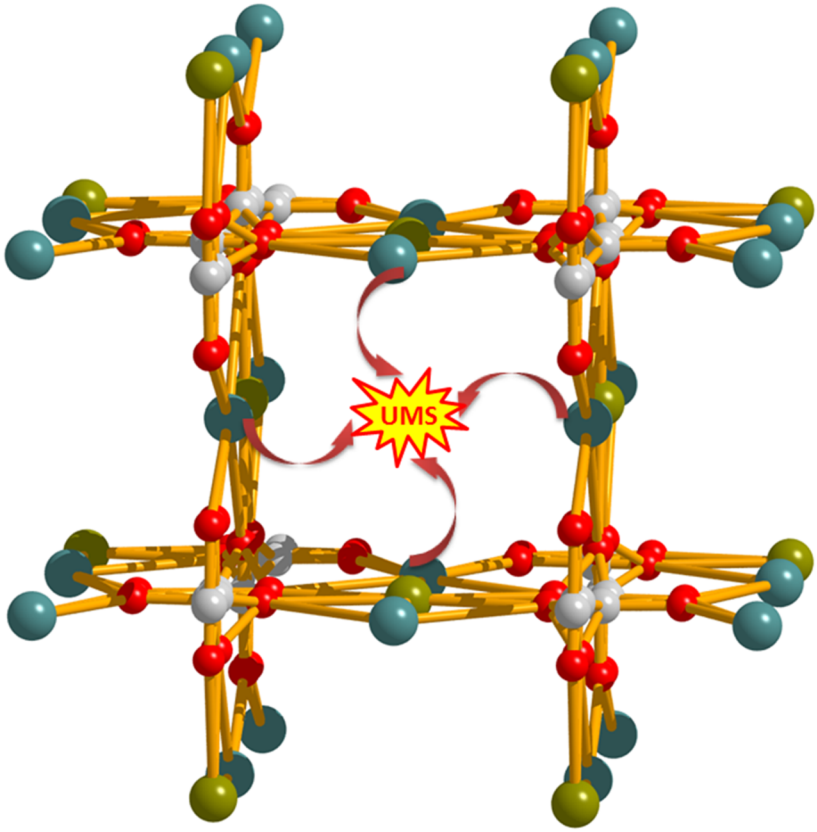

Fig. 7: Figure shows unsaturated metal sites (UMSs) in a Ho and K based MOF.

for a sorbent operating between 1.5-30 bar at 298 K.[16] One of the promising approaches for achieving stronger framework-H_2 interactions is to study metal-organic framework with exposed metal cation cites, particularly of light cations with a high charge density (Fig. 6).[17]

1.3.2: ***Hysteretic Hydrogen Adsorption***

In recent years, the hysteretic guest adsorption property of some flexible framework has dragged the immense interest, though it is not widely exposed for H_2 compare to that of CO_2, O_2, H_2O, CH_3OH, or C_2H_5OH molecules. The hysteretic H_2 adsorption has a great implication because it could provide an understanding of kinetic-based trapping mechanism of H_2 molecules which leads to the manufacture of an effective and promising hydrogen storage material.[18] The hysteresis offers the hydrogen molecules to be charged at higher pressure and stored at relatively lower and safer pressure. However, still the hysteretic hydrogen adsorption is not a common observation in metal-organic framework.[19] In this respect, recent reports indicate that the presence of unsaturated metal site (UMS) is crucial

for strong interaction of H_2 molecule and also largely enhances the value of enthalpy of adsorption (Fig. 7).[20]

1.4: ***Selective Adsorption by MOFs***

1.4.1: ***Selective Uptake of CO_2***

CO_2 adsorption by metal-organic frameworks (MOFs) was first reported[21] by Yaghi and co-workers and it is acclaimed that porous MOFs have great potential in CCST (carbon capture and sequestration technology),[22] as the CO_2 storage property of MOFs is greater than that of other classes of porous solids.[23, 24] This can be attributed to their modular nature that they can be decorated with organic[25] and inorganic[26] moieties which are suitable for molecular recognition of CO_2. Beside those fats, the selective uptake of CO_2 by MOF can also be correlated with the well-established fact that the electric field generated in the framework by UMSs (unsaturated metal sites) and aromatic π-cloud (organic ligand having aromatic ring) interacts firmly with the quadrupole moment of CO_2 (-1.4×10^{-39} C m^2) causing a rapid uptake even at very low pressure (Fig. 8).

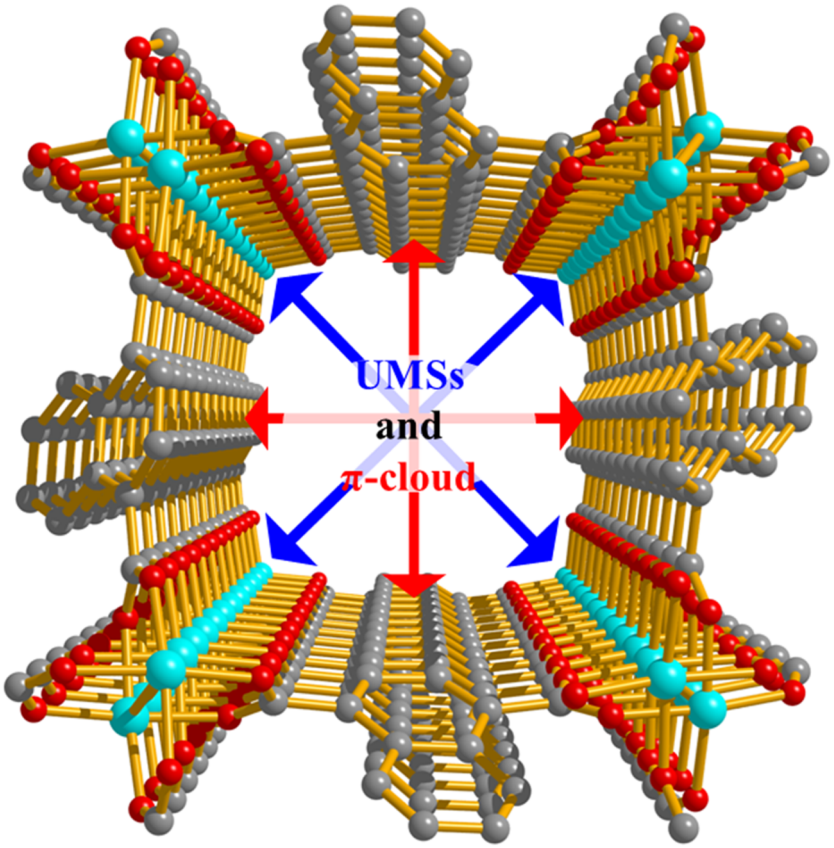

Fig. 8: UMSs and aromatic π clouds are very essential for selective uptake of CO_2.

Apart from that, porous metal–organic frameworks (MOFs), which have emerged as new zeolite alternatives, have attracted considerable research interest in the past decades.[27] As compared to traditional zeolites, they possess a high surface area, modifiable surface, and tuneable pore size which lead to an enormous application potential for MOFs in gas storage and adsorptive separation.

1.4.2: ***Selective Uptake of Hydrocarbons***

On the other hand the separation between C_8-alkyl aromatic compounds is another challenging issue in petroleum industry because of the similarity of their boiling points (e.g. *p*-xylene: 138 ºC, m-xylene: 138–139 ºC, and ethylbenzene: 136 ºC) makes it difficult to separate the isomers.[28] Distillation is only feasible for the removal of *o*-xylene, where it fails to separate the other three isomers. Similarly another example of separation where hexane isomers are separated[29] to boost octane ratings in gasoline has been a very important process and predominantly practiced by cryogenic distillation which is found to be costly.

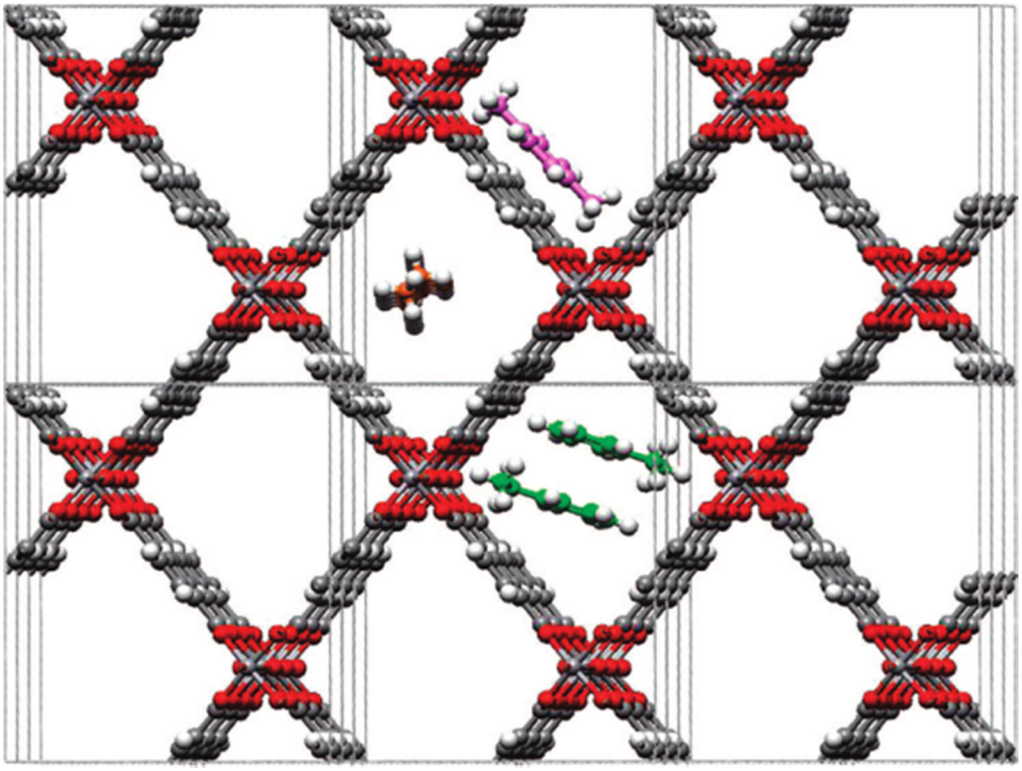

Fig. 9: The MIL-47 framework with octane (orange), *p*-xylene (purple), and ethylbenzene adsorbed inside its uni-dimensional pores (grey lines indicate the borders of a unit cell).

Because the old-hat processes are energy consuming and cost effective, there is an increasing demand to develop novel materials and technologies as an alternative trial. Recently, Jhu and co-workers[30] synthesised a new material which selectively adsorbs *p*-xylene over the other two isomers. By the fine tune of the pore size they have smartly included *p*-xylene in a selective manner. Denayeret. al has reported the study of vapour adsorption of MIL-47 where they have showed (Fig. 9) the effect of temperature on adsorption coefficient.[31]

1.5: ***Magnetism in MOFs***

1.5.1: ***Magnetic Materials***

Magnetism is one of the most fundamental physical phenomenon and it was commonly used in our daily life from a long time. Magnetism is explained as a phenomenon by which material exerts attractive or repulsive forces on other materials. Some well-known materials that exhibit easily detectable magnetic property, so called magnets are nickel, iron, cobalt and their alloys, metal oxides. Generally all materials are classified into two types, and they are paramagnet which increases the internal magnetic flux density under the external field and the other one is diamagnet which decreases it *vice versa*. The so called magnet generally means "ferromagnet" which exhibits a spontaneous magnetisation based on spin ordering without the presence of external field.

In the presence of external field they show a magnetic hysteresis with remnant magnetisation and cohesive force (Fig. 10) which has a great impact in preparing magnetic material based memory devices.

Though the history of magnets have been started in the ancient time, but the application of magnetic technology became indispensable after discovering the electromagnets and it was applied into magnetic devices, switching materials, motors, dynamics and magnetic cards which supports our modern society. On the other hand, magnetic and electromagnetic phenomenon led to the development of physics and created a new scientific area. Meanwhile the molecular-based magnets (MMs) have been appeared substantially in the late 1980s as a new class of magnetic materials.[32] MMs are of magnetic materials consisting of paramagnetic molecules, e.g. organic molecules, metal complexes and show a long range ordering as well as general magnets. To achieve the magnetic ordering it is necessary to provide highly ordered array structure of magnetic centre and long range control of magnetic interaction.

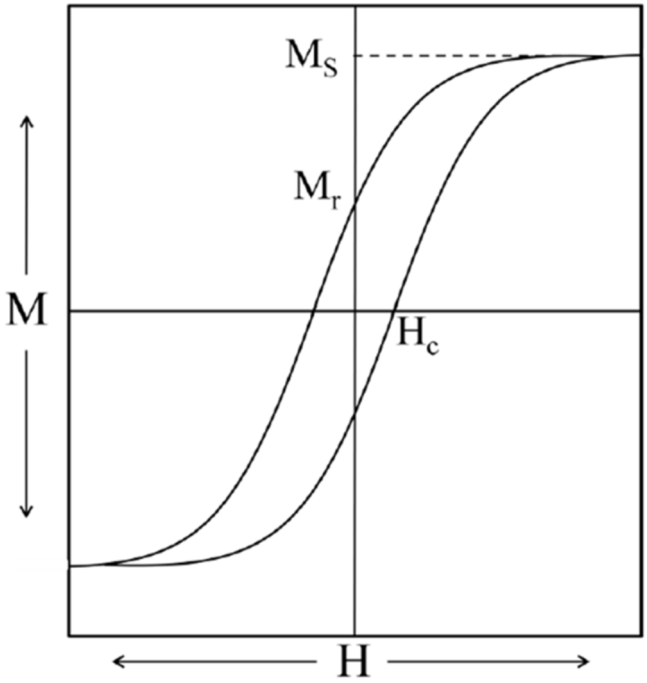

Fig. 10: Hysteresis loop of a typical ferromagnetic material. Where H_c = Coercive field M_r = Remnant magnetization M_s = Saturation magnetization.

This type of magnets has advantages over the conventional magnets (metal oxides, alloys etc.) due to their systematic study based on elaborate molecular design. In the arena of molecular magnetism, research has been focussed on the elucidation of magneto-structural relationship which is later shifted on the advanced one "achievement of multiple properties and multi-functionalized MMs".

1.5.2: ***Coordination Polymer Based Magnets***

After the establishment of the concept of metal complex by Alfred Warner, the versatile metal complexes based on the coordination bonds between metal ions and organic or inorganic ligands have been systematically investigated and their characteristics have been clarified. Prussian blue, $Fe^{III}_4[Fe^{II}(CN)_6]_3 \cdot nH_2O$ would be the history's first coordination polymer (CP), which has a 3D face centered cubic framework based on hexacyanoferrate and was accidentally synthesised by Heinrich Diesbach in Berlin in 1974 and later ferromagnetic ordering at 5.6 K was also observed for the same.[13] The magnetic interaction is sensitive to the bridging structure and electronic configuration of metal ions. From this aspect, structural information is crucial for the discussion of magnetic behaviour. So, the progress of the study of MMs had to wait for the development of X-ray diffractometer and analyser.

1.5.3: ***Prussian Blue and it's Analogue***

Prussian blue (Fig. 11) shows a blue colour and has been used as a dye material. However, Prussian blue's attraction lies not only in its optical properties but also in its magnetic properties: it shows a long-range ferromagnetic ordering at T_c= 5.6 K.[33] Moreover, various interesting magnetic properties have been reported recently with its analogues. For example, a series of Prussian blue analogous composed of hexacyanochromate; $A^{II}_y[Cr^{III}(CN)_6]$ (A = V, Cr, Mn, Ni and Cu), draw an attention due to their high T_c values.[34] Particularly, Verdaguer and co-workers reported a critical temperature of 315K for the magnetic spin ordering with $V[Cr(CN)_6]_{0.86}\cdot 2.8H_2O$.[35] In addition, Hatlevik et.al.[36] and Girolami and Holmes[37], respectively, reported the crystalline powder $K^IV^{II}[Cr^{III}(CN)_6]$, with a T_c value of 103ºC, and the amorphous powder $K^I_{0.058}V^{II/III}[Cr^{III}(CN)_6]_{0.79}(SO_4)_{0.058}\cdot 0.93H_2O$, with a T_c value of 99ºC.

1.5.4: ***Origin of Magnetism in Prussian Blue and it's Analogue***

The magnetic coupling of metals in Prussian blue analogues is described in terms of a superexchange mechanism through the cyanide ligands. The superexchange mechanism is summarized on the basis of the Goodenough–Kanamori rule[38], which includes consideration of the bond angle and the symmetry of the metal and ligand orbitals concerned. There are two mechanisms for superexchange interactions: the kinetic exchange mechanism (J_{KE}) and the potential exchange mechanism (J_{PE}) (Fig. 12).[39a] On one hand, kinetic exchange is mediated by a direct pathway of the overlapping orbitals, which connects the two interacting magnetic orbitals.

It is antiferromagnetic in nature as a consequence of the Pauli principle, leading to an antiparallel spin ordering via a common covalent bond. On the other hand, potential exchange is effective between orthogonal magnetic orbitals with comparable orbital energy. In this case Hund's rule leads to a parallel spin alignment, i.e. a ferromagnetic interaction. In the case of Prussian blue analogues, the metal *d*-orbitals are split into t_{2g} and e_g set by the CN ligands. Therefore, based on magnetic orbital symmetry, we can understand whether the orbital superexchange among each of the orbitals on metal ions is J_{KE} or J_{PE}. When the magnetic orbital symmetries of the metals are the same, the superexchange interaction is J_{KE}. Conversely, when the magnetic orbital symmetries of the metals are different, the superexch-

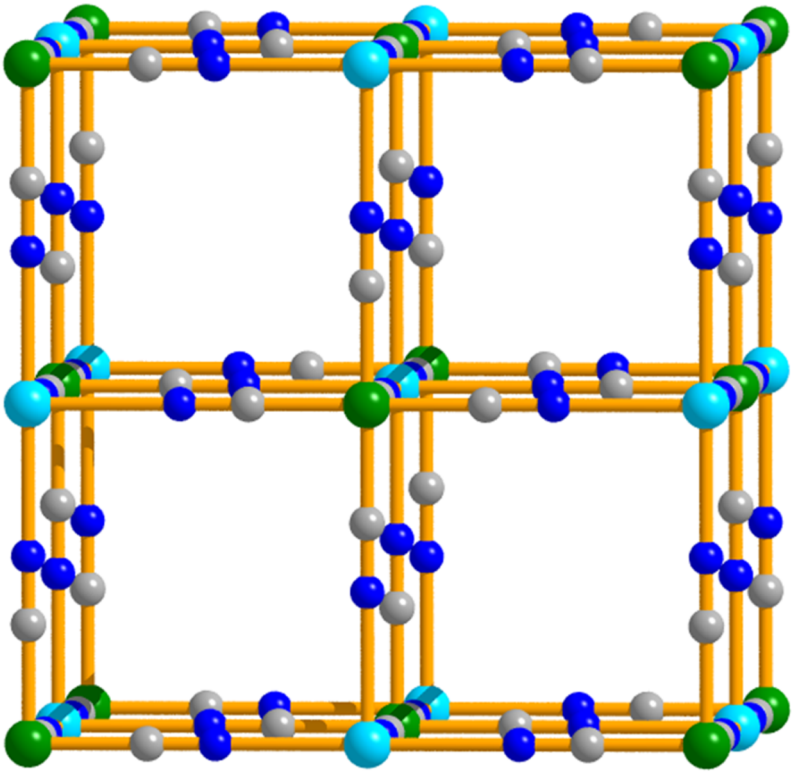

Fig. 11: Crystal structure of Prussian blue. Blue and grey coloured atoms are representing N and C respectively. Comparatively larger atoms (green and sky) represent the metal nodes.

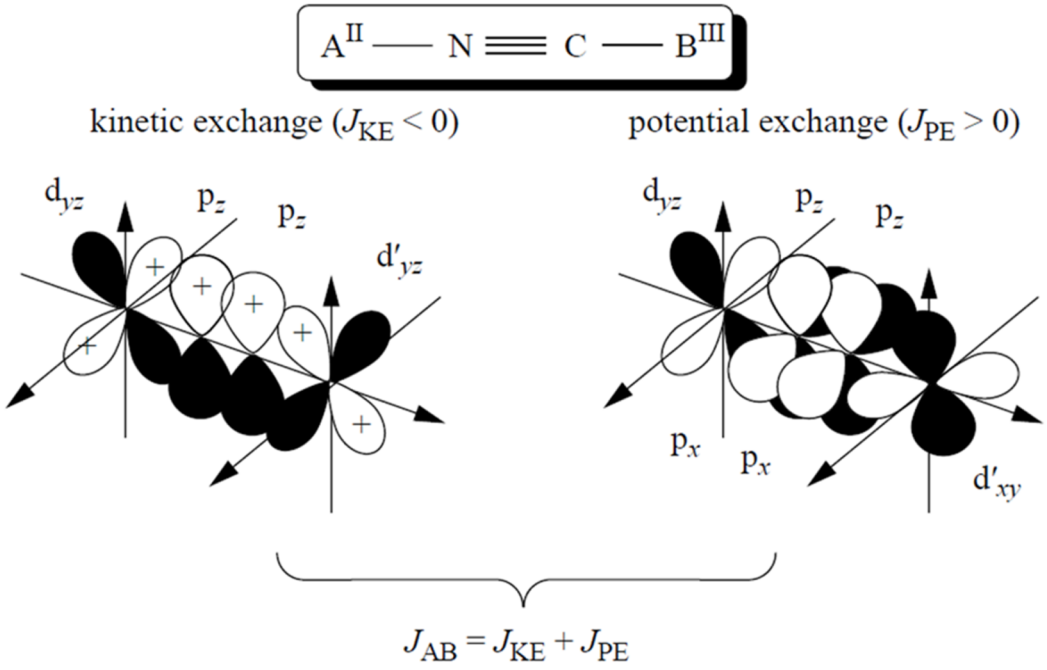

Fig. 12: The two basic mechanisms for the isotropic exchange in the magnetic coupling between the AII and BIII ions in the CN-bridged complex. On the left is one of the significant kinetic exchange (J_{KE}) pathways ($d_{yz} \parallel \pi_z \parallel d_{yz'}$), and on the right is one of significant potential exchange (J_{PE}) pathways ($d_{yz} \parallel \pi_z \perp \pi_x \parallel d_{xy'}$). The superexchange coupling between A^{II} and B^{III} (J_{AB}) involves a superposition of J_{PE} and J_{KE}.

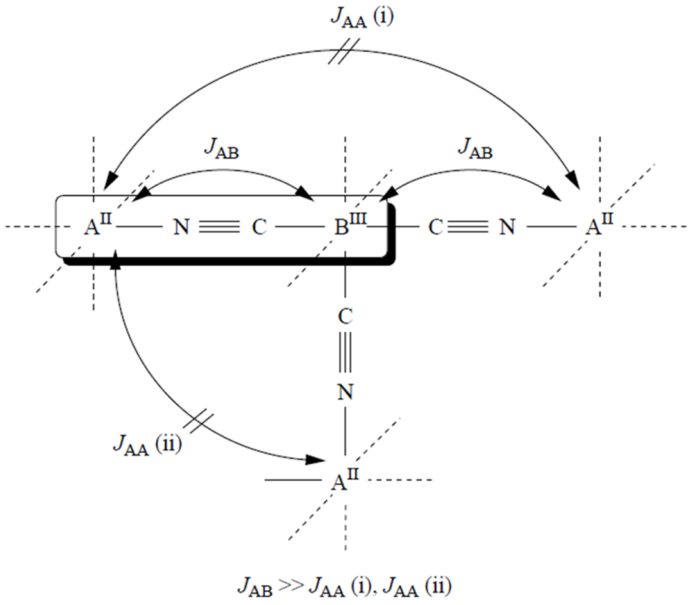

Fig. 13: In the Prussian blue structure, superexchange interactions at a 180 ºangle between A^{II} and B^{III} are dominant over superexchange interactions of the second nearest-neighbour metals (J_{AA}(i)) and direct exchange interactions (J_{AA}(ii)).

-ange interaction is J_{PE}. The total superexchange interaction is given by the sum of all of the orbital exchange contributions between the transition metal ions.[39]

As an example, we consider the case of the hexacyanochromate cyanide $A^{II}_{y}[Cr^{III}(CN)_6]$, with Cr^{III} being $(t_{2g})^3$ and S_{Cr}= 3/2 . There is no overlap between Cr^{III} and A^{II} magnetic orbitals, if all of the magnetic orbitals of A^{II} have e_g symmetry. In this situation, the potential exchange mechanism becomes dominant, leading to a ferromagnetic interaction between Cr^{III} and A^{II}. In fact, in $Cs^{I}Ni^{II}[Cr^{III}(CN)_6]$, with a high-spin state for $Ni^{II}((t_{2g})^6(e_g)^2$, S_{Ni} = 1), a ferromagnetic interaction operates between Cr^{III} and Ni^{II}.[14b] In contrast, when all of the A^{II} magnetic orbitals have t_{2g} symmetry, the overlap between the t_{2g} (A) and t_{2g} (Cr) orbitals gives rise to kinetic exchange, leading to an antiferromagnetic interaction. If both t_{2g} and e_g electrons are present on A^{II}, the superexchange coupling constant (J_{AB}) is described as the sum of the ferromagnetic (J_{PE}>0) and antiferromagnetic (J_{KE}<0) orbital contributions (Fig. 12, 13). Kinetic exchange usually operates in preference to potential exchange, i.e. $|J_{KE}| > |J_{PE}|$. For example, in $Cs^{I}Mn^{II}[Cr^{III}(CN)_6]$, with a high-spin state for $Mn^{II}((t_{2g})^3(e_g)^2$, S_{Mn}= 5/2), the interaction between Cr^{III} and Mn^{II} is antiferromagnetic, and the compound is a ferrimagnet.[14a] We can thus design the exchange interactions in Prussian blue analogs simply. Therefore, we have used Prussian blue analogs for the design of functional magnets. A rational concept and design approach would be to choose a polycyanometallate anion, $[(M_A(CN)_n]^{m-}$ (n = 2-8), as a hub which can link to another metal M_B to create a magnetic

path way M_B–NC–M_A–CN–M_B and leads to a 2D sheet. These 2D sheets can be further linked by organic linker to invoke long range magnetic ordering.

1.6: ***Porous Magnets Based on Hexcyanometallate***

Prussian blue analogues are the most known and studied cyanide-based frameworks, and constitute one of the most promising classes of potentially porous magnetic materials. In these compounds, octahedral $[M'(CN)_6]^{x-}$ complexes are linked via octahedrally-coordinated, nitrogen-bound M^{y+} ions to give a 2D sheet of mixed metals connected via cyanide linker (Fig. 14).

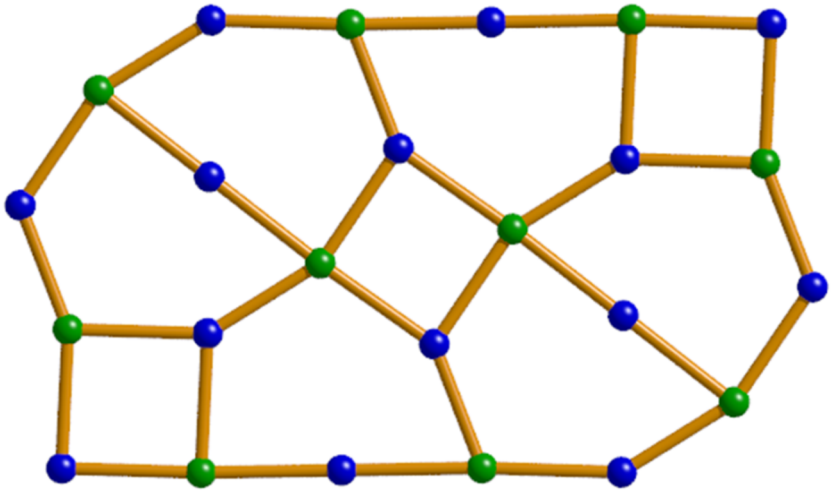

Fig. 14: Creating a 2D sheet by metal ions and cyanide ligands.

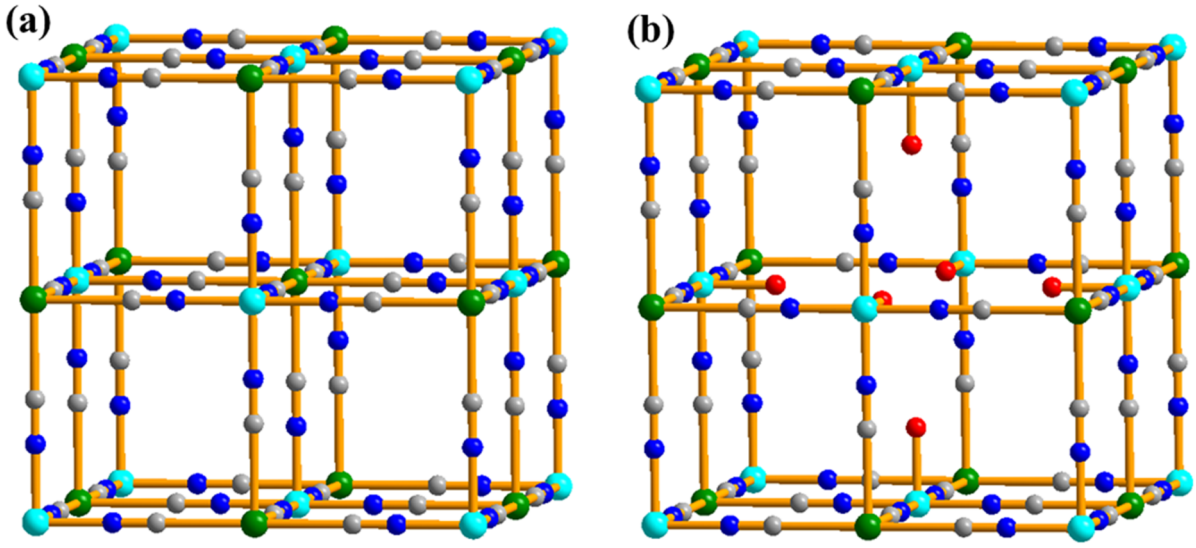

Fig. 15: (a) Portion of the crystal structure of the Prussian blue analogues $M^{II}_3[M'^{III}(CN)_6]_2$ and (b) $A^{I}M^{II}[M'^{III}(CN)_6]\cdot nH_2O$.

These 2D layers can be further connected by the pending cyanide linkers to grow along the 3rd direction (Fig. 15a). With a suitable choice of the transition metal ions M and M′, a number of Prussian blue analogues with high magnetic ordering temperatures have been elaborated, reaching up to 376 K for $KV[Cr(CN)_6]_2 \cdot 2H_2O$. Furthermore, based on empirical and theoretical studies, the nature (ferro- versus antiferro-) and an estimation of the strength of the magnetic coupling through the cyanide bridges can be predicted, facilitating rational design of the magnetic properties of these compounds.

Depending on the stoichiometry M′/M and the respective oxidation states, the structure can also contain monocationic counterions, located in the cavities of the cubic structure. When such vacancies are present, the available coordination sites on M are occupied by bound water molecules (Fig. 15b). Other water or small solvent molecules can also be situated within the pores of the cubic framework. Motivation collected by these facts makes us thinking that if we can link these 2D layers by any organic linker then magnetic and porosity both can be combined in a single framework.

1.7: ***Our Approach: Leading to the Preparation of Multifunctional Materials***

Recently, focus on multifunctional materials *i.e.* materials which combine a set of well-defined properties (e.g. porosity and magnetism, porosity and optical) for specific applications are gaining importance. Such synergism, where two different functionalities are combined, would open up the possibility and prospect of finding novel physical phenomena for designing smart materials.

Combining porosity and magnetic ordering in a single material presents a significant challenge because magnetic exchange generally requires short bridges between the spin carriers, whereas oppositely, porosity usually increases with the use of long diamagnetic connecting ligands. Despite this apparent in compatibility, tremendous successes have been achieved in the past decades generating truly microporous solids with high magnetic ordering temperatures. The introduction of simple organic bridging ligands along with metal ions revolutionized the field of porous magnet. From the combination of both properties can also result immerging features such as guest dependent magnetic behaviour. A significant number of porous magnets (Fig. 16) have been reported so far, with variable performances. Among them, Prussian blue analogues deserve particular attention, since they can feature high surface area together with magnetic ordering temperatures even at high temperature. In this dissertation, I have tried to give an overview of this emerging class of multifunctional materi-

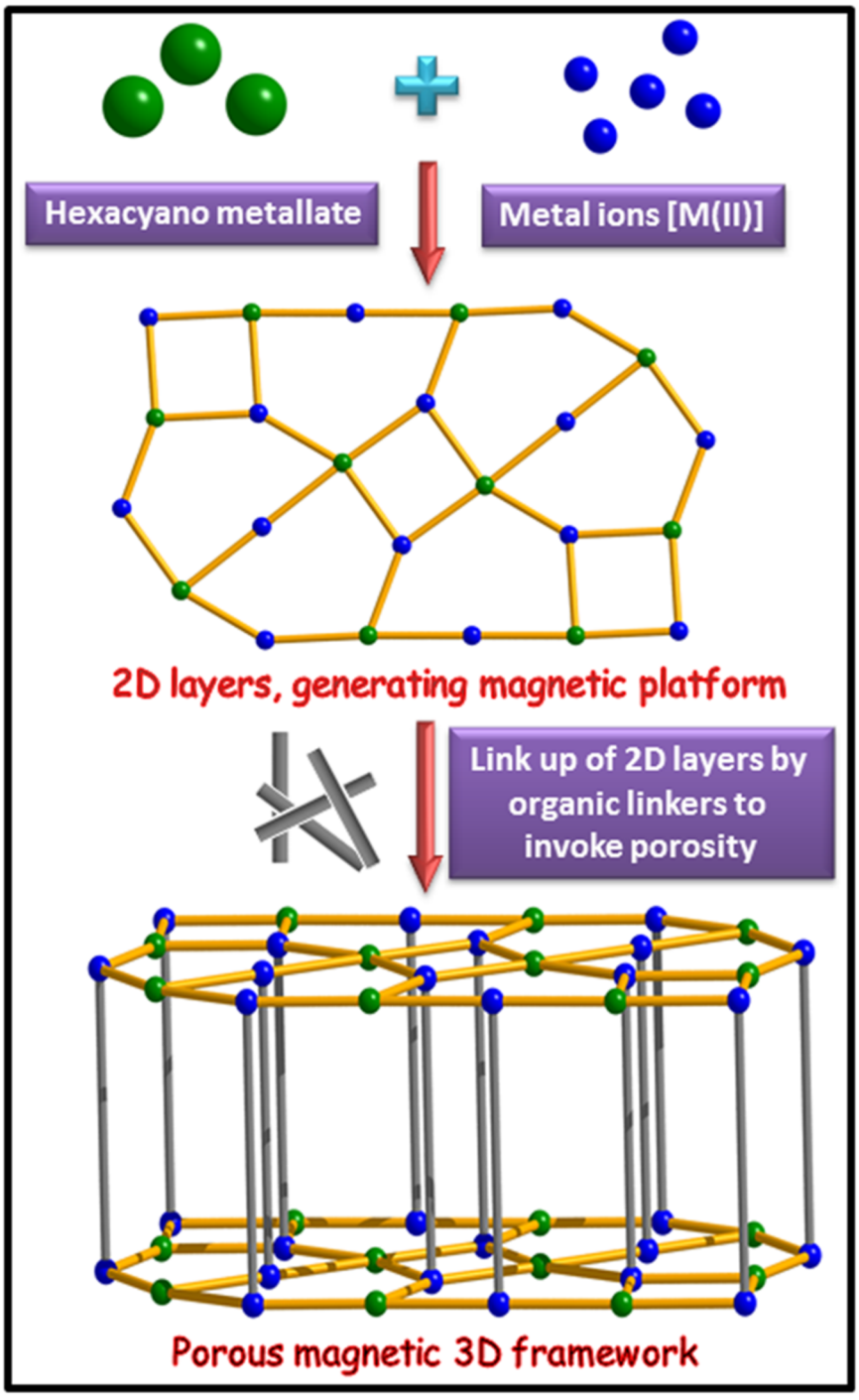

Fig. 16: Schematic diagram of the preparation of porous magnet.

-als with particular emphasis on synthetic strategies and their possible applications.

Based on the above discussion, we have tried to generate 2D layers with the help of metal cyanide which is further connected by organic ligand to extend along third direction for preparing multifunctional smart materials.

1.8: ***Concluding Remarks***

The last two decades have seen an explosion in the field of Coordination Polymers (CPs) research not only in terms of academic interest but also in terms of real applications. A large number of papers, reviews and books published in the last few years bear a testimony to this fact. However to bring these type of materials in use in daily life, large scale synthesis and cost reduction of devices is essential. Though there has been significant effort towards end, this major progress is still awaited. It is clearly an exciting time to pursue work on synthesis properties and applications of such multi-functional inorganic-organic hybrid materials.

1.9: ***References***

1. P. J. Langley, J. M. Rawson, J. N. B. Smith, M. Schuler, R. Bachmann, A. Schweiger, F. Palacio, G. Antorrena, G. Gescheidt, A. Quintel, P. Rechsteiner and J. Hulliger, *J. Mater. Chem.*, **1999**, *9*, 1431.
2. M. E. Brown and M. D. Hollingsworth, *Nature,***1995**, *376*, 323.
3. V. Ramamurthy and D. F. Eaton, *Chem. Mater.*, **1994**, *6*, 1128.
4. F. Toda, S. Hyoda, K. Okada and K. Hirotsu, *J. Chem. Soc., Chem. Commun*., **1995**, 1531.
5. K. Endo, T. Koike, T. Sawaki, O. Hayashida, H. Masuda and Y. Aoyama, *J. Am. Chem. Soc*., **1997**, *119*, 4117.
6. (*a*) C. L. Chen and A. M. Beatty, *J. Am. Chem. Soc.*, **2008**,*130***,** 17222; (*b*) M. B. Dewal, M. W. Lufaso, A. D. Hughes, S. A. Samuel, P. Pellechia and L. S. Shimizu, *Chem. Mater.,* **2006**, *18*, 4855; (*c*) S. A. Dalrymple and G. K. H. Shimizu, *Chem. Commun.,* **2006**, 956.
7. (*a*) O. M. Yaghi, H. L. Li, , C. Davis, D. Richardson and T. L. Groy. *Acc. Chem. Res.* **1998**, *31*, 474; (*b*) S. Kitagawa and M. Kondo.*Bull. Chem. Soc. Jpn*. **1998**, *71***,** 1739; (*c*) A. J. Blake *et al*. *Coord. Chem. Rev.* **1999**, *183*, 117; (*d*) B. Moulton and M. J. Zaworotko. *Chem. Rev.* **2001**, *101***,** 1629; (*e*) S. L. James *Chem. Soc.* Rev. **2003**, *32*, 276.
8. (*a*) T. Tanaka, T. Tasaki and Y Aoyama, *J. Am. Chem. Soc.* **2002**, *124*, 12453; (*b*) J. L. Atwood, L. J. Barbour and A Jerga. *Science*, **2002**, *296*, 2367.

9. D. V. Soldatov *et al. J. Am. Chem. Soc.* **1999**, *121*, 4179.
10. (*a*) A. J. Fletcher, K. M. Thomas and M. J. Rosseinsky, *J. Solid State Chem.* 2005, **178,** 2491; (*b*) K. Uemura, R. Matsuda and S. Kitagawa, *J. Solid State Chem.* 2005, *178*, 2420.
11. H. Hayashi, A. P. Côté, H. Furukawa, M. O'Keeffe, O. M. Yaghi, *Nat. Mater.*, **2007**, *6*, 501.
12. (*a*) M. Eddaoudi, J. Kim, N. Rosi, D. Vodak, J. Wachter, M. O'Keeffe and O. M. Yaghi, *Science*, **2002**, *295*, 469; (*b*) S. Kitagawa, R. Kitaura and S.-I. Noro, *Angew. Chem., Int. Ed.*, **2004**, *43*, 2334; (*c*) A. R. Millward and O. M. Yaghi, *J. Am. Chem. Soc.*, **2005**, *127*, 17998; (*d*) H. Furukawa, M. A. Miller and O. M. Yaghi, *J. Mater. Chem.*, **2007**, *17*, 3197; (*e)* G. Férey, *Chem. Soc. Rev.*, **2008**, *37*, 191; (*f*) S. Ma, D. Sun, J. M. Simmons, C. D. Collier, D. Yuan and H.-C. Zhou, *J. Am. Chem. Soc.*, **2008**, *130*, 1012; (*g*) R. E. Morris and P. S. Wheatley, *Angew. Chem., Int. Ed.*, **2008**, *47*, 4966; (*h*) L. J. Murray, M. Dincă and J. R. Long, *Chem. Soc. Rev.*, **2009**, *38*, 1294.
13. L. Schlapbach and A. Zűttel, *Nature*, **2001**, *414*, 353.
14. (*a*) L. J. Murray, M. Dincă and J. R. Long, *Chem. Soc. Rev.*, **2009**, *38*, 1294; (*b*) K. M. Thomas, *Dalton Trans.*, **2009**, 1487.
15. M. Dincã and J. R. Long, *Angew. Chem. Int. Ed.*, **2008**, *47*, 6766.
16. (*a*) S. K. Bhatia and A. L. Myers, *Langmuir*, **2006**, *22*, 1688. (*b*) Note that the consideration of an enthalpy–entropy correlation for H_2 adsorption in metal–organic frameworks results in an even greater magnitude for the optimal enthalpy of adsorption (–20 to –25 kJ mol^{-1}); (*c*) E. Garrone, B. Bonelli and C. Otero Areăn, *Chem. Phys. Lett.*, **2008**, *456*, 68; (*d*) C. Otero Areăn, S. Chavan, C. P. Cabello, E. Garrone and G. T. Palomino, *ChemPhysChem*, **2010**, *11*, 3237.
17. (*a*) M. Dincă and J. R. Long, *J. Am. Chem. Soc.*, **2005**, *127*, 9376; (*b*) A. Vimont, J.-M. Goupil, J.-C. Lavalley, M. Daturi, S. Surblé , C. Serre, F. Millange, G. Férey and N. Audebrand, *J. Am. Chem. Soc.*, **2006**, *128*, 3218; (*c*) H. R. Moon, N. Kobayashi and M. P. Suh, *Inorg. Chem.*, **2006**, *45*, 8672; (*d*) M. Dincă , A. Dailly, Y. Liu, C. M. Brown, D. A. Neumann and J. R. Long, *J. Am. Chem. Soc.*, **2006**, *128*, 16876; (*e*) K. Sumida, S. Horike, S. S. Kaye, Z. R. Herm, W. L. Queen, C. M. Brown, F. Grandjean, G. J. Long, A. Dailly and J. R. Long, *Chem. Sci.*, **2010**, *1*, 184; (*f*) P. D. C. Dietzel, Y. Morita, R. Blom and H. Fjellvag, *Angew. Chem., Int. Ed.*, **2005**, *44*, 6354; (*g*) N. L. Rosi, J. Kim, M. Eddaoudi, B. Chen, M. O'Keeffe and O. M. Yaghi, *J. Am. Chem.*

Soc., **2005**, *127*, 1504; (*h*) P. D. C. Dietzel, B. Panella, M. Hirscher, R. Blom and H. Fjellvag, *Chem. Commun.*, **2006**, 959; (*i*) S. R. Caskey, A. G. Wong-Foy and A. J. Matzger, *J. Am. Chem. Soc.*, **2008**, *130*, 10870; (*j*) P. D. C. Dietzel, R. Blom and H. Fjellvag, *Eur. J. Inorg. Chem.*, **2008**, 3624; (*k*) P. D. C. Dietzel, P. A. Georgiev, J. Eckert, R. Blom, T. Strässle and T. Unruh, *Chem. Commun.*, **2010**, *46*, 4962.

18. (*a*) K. L. Mulfort, O. K. Farha, C. D. Malliakas, M. G. Kanatzidis and J. T. Hupp, *Chem. –Eur. J.*, **2010**, *16*, 276; (*b*) J. T. Culp, M. R. Smith, E. Bittner and B. Bockrath, *J. Am. Chem. Soc.*, **2008**, *130*, 12427; (*c*) C. Serre, C. Mellot-Draznieks, S. Surblé, N. Audebrand, Y. Filinchuk and G. Férey, *Science*, **2007**, *315*, 1828; (*d*) P. L. Llewellyn, S. Bourrelly, C. Serre, Y. Filinchuk and G. Férey, *Angew. Chem., Int. Ed.*, **2006**, *45*, 7751; (*e*) T. K. Maji, G. Mostafa, R. Matsuda and S. Kitagawa, *J. Am. Chem. Soc.*, **2005**, *127*, 17152.
19. (*a*) Z. Guo, G. Li, L. Zhou, S. Su, Y. Lei, S. Dang and H. Zhang, *Inorg. Chem.*, **2009**, *48*, 8069; (*b*) H. J. Choi, M. Dincă and J. R. Long, *J. Am. Chem. Soc.*, **2008**, *130*, 7848; (*c*) S. Ma, X. S. Wang, E. S. Manis, C. D. Collier and H. C. Zhou, *Inorg. Chem.*, **2007**, *46*, 3432; (*d*) C. Yang, X. Wang and M. A. Omary, *J. Am. Chem. Soc.*, **2007**, *129*, 15454; (*e*) X. Zhao, B. Xiao, A. J. Fletcher, K. M. Thomas, D. Bradshaw and M. J. Rosseinsky, *Science*, **2004**, *306*, 1012;
20. A. Hazra, P. Kanoo and T. K. Maji, *Chem. Commun.*, **2010**, *47*, 538.
21. H. Li, M. Eddaoudi, T. L. Groy, O. M. Yaghi, *J. Am. Chem. Soc.,* **1998**, *120*, 8571.
22. (*a*) D. M. D'Alessandro, B. Smit, J. R. Long, *Angew. Chem., Int. Ed.,* **2010**, *49*, 2. (*b*) S. Q. Ma, H. C. Zhou, *Chem. Commun*., **2010**, *46*, 44.
23. (*a*) A. R. Millward, O. M. Yaghi, *J. Am. Chem. Soc.* **2005**, *127*, 17998. (*b*) P. L. Llewellyn, S. Bourrely, C Serre, A. Vimont, M. Daturi, L. Hamon, G. D. Weireld, J.-S. Chang, D.-Y. Hong, Y. K Hwang, S. H. Jhung, G. Férey; *Langmuir*, **2008**, *24*, 7245.
24. (*a*) J. Zhang, R. Singh, P. A. Webley,*Microporous Mesoporous Mater.* **2008**, *111*, 478. (*b*) S. Cavenati, C. A. Grande, A. E. Rodrigues, *J. Chem. Eng. Data*, **2004**, *49*, 1095. (*c*) S. Himeno, T. Komatsu, S. *J.* Fujita, *Chem. Eng. Data*, **2005**, *50*, 369.
25. (*a*) F. Debatin, A. Thomas, A. Kelling, N. Hedin, Z. Bacsik, I. Senkovska, S. Kaskel, M. Junginger, H. Müuller, U. Schilde, C. Jäger, A. Friedrich, H.-J. Holdt, *Angew. Chem., Int. Ed*. **2010**, *49*, 1258. (*b*) J. An, S. J. Geib, N. L. Rosi, *J. Am. Chem. Soc*. **2010**, *132*, 38. (*c*) R. Vaidhyanathan, S. S. Iremonger, K. W. Dawson, G. K. H. Shimizu, *Chem. Commun.* **2009**, 5230; (*d*) B. Arstad, H. Fjellvag, K. O. Kongshaug,

O. Swang, R. Blom, *Adsorption*, **2008**, *14*, 755; (*e*) S. Couck, J. F. M. Denayer, G. V. Baron, T. Remy, J. Gascon, F. Kapteijn, *J. Am. Chem. Soc.* **2009**, *131*, 6326; (*f*) J. -B. Lin, J.-P. Zhang, X. -M. Chen, *J. Am. Chem. Soc.* **2010**, *132*, 6654; (*g*) A. Torrisi, R. G. Bell, C. Mellot-Draznieks, *Cryst. Growth Des.* **2010**, *10*, 2839.

26. A. Demessence, D. M. D'Alessandro, M. L. Foo, J. R. Long, *J. Am. Chem. Soc.*, **2009**, *131*, 8784.
27. (*a*) M. Dincã, and J. R. Long, *J. Am. Chem. Soc.* **2005**, *27*, 9376. (*b*) A. J. Fletcher, E. J. Cussen, T. J. Prior, M. J. Rosseinsky, C. J. Kepert, K. M. Thomas. *J. Am. Chem. Soc.***2001**, *123*, 10001. (*c*) S. I. Sandler, and S. Chempath, *Langmuir*, **2007**, *23,* 659. (*d*) B. Zheng, J. Bai, J. Duan, L. Duan, M. J. Zaworotko. *J. Am. Chem. Soc.*doi.org/10.1021/ja110042b. (*e*) S. Ma, X.S. Wang, E. S. Manis, C. D. Collier, H. C. Zhou, *Inorg. Chem.* **2007**, *46*, 3432. (*f*) A. Demessence, and J. R. Long, *Chem. Eur. J.* **2010**, *16*, 5902.
28. (*a*) *Ullmann&sEncyclopedia of Industrial Chemistry*, 6th ed., **2000** electronic release; (*b*) R. Meyers, *Handbook of Petroleum Refining Processes, 3th ed., McGraw-Hill, New York*, 2003, pp. 2.47; (*c*) A. Méthivier in *Zeolites for Cleaner Technologies, Catalytic Science Series*, Vol. 3 (Eds.: M. Guisnet, J. P. Gilson), Imperial College Press, London, 2002, 209.
29. P. S. Bárcia, F. Zapata, J, A. C. Silva, A. E. Rodrigues, B. Chen. *J. Phys. Chem. B*, **2007**, *111,* 6101.
30. Z. Jin, H. Y. Zhao, X. J. Zhao, Q. R. Fang, J. R. Long and G. S. Zhu, *Chem. Commun.,* **2010**, *46*, 8612.
31. V. Finsy, H. Verelst, L. Alaerts, D. D. Vos, P. A. Jacobs, G. V. Baron, and J. F. M. Denayer, *J. Am. Chem. Soc.***2008**, *130*, 7110.
32. (*a*) J. S. Miller, J. C. Calabrese, H. Rommelmann, S. R. Chittipeddi, J. H. Zhang, W. M. Reiff and A. J. Epstein, *J. Am. Chem. Soc.*, **1987**, 109, 769; (*b*) J. S. Miller, A. J. Epstein, W. M. Reiff, *Chem. Rev.*, **1988**, 88, 201.
33. W.E. Buschmann, J. Ensling, P. Gulich, J. S. Miller, *Chem. Eur. J.*, **1999**, *5*, 3019.
34. (*a*) W.D. Griebler, D. Babel, Z. Naturforsch. *Teil B*, **1982**, 87, 832. (*b*) V. Gadet, T. Mallah, I. Castro, P. Veillet, M. Verdaguer, *J. Am. Chem. Soc.*, **1992**, *114*, 9213. (*c*) T. Mallah, S. Thiebaut, M. Verdaguer, P. Veillet, *Science*, **1993**, *262*, 1554. (*d*) W.R. Entley, G.S. Girolami, *Inorg. Chem.*, **1994**, *33*, 5165. (*e*) R.E. William, G.S. Girolami, *Science*, **1995**, *268*, 397. (*f*) O. Sato, T. Iyoda, A. Fujishima, K. Hashimoto, *Science*, **1996**, *271*, 49.

35. (*a*) S. Ferlay, T. Mallah, R. Ouahs, P. Veillet, M. Verdaguer, *Nature*, **1995**, *378*, 701. (*b*) E. Dujardin, S. Ferlay, X. Phan, C. Desplanches, C. Cartier dit Moulin, P. Sainctavit, F. Baudelet, E. Dartyge, P. Veillet, M. Verdaguer, *J. Am. Chem. Soc.*, **1998**, *120*, 11347.

36. Ø. Hatlevik, W. E. Bushmann, J. Zhang, J. L. Manson, J. S. Miller, *Adv. Mater.*, **1999**, *11*, 914.

37. S.M. Holmes, G. S. Girolami, *J. Am. Chem. Soc.*, **1999**, *121*, 5593.

38. (*a*) J. B. Goodenough, *Phys. Rev.*, **1959**, *100*, 564; (*b*) J. B. Goodenough, *J. Phys. Chem. Solids*, **1958**, *6*, 287; (*c*) J. Kanamori, *J. Phys. Chem. Solids*, **1959**, *10*, 87.

39. (*a*) A.P. Ginsberg, *Inorg. Chim. Acta. Rev.*, **1971**, *5*, 45. (*b*) M. Nishino, S. Kubo, Y. Yoshioka, A. Nakamura, K. Yamaguchi, Mol. Cryst. Liq. Cryst. 1997, 305, 109.

Chapter-2

Part-A

Flexible Supramolecular Host with a Crowned Chair Octameric Water Cluster and Highly Selective Adsorption Properties

Abstract:

A novel supramolecular porous host $\{(H\text{-}bipy)_3 \cdot [Fe(CN)_6] \cdot 8H_2O\}$ **(1)** was obtained by the reaction of $K_3[Fe(CN)_6]$ and 4,4′-bipyridyl (bipy) under acidic medium (pH ≈ 3). The host structure of **1** is predominantly made up of non-covalent forces viz. hydrogen bonding and π-π interactions. The porous host houses a discrete octameric water cluster with the conformation of 1,4-substituted cyclohexane molecule where six water molecules are positioned on the vertices of the cyclohexane ring and the seventh and eighth occupy the 1,4-equatorial positions of the ring. The DFT calculation suggests, this conformation is more stable (-73.08 kcal/mol) compare to the *a,e* or *a,a* conformation. Upon removal of the water molecules, host network of **1** undergoes structural transformation and the dehydrated phase, **1′** exhibits three step uptake of H_2O molecules and completely excludes CO_2 gas and other organic solvent molecules (CH_3OH, CH_3CN, EtOH).

2.1.1: ***Introduction***

Modular synthesis of soft materials, e.g. block copolymers, organic thin films, molecular inclusion compounds promise precession engineering of specific properties and functions. Amongst them, the class of molecular compounds (also termed as inclusion compounds) is of particular interest because of their widespread applications in the field of magnetism,[1] ferroelasticity,[2] nonlinear optical effect,[3] chemical storage[4] and catalysis.[5] Moreover, extended networks sustained solely by noncovalent interactions exhibits greater degree of flexibility resulting selectivity in terms of guest accommodation.[6] Such network of soft interactions is often amenable to switching properties and reversible changes from an absorbing state to a close packed inactive polymorph can be triggered by thermal, mechanical, or radiative stimuli.[7] Open framework solids act as a coffer for the templating solvent molecules and they stabilize the overall crystal host and often they formed cluster, particularly water molecules by H-bonding interactions. Exploration of the possible structures and stabilities of water clusters is of immense interest to chemist as well as to physicist because of their unusual properties and of importance to life.[8] The importance in relevance to physical, chemical and biological processes have propelled the scientists to investigate water clusters extensively.[9] Indeed, it is possible to understand the complex nature of bulk water as well as ice by a detail study of numerous possible structures of water clusters found in supramolecular networks.[10] Although a number of water structures are reported in literature,[11-14] our emphasis in this report would be on conformations of octameric water clusters. Octameric clusters observed in organic or inorganic-organic host structures exhibit conformations of cubane,[13a] opened cube,[13b] cyclic ring,[13c] book-shaped,[13d] crowned chair[13e,f] due to different environments imposed by the hosts. Of particular interest is the octameric cluster with hexameric core, which has received increased attention in recent years as the hexamer is believed to be the smallest possible unit that can show many properties of bulk water. Nauta *et al*.[15] have reported a less stable cyclic hexamer in liquid helium which is the building block of ice I_h[16] and is also relevant to liquid water.[17] Recently, Hong *et al*.[13i] reported a new type of octameric water cluster formed by a planar water tetramer and two dangling water dimers.

2.1.2: ***Scope of the study***

Strong noncovalent interactions viz., H-bonding and π-π interactions are prerequisite for the stability of functional supramolecular networks. Therefore, choice of molecular subunits is crucial whose structure and functions may be tuned using appropriate strategies with the help of crystal engineering. For this purpose, we have deliberately use $[Fe(CN)_6]^{3-}$ and protonated 4,4′-bipy (H-bipy) as donor and acceptor molecules for designing supramolecular host with focussing specific interactions on the channel core. Here we report synthesis and structural characterization of a supramolecular host $\{[Fe(CN)_6]\cdot(H\text{-}bipy)_3\cdot 8H_2O\}$ (**1**) with a unique octameric water cluster accomodated in the pore. The dehydrated form of **1** shows interesting selective gated adsorption properties with H_2O vapor compare to the other organic vapor.

2.1.3: *Experimental Section*

2.1.3.1: *Materials*

All the reagents and solvents employed were commercially available and used as supplied without further purification. $K_3[Fe(CN)_6]$ and 4,4′-bipyridyl were obtained from the Aldrich Chemical Co.

2.1.3.2: *Synthesis*

Synthesis of {(H-bipy)$_3$·[Fe(CN)$_6$]·8H$_2$O} (1): The cocrystal, **1** was synthesized according to the following procedure. $K_3[Fe(CN)_6]$, 1.0 mmol (0.329 g) was dissolved in 7 mL water in a beaker. In another beaker, 1.5 mmol (0.234 g) of 4,4′-bipyridyl was dissolved in 1.5 %(v/v) 7 mL HCl solution. Then both the solutions were mixed together and stirred until some yellow solid separated out. The reaction temperature was maintained around 10-15 °C. The solution was filtered and light yellow precipitate was discarded and filtrate was kept in open atmosphere for slow evaporation. After one day, yellow block shaped crystals of 1 were separated. The crystals are highly sensitive to open atmosphere and slowly loose single crystallinity. Good quality single crystals were picked up from the mother liquor and immediately covered with paraffin oil and crystal data was collected at 100 K. Yield: 77%, relative to Fe. Anal. Calcd for $C_{36}H_{43}FeN_{12}O_8$: C, 52.19; H, 5.19; N, 20.29. Found: C, 52.01; H, 5.32; N, 20.09. IR (KBr, cm^{-1}): νH_2O 3440, 3374; νAr(C-H) 3087, 3052; νCN 2117; νAr(C=C) 1618. IR spectrum of 1 shows two strong and sharp bands around 3375 and 3442 cm^{-1} suggesting the presence of water molecules (Fig. S1a). A strong band around 2117 cm^{-1} corroborate to ν(CN) stretching frequency and a band around 1618 cm^{-1} indicates the presence bipy molecule.

Preparation of {(H-bipy)$_3$·[Fe(CN)$_6$]} (1a): Compound **1** was placed in a glass sample cell and heated at 80 ºC for 5h under reduced pressure of 0.1 Pa that results **1a**. Removal of water molecules was confirmed by IR (Fig. 1a) and CHN analysis. Anal. Calcd for $C_{36}H_{27}FeN_{12}$: C, 63.26; H, 3.98; N, 24.59. Found: C, 62.61; H, 3.21; N, 23.89.

Preparation of {(H-bipy)$_3$·[Fe(CN)$_6$]} (1b): Compound **1** was placed in a glass sample cell and outgassed at room temperature for 20 h under reduced pressure of 0.1 Pa that results **1b**. Removal of water molecules was confirmed by IR (Fig. 1b) and CHN analysis. Anal. Calcd for $C_{36}H_{27}FeN_{12}$: C, 63.26; H, 3.98; N, 24.59. Found: C, 62.47; H, 3.33; N, 24.01.

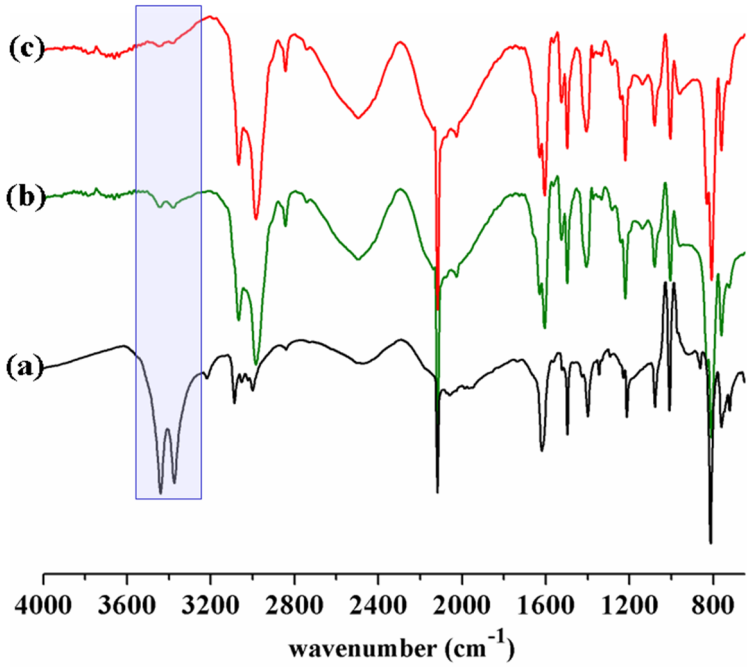

Fig. 1: IR spectra of compounds **1**(a), **1a** (c) and **1b** (b).

2.1.3.3: ***Physical Measurements***

The elemental analyses of each compounds and their different state were carried out on a Thermo Fisher Flash 2000 Elemental Analyser. Infra-red (IR) spectroscopic studies was carried out in the mid-IR region as KBr pellet (Bruker IFS-66v). Thermogravimetric analysis (TGA) was carried out (Metler Toledo) in nitrogen atmosphere (flow rate = 50 ml min^{-1}) in the temperature range 30 – 650 °C (heating rate = 2°C min^{-1}). Powder XRD pattern of the products were recorded by using Cu-K_α radiation (Bruker D8 Discover; 40 kV, 30 mA).

2.1.3.4: ***Single Crystal X-ray Diffraction***

A suitable yellow colour single crystal of compound **1** was mounted on a thin glass fibre with commercially available super glue. X-ray single crystal data was collected on a Bruker Smart-CCD diffractometer equipped with a normal focus, 2.4 kW sealed tube X-ray source with graphite monochromated Mo-*Kα* radiation (λ = 0.71073 Å) operating at 50 kV and 30 mA. The program SAINT was used for integration of diffraction profiles and absorption correction was made with SADABS program. The structure was solved by SIR 92[18] and refined by full matrix least square method using SHELXL.[19] All the hydrogen atoms were fixed by HFIX and placed in ideal positions. Potential solvent accessible area or void space was calculated using the PLATON[20] multipurpose crystallographic software. The coordinates, anisotropic displacement parameters and torsion angles for **1** is submitted as

supplementary information in CIF format. All crystallographic and structure refinement data of **1** are summarized in Table 1. Selected bond distances and angles are shown in Table S1. All calculations were carried out using SHELXL 97,[19] PLATON,[20] SHELXS 97[21] and WinGX system, Ver 1.70.01.[22]

The $[Fe(CN)_6]^{3-}$ part of the structure was easily solved with direct methods and Patterson method in both space groups *P*1 and *P*$\bar{1}$. Initial attempts to model the structure in the space group *P*$\bar{1}$ with Fe atom on the origin gave moderately good agreement with the diffraction data but attempts to use the resulting phases to generate a Fourier map gave an uninterpretable result and the refinement was not at all satisfactory. The structure was then modeled in the space group *P*1 and the phase extension agreed well with the diffraction data with the appearance chemically feasible structure. During refinement, we observed that ADDSYM detects a pseudo center of symmetry. A closer look into the refinement of data for compound **1** revealed a Flack parameter of ~0.26. We assigned the additional apparent pseudo-symmetry to be due to the presence of highly symmetrical $[Fe(CN)_6]^{3-}$ moiety coupled with the existence of twinning. Further a transformation of coordinates of *P*1 to *P*$\bar{1}$ gives chemically unfeasible structure. All the reasons unequivocally establish the space group as *P*1. Therefore, the ADDSYM message can be regarded as harmless.

2.1.3.5: ***Adsorption Study***

CO_2 adsorption-desorption isotherms of **1** was measured at 195 K with the dehydrated sample of **1** (**1a**) prepared at 353 K under high vacuum in QUANTACHROME AUTOSORB-1C analyser. The adsorption of different solvents like MeOH at 293K and H_2O, EtOH, CH_3CN at 298 K were measured in the vapour state by using BELSORP-aqua3 analyser. In all the measurements, in the sample tube adsorbent sample (~100 –150 mg) was placed which was prepared at 353 K for about 5 hours (sample **1a**) or at RT for 20 hours (sample **1b**) under vacuum prior to measurement of the isotherms. The different solvent molecules used to generate the vapour were degassed fully by repeated evacuation. Dead volume was measured with helium gas. The adsorbate was placed into the sample tube, then the change of pressure was monitored and the degree of adsorption was determined by the decrease in pressure at the equilibrium state. All operations were computer controlled and automatic.

2.1.4: ***Results and Discussion***

2.1.4.1: ***Crystal Structure Description of 1***

Compound **1** crystallizes in triclinic system with *P*1 space group. The asymmetric unit consists of one molecule of $[Fe(CN)_6]^{3-}$, three protonated 4,4′-bipyridyl (H-bipy) linkers and eight lattice water molecules (Fig. 2). Fe(III) in **1** locates itself in a distorted octahedral geometry with six coordination furnished by six cyanide ligands. Distortion from perfect octahedral geometry is reflected in *cisoid* (87.5(3)-92.3(3)º) and *transoid* (178.4(6)-179.8(8)º) angles. Fe-C bond lengths are fairly uniform and it ranges from 1.921(9)-1.955(7) Å. C-N bond length in cyanide ligand ranges from 1.132(9)-1.180(9) Å.

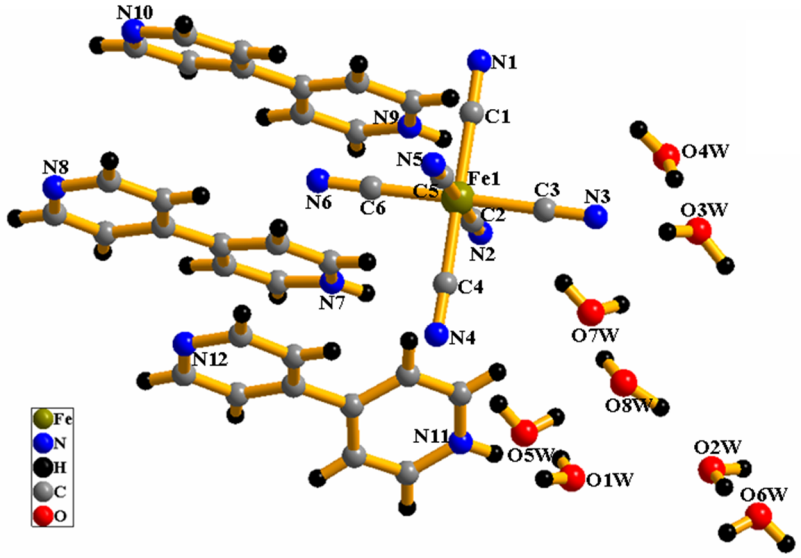

Fig. 2: View of the asymmetric unit of supramolecular host **1** shows one molecule of $[Fe(CN)_6]^{3-}$, three protonated bipy molecule and eight lattice water molecules.

Each singly protonated bipy molecules form a linear chain through N···H–N hydrogen bonding interaction (2.692(10) – 2.707(8) Å) in *a* direction. Three independent chains are associated through π-π interactions (cg···cg distances are in the range of 3.795(4) – 5.425(4) Å) to form a 2D corrugated sheet lying in the crystallographic *ab* plane (Fig. 3). The most interesting structural aspect of **1** is the presence of an octameric water cluster where the eight lattice water molecules assembled through hydrogen bonding interactions (2.692(8) – 2.750(9) Å) (Fig. 4a).The structure of the water cluster is very fascinating and is similar to a e,e-1,4- substituted cyclohexane molecule where six water molecules are positioned on the vertices of the cyclohexane ring and the seventh and eighth occupy the

1,4-equatorial positions of the ring. Each octameric water cluster is connected to four nearest $[Fe(CN)_6]^{3-}$ moiety through O–H···N hydrogen bonding (2.802(8) – 2.977(8) Å) between O-atom of water molecules and N-atom of cyanide ligands to form a sheet like structure (Fig. 4b). Further hydrogen bonding between water clusters and cyanide ligands in *a* and *b* directions extend the 2D sheet in the *ab* plane.

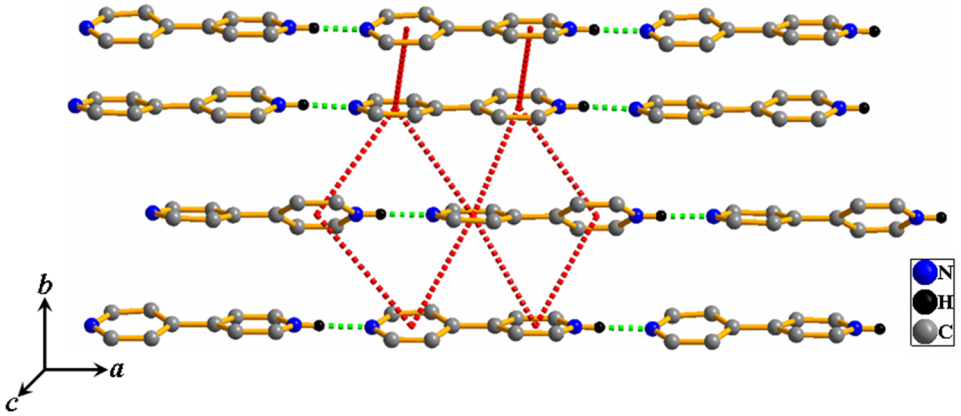

Fig. 3: View of the 2D sheet formed by N-H···N H-bonding (green dashed lines) and π-π interactions (red dashed lines) between the ring centroids of H-bipy cations.

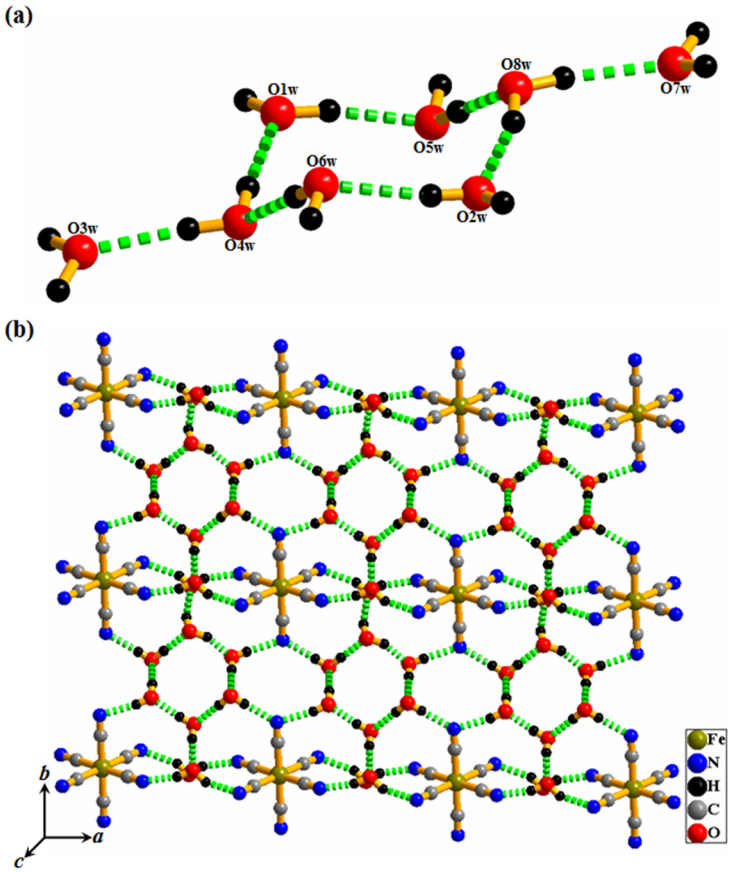

Fig. 4: (a) View of the 1,4-substituted chair conformer of octameric water cluster in **1**. (b) Figure shows each water cluster is in close contact with four neighboring $[Fe(CN)_6]^{3-}$ anions by hetero-molecular O-H···N H-bonding to form a extended sheet like structure.

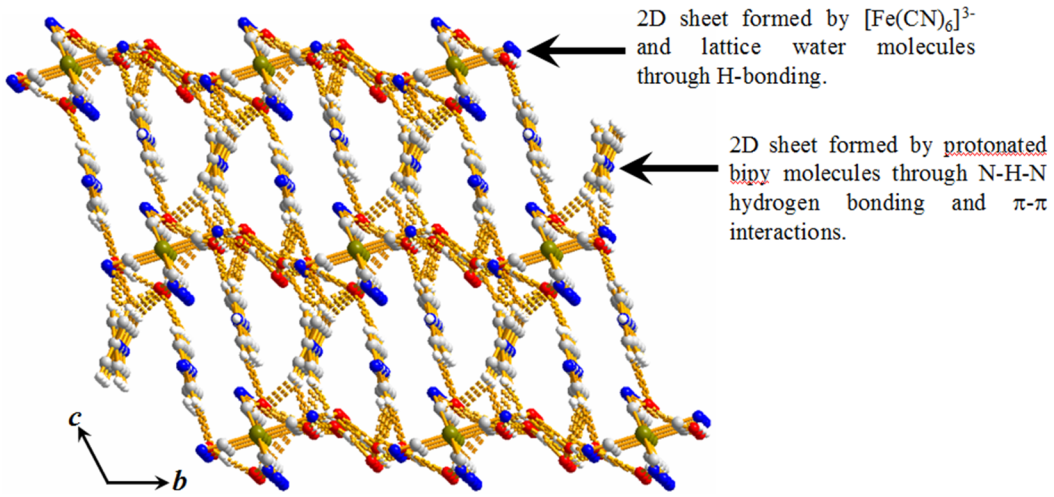

Fig. 5: Figure shows the ABAB type stacking of 2D sheets in host network **1**.

The H-bipy corrugated sheets and the 2D sheets formed by $[Fe(CN)_6]^{3-}$ and water clusters stack in AB fashion along *c* direction (Fig. S4). C–H···N and C–H···O hydrogen bonding between these 2D sheets results a 3D supramolecular host with six-sided voids along *b* direction occupied by lattice water molecules (Fig. 6 and 7).

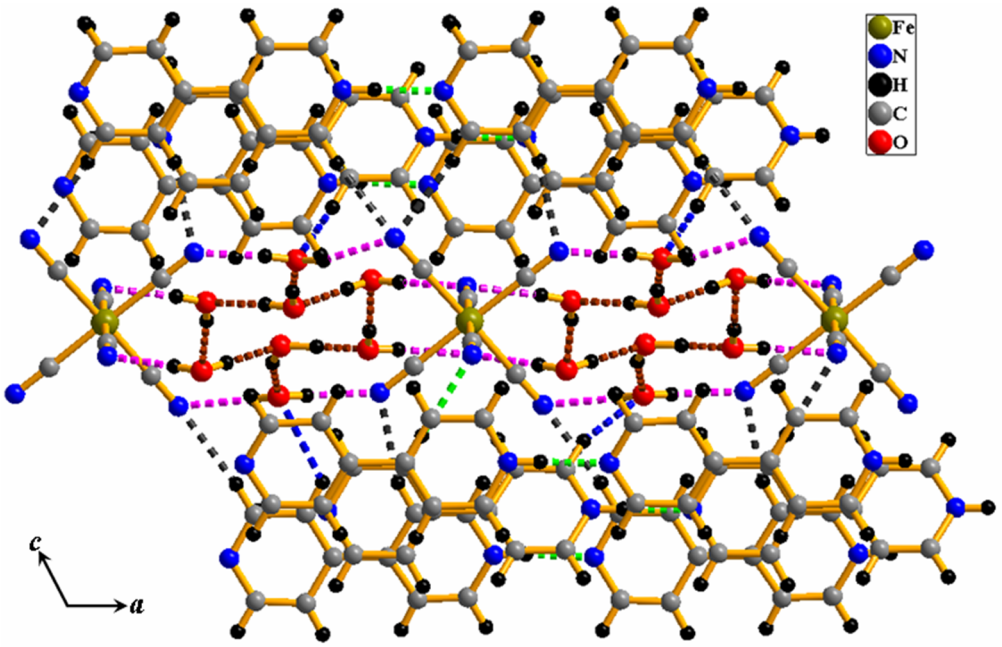

Fig. 6: 3D supramolecular host **1** generated by H-bonding and π-π interactions with the channels occupied by lattice water molecules. H-bonding specification (dashed lines): brown, O-H···O; pink, O-H···N; green, N-H···N; blue, C-H···O; C-H···N, grey.

The dimension of the channels is about 4.6 x 2 $Å^2$, calculated considering the van der Walls radii of the atoms. The void volume of the host calculated by PLATON[20] after removal of the lattice water molecules is about 22.2% to the total unit cell volume.

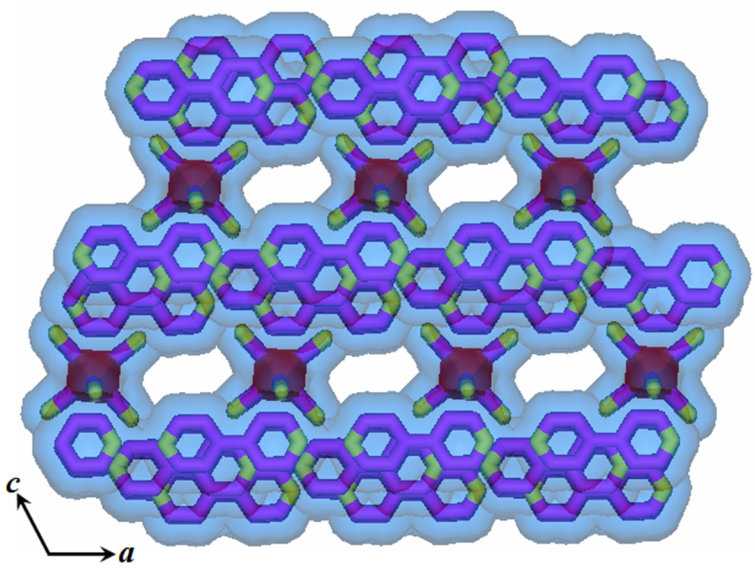

Fig. 7: Surface stick view of supramolecular host **1** after removal of water molecules showing 1D channels of 4.6 x 2 Å along crystallographic *b* direction.

2.1.4.2: ***Water cluster conformation***

Six lattice water molecules O1W, O2W, O4W, O5W, O6W and O8W attain chair conformation of cyclohexane by cooperative H-bonding to form a hexameric core. The remaining two molecules O3W and O7W are crowned at 1,4-equatorial positions of the cyclohexane ring to form a discrete octameric water cluster with S_2 symmetry. A schematic diagarm showing the conformations of different water octamers with their corresponding energies is given in Fig. 8.

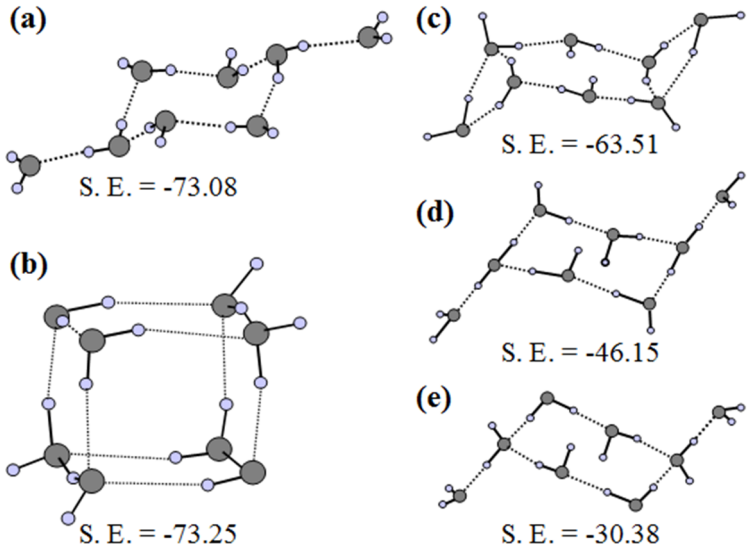

Fig. 8: Comparison of the stabilization energies of various octamers (S. E. is stabilization energy in kcal/mol). Conformer 'a' is presented in this report and its energy calculation is mentioned in the text. Energy calculations for the conformers 'b-e' can be found in reference 13f.

Table 1: Crystal data and structure refinement parameters for **1**.

Parameters	**1**
Empirical formula	$C_{36}H_{43}FeN_{12}O_8$
M	827.67
Crystal system	Triclinic
Space group	*P*1 (No. 1)
a (Å)	9.7496(10)
b (Å)	10.3079(5)
c (Å)	11.9451(6)
α (°)	114.920(2)
β (°)	110.933(4)
γ (°)	91.374(3)
V(Å^3)	995.02(13)
Z	1
T (K)	100
λ (Mo-K$_\alpha$)	0.71073
D_c (g cm^{-3})	1.381
μ (mm^{-1})	0.445
θ_{max} (°)	25.1
Total data	14096
Data [$I>2\sigma(I)$]	5346
R^a	0.0493
$R_W{}^b$	0.1028
GOF	1.01
Flack (x)	0.26(2)

$^a R = \sum||Fo|-|Fc||/\sum|Fo|$; $^b R_w = [\sum\{w(Fo^2-Fc^2)^2\}/\sum\{w(Fo^2)^2\}]^{1/2}$

The host lattice plays a crucial role in determining the conformation of the water cluster. A good comparison can be made with the octameric water cluster found in host **1** to that reported by Rajsekharan et al.[13f] Both the clusters have hexameric core, however, 1,4-

substitution in the water cluster reported by Rajsekharan *et al.* is axial type instead of equatorial as found in **1**, and for good reasons. They showed that the 1,4-axially substituted water molecules are involved in hydrogen bonding with carboxylate oxygens of the dipicolinate ligand. The 1,4-equatorial positioning of the water molecules will miss these hydrogen bonding interactions and hence, favours the axial conformation. In case of host **1**, the 1,4-equatorially substituted water molecules are involved in hydrogen bonding with the cyanide groups of $[Fe(CN)_6]^{3-}$ moiety. On the other hand, 1,4-axial positioning of these water molecules would be lacking such hydrogen bonding interactions and hence favours the more stable equatorial conformation. The average O-O distance in the cluster is 2.733 Å at 100 K as determined from X-ray crystallography. The corresponding value in Ice–I_h at 183 K is 2.759 Å. On the basis of the accuracy of the water structure as well as the proper hydrogen-bond donor-acceptor matching, the indicated positions of the hydrogen atoms are believed to be correct. The H-bonding saturation inside the hexameric core is not reached, and therefore further stabilization of the cluster results from the O-H···N H-bonding assisted by the presence of CN groups in $[Fe(CN)_6]^{3-}$ anions.

2.1.4.3: ***Stability of the water cluster***

Studies based on isomeric water clusters isolated in different host led us to compute the effect of spatial confinement on the properties of the water cluster, its stabilization due to the confinement by ranking in energy and the complementarity relationship. Hence, for a quantitative understanding about the stability of the water cluster, we performed ab initio geometry optimization of the H-atom positions with 6-31++G(d,p) basis set by freezing the positions of the heavy oxygen atoms. The corrected stabilization energy of the water cluster was found to be –73.08 kcal/mol and the value is almost equal to the cubic conformer (–73.25 kcal/mol, higher than the axial conformer) which is reported as the most stable one (Fig. 3).[13f] Corrected stabilization energy includes the basis set superposition error (BSSE) and has been defined as $E_{int}=\{(E_{water\text{-}n\text{-}mer} + BSSE_{water\text{-}n\text{-}mer}) - (n*E_{water})\}$. The optimized configuration of $(H_2O)_8$ cluster with the conformation of *e,e*–1,4–substituted cyclohexane is shown in Fig. S6 and is found to be similar as observed in compound **1**, suggesting *e,e*-1,4-substituted cyclohexane chair conformation is the most stable with the resemblence of organic molecules.

2.1.4.4: *TGA and PXRD analysis*

Thermogravimetric analysis (TGA) and powder X–ray diffraction (PXRD) measurement were carried out to study the stability of the supramolecular framework (Fig. S7 and 4). TGA measurement suggests weight loss of 9.96 wt% in the temperature range of 40-80 °C which is less than eight lattice water molecules (20 wt%) occupied in the channels. The inconsistency of TGA can be correlated with the release of some lattice water molecules at room temperature. We observed that **1** looses single crystallinity slowly after taking out the crystals from mother liquor. The dehydrated compound is stable up to 200 °C without further weight loss; after that framework decomposes to unidentified product.

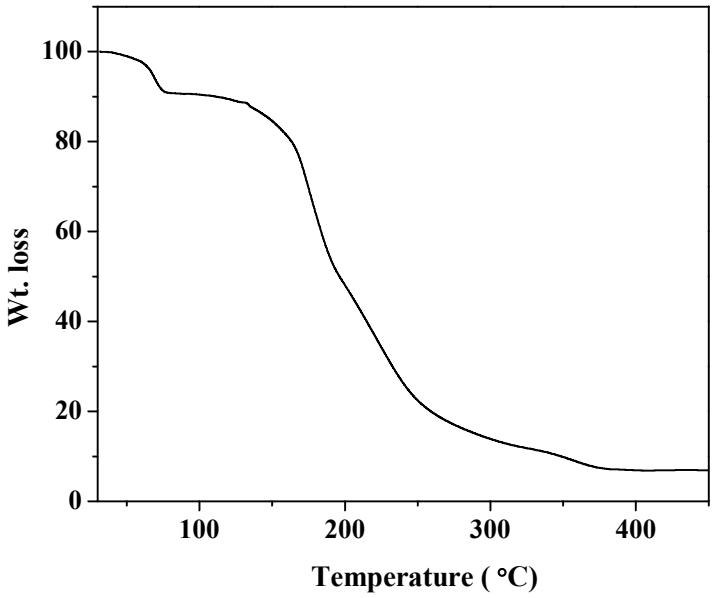

Fig. 9: TGA curve of **1** in the temperature range 30 – 450 °C (Heating rate 5 °C/min under nitrogen).

The PXRD pattern of **1a** shows drastic change with shifting of peaks and also appearance of some new peaks after removal of water molecules. However, we were able to index the pattern using the program TREOR that suggest a monoclinic crystal system with unit cell parameters, a = 18.5208 Å, b = 7.3948 Å, c = 16.8450 Å and β = 110.622 º. A change in crystal system from triclinic to monoclinic together with noticeable changes in cell parameter suggest significant structural transformation upon removal of water molecules from **1**.

The PXRD pattern of **1b** (Fig. 11) also shows difference in peak positions suggesting structural transformation upon removal of water molecules. The PXRD patterns of water vapor exposed smaples of **1a** (Fig. 4) and **1b** do not match well with **1**, suggesting structure is not completely reversible upon rehydration.

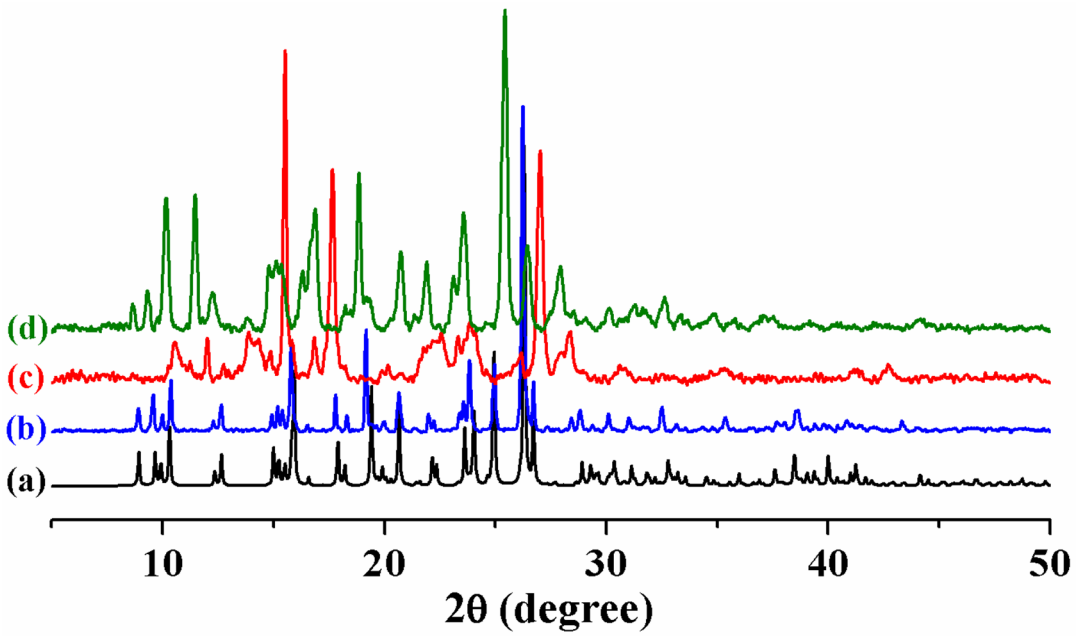

Fig. 10: PXRD patterns of **1** in different state: (a) simulation based on single crystal X-ray analysis, (b) assynthesized, (c) dehydrated at 80 °C, and (d) exposed to the water vapor for three days.

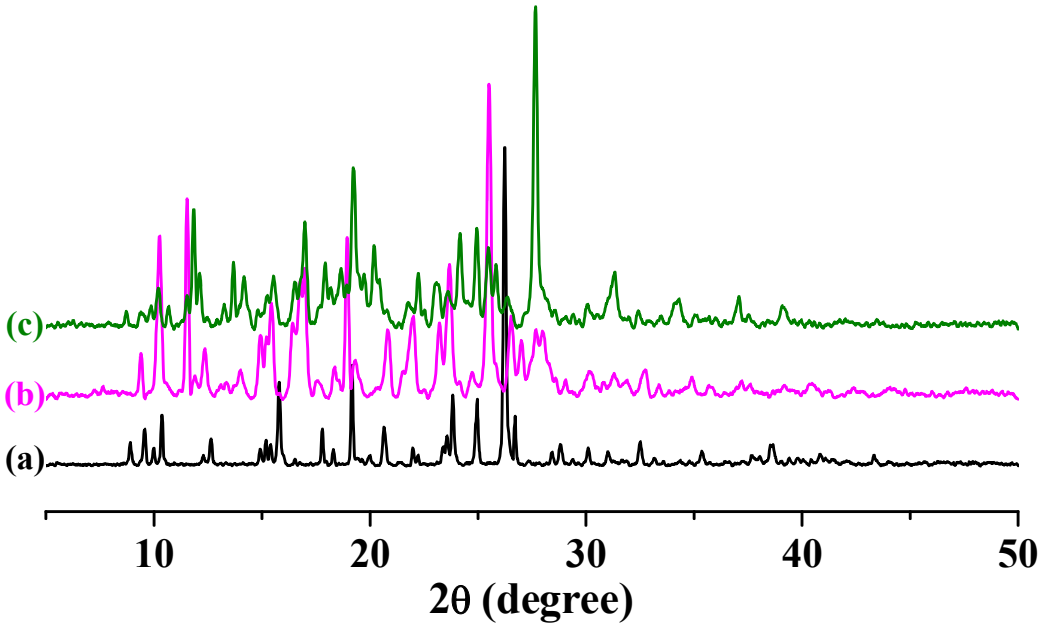

Fig. 11: PXRD patterns of **1** in different state: (a) assynthesized **1**, (b) outgassed at RT for 20h, **1b** and (c) exposed to the water vapor for three days.

Elemental analyses suggest that water vapour exposed samples of **1a** and **1b** can hold ~6 and ~7 number of water molecules, respectively. The host **1**, **1a** and **1b** dissolves when directly poured in water at RT.

2.1.4.5: ***Adsorption Property***

The presence of lattice water molecules in the supramolecular framework of **1** propelled to carry out adsorption study with dehydrated samples of **1**. CO_2 adsorption (kinetic diameter, 3.4 Å) study at 195 K reveals no uptake indicating nonporous nature of **1a** (Fig. S9). This may be due to the smaller channel size compare to kinetic diameter of CO_2. However, interesting results were obtained with solvent vapor adsorption study.

Multistep isotherm was obtained with H_2O adsorption experiment at 298 K as shown in Fig. 12.The adsorption isotherm of **1a** reveals, initially at low P/P_0 it is difficult for the H_2O molecules to get adsorbed and hence up to P/P_0 ~0.55 the uptake is only about 32 mLg^{-1}. Then there is a sudden adsorption jump at P/P_0~0.62 and the uptake volume reaches to about 120 mLg^{-1}. This steep uptake suggests a kind of gate opening at P/P_0~0.55 because of structural transformation upon dehydration which blocks the H_2O molecules at low pressure. Once the gate opens, adsorption gradually increases with pressure and ends without saturation with net adsorption amount of 189 mLg^{-1} at P/P_0~1.

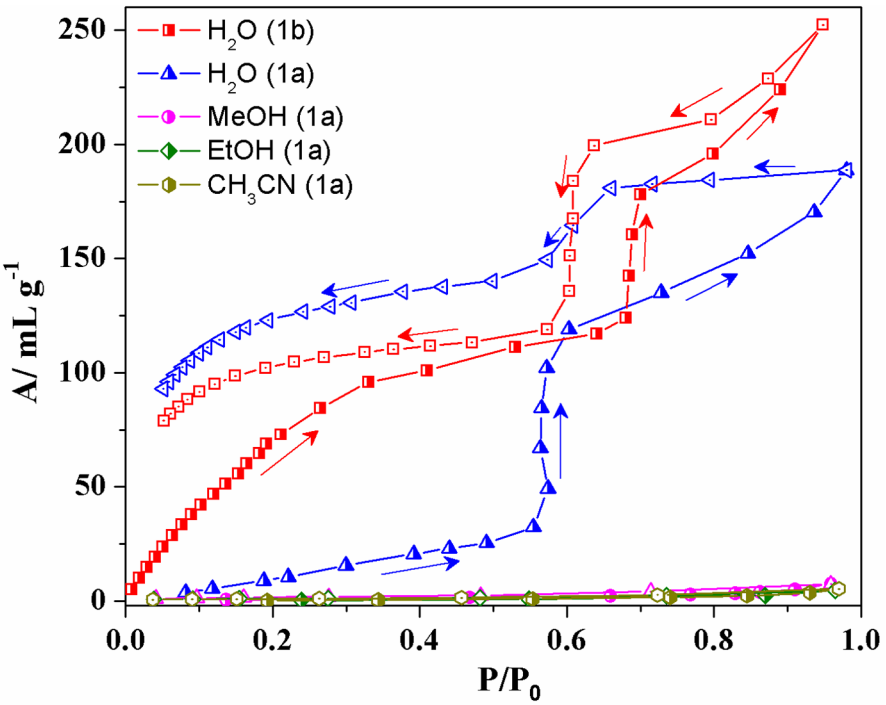

Fig. 12: Solvent vapor adsorption isotherms of **1a** and **1b**; H_2O (blue, **1a** and red, **1b**), EtOH, CH_3CN at 298 K and MeOH at 293 K, shows selective adsorption of H_2O vapor over organic solvents.

Interestingly, desorption also occurs in a stepwise fashion and exhibits large hysteresis. The desorption isotherm does not retrace the adsorption one; instead it shows abrupt

decrease at P/P_0~0.66 to reach P/P_0~0.57 and then decreases gradually. Therefore certain adsorption jump with gate opening phenomenon and desorption drops suggest structural transformation with pore opening at some threshold pressure. This type of phenomena is well documented for flexible metal-organic coordination frameworks.[23] However, to the best of our knowledge, such stepwise adsorption in supramolecular host composing of two discrete molecular entities is yet to be reported. Calculation using the final adsorption amount suggests that only 5.6 molecules of H_2O are occluded into the host **1a**, less than the assynthesized compound **1**, which is also reflected from unsaturated adsorption profile at P/P_0~1. Realising significant structural transformation upon dehydration at 80 ºC from PXRD and closed structure of **1a** from adsorption studies, we decided to outgass the sample of **1** at room tempearture under vacuum and then check the H_2O adsorption property. The removal of H_2O molecules at RT under vacuum in the outgassed sample (**1b**) has been confirmed by IR and elemental analysis. Surprisingly, the H_2O adsorption of **1b** also shows stepwise profile but different than **1a** (Fig. 5). Unlike **1a**, **1b** allows the H_2O molecules to diffuse through it even at low P/P_0. The profile of **1b** shows gradual uptake of H_2O molecules up to P/P_0 ~ 0.7 and then there is a sudden adsorption jump and finally reaches to maximum uptake volume of 252 mL/g at P/P_0~1. This indictes that even at room temperature the removal of H_2O molecules led to the shrinkage in the host structure that completely opens up at P/P_0~0.7. It is worth mentioning that, H_2O uptake at P/P_0~0.55 for **1a** and **1b** differs significantly and corresponding values are 32 mL/g for **1a** and 113 mL/g for **1b**. Higher H_2O uptake of **1b** at low pressures indicate that structure of **1b** is more open than **1a**. Calculation using the final adsorption amount suggests that total 7.7 molecules of H_2O invade into the host **1b**. Similar to **1a**, desorption occurs in a stepwise fashion and at the end of the adsorption process **1b** holds ~2.4 number of water molecules. The value of βE_0, which reflects adsorbate-adsorbent affinity, is about 4.29 kJ/mol for **1a** and and 5.43 kJ/mol for **1b**, suggests that the later has stronger hydrophilicity than **1a**. The number of H_2O molecules adsorbed per formula unit, by **1a** and **1b,** are in good agreement with elemental analysis of H_2O vapour exposed samples and adsorption experiments. MeOH (293 K), CH_3CN (298 K), and EtOH (298 K) adsorption studies of **1a** suggest only surface adsorption as revealed by their type-II adsorption properties. The size of these adsobates is larger than the pore size, correlating the non inclusion of such organic vapors in **1a**.

2.1.5: ***Conclusion***

In conclusion, we have shown a recipe for the fabrication of an unprecedented flexible supramolecular host that shows stepwise sorption property by exploiting simple molecular building units, $[Fe(CN)_6]^{3-}$ and protonated 4,4′-bipy. $[Fe(CN)_6]^{3-}$ acts as an acceptor in three dimension, whereas H_2O as a donor with charge neutralization by H-bipy. The supramolecular host is stabilized by a novel octameric water cluster that have stable chair conformation with two water molecules at 1,4-equatorial positions. This type of flexible supramolecular host stabilized by non-covalent interaction that accomodates specific molecules selectively would be useful for separation technique.

2.1.6: ***References:***

1. P. J. Langley, J. M. Rawson, J. N. B. Smith, M. Schuler, R. Bachmann, A. Schweiger, F. Palacio, G. Antorrena, G. Gescheidt, A. Quintel, P. Rechsteiner and J. Hulliger, *J. Mater. Chem.*, **1999**, *9*, 1431.
2. M. E. Brown and M. D. Hollingsworth, *Nature,* **1995**, *376*, 323.
3. V. Ramamurthy and D. F. Eaton, *Chem. Mater.*, **1994**, *6*, 1128.
4. F. Toda, S. Hyoda, K. Okada and K. Hirotsu, *J. Chem. Soc., Chem. Commun*., **1995**, 1531.
5. K. Endo, T. Koike, T. Sawaki, O. Hayashida, H. Masuda and Y. Aoyama, *J. Am. Chem. Soc*., **1997**, *119*, 4117.
6. (*a*) C. L. Chen and A. M. Beatty, *J. Am. Chem. Soc.*, **2008**, *130***,** 17222; (*b*) M. B. Dewal, M. W. Lufaso, A. D. Hughes, S. A. Samuel, P. Pellechia and L. S. Shimizu, *Chem. Mater.,* **2006**, *18*, 4855; (*c*) S. A. Dalrymple and G. K. H. Shimizu, *Chem. Commun.,* **2006**, 956.
7. (*a*) T. Friščić, A. V. Trask, W. D. S. Motherwell and W. Jones, *Cryst*. *Growth Des*. **2008**, *8*, 1605; (*b*) G. J. Halder, C. J. Kepert, B. Moubaraki, K. S. Murray and J. D. Cashion, *Science,* **2002**, *298*, 1762.
8. (*a*) R. Ludwig, *Angew. Chem., Int. Ed*., **2001**, *40*, 1808; (*b*) D. Eisenberg and W. Kauzmann, *The Structure and Properties of Water,* Oxford University Press, Oxford, 1969.
9. (*a*) K. Mitsuoka, K. Murata, T. Walz, T. Hirai, P. Agre, J. B. Heymann, A. Engel and Y. *J.* Fujiyoshi, *Struct. Biol*., 1999, **128**, 34; (*b*) E. Tajkhorshid, P. Nollert, M .Ø. Jensen, L. J. W. Miercke, J. O'Connell, R. M. Stroud and K. Schulten, *Nature*, **2002**, **296**, 525.
10. (*a*) M. Yoshizawa, T. Kusukawa, M. Kawano, T. Ohhara, I. Tanaka, K. Kurihara, N. Nimura and M. Fujita, *J. Am. Chem. Soc.*, **2005**, *127***,** 2798; (*b*) B. Sreenivasulu and J. Vittal, *Angew. Chem. Int. Ed*., **2004**, *43***,** 5769; (*c*) B. Q. Ma, H. L. Sun and S. Gao, *Angew. Chem., Int. Ed.*, **2004**, *43*, 1374; (*d*) C. Biswas, M. G. B. Drew and A. Ghosh, *Inorg. Chem.*, **2008**, *47***,** 4513; (*e*) M. T. Ng, T. C. Deivaraj, W. T. Klooster, G. J. McIntyre and J. J. Vittal, *Chem. Eur. J.*, **2004**, *10***,** 5853; (*f*) K. V. Katti, P. K. Bharadwaj, J. J. Vittal and R. Kannan, *Synthesis and Reactivity in Inorganic, Metal-Organic and Nano-Metal Chemistry* **2008**, *38*, 1.

11. Dodecameric Cluster: (*a*) S. K. Ghosh and P. K. Bharadwaj, *Angew. Chem., Int. Ed.*, **2004**, *43*, 3577; (*b)* S. Neogi, G. Savitha and P. K. Bharadwaj, *Inorg. Chem*., **2004**, *43***,** 3771; (*c*) S. Nishikiori and T. Iwamoto, *Chem. Commun.,* **1993**, 1555.
12. Decamer: (*a*) L. J. Barbour, G. W. Orr and J. L. Atwood, *Nature,* **1998**, *393*, 671; (*b*) A. Michaelides, S. Skoulika, E. G. Bakalbassis and J. Mrozinski, *Cryst. Growth Des.*, **2003**, *3*, 487; (*c*) R. D. Bergougnant, A. Y. Robin and K. M. Fromm, *Cryst. Growth Des*., **2005**, *5*, 1691.
13. Octamer: (*a*) W. B. Blanton, S. W. Gordon-Wylie, G. R. Clark, K. D. Jordan, J. T. Wood, U. Geiser and T. J. Collins, *J. Am. Chem. Soc.*, **1999**, *121***,** 3551; (*b*) R. J. Doedens, E. Yohannes and M. I. Khan, *Chem. Commun.*, **2002**, *62*; (*c*) J. L. Atwood, L. J. Barbour, T. J. Ness, C. L. Raston and P. L. Raston, *J. Am. Chem. Soc.,* **2001**, *123*, 7192; (*d*) B. –Q. Ma, H. –L. Sun and S. Gao, *Chem. Commun*., **2005**, 2336; (*e*) S. K. Ghosh and P. K. Bharadwaj, *Inorg. Chim. Acta*, **2006**, *359*, 1685; (*f*) T. K. Prasad and M. V. Rajasekharan, *Cryst. Growth Des.*, **2006,** *6,* 488; (*g*) D. Li, Y. Wang, X. Luan, P. Liu, C. Zhou, H. Ma, and Q. Shi, *Eur. J. Inorg. Chem.*, **2005**, 2678; (*h*) S. Das and P. K. Bharadwaj, *Cryst. Growth Des.,* **2006**, *6,* 187; (*i*) W. Wei, F. Jiang, M. Wua, Q. Gao, Q. Zhang, C. Yan, L. Ning and M. Hong, *Inorg. Chem. Commun.*, **2009**, *12*, 290. (*j*) J. –Y. Wua, J. –F. Yin, T. –W. Tseng and L. -L. Kuang, *Inorg. Chem. Commun.*, **2008**, *11*, 314; (*k*) S. K. Ghosh and Bharadwaj, *Eur. J. Inorg. Chem.*, **2005**, 4886.
14. Hexamer: (*a*) R. Custecean, C. Afloroaei, M. Vlassa and M. Polverejan, *Angew. Chem., Int. Ed.,* **2000**, *39*, 3094; (*b*) B. -Q. Ma, H. -L. Sun and S. Gao, *Chem. Commun.,* **2005**, 2336; (*c*) B. -H. Ye, B. -B. Ding, Y. -Q. Weng and X. -M. Chen, *Inorg. Chem.,* **2004**, *43*, 6866; (*d*) K. M. Park, R. Kuroda and T. Iwamoto, *Angew. Chem., Int. Ed.,* **1993**, *32*, 884; (*e*) J. N. Moorthy, R. Natarajan and P. Venugopalan, *Angew. Chem., Int. Ed*., **2002**, *41*, 3417; (*f*) K. -M. Park, R. Kuroda and T. Iwamoto, *Angew. Chem., Int. Ed. Engl.*, **1993**, *32*, 884; (*g*) U. Mukhopadhyay and I. Bernal, *Cryst. Growth Des.*, **2005**, *5*, 1687; (*h*) Y. -C. Liao, Y. -C. Jiang and S. -L. Wang, *J. Am. Chem. Soc.*, **2005**, *127***,** 12794; (*i*) Y. -P. Ren, L. -S. Long, B. -W. Mao, Y. -Z. Yuan, R. -B. Huang and L. -S. Zheng, *Angew. Chem., Int. Ed.*, **2003**, *42*, 532; (*j*) S. K. Ghosh and P. K. Bharadwaj, *Inorg. Chem.,* **2003**, *42***,** 8250; (*k*) X. -M. Zhang, R. -Q.; Fang and H. -S. Wu, *Cryst. Growth Des.,* **2005**, *5,* 1335.
15. K. Nauta and R. E. Miller, *Science,* **2000**, *287*, 293.

16. D. Eisenberg and W. Kauzmann, *The Structure and Properties of Water,* Oxford university Press, Oxford, **1969**.
17. (*a*) R. J. Speedy, J. D. Madura and W. L. Jorgensen, *J. Chem. Phys.,* **1987**, *91*, 909; (*b*) A. C. Belch and S. A. Rice, *J. Chem. Phys*., **1987**, *86*, 5676.
18. A. Altomare, G. Cascarano, C. Giacovazzo and A. Gualaradi, *J. Appl. Cryst.* **1993**, *26*, 343.
19. G. M. Sheldrick, SHELXL 97 Program for the Solution of Crystal Structure, University of Göttingen, Germany, **1997**.
20. A. L. Spek, *J. Appl. Cryst.* **2003**, *36*, 7.
21. G. M. Sheldrick, SHELXS 97, Program for the Solution of Crystal Structure, University of Göttingen, Germany, **1997**.
22. L. J. Farrugia, WinGX - A Windows Program for Crystal Structure Analysis. *J. Appl. Crystallogr.* **1999**, *32*, 837.
23. (*a*) T. K. Maji, G. Mostafa, R. Matsuda and S. Kitagawa, *J. Am. Chem. Soc.,* **2005**, *127*, 17152; (*b*) T. K. Maji, K. Uemura, H. C. Chang, R. Matsuda and S. Kitagawa, *Angew. Chem. Int. Ed.*, **2004**, *43*, 3269.

Part-B

Soft Supramolecular Porous Framework: Supramolecular Isomerism and Effect of External Stimuli on Structural Transformation and Adsorption Properties

Abstract:

Three novel supramolecular hosts $\{(H_2\text{-bpee})_2[Fe(CN)_6]\cdot 5H_2O\}$ (**1**), $\{[(H_2\text{-bpee})(H\text{-bpee})][Fe(CN)_6]\}\cdot 4(H_2O)$ (**2**) and $\{[2(H\text{-bpee})\cdot H_3O][Fe(CN)_6]\}.4(H_2O)$ (**3**) (bpee = 1,2-bis(4-pyridyl)ethylene) were obtained by the reaction of 1,2-bis(4-pyridyl)ethylene (bpee), $K_4[Fe(CN)_6]$ (**1**), and 1,2-bis(4-pyridyl)ethylene (bpee), $K_3[Fe(CN)_6]$ (**2** and **3**). The supramolecular structures were constructed by non-covalent interaction *viz*. hydrogen bonding, π···π interaction. These host networks of **1**, **2** and **3** undergo a structural transformation when they are heated at 100 ºC under vacuum. Interesting stepwise vapour adsorption property was observed when they are evacuated under vacuum at room temperature. They completely exclude any gas molecule e.g. N_2, CO_2, H_2.

2.2.1: *Introduction*

The potential application of co-crystals including the generation of novel nonlinear optical materials,[1] synthesis of new supramolecular compounds,[2] homogeneous and heterogeneous separation,[3] host-guest chemistry[4] drags the immense interest of the scientist in the recent years. Parallelly these types of compounds (molecular compounds or inclusion compounds) have immediate importance because of their broad application in the field of magnetism,[5] ferroelasticity,[6] nonlinear optical effect,[7] chemical storage,[8] catalysis[9] and adsorption. Co-crystals are class of natural complexes where two or more components are bonded by non-covalent, non-ionic intermolecular interactions, with the proton remaining on the acidic constituent. The process of co-crystallization is governed by molecular recognition and self-assembly, rather than formation and deformation of covalent bonds, which are capable of meliorating pharmaceutical formulation.[10] However, here we have focused on the non-covalent synthesis of a series of new co-crystals applying host-guest molecular recognition which provides a greater degree of flexibility in term of guest accommodation.[11] Such type of network having soft interaction is suitable for depicting switching properties and reversible changes from an absorbing state to a close packed inactive polymorph and can be activated by thermal, mechanical, or radioactive stimuli[12]. Such soft materials demonstrate a good impact in the arena of drug delivery, vapour adsorption and gust selectivity.

Recently polymorphism and supramolecular isomerism have received increasing attention, since they can provide useful information on the factors that governs molecular self-assembly process as well as structure-property relationship in crystalline materials. Supramolecular isomerism is important for the better understanding of supramolecular synthons and corresponding chemical and physical properties. Supramolecular isomerism shows different magnetic optical properties depending on the different crystal packing. However different porous functionality in supramolecular isomerism is yet to be explored. Strong non-covalent interactions are prerequisite for the stability of functional supramolecular networks. Therefore building units (i.e. donor and accepter for H-bonding interaction) are vital whose structure and functions may be tuned by control over the synthetic route and crystallization condition such as concentration gradients, pH solvent, temperature etc. Here we have exploited the acceptor property of hexacyanometallate $[Fe(CN)_6]^{3-}$/$[Fe(CN)_6]^{4-}$ which is well studied in fabricating molecular based magnet. This type of metalloligands provides accepter site in three dimensions and linked with donor like protonated 1,2-bis (4-pyridyl) ethane (H-

bpee) or protonated 4,4′-bipy (H-bipy) which provides a greater flexibility in fabricating 3D supramolecular frameworks.

The fundamental physical and chemical properties of a crystalline solid solely depend on the identity of constituents and as well as also on their arrangements. Those are called crystalline solids where the arrangement of component atoms, molecules, or ions are regularly ordered and repeated in three dimensions. So it is quite possible for a single constituent to show the ability to exist in different arrangements[13]. This phenomenon in single-component organic crystal is called polymorphism and currently the subject of both experimental[14] and theoretical interests.[15] Polymorphism can be applied to organic compounds where it exhibited only in solid state i.e. the polymorphic structure can be spifflicated upon vaporization, melting or dissolution.[16] The reason is that relatively weak forces i.e. H-bonding, ionic interaction, and van der Waals attraction which hold the crystal, disrupted by the energy needed for melting, vaporization, or dissolution. In spite of that, researchers are interested to study the co-crystal growth strategies such as solid-state grinding,[17] sonication,[18] evaporation[19] and melting.[20] Hence organic polymorphism has some boundaries making it a unique domain of study.

2.2.2: ***Scope of the study***

Soft porous frameworks are bistable or multistable crystalline materials which exibits reversible transformability between the states and permanent porosity. These highly ordered networks show structural transformability by external stimuli in particular temperature, light, pressure etc. Moreover, extended networks sustained solely by non-covalent interactions (viz. H-bonding, π–π interactions), exhibits greater degree of softness and structural flexibility resulting in guest responsive fitting, framework breathing, guest induced structural asymmetry. Such soft networks composed of non-covalent interactions are often amenable to different state depending upon the strength of the external stimuli. Drastic change in structure may results from extreme condition whereas such change is avoidable in comparatively gentle condition.

To get hold of optimized condition for co-crystallization process, we must carry out several techniques with varying conditions as the success of co-crystallization is hardly predictable[21].

In the present work, with the help of crystal engineering, we have purposely chosen systems where the primary intermolecular attraction is based on hydrogen bonding and π···π interaction[22]. For this, we have deliberately used $[Fe(CN)_6]^{4-}$, $[Fe(CN)_6]^{3-}$ as donor and protonated 1,2-bis(4-pyridyl)ethylene (bpee) as accepter for designing supramolecular host with focussing specific interactions on the channel core. Here we are reporting the synthesis, structural characterization and interesting solvent vapour adsorption property of three new co-crystals $\{(H_2\text{-bpee})_2[Fe(CN)_6]\cdot 5H_2O\}$ (**1**), $\{[(H_2\text{-bpee})(H\text{-bpee})][Fe(CN)_6]\}.4(H_2O)$ (**2**) and $\{[2(H\text{-bpee})\cdot H_3O][Fe(CN)_6]\}\cdot 4(H_2O)$ (**3**) where **2** and **3** shows supramolecular isomerism.

2.2.3: *Experimental Section*

2.2.3.1: *Materials*

All the reagents and solvents employed were commercially available and used as supplied without further purification. $K_4[Fe(CN)_6]$, $K_3[Fe(CN)_6]$ and 1,2-bis(4-pyridyl)ethylene were obtained from the Aldrich Chemical Company.

2.2.3.2: *Synthetic procedure*

Synthesis of $\{(H_2\text{-bpee})_2[Fe(CN)_6]\cdot 5H_2O\}$ (1): The co-crystal **1** was synthesized according to the following procedure. 0.354 g (1 mmol) of $Fe(III)(ClO_4)_3$ was dissolved in 50 mL of water and 0.5 mmol (0.091g) of 1,2-bis(4-pyridyl)ethylene (bpee) was dissolved in 50mL of ethanol. These two solutions were mixed together, stirred for 15 min. $K_4[Fe(CN)_6]$ solution was prepared by dissolving 0.5 mmol (0.211g) in 100 mL water. 2 mL of as prepared ligand solution was slowly and carefully layered on top of the metal solution (2 mL) by employing 1 mL buffer (H_2O:EtOH = 1:1) in a 15 cm long crystal tube. These crystal tubes were left undisturbed for four weeks for crystal growth. During this time the slow diffusion of the ligand solution occurs and it reacts with metal solution which results in the formation of deep blue needle shaped crystals in the middle of the tubes. These crystals were collected by cutting the crystal tube carefully and observed under a polarizing microscope in the absence of mother liquor. Good quality single crystals were picked up from the mother liquor and immediately covered with paraffin oil and crystal data was collected at 293 K.

Different procedure was employed for the preparation of the sample in bulk amount. 0.5mmol of 1,2-bis(4-pyridyl)ethylene was dissolved in 7mL of 1 N of HCl solution to make the bpee molecules be protonated. Above solution was stirred for 15min and then it was added to 0.5 mmol of $K_4[Fe(CN)_6]$ taken in 15mL water. Before mixing the solutions, both of them were cooled in an ice bath and the reaction was carried out at the same temperature. Blue coloured precipitate was obtained by the addition of the protonated ligand and the resulting mixture was stirred for overnight. The precipitate was then filtered and air dried and subjected for powder X-ray diffraction.

Yield: 77%, relative to Fe. Anal. Calcd for $C_{30}H_{36}FeN_{10}O_6$: C, 52.33; H, 5.27; N, 20.34. Found: C, 51.73; H, 5.20; N, 21.25. IR (KBr, cm^{-1}): $\nu(H_2O)$ 3456, 3374; ν(ArC-H) 3058, 3077; $\nu(C\equiv N)$ 2049, 2026; ν(ArC=C) 1623, 1589. IR spectrum of **1** (Fig. 1) show strong and

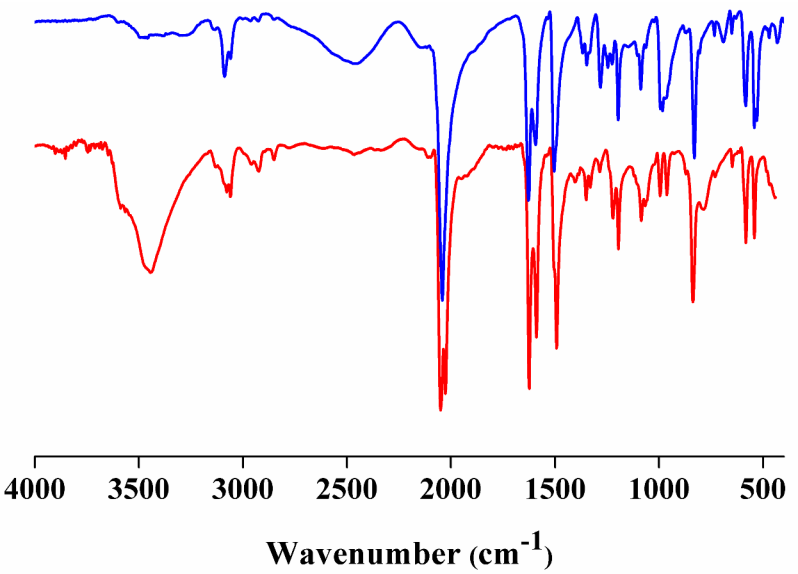

Fig. 1: IR spectrum of **1**. Red as-synthesised and blue corresponds to **1″**.

sharp bands around 3456 cm^{-1} suggesting the presence of water molecules. A strong band around 2049 cm^{-1} corroborate to free ν(C≡N) stretching frequency and a band around 1617 cm^{-1} indicates the presence bpee molecule.

Preparation of {(H_2-bpee)$_2$[Fe(CN)$_6$]} (1′): Compound **1** was placed in a glass sample cell and heated at 100 ºC for 8 h under reduced pressure of 0.1 Pa that yields **1′**. Removal of water molecules was confirmed by CHN analysis. Anal. calcd for $C_{30}H_{24}FeN_{10}$: C 62.08, H 4.17, N 24.14. Found: C 61.81, H 4.58, N 23.89.

Preparation of {(H_2-bpee)$_2$[Fe(CN)$_6$]}(1″): Compound **1** was placed in a glass sample cell under vacuum for 24 h (under reduced pressure of 0.1 Pa) at room temperature that yields **1″**. Removal of water molecules was confirmed by IR and CHN analysis. Anal. calcd for $C_{30}H_{24}FeN_{10}$: C 62.08, H 4.17, N 24.14. Found: C 60.01, H 4.51, N 23.15. IR (KBr, cm^{-1}): ν(ArC-H 3088), 3059; ν(C≡N) 2041; ν(ArC=C) 1627, 1592. IR spectrum of **1″** (Fig. 1) shows a strong band around 2041 cm^{-1} corroborate to free ν(C≡N) stretching frequency and a band around 1617 cm^{-1} indicates the presence bpee molecule.

Synthesis of {[(H_2-bpee)(H-bpee)][Fe(CN)$_6$]}.4H_2O (2): The method used for the synthesis of compound **2** is same as previous. Briefly 1 mmol (0.354 g) of Fe(III)(ClO_4)$_3$ (50mL of water) was mixed with 0.5 mmol (0.091g) of 1,2-bis(4-pyridyl)ethylene (50mL ethanol) and stirred for 15 min. K_3[Fe(CN)$_6$] solution was prepared by dissolving 0.5 mmol (0.1646 g) in 100 mL water. 2 mL of ligand solution was carefully layered on top of the metal solution (2

mL) by employing 1 mL buffer (H_2O:EtOH = 1:1) in a 15 cm long crystal tube and left undisturbed for four weeks. Greenish yellow block shaped crystals were collected and taken for single crystal XRD.

For the bulk synthesis of compound **2**, 0.25 mmol of 1,2-bis(4-pyridyl)ethylene (in 5 ml EtOH) and 0.25 mmol of $K_3[Fe(CN)_6]$ (in 5 ml H_2O) solution were prepared and they are separately allowed to stand in an ice bath. Then the both solution were mixed under stirring condition. Immediately after mixing, ice cold $Fe(ClO_4)_3$ (0.25 mmol in 5ml H_2O) solution was added following by 5 min stirring. Greenish yellow precipitate was filtered, washed with cold water and ethanol for several time and subjected to PXRD analysis.

Yield: 79%, relative to Fe. Anal. Calcd for $C_{30}H_{31}FeN_{10}O_4$, **(2)**: C, 55.31; H, 4.80; N, 21.50. Found: C, 54.81; H, 5.12; N, 22.01. IR (KBr, cm^{-1}): $\nu(H_2O)$ 3426; ν(ArC-H) 3089, 3060; ν(C≡N) 2113; ν(ArC=C) 1619, 1587. IR spectrum of **2** (Fig. 2) shows strong and broad bands around 3426cm^{-1} suggesting the presence of water molecule. A strong band around 2113 cm^{-1} affirm to free ν(C≡N) stretching frequency and a band around 1617 cm^{-1} indicates the presence bpee molecule.

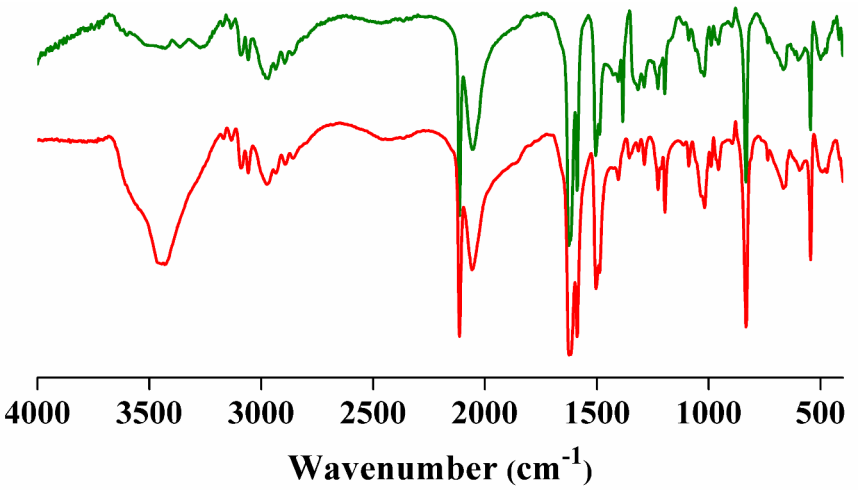

Fig. 2: IR spectrum of **2**. Red as-synthesised and green corresponds to **2″**.

Preparation of {[(H_2-bpee)(H-bpee)][$Fe(CN)_6$]}(2′): Compound **2** was placed in a glass sample cell and heated at 100 ºC under vacuum for 8 h (under reduced pressure of 0.1 Pa) that yields **2′**. Removal of water molecules was confirmed by CHN analysis. Anal. calcd for $C_{30}H_{23}FeN_{10}$: C 62.19, H 4.00, N 24.17. Found: C 61.76, H 4.12, N 23.91.

Preparation of {[(H_2-bpee)(H-bpee)][$Fe(CN)_6$]}(2″): Compound **2** was placed in a glass sample cell under the reduced pressure of 0.1 Pa at room temperature for 24 hours which yields **2″**. Removal of water molecules was confirmed by IR and CHN analysis. Anal. calcd for $C_{30}H_{24}FeN_{10}$: C 62.19, H 4.00, N 24.17. Found: C 61.24, H 4.11, N 23.81. IR (KBr, cm^{-1}): *ν*ArC-H 3086, 3059; *ν*C≡N 2114; *ν*ArC=C 1619, 1587. IR spectrum of **2″** (Fig. 2) shows a strong band around 2114 cm^{-1} corroborate to free *ν*(C≡N) stretching frequency and band around 1619 and 1587 cm^{-1} indicates the presence bpee molecule.

Synthesis of {[2(H-bpee)·H_3O][$Fe(CN)_6$]·$4H_2O$} (3): For the synthesis of compound **3**, briefly, 0.25 mmol (0.165g) of $K_3[Fe(CN)_6]$ (in 25mL of water) was mixed with 0.25 mmol (0.091g) of 1,2-bis(4-pyridyl)ethylene (25mL ethanol) and stirred for 15 min. Later this solution was added to 0.5 mmol of $Fe(III)(ClO_4)_3$ in 50mL water, stirred for 4 hour, further the solution was filtered and keep the filtrate for slow evaporation at room temperature. Orange block shaped crystals were found after two days of evaporation which is then filtered and washed with water and ethanol. Good quality single crystals were picked up and immediately covered with paraffin oil and crystal data was collected at 293 K.

For the bulk synthesis of the compound **3**, 0.25 mmol (0.083 g) of $K_3[Fe(CN)_6]$ was taken in 10mL water and first it was mixed with 0.25 mmol of $Fe(ClO_4)_3$ (in 10mL water). Before mixing, the both solutions were kept in an ice bath. The above solution was stirred for 5 min and then 0.5 mmol (0.092 g) of ice cold 1,2-bis(4-pyridyl)ethylene was added to it. Above final solution was stirred for 30min and then oranges brown precipitate was filtered and air dried and subjected to PXRD. Yield: 68%, relative to Fe. Anal. Calcd for $C_{30}H_{36}FeN_{10}O_6$, **(3)**: C, 53.82; H, 4.97; N, 20.93. Found: C, 52.41; H, 5.13; N, 20.39. IR (KBr, cm^{-1}): *ν*(H_2O)

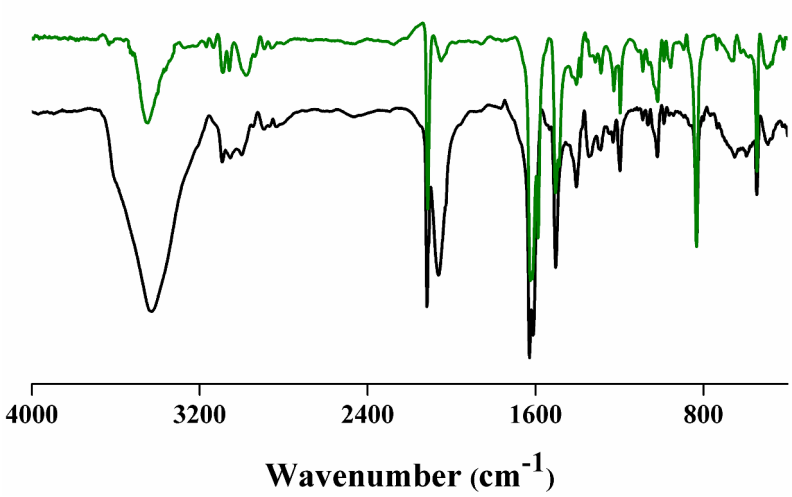

Fig. 3: IR spectrum of **3**. Red as-synthesised and green corresponds to **3″**.

3430; ν(ArC-H) 3093, 3053; *ν*(C≡N) 2118, 2063; *ν*(ArC=C) 1628, 1612. IR spectrum of **3** (Fig. 3) shows strong and broad bands around 3430 cm^{-1} suggesting the presence of water molecule. A strong band around 2118 cm^{-1} affirm to free *ν*(C≡N) stretching frequency and a band around 1628 cm^{-1} indicates the presence of bpee molecule.

Preparation of {[2(H-bpee)·(H_3O)][$Fe(CN)_6$]} (3′): Compound **3** was placed in a glass sample cell and heated at 100 ºC for 8 h under reduced pressure of 0.1 Pa that yields **3′**. Removal of water molecules was confirmed by CHN analysis. Anal. calcd for $C_{30}H_{25}FeN_{10}O$: C 60.31, H 4.21, N 24.45. Found: C 59.91, H 4.16, N 23.29.

Preparation of {[2(H-bpee)·(H_3O)][$Fe(CN)_6$]·H_2O}(3″): Compound **3** was placed in a glass sample cell under vacuum for 24 h (under reduced pressure of 0.1 Pa) at room temperature that yields **3″**. Removal of water molecules was confirmed by IR and CHN analysis. Anal. calcd for $C_{30}H_{27}FeN_{10}O_2$: C 58.55, H 4.42, N 22.79. Found: C 58.08, H 4.54, N 22.59. IR (KBr, cm^{-1}): *ν*H_2O 3451; *ν*ArC-H 3089, 3058; *ν*C≡N 2114; *ν*ArC=C 1625, 1616. IR spectrum of **3″** shows a strong band around 2114 cm^{-1} corroborate to free *ν*(C≡N) stretching frequency and band around 1625 cm^{-1} indicates the presence of bpee molecule. Due to having one protonated water molecule in compound **3,** the IR spectrum of **3″** (Fig. 3) shows a peak at ~ 3400 cm^{-1}.

2.2.3.3: ***Physical Measurements***

The elemental analyses of each compounds and their different state were carried out on a Thermo Fisher Flash 2000 Elemental Analyser. Infra-red (IR) spectroscopic studies was carried out in the mid-IR region as KBr pellet (Bruker IFS-66v). Thermogravimetric analysis (TGA) was carried out (Metler Toledo) in nitrogen atmosphere (flow rate = 50 ml min^{-1}) in the temperature range 30 – 650 °C (heating rate = 2°C min^{-1}). Powder XRD pattern of the products were recorded by using Cu-K_α radiation (Bruker D8 Discover; 40 kV, 30 mA).

2.2.3.4: ***Single Crystal X-ray Diffraction***

Suitable yellow colour single crystals of compound **1**, **2** and **3** were mounted on a thin glass fiber with commercially available super glue. X-ray single crystal structural data were collected on a Bruker Smart-CCD diffractometer equipped with a normal focus, 2.4 kW sealed tube X-ray source with graphite monochromated Mo-*Kα* radiation (λ = 0.71073 Å)

operating at 50 kV and 30 mA. The program SAINT was used for integration of diffraction profiles and absorption correction was made with SADABS program. All the structures were solved by SIR 92[18] and refined by full matrix least square method using SHELXL.[19] All the hydrogen atoms were fixed by HFIX and placed in ideal positions. Potential solvent accessible area or void space was calculated using the PLATON[20] multipurpose crystallographic software. The coordinates, anisotropic displacement parameters and torsion angles for **1**, **2** and **3** are submitted as supplementary information in CIF format. All crystallographic and structure refinement data of **1**, **2** and **3** are summarized in Table 1. All calculations were carried out using SHELXL 97[19], PLATON[20], SHELXS 97[21] and WinGX system, Ver 1.70.01.[22]

2.2.3.5: ***Adsorption Study***

The adsorption of different solvents like MeOH at 293K and H_2O, EtOH, CH_3CN at 298 K were measured in the gaseous state by using BELSORP-aqua-3 analyzer. In all the measurements, in the sample tube adsorbent samples (~100 – 150 mg) were placed which were prepared at 100 ºC for about 8 hours (**1′**, **2′**, **3′**) or at RT for about 24 hours (**1″**, **2″**, **3″**) under vacuum prior to measurement of the isotherms. The different solvent molecules used to generate the vapour were degassed fully by repeated evacuation. Dead volume was measured with helium gas. The adsorbates were placed into the sample tubes, then the change of the pressure was monitored and the degree of adsorption was determined by the decrease in pressure at the equilibrium state. All operations were computer controlled and automatic. N_2 and CO_2 adsorption studies were carried out with the dehydrated samples (i.e. **1′**, **2′**, **3′**) prepared at 100 ºC under high vacuum ($<10^{-1}$ Pa) for 8 hours by using QUANTACHROME QUADRASORB *SI* analyser at 77 and 195 K, respectively.

2.2.4: ***Results and Discussion***

2.2.4.1: ***Structural description of {(H_2-bpee)$_2$[Fe(CN)$_6$]·5H_2O} (1)***

Compound **1** crystallizes in monoclinic system with *C*2/m space group. The asymmetric unit consist of one molecule of $[Fe(CN)_6]^{4-}$, two doubly protonated 1,2-bis(4-pyridyl)ethylene (H_2-bpee) and five lattice water molecules (Fig. 4).

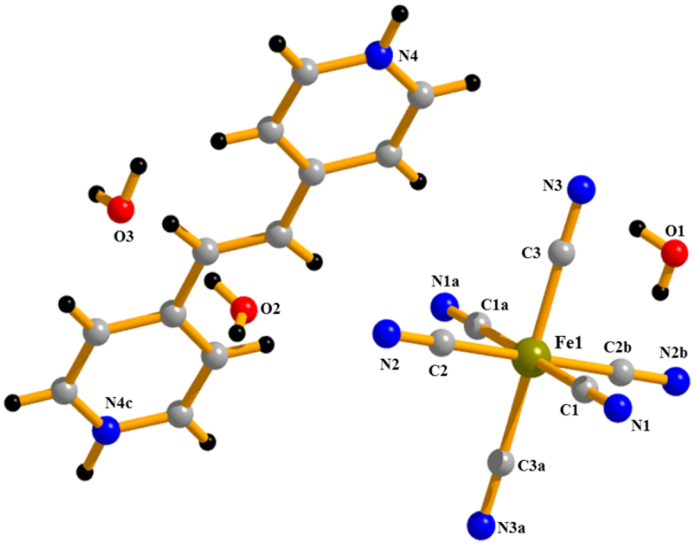

Fig. 4: Asymmetric unit of **1**. Symmetry codes: a = 1-x, y, 1-z; b = 1-x, -y, 1-z; c = 0.5-x, 0.5-y, -z.

Each Fe(II) atom is hexacoordinated and linked with six cyanide ions. In compound **1**, Fe(II) centre is in a slightly distorted octahedral geometry which is clearly reflected from the *cisoid* (88.5-91.5º) angles. Fe-C bond lengths varies from 1.907(8) to 1.925(10) Å. C-N bond distance in cyanide legand also ranges from 1.160(14) Å to 1.167(9) Å. The most fascinating feature is the formation of R4 cyclic quasi-planar water tetramers with D_{2h} configuration (Fig. 5b) where the water molecules (O2 and O3) are assembled through hydrogen bonding interaction (2.770(3) Å). These water molecules are involved in an extensive network of H-bonding (Fig. 5a) with the nitrogen atom of $Fe(CN)_6$ and form a 2D layer in *ac* plane. Each oxygen atom in the cluster is in a tetrahedral environment where it is involved in the formation of four hydrogen bonds, two with water molecules in the cluster itself and the another two with H_2-bpee molecules (N-H···O1 = 3.043(4) Å) for O1 (Fig. 2c) and $[Fe(CN)_6]^{4-}$ moiety for O2 (O2-H···N= 2.732(5) – 2.770(8) Å) (Fig 5a).

H_2-bpee molecules form a 1D chain through H-bonding with water and $[Fe(CN)_6]$ moiety which leads to 2D sheet (Fig. 5c) through π-π interaction (cg···cg distance are in the range of3.695 to 3.912 Å) along the crystallographic *bc* plane. The 2D layers generated by H_2O and

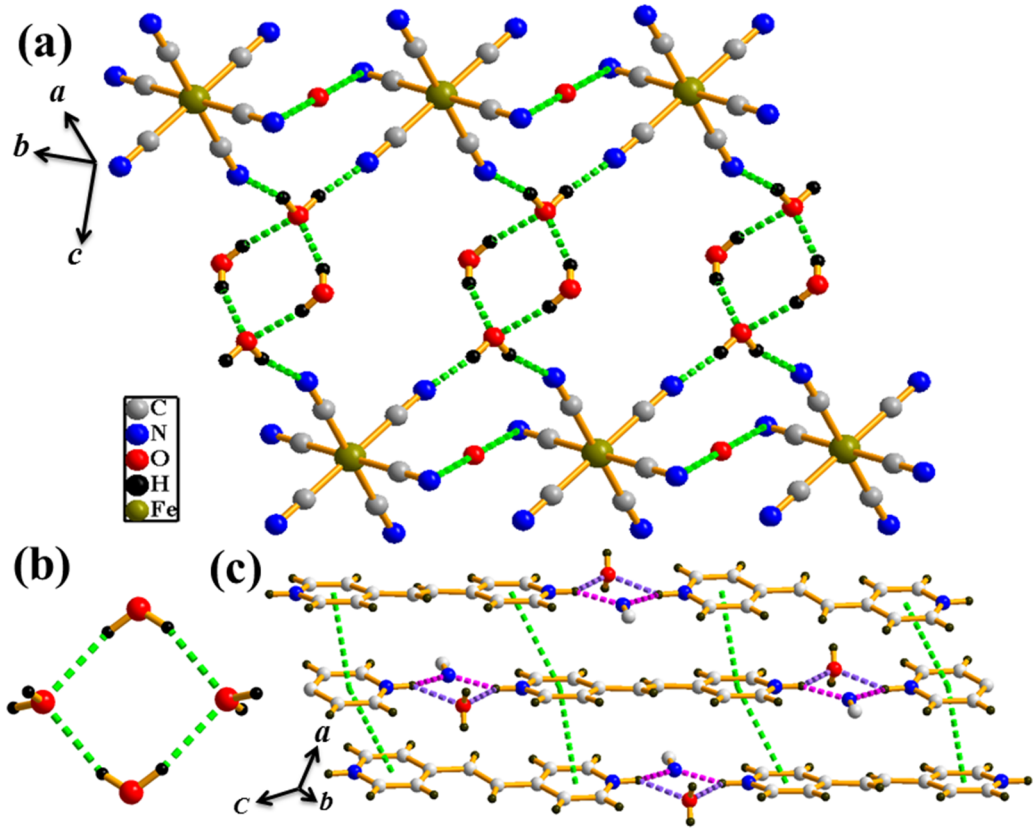

Fig. 5: (a) Figure shows the interaction between tetrameric water cluster and $[Fe(CN)_6]^{4-}$ by heteromolecular O–H---N H-bonding to form an extended sheet like structure. (b) Tetra nuclear water cluster formed in the pore of **1**. (c) ABAB stacking between the bpee molecules.

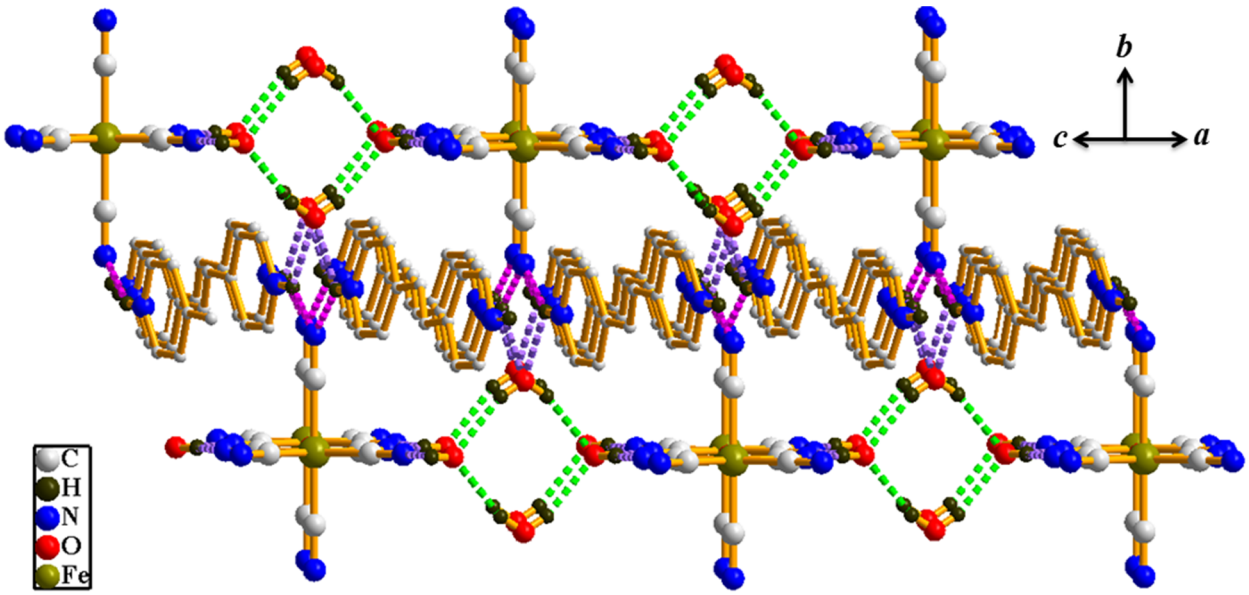

Fig. 6: Figure shows the different type of Hydrogen bonding which leads to 3D supramolecular architecture in **1**.

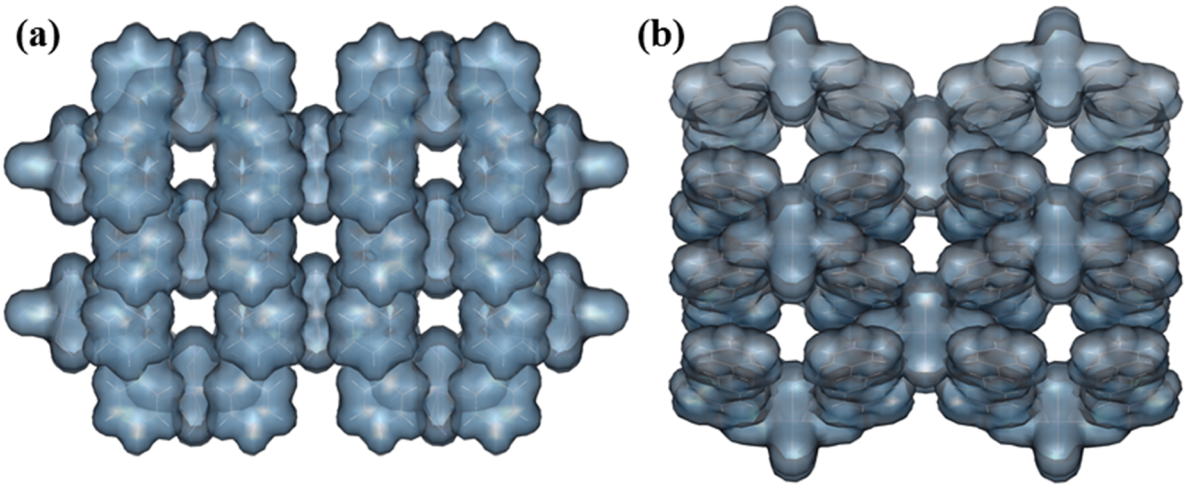

Fig. 7: View of different types of pore in **1**; (a) along crystallographic *c* direction and (b) along [101] direction.

$[Fe(CN)_6]$ are connected to H_2-bpee molecules through N-H···O and N-H···N H-bonding and leads to 3D supramolecular architecture (Fig. 6) with two type void along (101) and *c* direction.

The dimension of the voids are 2.6 × 1.7 $Å^2$ (along *c* direction) and 3.23 × 3.23 $Å^2$ (along [101] direction) calculated considering van der Walls radii of the atom (Fig. 7). After removal of the lattice water molecules, calculation using PLATON suggest 20.7% void volume per unit cell volume in **1**.

2.2.4.2: ***Structural description of {[(H_2-bpee)(H-bpee)][$Fe(CN)_6$]}.4(H_2O) (2)***

Compound **2** crystallizes in monoclinic system with *P*ī space group. The asymmetric unit consist of two molecule of $[Fe(CN)_6]^{3-}$ unit, one doubly protonated 1,2-bis(4-pyridyl)ethylene (H_2-bpee) molecule, one singly protonated 1,2-bis(4-pyridyl)ethylene (H-bpee) and four lattice water molecules (Fig. 8). In compound **2**, Fe(III) centres are slightly distorted from the perfect octahedral geometry which is reflected from the Fe-C-Fe *cisoid* (89.2(3) − 90.8º(3)) angles and Fe-C bond lengths (1.923(7) to 1.949(7) Å). Three crystalline water molecules (O2, O3, and O4) form a trimeric water cluster through H-bonding (Fig. 9b) where each oxygen atom is further connected to nearest nitrogen atom of $[Fe(CN)_6]^{3-}$ (Fe2) moiety through O−H···N H-bonding and leads to a 2D layer along the *ab* plane.

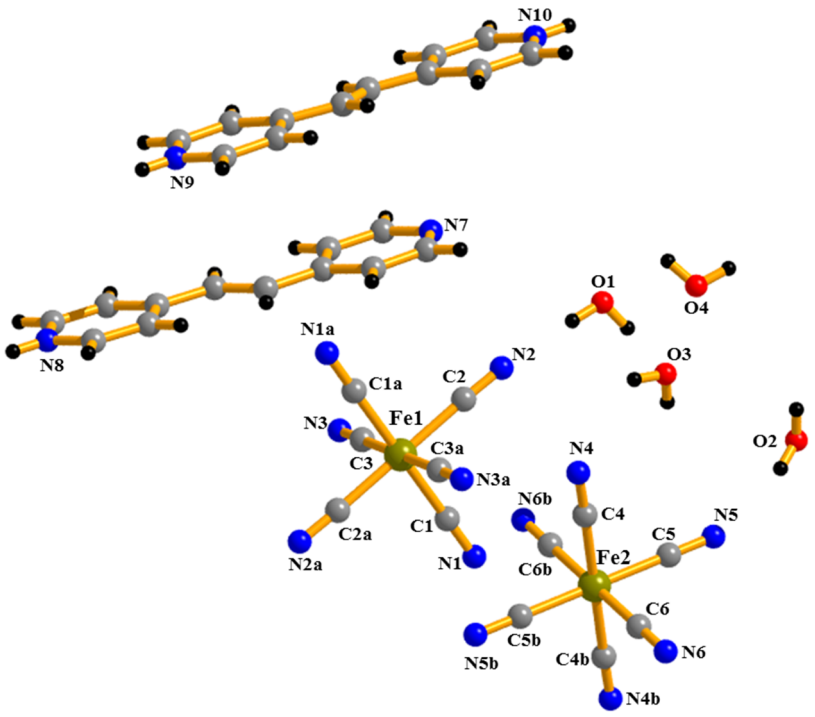

Fig. 8: Asymmetric unit of **2**. Symmetry codes: a = -x, -y, 1-z; b = -x, -y, -z.

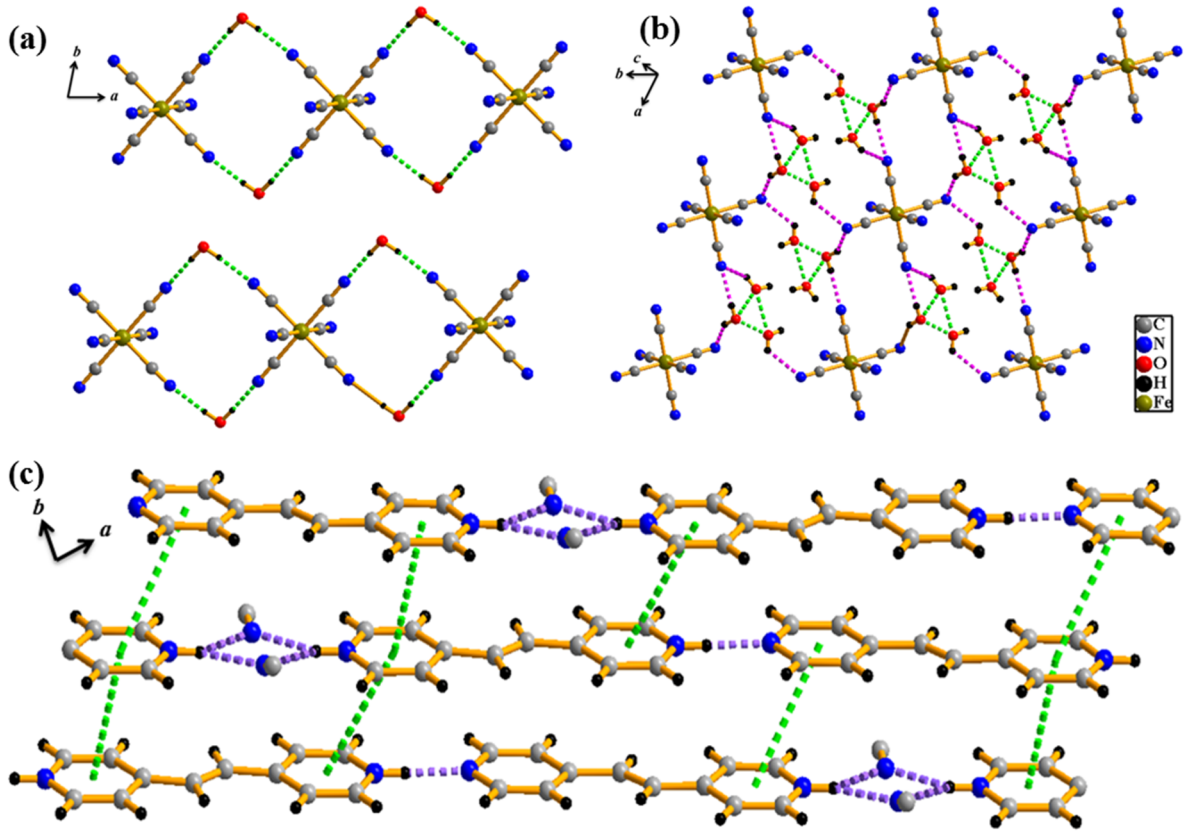

Fig. 9: (a) H-bonding interaction between $[Fe(CN)_6]$ (Fe1 centre) unit and H_2O molecule in **2** resulting 1D chain along crystallographic *a* direction, (b) H-bonding interaction between $[Fe(CN)_6]$ (Fe2 centre) unit and H_2O molecule in **2** resulting 2D layer, (c) ABAB stacking between the bpee molecule.

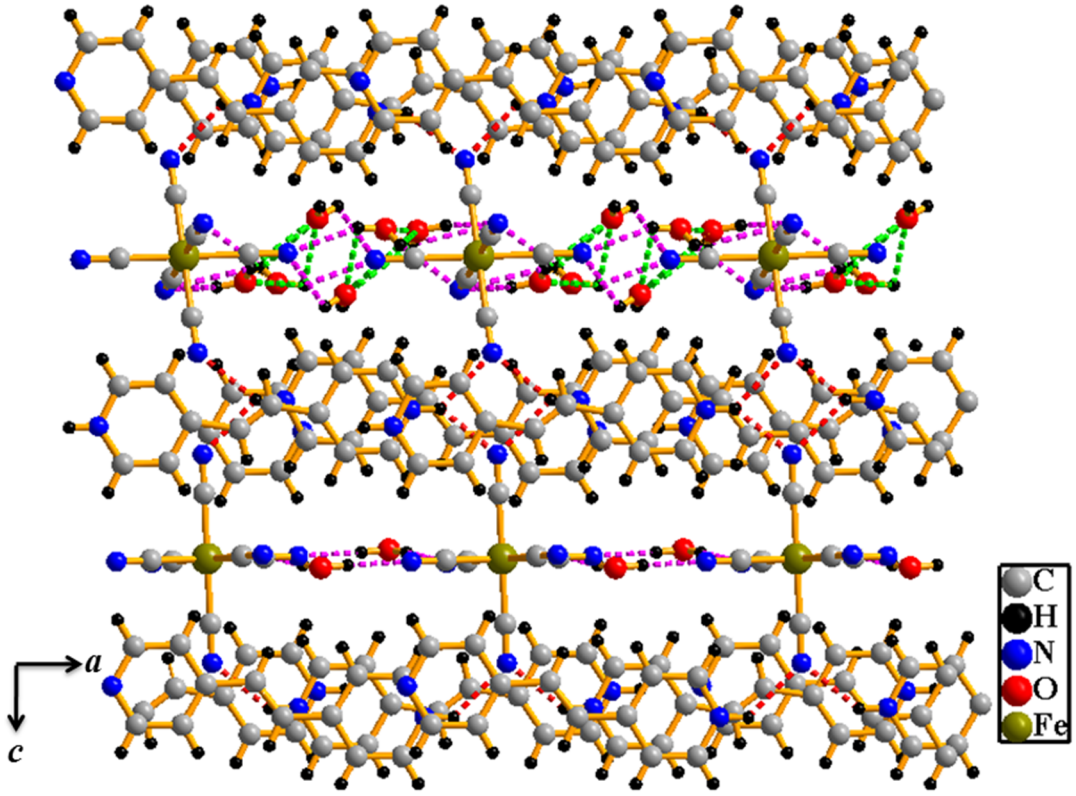

Fig. 10: Figure shows the different type of Hydrogen bonding along crystallographic *c* direction which leads to 3D supramolecular architecture to form **2**.

Another $[Fe(CN)_6]^{3-}$ (Fe(1)) moiety is connected by one water molecule (O1) through O−H···N H-bonding (bond distance varies from 2.866(8) to 2.882(9) Å) and thus forming a 1D chain along *a* direction (Fig. 9a). The two types of bpee molecules i.e. H_2-bpee and H-bpee are connected by two different type of N-H···N H-bonding (Fig. 9c) to form a 1D chain along *a* direction. π-π interaction (cg···cg distance are in the range of 3.590 to 4.487 Å) between these chains generates a 2D corrugated sheet along the crystallographic *ab* plane.
The 1D chains and 2D sheets formed by the $[Fe(CN)_6]^{3-}$ and water, which interacts with the bpee (H_2-bpee and H-bpee) sheets through N-H···N hydrogen bonding (varies from 2.860(7) to 2.999(8) Å) and stack in a ABAB fashion along *c* direction (Fig. 10) resulting a 3D supramolecular host.

The host houses two types of void (Fig. 11) along crystallographic *a* direction occupied by the lattice water molecules. After removal of the lattice water molecules, calculation using PLATON suggest 16.2% void volume per unit cell volume in **2**. The dimension of the voids are 3.60 × 2.66 $Å^2$ and 2.66 × 1.60 $Å^2$ calculated considering van der Walls radii of the atom (Fig. 11).

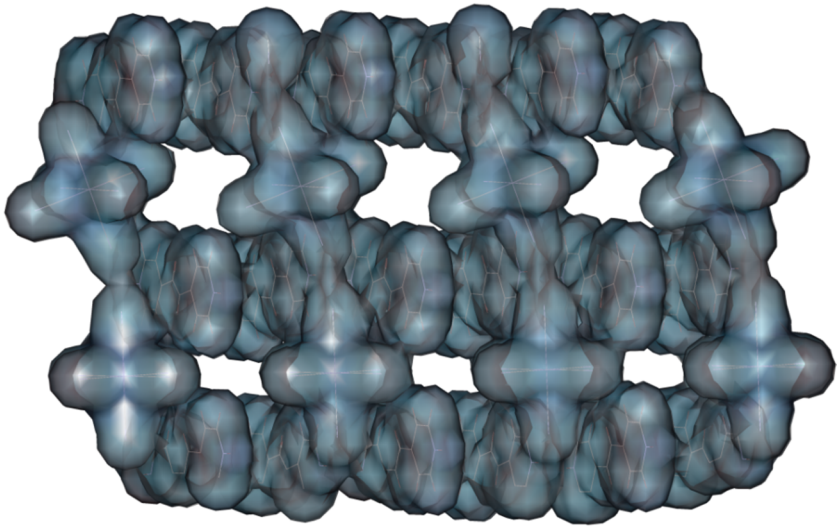

Fig. 11: View of different types of pore in **2** along crystallographic *a* direction.

2.2.4.3: ***Structural description of {[2(H-bpee)·H_3O][$Fe(CN)_6$]}·$4H_2O$ (3)***

Compound **3** crystallizes in triclinic space group *P*ī. The formula unit of compound **3** contains one molecule $[Fe(CN)_6]^{3-}$ unit, two singly protonated 1,2-bis(4-pyridyl)ethylene (H-bpee) molecules, one protonated water molecule and four lattice water molecules (Fig. 12).

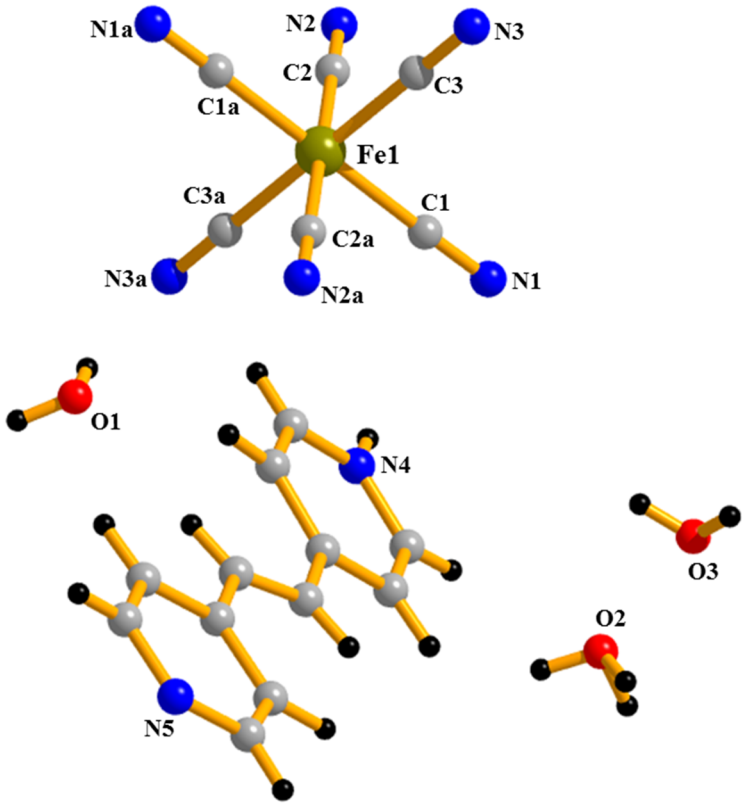

Fig. 12: Asymmetric unit of **3**. Symmetry code: a = 2-x, 2-y, z.

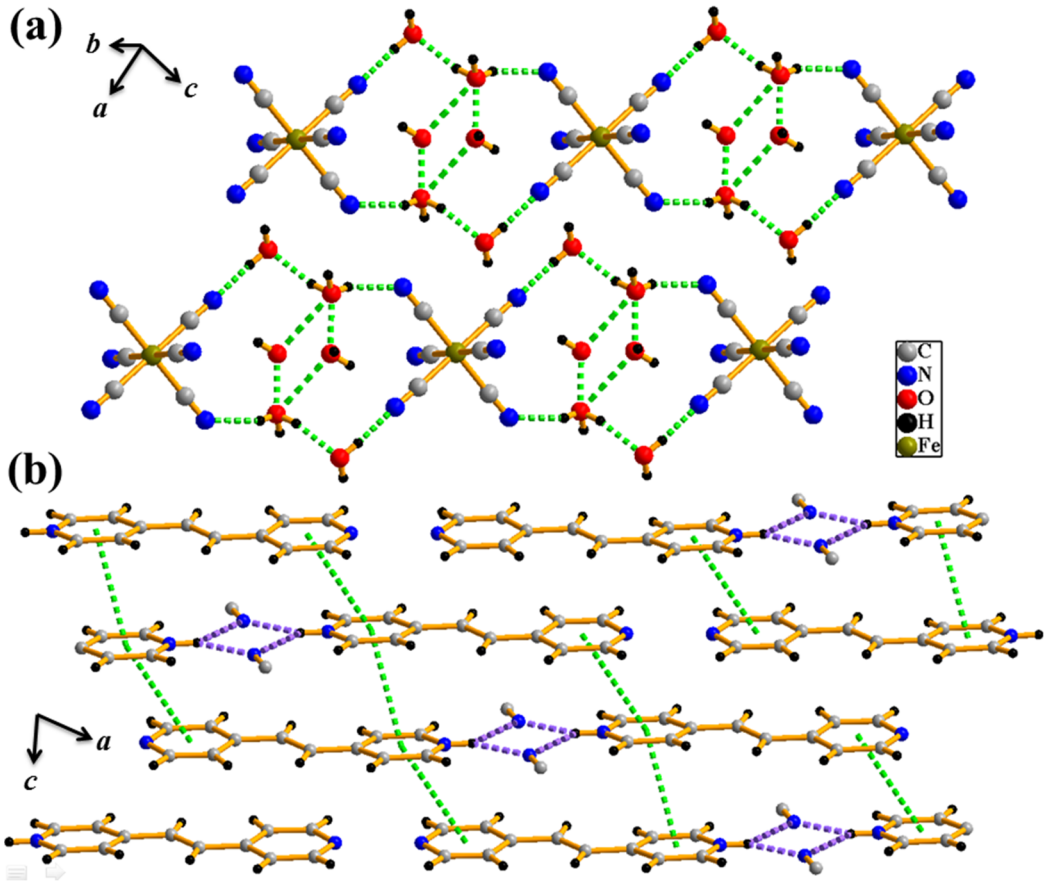

Fig. 13: (a) Figure shows the interaction between tetrameric water cluster and $[Fe(CN)_6]^{3-}$ by heteromolecular O–H---N H-bonding to form an extended sheet like structure. (b) ABAB stacking between the bpee molecules in **3**.

The coordination environment of Fe(III) centre in compound **3** is similar to that of compound **1** and **2**, that is it locates itself in a slightly octahedral centre which is clearly reflected from the *cisoid* angles (87.8(2) - 92.2(2)º) and different Fe−C bond lengths (1.931(7) – 1.944(7) Å). Each hexameric water cluster is connected to two nearest $[Fe(CN)_6]^{3-}$ moiety through O–H···N hydrogen bonding (2.798(8) – 2.837(14) Å) between O-atom of water molecules and N-atom of cyanide ligands to form a 2D sheet like structure.

The H-bpee molecules form a dimer which leads to 1D chain along *a* direction through N-H···N hydrogen bonding. Each N4 atom of H-bpee is connected to pendant cyanide ligand of $[Fe(CN)_6]^{3-}$ through N-H···N hydrogen bonding. These 1D chains are stacked through π···π interaction (cg···cg distance are in the range of 3.778 to 3.898 Å) in ABC fashion along the crystallographic *ac* plane resulting a 2D corrugated sheet (Fig. 13b). The H-bpee corrugated sheets and the 2D sheets formed by $[Fe(CN)_6]^{3-}$ and water clusters interacts in ABAB fashion along *b* direction. N-H···N hydrogen bonding between these 2D sheets resulting in a 3D

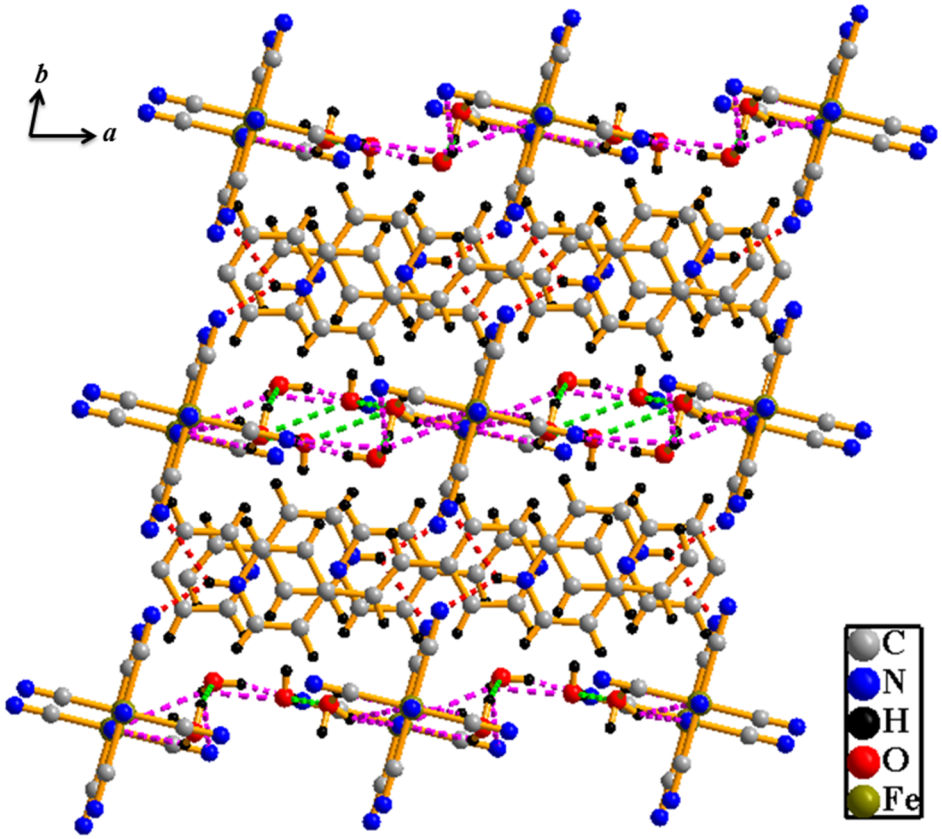

Fig. 14: Figure shows the different type of Hydrogen bonding along crystallographic *c* direction which leads to 3D supramolecular architecture to form **3**.

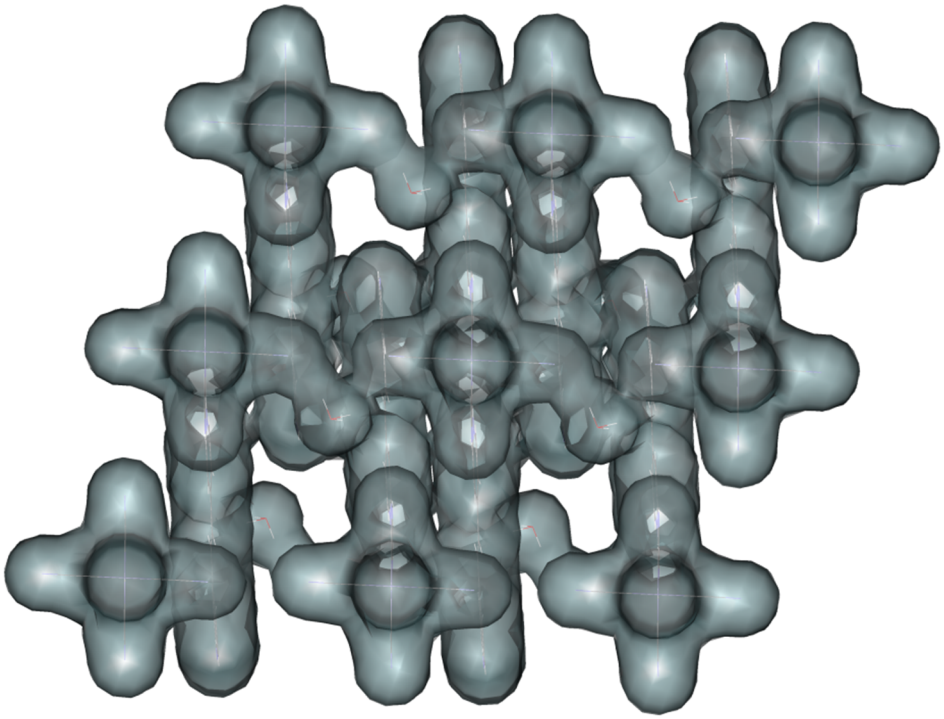

Fig. 15: Figure shows the pore in **3** along crystallographic *a* direction.

supramolecular host with voids along *a* direction which is occupied by lattice water molecules (Fig. 14). After removal of the lattice water molecules, calculation using PLATON suggest only 3.1% void volume per unit cell volume in **3**. The dimension of the void is 3.23 × 1.85 $Å^2$ calculated considering van der Walls radii of the atom (Fig. 15). The interesting feature of **3** is the formation of hexameric water cluster with teterameric core (Fig. 13a). In tetrameric core the average distance between the oxygen molecules (O2 and O3) varies from 2.129 to 3.004 Å, whereas the 5^{th} and 6^{th} oxygen molecules are almost perpendicular to the tetrameric core (distance = 2.805 Å).

Table 1 Crystal data and structure refinement parameters for **1, 2,** and **3**.

	1	**2**	**3**
Empirical formula	C_{30} H_{32} N_{10} FeO_6	$C_{30}H_{32}$ N_{10} Fe O_4	$C_{30}H_{32}$ N_{10} Fe O_6
M	668.51	652.51	688.54
cryststystem	Monoclinic	Triclinic	Triclinic
space group	*C*2/m (No. 12)	*P*-1 (No. 2)	*P*-1 (No. 2)
a (Å)	13.3574(5)	8.9644(2)	9.1823(8)
b (Å)	16.1239(5)	10.3952(3)	9.2949(8)
c (Å)	10.8192(4)	18.1383(5)	9.9680(9)
α(deg)	90	79.091(2)	86.070(5)
β (deg)	137.0150(10)	82.964(2)	71.890(4)
γ (deg)	90	75.009(2)	76.950(4)
V ($Å^3$)	1588.72(10)	1598.39(8)	787.72(12)
Z	2	2	1
T(K)	293	293	293
λ(Mo $K_α$)	0.71073	0.71073	0.71073
D_c (g cm^{-3})	1.398	1.356	1.452
μ (mm^{-1})	0.530	0.523	0.539
$θ_{max}$ (deg)	21.6	22.2	22.8
total data	5349	15627	10795
uniquereflection	974	3944	2117
R_{int}	0.027	0.029	0.038
data [$I > 2σ(I)$]	900	3106	1925
R^a	0.0342	0.0691	0.0705
$R_w{}^b$	0.0938	0.2245	0.2004
GOF	1.14	1.07	1.05

$^a R = \sum||Fo|-|Fc||/\sum|Fo|$; $^b R_w = [\sum\{w(Fo^2-Fc^2)^2\}/\sum\{w(Fo^2)^2\}]^{1/2}$

2.2.4.4: ***Thermogravimetric (TG) and PXRD analysis***

Thermogravimetric analysis (TGA) and powder X–ray diffraction (PXRD) measurement were carried out to study the stability of the supramolecular framework. TGA of compounds **1-3** were performed in the temperature range 30 – 600 ºC under nitrogen atmosphere (Fig. 16). Compound **1** shows release of ≈ 4 water molecules in temperature range 120-130 ºC (wt. loss 89.80% at 130 ºC). After that it gradually decomposes into undetermined structure. The TGA plot of Compound **2** shows a weight loss of 9.50% at 130 ºC corroborate the release of all 3.46 lattice water molecules. The dehydrated compound of **2** stable up to 170 ºC without any further weight loss and then goes to an undetermined structure.

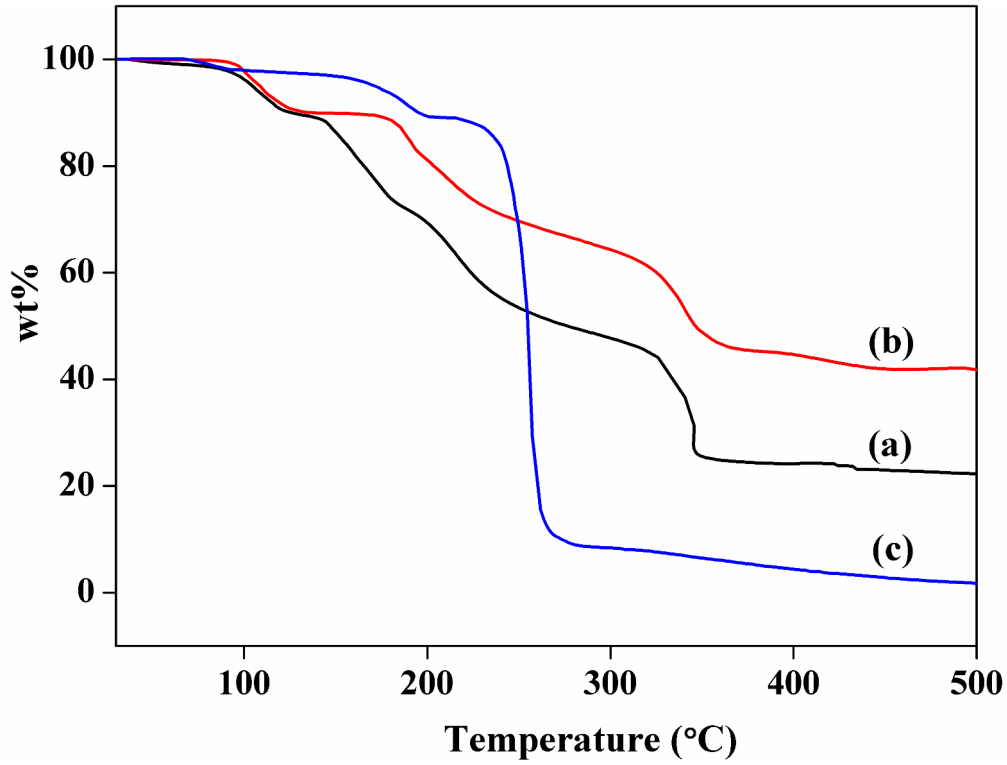

Fig. 16: TGA plot of **1** (a), **2** (b) and **3** (c).

Compound **3** also shows some steps in its TGA plot. The first one indicates the release of one water molecules (wt. loss = 2.52%) at 125 ºC, and the second one corresponds the release of total four water molecules (wt. Loss = 10.74%) at 106 ºC. Finally it loses all the five water molecules which leads to an unidentified structure.

The PXRD pattern of compounds **1-3** are shown in Fig. 17, 18, 19. The position of the different peaks in simulated and as-synthesised pattern corresponds well indicating the purity of the as-synthesised compounds.

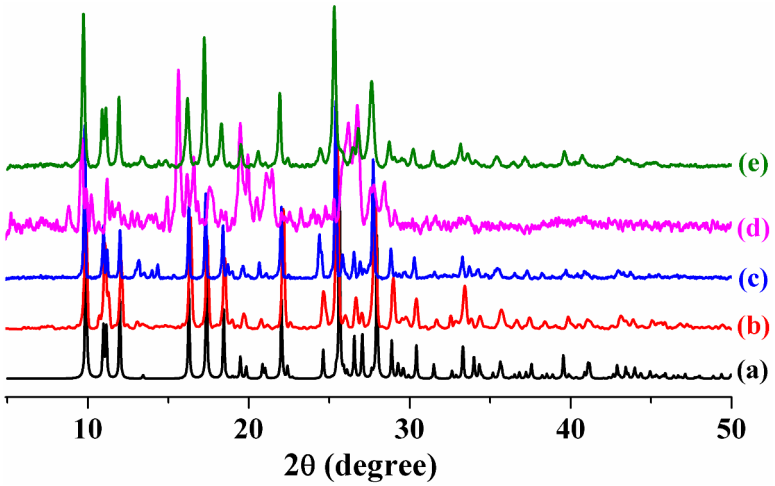

Fig. 17: PXRD Pattern of comp1. (a) Simulated, (b) as-synthesised, (c) heated at room temperature, (d) heated at 100 ºC (e) rehydrated.

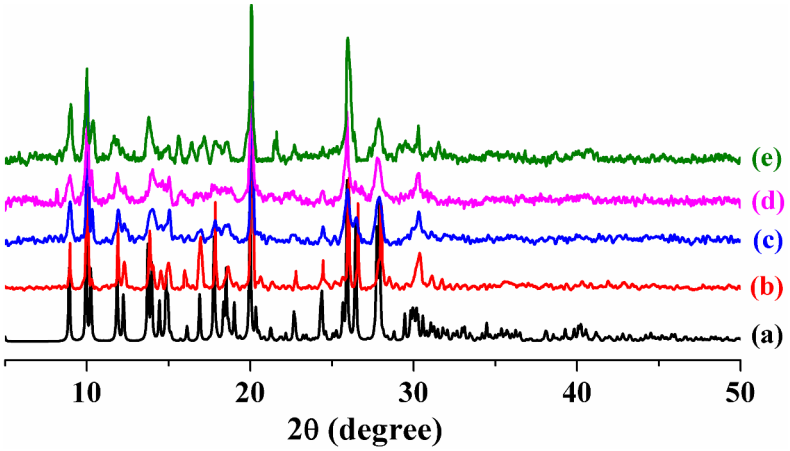

Fig. 18: PXRD Pattern of **2**. (a) simulated, (b) as-synthesised, (c) heated at room temperature, (d) heated at 100 ºC (e) rehydrated.

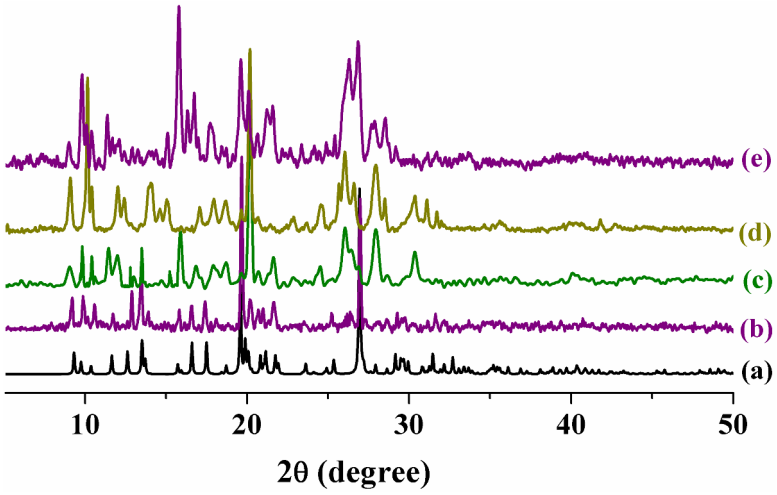

Fig. 19: PXRD Pattern of comp **3**. (a) Simulated, (b) as-synthesised, (c) heated at room temperature, (d) heated at 100 ºC (e) rehydrated.

Similarity between the PXRD pattern of **1** and **1″** indicates that there is no structural change upon degassing the as-synthesised compound at room temperature (Fig. 17). The PXRD pattern of **2″** (Fig. 18) is almost similar to that of **2** with negligible loss in crystallinity. But in case of **3** the PXRD pattern (Fig. 19) suggests a definite structural change occurred in **3″** even after the removal of water molecules at room temperature.

2.2.4.5: *Adsorption study*

The presence of lattice water molecules in the three supramolecular structures motivates for the solvent vapour adsorption which shows interesting results. I have studied the adsorption properties for the dehydrated samples of **1**, **2**, and **3** with different solvent molecules (H_2O, MeOH, EtOH, and CH_3CN).

2.2.4.5.1: *Solvent adsorption study of {$(H_2$-bpee$)_2[Fe(CN)_6]\cdot 5H_2O$} (1)*

The H_2O (kinetic diameter=2.68Å) adsorption profile for **1′** shows a gradual uptake with increasing pressure and reaches an amount of 104.43 mL g^{-1} (P/P_0 = 0.98, 2.60 molecules per formula unit) without showing any step. Desorption curve does not follow the same path and shows large hysteresis evidencing the hydrophilic nature of the pore (Fig. 20b). Interesting results were obtained when we decided to perform the same adsorption experiment with **1″** i.e. by degassing the samples at room temperature. The removal of water molecules at room temperature under vacuum were confirmed by IR analysis. Surprisingly the adsorption profile of **1″** showed a stepwise uptake which is totally different from that of **1′** (Fig. 20a).

Unlike **1′**, the water molecules can easily diffuse into **1″** even at low P/P_0= 0.095 (uptake ≈ 40mL g^{-1}) where the earlier compound adsorbs only 9.65 mL g^{-1} at the same P/P_0. The profile of **1″** shows steep uptake up to P/P_0~ 0.13 and then gradually reaches at an amount of 86 mL g^{-1} (P/P_0 ~ 0.62). After that there is a sudden jump and the profile ends at a final uptake of 160 mL g^{-1} (4 H_2O molecules per formula unit) suggesting a kind of gate opening at P/P_0 = 0.62. This clearly indicates the shrinkage of the structure upon removal of H_2O molecule at room temperature that opens up at P/P_0= 0.62. The βE_0 values, reflecting the interaction between adsorbate and adsorbent molecule are about 2.13 $kJmol^{-1}$ for **1′** and 8.82 kJ mol^{-1} **1″** which clearly indicates that the latter is more hydrophilic than **1′**.

The sorption studies of MeOH are shown in figure 21b. Compound **1′** reveals a type-I uptake with a final amount of 30 mL g^{-1} at P/P_0 = 0.98.

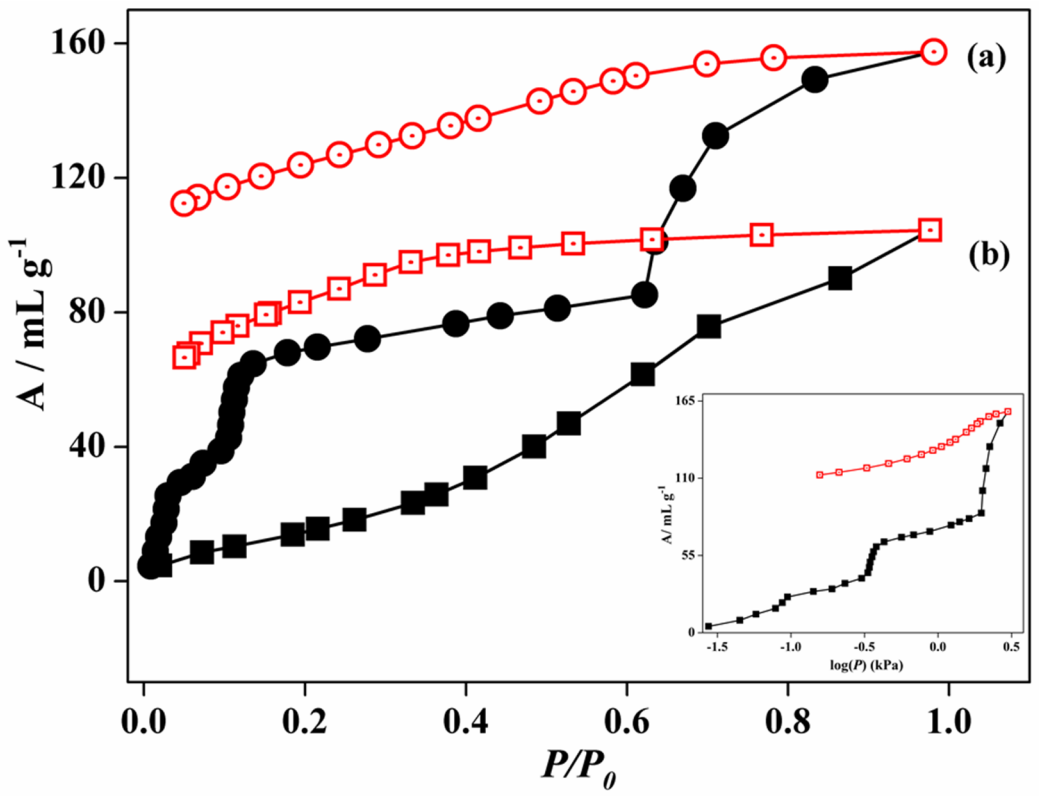

Fig. 20: Water adsorption profile of **1″** (*a*) and **1′** (*b*), Inset figure showing steps in the adsorption profile of **1″.**

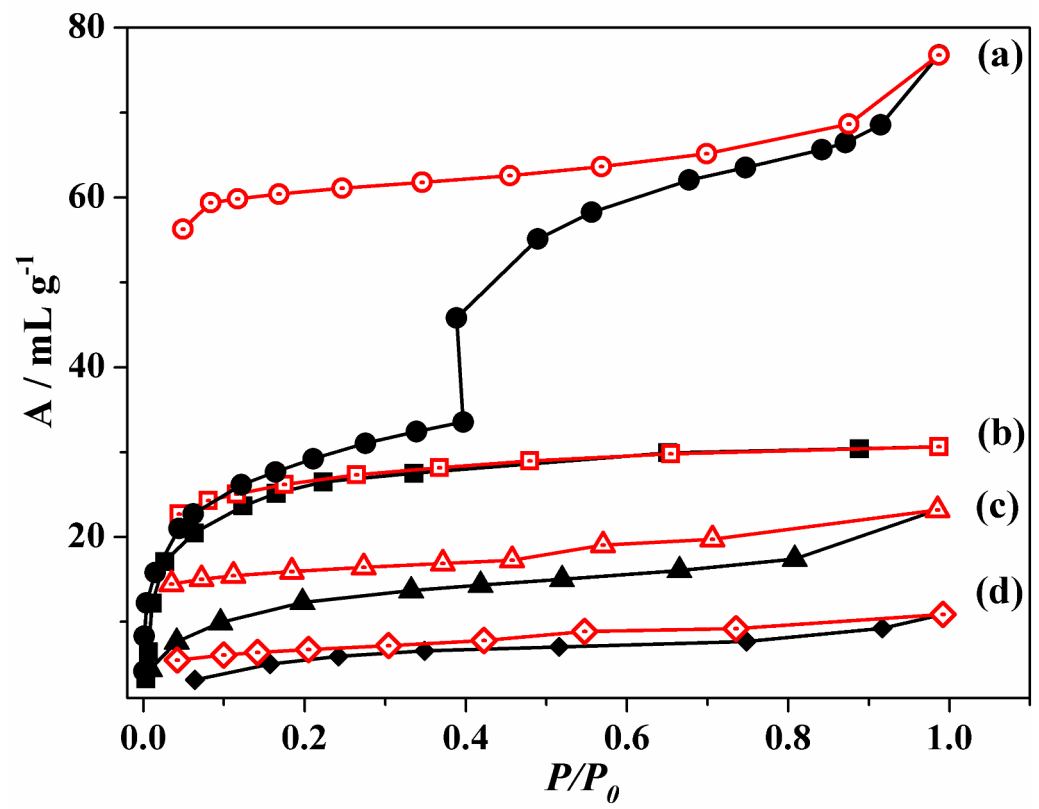

Fig. 21: Methanol adsorption profile of **1″** (a), **1′** (b) and Ethanol adsorption profile of **1″**(c), **1′** (d).

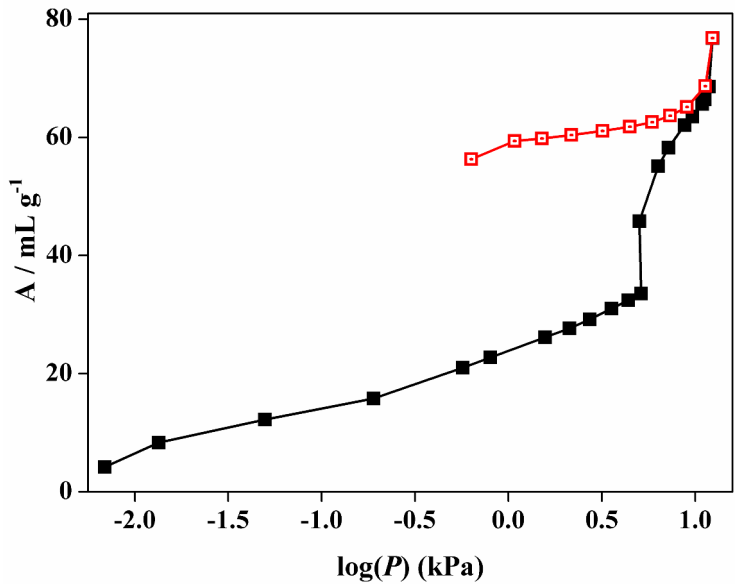

Fig. 22: Figure showing steps in the methanol adsorption profile of **1″**.

But a different profile was obtained in case of **1″** where it shows a typical type-I curve up to P/P_0 = 0.39 and exhibit a sudden jump at this point (Fig. 21a). After that it reaches an amount of 76.8 mL g^{-1} at P/P_0 = 0.98. The sudden adsorption jump in MeOH sorption at a certain pressure, called the gate-opening pressure, correlates to the structural transformation of the structure.

2.2.4.5.2: *Solvent adsorption study of {[(H_2-bpee)(H-bpee)][Fe(CN)$_6$]}.4(H_2O) (2)*

The H_2O adsorption profile for **2′** shows a gradual uptake with increasing pressure and reaches an amount of 115.2 mL g^{-1} (P/P_0 = 0.97, 3 molecules per formula unit) without showing any step (Fig. 23b). Again we have performed same experiment with **2″** and the removal of water molecules was confirmed by IR and elemental analysis.

The adsorption isotherm of **2″** shows gradual uptake of H_2O up to $P/P_0 \sim 0.2$ (uptake volume ~ 53mL g^{-1}) and then a sudden jump occurs at around $P/P_0 \sim 0.25$ where the profile shows a second step adsorption that leads to final uptake of 145 mL g^{-1} (3.76 H_2O molecules per formula unit) at P/P_0 = 0.98 (Fig. 23a).

Like compound **1** the same property was observed when we found the inclusion of H_2O molecules is easier in **2″** compare to **2′** even at low pressure. Compound **2″** takes 28 mL g^{-1} at P/P_0= 0.05 while the uptake of **2′** is only 8 mL g^{-1} at the same pressure. The βE_0 value of **2″** (6.87 kJmol^{-1}) is larger than **2′** (2.09 kJ mol^{-1}) reflecting the higher hydrophilic nature of **2″**.

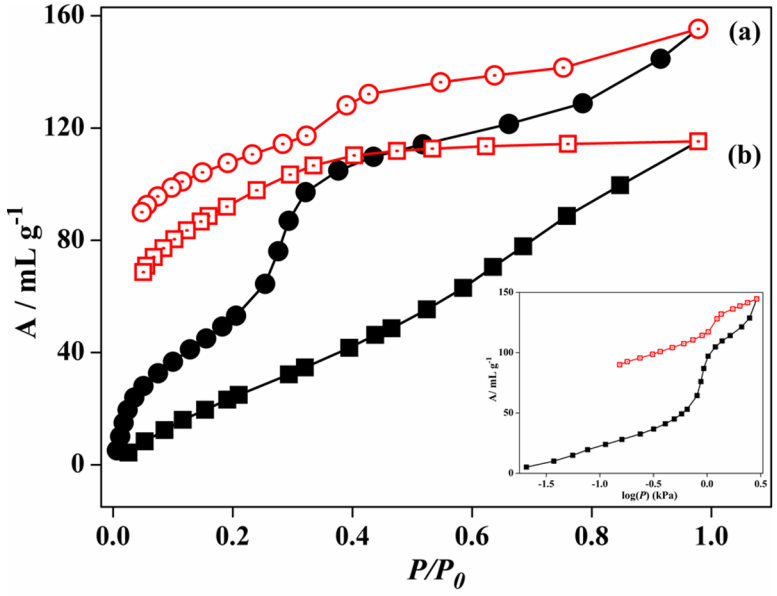

Fig. 23: (a) Water adsorption profile of **2″** (*a*) and **2′**(*b*), Inset figure showing steps in the water adsorption profile of **2″**.

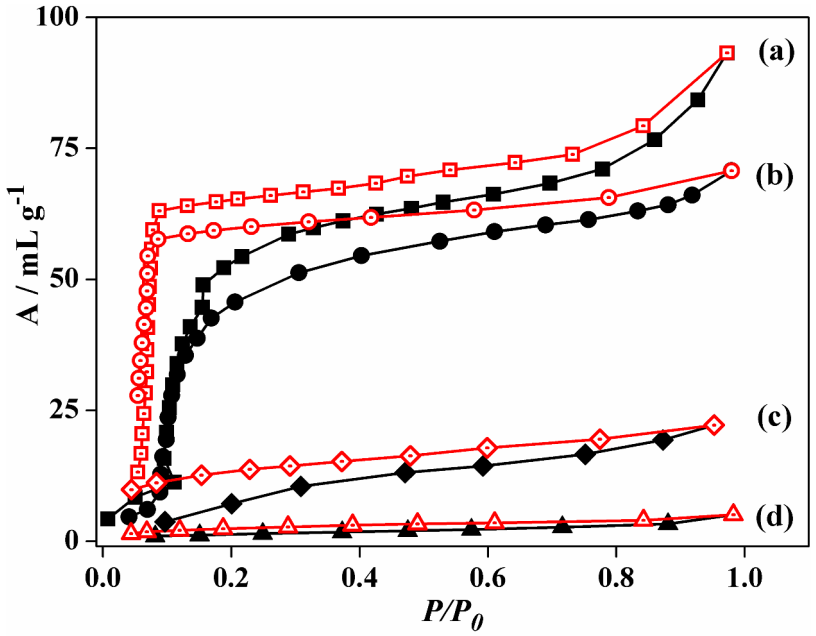

Fig: 24: Methanol adsorption profile of **2″** (a), **2′** (b) and Ethanol adsorption profile of **2″**(c), **2′** (d).

The MeOH adsorption profile of **2′** shows a steady uptake up to P/P_0 = 0.16 and then shows a gradual curve with increasing pressure which reaches an final amount of 73.74 mL g^{-1} at P/P_0 = 0.96 (Fig. 24). Like the earlier case a different profile was obtained in case of **2″**. A gate opening type phenomenon was observed at P/P_0 = 0.11 and after that a sudden jump occursfrom this point. The final uptake was 93 mL g^{-1} at P/P_0 = 0.97 (Fig. 24).

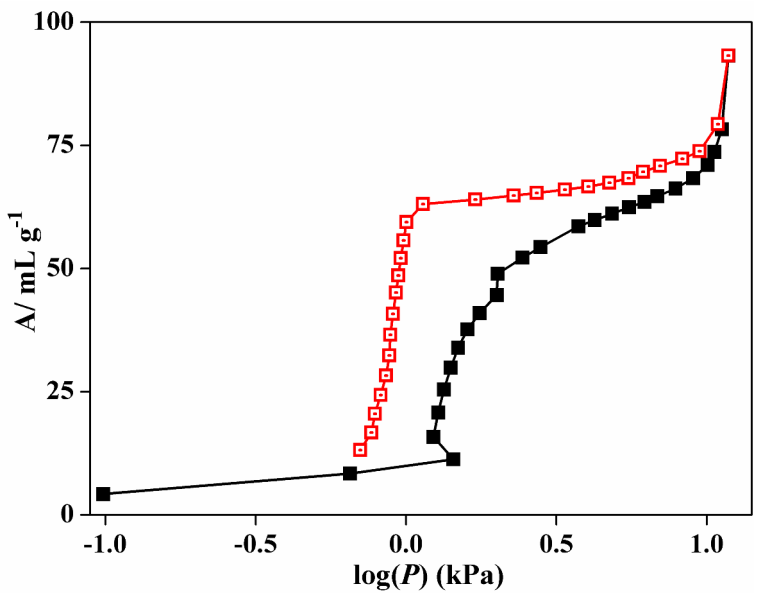

Fig. 25: Figure showing steps in the methanol adsorption profile of **2″**.

2.2.4.5.3: *Solvent adsorption study of {[2(H-bpee)·H_3O][Fe(CN)$_6$]}·4(H_2O) (3)*

Though the calculation from PLATON suggests very small pore size in **3** but still the high amount of uptake can be attributed from the structural change observed in PXRD.

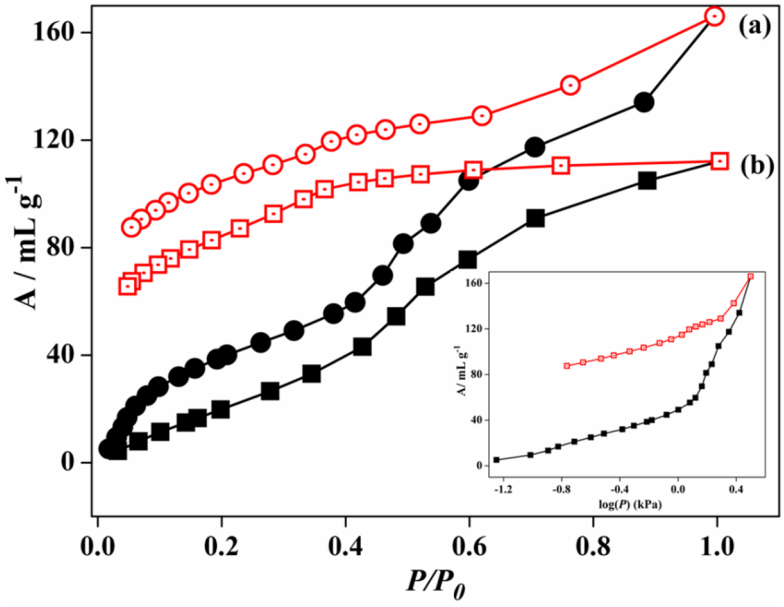

Fig. 26: (a) Water adsorption profile of **3″** (*a*) and **3′**(*b*), Inset figure showing steps in the water adsorption profile of **3″**.

The H_2O adsorption profile for **3′** shows a gradual uptake with increasing pressure and reaches an amount of 112 mL g^{-1} (P/P_0 = 0.99) without any step. The water adsorption profile

of **3″** shows a gradual uptake up to P/P_0 = 0.42 (uptake volume = 60 mL g^{-1}) and then the rate of uptake increases which ends at P/P_0 = 0.99 with a final amount of 166 mL g^{-1}(Fig. 26b). Like the previous cases the inclusion of H_2O molecule is easier in **3″** compare to **3′** at low P/P_0. Compound **3″** takes 22 mL g^{-1} at P/P_0= 0.065 while the uptake of **3′** is 8 mL g^{-1} at the same pressure (Fig. 26a). The βE_0 value of **3″** (6.87 kJ mol^{-1}) is larger than **3′** (4.5 kJ mol^{-1}) reflecting the hydrophilic nature of **3″**.

The MeoH adsorption profile of 3 shows a gradual uptake up to P/P_0 = 0.1 and a sudden jump occurs at this point. After that it shows type-I curve and reaches a final uptake of 60 mL g^{-1} at P/P_0 = 0.99. When the same experiment was performed with **3″** the final uptake was 75 mL g^{-1} with a sudden jump at P/P_0 =0.11. In both cases the desorption curve does not follow the adsorption one and shows large hysteresis indicating the hydrophilic nature of the channels (Fig27).

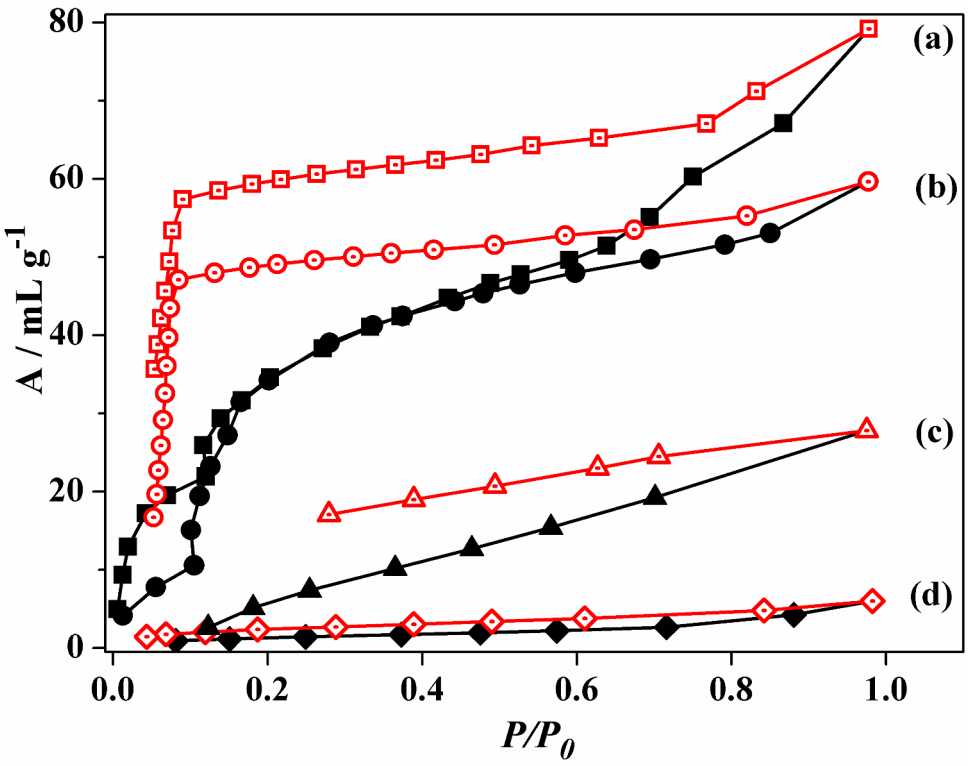

Fig. 27: Methanol adsorption profile of **3″** (a), **3′** (b) and Ethanol adsorption profile of **3″**(c), **3′** (d)

CH_3CN and EtOH sorption studies suggest only surface sorption as revealed by their type-II sorption properties. The size of these adsorbates is larger than the pore size, correlating the non-inclusion of such organic vapors in the dehydrated compound of **1**, **2**, and **3** (Fig. 21, 24 and 27).

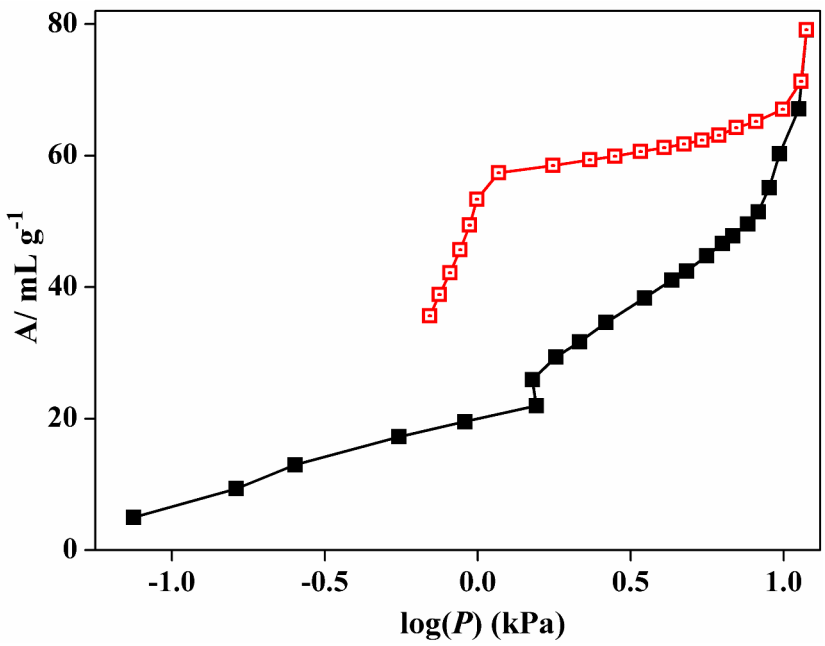

Fig. 28: Figure showing steps in the methanol adsorption profile of **3″**.

But CO_2 (kinetic diameter, 3.4 Å) and N_2 (kinetic diameter, 3.6 Å) adsorption studies at 195 K and 77 K reveal a very less amount of uptake indicating nonporous nature of the dehydrated phase **1**, **2** and **3**. This may be due to the smaller channel size compare to kinetic diameter of CO_2 and N_2.

2.2.5: ***Conclusion***

We have successfully synthesised three new co-crystals by exploiting the simple molecular building unit of $[Fe(CN)_6]^{4-}$ or $[Fe(CN)_6]^{3-}$ and protonated 1,2-bis(4-pyridyl)ethylene molecule. We have also successfully determined their structures by X-Ray crystallography. We have measured solvent adsorption property of the dehydrated form of three compounds. Stepwise uptake was observed when they are activated under vacuum at room temperature. But the same was not observed when they are evacuated at 100 ºC and the final uptake also differ from the previous one. This may be due to the structural change, takes place when they were heated under vacuum. Currents efforts are going on to investigate different co-crystals and discover the nature of different non-covalent interactions.

2.2.6: ***References:***

1. (*a*) K. Huang, D. Britton, M.C. Etter, S.R. Byrn, *J. Mater. Chem.* **1997**, *7*, 713.
2. (*a*) K. Endo, T. Koike, T. Sawaki, O. Hayashida, H. Masuda, Y. Aoyama, *J. Am. Chem. Soc.* **1997**, *119,* 4117; (*b*) R. Martinez-Manez, R. Sancenon, *Chem. Rev.* **2003**, *103*, 4419; (*c*) G.S. Kottas, L.I. Clarke, D. Horinek, J. Michl, *Chem. Rev.* **2005**, *105*,1281; (*d*) R.J. Sarma, J.B. Baruah, *Cryst. Growth Des.* **2007**, *7*, 989; (*e*) Filipe A.A. Paz, J. Klinowski, *CrystEngComm* **2003**, *5*, 238.
3. (*a*) B. Chen, C. Liang, J. Yang, D. S. Contreras, Y. L. Clancy, E. B. Lobkovsky, O. M. Yaghi, S. Dai, *Angew. Chem., Int. Ed.* **2006**, *45*, 1390. (*b*) Z. Zhang, S. Xiang, Y. S. Chen, S. Ma, Y. Lee, T. Phely-Bobin, B. Chen, *Inorg. Chem.* **2010**, *49*, 8444; (*c*) B. Chen, S. Xiang, G. Qian, *Acc. Chem. Res*. **2010**, *43*, 1115.
4. (*a*) B.Q. Ma, Y. Zhang, P. Coppens, *Cryst. Growth Des. 2* (**2002**) 7; (*b*) B.Q. Ma, Y. Zhang, P. Coppens, *Cryst. Growth Des.* **2001**, *1*, 271; (*c*) L. R. MacGillivray, J.L. Reid, J.A. Ripmeester, *Chem. Commun.* **2001**, 1034; (*d*) S. Hoger, D. L. Morisson, V. Enkelman, *J. Am. Chem. Soc.* **2002**, *124*, 6734.
5. P. J. Langley, J. M. Rawson, J. N. B. Smith, M. Schuler, R. Bachmann, A. Schweiger, F. Palacio, G. Antorrena, G. Gescheidt, A. Quintel, P. Rechsteiner and J. Hulliger, *J. Mater.Chem.*, **1999**, *9*, 1431.
6. M. E. Brown and M. D. Hollingsworth, *Nature,* **1995**, *376*, 323.
7. V. Ramamurthy and D. F. Eaton, *Chem. Mater*., **1994***, 6*, 1128.
8. F. Toda, S. Hyoda, K. Okada and K. Hirotsu, *J. Chem. Soc., Chem. Commun*., **1995**, 1531.
9. (*a*) K. Endo, T. Koike, T. Sawaki, O. Hayashida, H. Masuda and Y. Aoyama, *J. Am. Chem.Soc*., **1997,** *119*, 4117. (*b*) Yoo, S.; Ryu, J. Y.; Lee, J. Y.; Kim, C.; Kim S.; Kim Y. Dalt. Trans **2003**, 1454
10. (*a*) J. C. MacDonald, G.M. Whitesides, *Chem. Rev.* **1994**, *94*, 2383; (*b*) J.F. Remenar, S.L. Morissette, M. L. Peterson, B. Moulton, J. M. MacPhee, H.R.Guzmán, Ö. Almarsson, *J. Am. Chem. Soc.* **2003**, *125*, 8456; (*c*) S.L. Childs, L.J. Chyall, J.T. Dunlap, V.N. Smolenskaya, B.C. Stahly, G.P. Stahly, *J. Am. Chem. Soc.* **2004**, *126*, 13335; (*d*) G. Bettinetti, M.R. Caira, A. Callegari, M. Merli, M. Sorrenti, C. Tadini, *J.Pharm. Sci.* **2000**, *89*, 478; (*e*) N. Schultheiss, A. Newman, *Cryst. Growth Des.* **2009**, *9*, 2950; (*f*) B. R. D. Walsh, M. W. Bradner, S. Fleischman, L. A. Morales, B. Moulton, N. Rodrı´guez-Hornedo, M. J. Zaworotko, *Chem. Commun.* **2003**, 186; (*g*)

I. D. H. Oswald, D. R. Allan, P. A. McGregor, W. D. S. Motherwell, S. Parson, C. R. Pulham, *Acta Crystallogr., Sect. B: Struct. Crystallogr. Cryst. Chem*. **2002**, *B58*, 1057; (*h*) P. Vishweshwar, J. A. McMahon, J. A. Bis, M. J. Zaworotko, *J. Pharm. Sci.* **2006**, *95*, 499.

11. (*a*) C. L. Chen and A. M. Beatty, *J. Am. Chem. Soc.*, **2008**, *130***,** 17222; (*b*) M. B. Dewal, M. W. Lufaso, A. D. Hughes, S. A. Samuel, P. Pellechia and L. S. Shimizu, *Chem. Mater.,* **2006**, *18*, 4855; (*c*) S. A. Dalrymple and G. K. H. Shimizu, *Chem. Commun.,* **2006**, 956; (*d*) A. Hazra.; P. Kanoo.; S. Mohapatra.; G. Mostafa.; T. K. Maji.; *CrystEngComm* **2010**, *12*, 2775.
12. (*a*) T. Friščić, A. V. Trask, W. D. S. Motherwell and W. Jones, *Cryst*. *Growth Des*. **2008**, *8*, 1605; (*b*) G. J. Halder, C. J. Kepert, B. Moubaraki, K. S. Murray and J. D. Cashion, *Science,* **2002**, *298*, 1762.
13. (*a*) K. R. Seddon, M. J Zaworotko; *Crystal Engineering: The Design and Application of Functional Solids*; NATO-ASI Series; Kluwer: Dordrecht, The Netherlands, **1999**; Vol. 539; (*b*) D. J. W. *Nat. Re*V. *Drug Disco*V*ery*, **2004**, *3*, 42; (*c*) *Making Crystals by Design-from Molecules to Molecular Materials, Methods, Techniques, Applications*; Grepioni, F.; Braga, D. Eds.; Wiley-VCH: Weinheim, Germany, **2007**.
14. R. J. Davey, N. Blagden, G. D. Potts and R. Docherty, *J. Am. Chem. Soc.*, **1997**, *119*, 1767.
15. (*a*) A. Gavezzotti and G. Fillipini, *J. Am. Chem. Soc.*, **1996**, *118*, 7153; (*b*) S. L. Price and K. S. Wibley, *J. Phys. Chem. A.*, **1997**, *101*, 2198.
16. G. Patrick Stahly, *Crystal Growth Des,* **2007**, *7,*1007.
17. One general example: T. Friščić, W. Jones, *Cryst. Growth Des* **2009**, *9*, 1621.
18. T. Friščić,, S. L. Childs, S. A. A. Rizvi, W. Jones, *CrystEngComm* **2009**, *11*, 418.
19. One general example: Weyna, D. R.; Shattock, T.; Vishweshwar, P.; Zaworotko, M. J. *Cryst. Growth Des* **2009,** *9*, 1106.
20. N. Blagden, D. J. Berry, Parkin, A.; H. Javed,; Ibrahim, A.; Gavan, P. T.; De Matos, L. L.; Seaton, C. C. *New J. Chem.* **2008**, *32*, 1659.
21. Computational attempts are ongoing to predict cocrystal formation. Issa, N.; Karamertzanis, P. G.; Welch, G. W. A.; Price, S. L. *Cryst. Growth. Des.* **2009**, *9*, 442.
22. (*a*) C. B. Aakeroy, D. J. Salmon *CrystEngComm*, **2005**, *7*, 439; (*b*) G. R. Desiraju, *Angew. Chem., Int. Ed.*. **1995**, *34*, 2311; (*c*) T. Steiner, *Angew. Chem. Int. Ed.* **2002**, *41*, 48; (*d*) C. B. Aakeröy,; N. Schultheiss, Assembly of Molecular Solids via Non-covalent Interactions, In *Making Crystals by Design-from Molecules to Molecular*

Materials, Methods, Techniques, Applications; Grepioni, F.; Braga, D. Eds.; Wiley-VCH: Weinheim, Germany, **2007**; (*e*) T. R. Shattock, K. K. Arora, P. Vishweshwar, M. J. Zaworotko, *Cryst. Growth Des.* **2009**, *8*, 4533.

Chapter-3

High Heat of Hydrogen Adsorption and Guest-Responsive Magnetic Modulation in a 3D Porous Pillared-Layer Coordination Framework

Abstract:

A bimetallic pillared-layer coordination framework, **{[Mn_3(bipy)$_3$(H_2O)$_4$][Cr(CN)$_6$]$_2$·2(bipy)·4(H_2O)}$_n$** has been constructed using a cyanometallate anion ($[Cr(CN)_6]^{3-}$) and an organic linker (4,4′-bipyridyl) that provides high heat of hydrogen adsorption (~11.5 kJ mol^{-1}) and shows guest dependent magnetic modulation.

3.1: ***Introduction***

Metal-organic frameworks (MOFs) or porous coordination polymers (PCPs) are promising materials for applications in gas storage, separation, sensing, catalysis, magnetism, drug delivery etc.[1] Multifunctional materials, *i.e*. materials which combine a set of well defined properties (e.g. porosity and magnetism, porosity and optical) for specific applications are gaining importance recently.[1a,e,2] Such synergism, where two different functionalities are combined, would open up the possibility and prospect of finding novel physical phenomena for designing smart materials. Magnetism has generic dependence on distance while the porosity is enhanced with long linkers and hence combination of these two is not always easy or straightforward. A rational concept and design approach would be to choose a polycyanometallate anion, $[(M_A(CN)_n]^{m-}$ (n = 2-8), as a hub which can link to another metal M_B to create a magnetic path way M_B–NC–M_A–CN–M_B.[3] Once the magnetic platform has been constructed, it can be further linked by a long organic pillar (e.g. 4.4′-bipyridyl) to invoke porosity in the material. Presence of porosity provides the opportunity to study gas storage property, selectivity as well as guest-dependent magnetism[4] and magnetic sensing which are of particular interest for applications such as magnetic devices and sensors (Scheme 1).[2b,5] Several fascinating properties like guest-dependent spin crossover,[4d,6] magnetic ordering sensitive to guest removal/exchange,[7] and different magnetic behaviour corresponding to reversible solvent-induced structural changes[8] have been reported in porous magnets. On the other hand, the porous property of MOFs are gaining increased attention with time and the framework materials have emerged as an excellent storage alternative to high pressure and liquefied hydrogen tanks.[1a,9] In this respect, recent reports indicate that presence of unsaturated metal site (UMS) is crucial for strong interaction of H_2 molecule and also largely enhances the value of enthalpy of adsorption.[10,] Hence, it will be very promising for hydrogen storage material if we can incorporate UMS in a framework along with the permanent porosity.

3.2: ***Scope of the Study***

Here we have tried to combine various aspects: (i) use of cyanometallate anion, $[Cr(CN)_6]^{3-}$ as magnetic hub; (ii) use of long linker 4,4′-bipyridyl (bipy) to invoke porosity; (iii) generation of UMSs to enhance enthalpy of hydrogen adsorption, together in a single

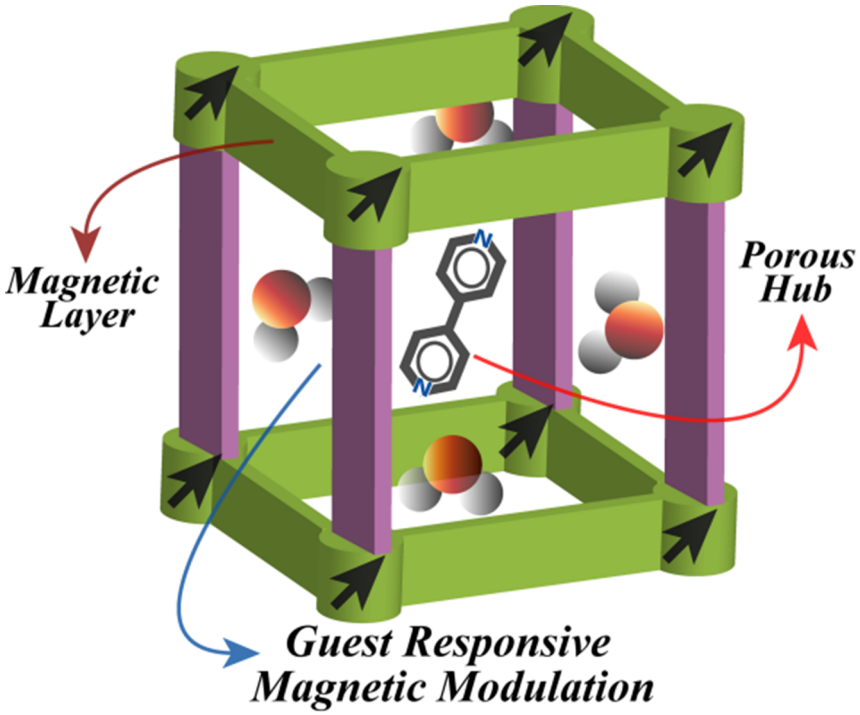

Scheme 1 Bimodal functionality in a framework material.

framework in cyanometallate systems for the first time, to the best of our knowledge (Scheme 1).

We have shown a new recipe for synthesizing a new $Mn^{II}Cr^{III}$ framework, $\{[Mn_3(bipy)_3(H_2O)_4][Cr(CN)_6]_2 \cdot 2(bipy)\cdot 4(H_2O)\}_n$ (**1**) (bipy = 4,4′-bipyridyl)that exhibits guest-dependent magnetic modulation and selective sorption of CO_2/H_2 over N_2. It is noteworthy that presence of UMSs in the framework leads to a very high value of enthalpy of adsorption for H_2 and is close to the highest reported value of 13.5 kJ mol^{-1}.[10b]

In this chapter, we will demonstrate the guest influenced magnetic modulation in a 3D porous framework along with the impact of UMS, present on the pore surface, on high affinity of the framework towards hydrogen molecule.

3.3: *Experimental Section*

3.3.1: *Materials*

All the reagents and solvents employed were commercially available and used as supplied without further purification. $K_3[Cr(CN)_6]$, bipy and $MnCl_2 \cdot 4H_2O$ were obtained from the Aldrich Chemical Co.

3.3.2: *Synthetic procedure*

Synthesis of $\{[Mn_3(bipy)_3(H_2O)_4][Cr(CN)_6]_2 \cdot 2(bipy) \cdot 4(H_2O)\}_n$ (1): An aqueous solution (12.5 mL) of $K_3[Cr(CN)_6]$ (0.25 mmol, 0.0426 g) was added to an ethanolic solution (12.5 mL) of bipyridyl (0.25 mmol, 0.039 g) and stirred for 30 min. $MnCl_2 \cdot 4H_2O$ (0.25 mmol, 0.0494 g) was dissolved in 12.5 ml distilled water and 2.5 mL of this metal solution was carefully layered with the 2.5 mL of mixed bipy and $K_3Cr(CN)_6$ solution using a ethanol : water buffer solution (1 mL, 1:1) in a crystal tube. After 15 days, transparent block crystals were appeared in the middle of the tube and separated and washed with ethanol (Yield ~ 60 %). The bulk amount of the sample was prepared by the direct mixing of the reagents in ethanol/water mixed solution with stirring for 24 h and the phase purity was checked with the PXRD and elemental analysis. This powdered sample was used for studying of different physical properties. IR: ν(C≡N) 2125, 2154 and 2170 cm^{-1}; ν(C=C): 1608 cm^{-1}, 1536 cm^{-1}; ν(O-H): 3477 cm^{-1} and 3592 cm^{-1}. Anal. cald. for $C_{62}H_{56}Cr_2Mn_3N_{22}O_8$: C, 49.44; H, 3.75; N, 20.46. Found: C, 48.98; H, 3.31; N, 20.66%.

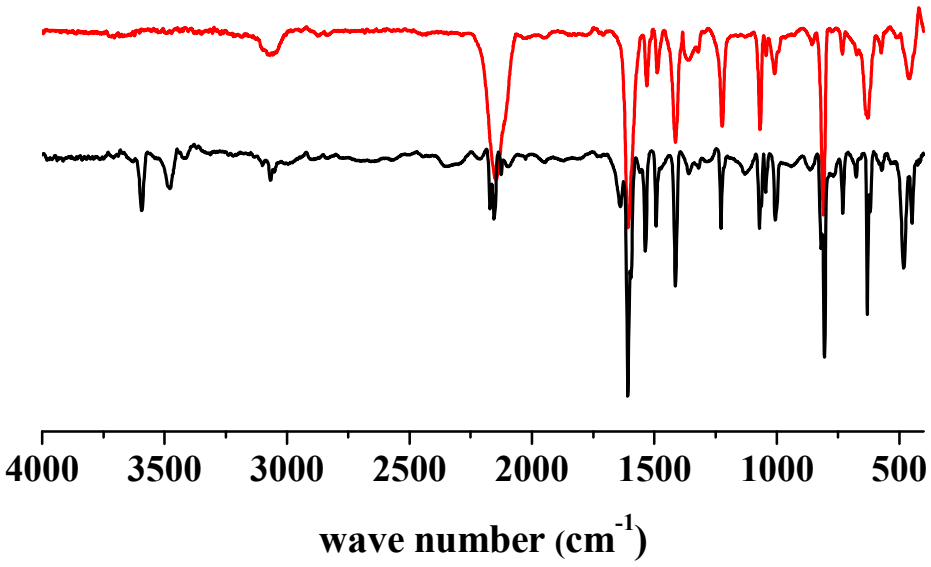

Fig. 1: IR spectra of **1** and **1a**.

Preparation of {[$Mn_3(bipy)_3$][$Cr(CN)_6$]$_2$} (1a): Compound **1a** was prepared by heating **1** at 165 ºC under vacuum (< 10^{-1} Pa) for 72 hours. This powdered sample was used for characterization of different physical properties. IR: ν(C≡N) 2162 cm^{-1}; ν(C=C): 1603 cm^{-1}, 1531 cm^{-1}. Anal. cald. for $C_{42}H_{22}Cr_2Mn_3N_{18}$: C, 48.16; H, 2.12; N, 24.07. Found: C, 47.52; H, 1.92; N, 23.66%.

Preparation of {[$Mn_3(bipy)_3$][$Cr(CN)_6$]$_2$·$8H_2O$} (1b): Compound **1b** was prepared by exposing water vapour into **1a** for 6 days. Anal. cald. for $C_{42}H_{38}Cr_2Mn_3N_{18}O_8$: C, 42.33; H, 3.21; N, 21.16. Found: C, 41.92; H, 3.34; N, 20.96%.

3.3.3: ***Physical Measurements***

The elemental analyses were carried out on a Thermo Fisher Flash 2000 Elemental Analyzer. Thermogravimetric analyses (TGA) was carried out with a METTLER TOLEDO TGA850 instrument under nitrogen atmosphere. IR spectra were recorded in the region 4000-400 cm^{-1} on a Bruker IFS 66v/S spectrophotometer with samples prepared in KBr pellets. Powder X-ray diffraction (PXRD) data were collected on a Bruker D8 Discover instrument using Cu-*K*α radiation.

3.3.4: ***Single Crystal X-ray Diffraction***

Suitable single crystal of compound **1** was mounted on a thin glass fibre with commercially available super glue. X-Ray single crystal structural data was collected on a Bruker Smart-CCD diffractometer equipped with a normal focus, 2.4 kW sealed tube X-ray source with graphite monochromated Mo-Kα radiation (λ = 0.71073 Å) operating at 50 kV and 30 mA. The data was collected at 296 K. The program SAINT[14] was used for integration of diffraction profile and absorption correction was made with SADABS[15] program. The structure was solved by SIR 92[16] and refined by full matrix least squares method using SHELXL-97.[17]The non-hydrogen atoms were refined anisotropically. The hydrogen atoms were fixed by HFIX command and placed in ideal positions (except for H_2O molecules which were located from Fourier map). Potential solvent accessible area or void space was calculated using the PLATON 99[18] multipurpose crystallographic software. The coordinates, anisotropic displacement parameters and torsion angles are available as ESI in CIF format. All crystallographic and structure refinement data of the compound **1** is summarized in Table 1. All calculations were carried out using SHELXL-97,[17] PLATON 99,[18] SHELXS-97[19] and WinGX system, Ver 1.70.01.[20]

3.3.5: *Adsorption Study*

N_2, H_2 and CO_2 adsorption studies were carried out with the dehydrated samples of **1** (i.e. **1a**, prepared at 438 K under high vacuum (<10^{-1} Pa) for 72 hours) by using QUANTACHROME QUADRASORB *SI* analyzer at 77 and 195 K, respectively. High-pressure hydrogen adsorption isotherm measurements at 77 and 87 K were carried out on a fully computer controlled volumetric BELSORP-HP, BEL JAPAN high pressure instrument. The hydrogen used for the high pressure measurements is of scientific/research grade with 99.999% purity. For the measurements, approximately 200 mg of sample was taken in a stainless-steel sample holder and degassed at 438 K for about 72 hours. Dead volume of the sample cell was measuredusing helium gas of 99.999% purity. Non-ideal correction for hydrogen gas was made by applying virial coefficients at the measurement temperature.

3.4: *Results and Discussion*

3.4.1: *Structural description of 1 ($\{[Mn_3(bipy)_3(H_2O)_4][Cr(CN)_6]_2\cdot 2(bipy)\cdot 3H_2O\}_n$)*

Single crystal X-ray crystallographic structure determination reveals that **1** is a neutral 3D coordination architecture of Mn(II) built by $[Cr(CN)_6]^{3-}$ and bipy with the formulation $\{[Mn_3(bipy)_3(H_2O)_4][Cr(CN)_6]_2\cdot 2(bipy)\cdot 3(H_2O)\}_n$.

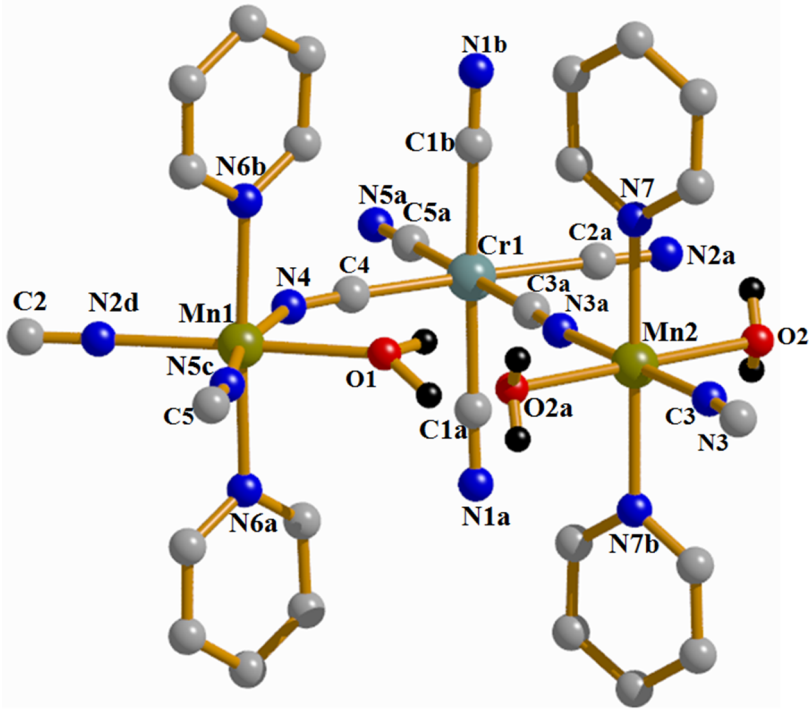

Fig. 2: View of coordination environment around Mn1, Mn2 and Cr1 in **1**. Symmetry codes: a = 2-x, 1-y, z; b = 2-x, 1-y, 1-z; c = 2.5-x, 0.5-y, 1-z; d = -0.5+x, 1.5-y, 1-z.

There are two crystallographically independent Mn (Mn1 and Mn2) atoms in the asymmetric unit and each octahedral Mn1 is coordinated to three CN groups from three different $[Cr(CN)_6]^{3-}$, one water molecule (O1) and two bipy, whereas each octahedral Mn2 is coordinated two CN groups, two bipy and two water molecules (O2, O2*) (Fig. 2). Both Mn1 and Mn2 are slightly distorted from the perfect octahedron as reflected in the *cisoid* angles (83.52–89.97 º**)** for Mn1 and (90.00–94.58 º**)** for Mn2. The Mn-N and Mn-O bond distances are in the range of 2.1854–2.2755 Å and 2.2125–2.2694 Å, respectively. In the 2D layers, the twelve-membered $Mn1_2Cr1_2(CN)_4$ ring surrounded by six eighteen-membered $Mn1Mn2_2Cr1_3(CN)_{12}$ rings and each 2D layer connected by the bipy linker through the Mn(II) centres forms a 3D pillared-layer network (Fig. 3, 5) with two kind of channels along the *c*-axis (Fig. 6).

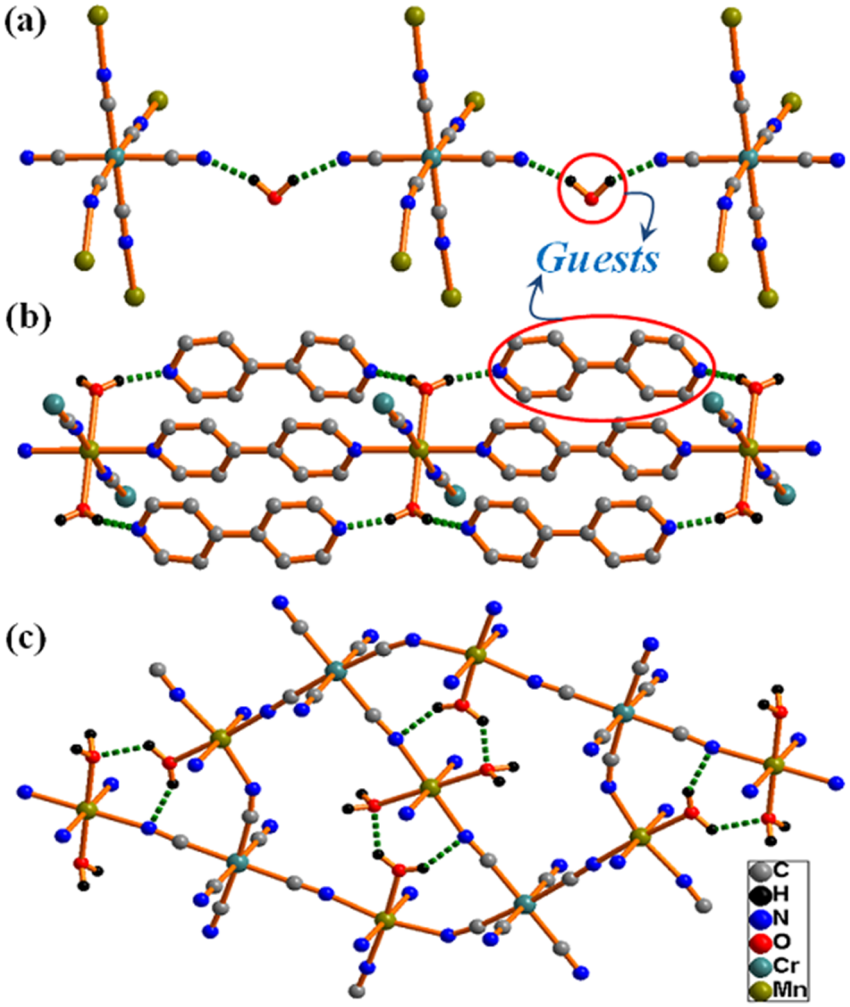

Fig. 3: The supramolecular interaction in **1**; (a) Two neighbouring Cr1 centres interact via N-H-O hydrogen bonding of coordinated CN and guest H_2O molecule, (b) Two Mn2 centres interact via hydrogen bonding of coordinated H_2O and guest bipy molecule, (c) In the 2D layer, coordinated water molecules are involved in H-bonding with each other and also with the CN groups.

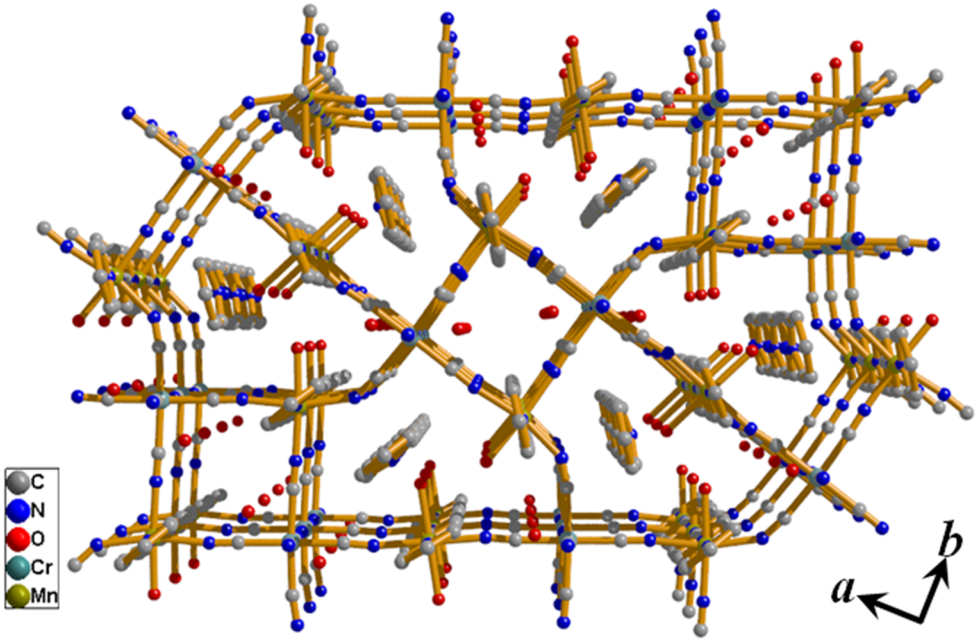

Fig. 4: 3D view of compound **1** along *c* direction shows two different type of channels; one square occupied by water molecules and the other distorted triangular occupied by water and guest bipy molecules.

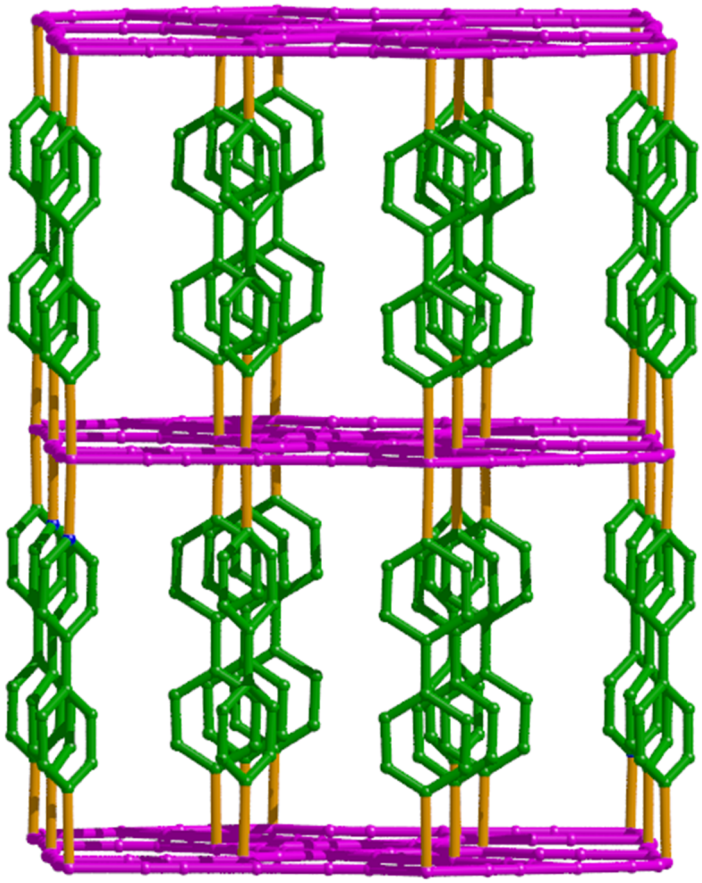

Fig. 5: Pillared-layer structure of **1**. The layers formed by $[Cr(CN)_6]^{3-}$ and Mn^{II} are shown in pink colour and the pillars (bipy) are shown in green colour.

Examination with TOPOS[23] reveals that **1** is a tri-nodal (4-c)3(5-c)2-periodic 3D net formed by 5-connected (5-c) Mn- nodes, (4-c) Cr-nodes and (2-c) bipy and CN linkers. In a layer, the vertex symbol for Mn1, Mn2 and Cr1 points are represented by Schläfli symbols, $\{4.6^8.8\}$, $\{6^5.8\}$and $\{4.6^5\}$, respectively. Further examination shows that **1** adopts an unprecedented network topology with the Schläfli symbol $\{4.6^5\}_2\{4.6^8.8\}_2\{6^5.8\}$. The square-shaped smaller channel (2.8 × 2.2 $Å^2$) contains two water molecules and the large channel (7.7 × 5.5 $Å^2$) contains one water and bipy molecule as guests, both of which providing about 34% void spaces to the total crystal volume. Thus, **1** acts as a biporous host. Upon removal of the coordinated water molecules, framework shows 40.3% void space to the total volume with coordinatively unsaturated Mn(II) centers on the pore surface (Fig 6).

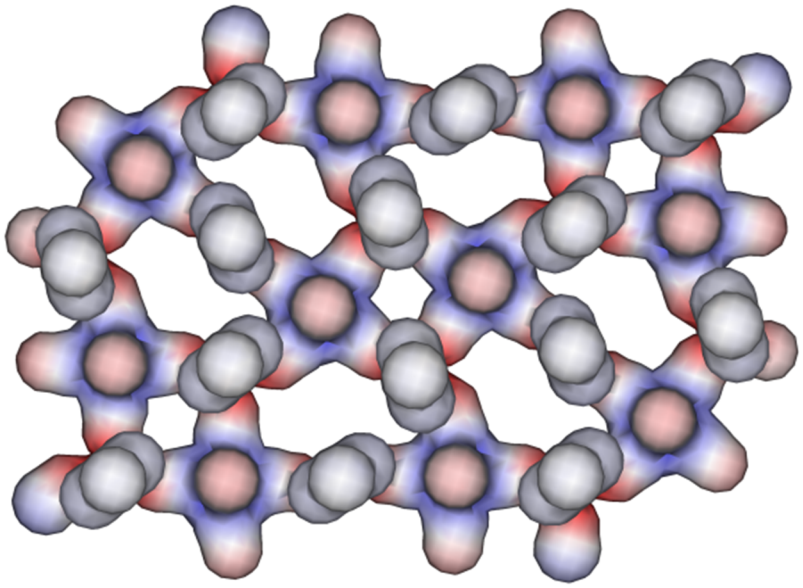

Fig. 6: View of two different kind of channels in **1** along *c* direction.

The guest water molecules O3 and O4 are H-bonded (O3···O4, 3.027Å) to each other, and O3 also making a bridge between the two layers through N1 of the pendant CN group (N1···O3, 2.944 Å). The guest bipy undergoes strong face to face and edge to face π–π interactions with two different coordinated bipy (cg···cg distances are in the range of 3.689–5.210 Å) linkers connected to Mn1 and Mn2 centres (Fig. 3). In the 3D network, separation between the layers through Mn(II)-bipy-Mn(II) is 11.628Å while in the 2D layer, the Mn1–Cr1 and Mn2–Cr1 distances are 5.230 Å and 5.240 Å , respectively.

Table S1: Crystal data and structure refinement parameters for compound 1

Parameter	Compound 1
Formula	$C_{62}H_{56}Cr_2Mn_3N_{22}O_8$
M	1506.06
crystal system	Orthorhombic
space group	*P*bam
a [Å]	16.7961(4)
b [Å]	18.1575(4)
c [Å]	11.6335(2)
α [º]	90
β [º]	90
γ [º]	90
V [Å^3]	3547.93(13)
Z	2
T[K]	296
μ[mm^{-1}]	0.883
ρ_c [g/cm^3]	1.405
F (000)	1528
reflections [$I>2\sigma(I)$]	3380
Unique reflections	3815
measured reflections	33673
GOF	1.35
$R_1[I>2\sigma(I)]$[a]	0.0947
$R_w[I>2\sigma(I)]$[b]	0.2279
$\Delta\rho$ max/min [e Å^{-3}]	0.092/-1.17

[a] $R = \sum||Fo|-|Fc||/\sum|Fo|$; [b] $R_w = [\sum\{w(Fo^2-Fc^2)^2\}/\sum\{w(Fo^2)^2\}]^{1/2}$

3.4.2:*Framework stability: Thermogravimetric (TG) and PXRD analyses*

Thermal studies were carried out to analyse the stability and integrity of the framework (Fig. 7). TG analysis under nitrogen flow suggests two-step release of guest and coordinated water molecules (obs. 9.1 %; calcd. 9.55 %) in the temperature range 40 – 180 ºC. However, when **1** is heated at 165 ºC under high vacuum (to prepare **1a**) we observed loss of guest bipy together with guest and coordinated water molecules. This was confirmed

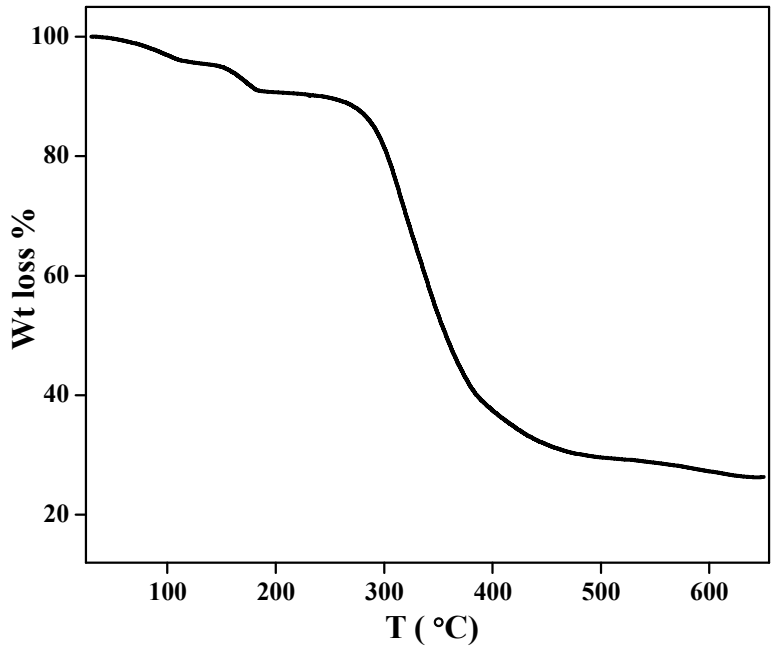

Fig. 7: TGA of **1** recorded under N_2 atmosphere in the temperature range 30 – 650 ºC.

by IR spetroscopy and elemental analysis.

Powder X-ray diffraction (PXRD) pattern of $\{[Mn_3(bipy)_3][Cr(CN)_6]_2\}$(**1a**) recorded after heating the sample at 165 ºC under vacuum suggests the 3D framework structure remains intact even it sustains loss of water (guest and coordinated) and guest bipy molecules (Fig. 8). However, decraese in intensity of peaks in **1a** indicate crystallinity of the deguest sample decreases.

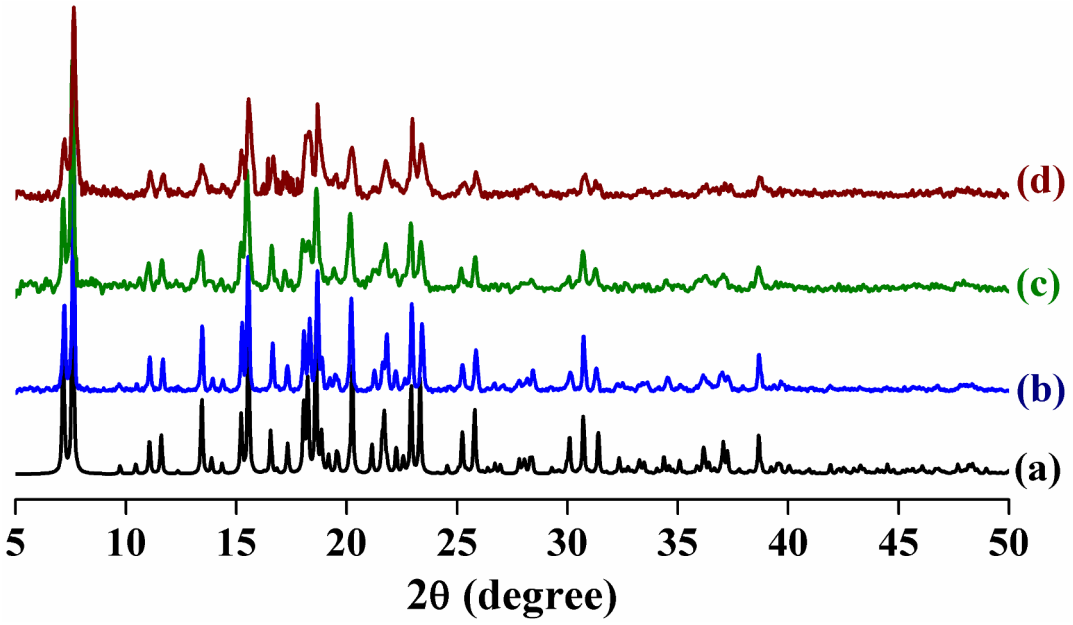

Fig. 8: PXRD plot of **1** at different states: (a) simulated; (b) assynthesized; (c) heated at 165 ºC under vacuum for 72 hrs and (d) rehydrated.

3.4.3: *Adsorption measurement*

Gas adsorption study: The desolvated framework **1a** was used for gas adsorption studies to establish the permanent porosity of the compound. N_2 adsorption at 77 K reveals a type II profile indicating only surface adsorption (Fig. 9).

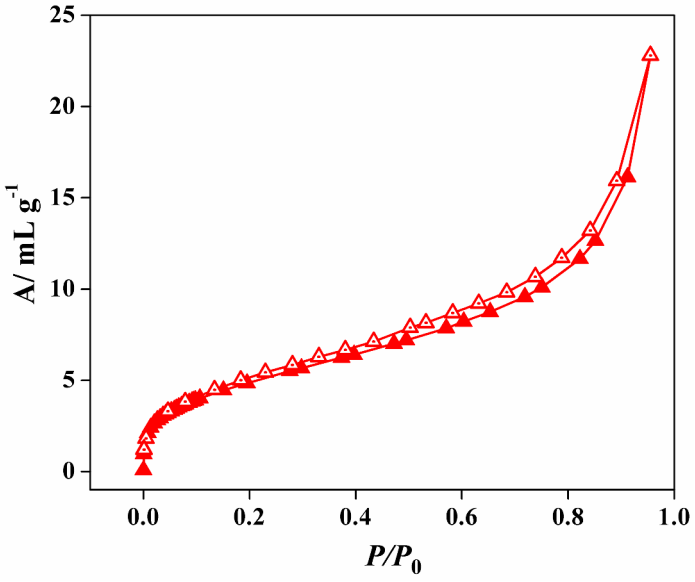

Fig. 9: N_2 adsorption isotherm of **1a** at 77K. ((P_0 is the saturated vapour pressure of N_2 at the measurement temperature).

On the contrary, CO_2 adsorption measurement at 195 K shows a typical type I profile with steep uptake at low pressure regions (Fig. 10). The Langmuir surface area calculated from CO_2 profile turns out to be 353 $m^2 g^{-1}$.

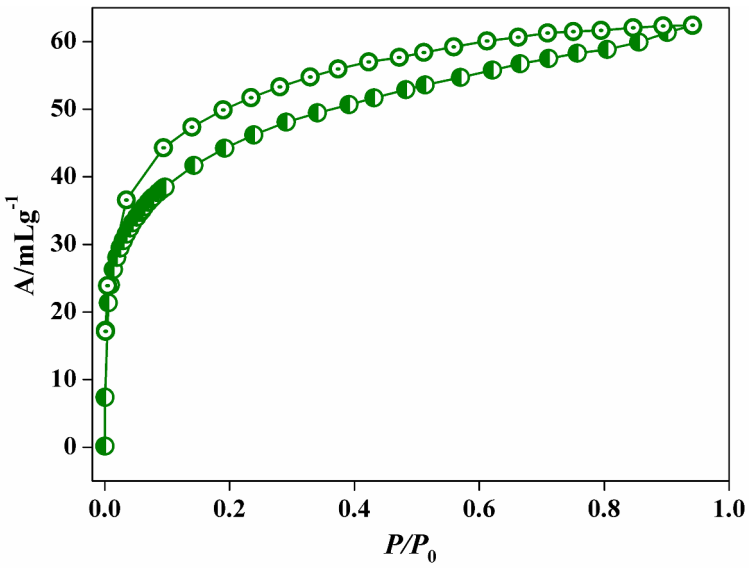

Fig. 10: CO_2 adsorption isotherm of **1a** at 195K which shows a small histeresis.

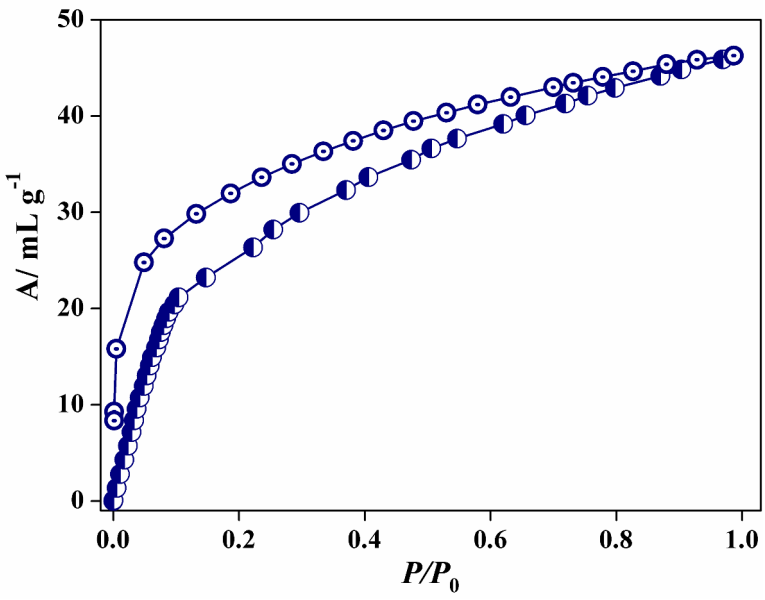

Fig. 11: H_2 adsorption isotherm of **1a** at 77 K (P_0 is the saturated vapour pressure of H_2 at the measurement temperature).

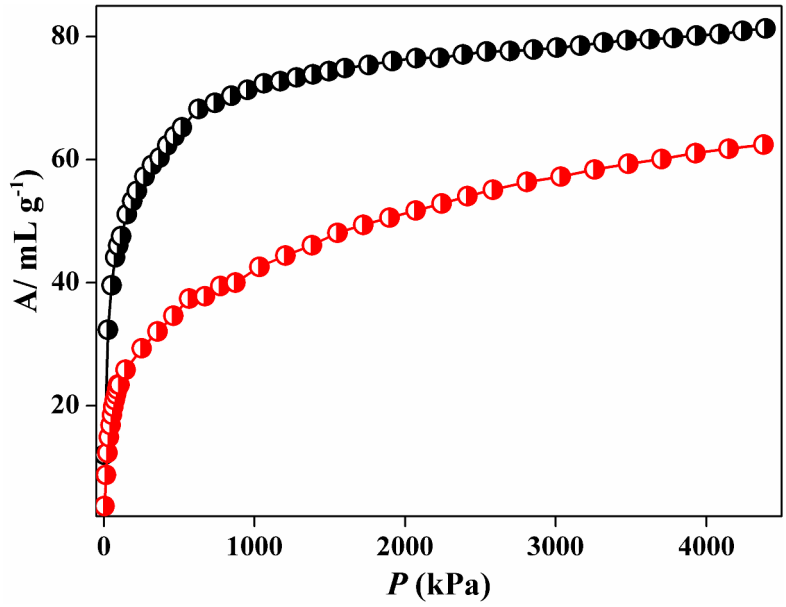

Fig. 12: High pressure H_2 isotherm (only adsorption) of **1a** measured at 77 K (black) and 87 K (Red).

The hysteretic sorption and large isosteric heat of adsorption, (q_{st},ϕ) value of ~34.3 kJ mol^{-1} (calculated using Dubinin-Radushkevich equation[12]) suggests strong interaction of CO_2 molecules with **1a**. This could be correlated with the well established fact where the electric field generated in the framework by UMSs and aromatic π-cloud interacts firmly with the quadrupole momentof CO_2 (-1.4×10^{-39} Cm^2) causing rapid uptake at low pressure.

1a was also tested for its H_2-storage capacity at cryogenic temperature. High pressure

adsorption measurement at 77 K reveals a type I profile with very steep uptake at low pressure and the final uptake volume is ~81 mLg^{-1} at ~ 45 bar. Interestingly, a careful measurement at 77 K and low pressure (P ~ 1 atm) (Fig. 11) shows a prominent hysteresis in the adsorption profile suggesting strong interaction of H_2 molecules with the pore surface.

The high pressure profiles measured at 77 and 87 K (Fig. 12) were used for the calculation of enthalpy of adsorption (ΔH_{ads}) applying Clausius-Clapeyron equation which provides a value of ~11.5 kJ mol^{-1} (Fig. 15).[10a] The high value of ΔH_{ads} can be linked to the highly polar nature of **1a** decorated with cyanide groups (free as well as coordinated) and unsaturated Mn^{II} sites (Mn1 and Mn2) which bind H_2 molecules strongly in the pore. This is also in line with the hysteresis obtained from the low pressure measurement. It is noteworthy that the value of ΔH_{ads} obtained for **1a** is one of the highest among the reported values.[10]

Analysis of Gas Adsorption Isotherms: Hydrogen adsorption isotherms were fitted to the Langmuir-Freundlich[21] equation instead of the more commonly used Langmuir equation.[22] An accurate fit was obtained by using this equation which results a precise prediction over the quantity of hydrogen adsorbed at saturation. A variant of the Clausius-Clapeyron equation was used to calculate enthalpy of adsorption.

$$l\,n\left(\frac{P_1}{P_2}\right) = \Delta H_{a\,d\,s} \times \left(\frac{T_2 - T_1}{R \times T_2 T_1}\right)$$

Where, P_n is = Pressure for isotherm n

T_n = Temperature for isotherm n

R = Universal Gas constant = 8.314 J mol^{-1} K^{-1}

Pressure as a function of amount of adsorption was determined by using the Langmuir-Freundlich fit for each isotherm.

$$\frac{Q}{Q_m} = \frac{B \times P^{\left(\frac{1}{t}\right)}}{1 + \left(B \times P^{\left(\frac{1}{t}\right)}\right)}$$

Where, Q = moles adsorbed

Q_m = moles adsorbed at saturation

P = Pressure

B and t = constant

By rearranging this equation we get

$$P = \left(\frac{\frac{Q}{Q_m}}{B - \left(B \times \frac{Q}{Q_m}\right)}\right)^t$$

Substituting this into Clausius-Clapeyron equation we get

$$\Delta H_{ads} = \frac{R \times T_1 \times T_2}{T_2 - T_1} \ln \frac{\left(\frac{\frac{Q}{Q_{m\,1}}}{B_1 - (B_1 \times \frac{Q}{Q_{m\,1}})}\right)^{t_1}}{\left(\frac{\frac{Q}{Q_{m\,2}}}{B_2 - (B_2 \times \frac{Q}{Q_{m\,2}})}\right)^{t_2}}$$

Where, the subscript 1 and 2 are representing the data corresponding to 77 and 87 K respectively.

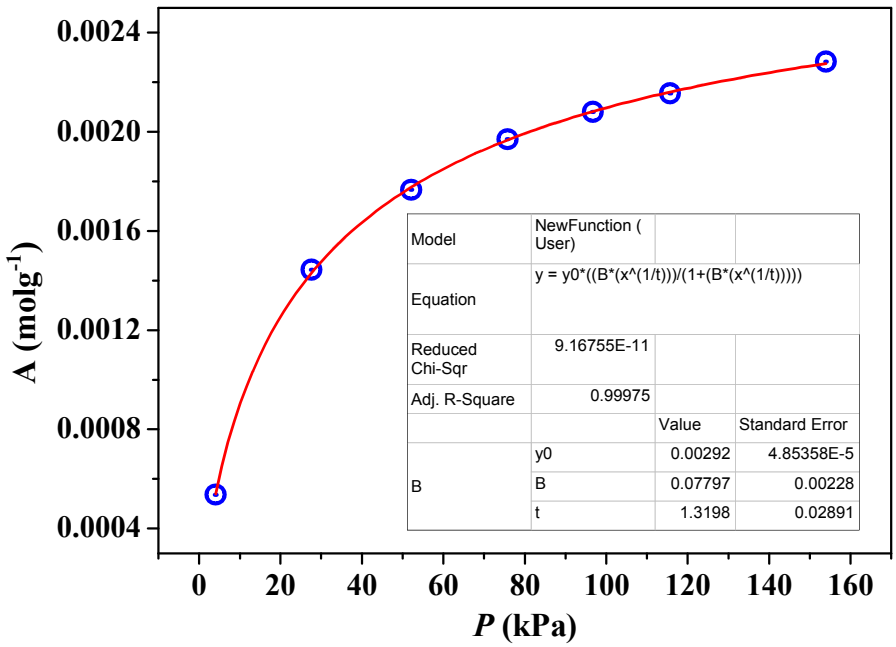

Fig. 13: H_2 adsorption isotherm for **1a** at 77 K. The solid line represents the best fit to the data using the Langmuir-Freundlich equation, as described above.

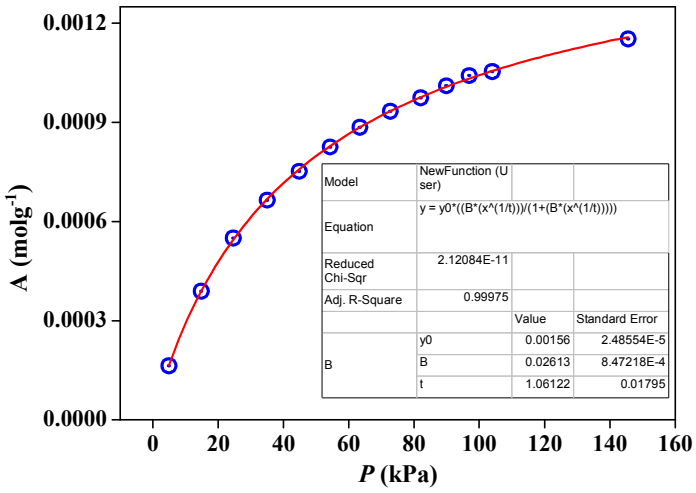

Fig. 14: H_2 adsorption isotherm for **1a** at 87 K. The solid line represents the best fit to the data using the Langmuir-Freundlich equation, as described above.

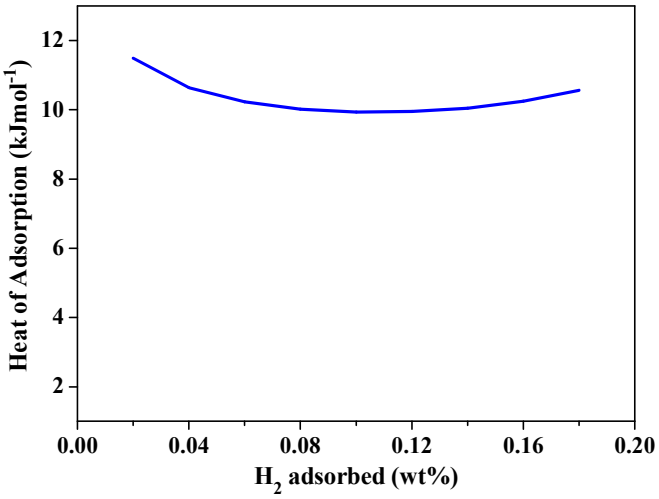

Fig. 15: Enthalpy of H_2 adsorption for **1a** calculated using Clausius-Clapeyron equation.

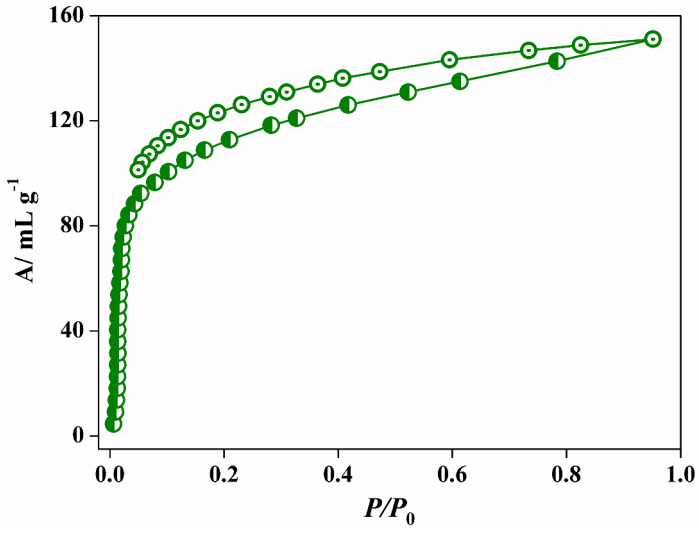

Fig. 16: H_2O adsorption isotherm of **1a** which exhibit typical type-I curve.

The polar nature of **1a** is also reflected in H_2O sorption that display unsusual type I profile (Fig. 16) with steep uptake at low pressure region where the framework shows uptake of eight water molecules resulting in $\{[Mn_3(bipy)_3][Cr(CN)_6]_2 \cdot 8H_2O\}$ (**1b**).

3.4.4: ***Magnetic Measurement***

We have successively measured magnetic data of assynthesized **1**, **1a** and **1b** (rehydrated). The dc magnetic susceptibilities are shown in the form $\chi_M T$ vs T (**1** and **1a**) in Fig. 18.

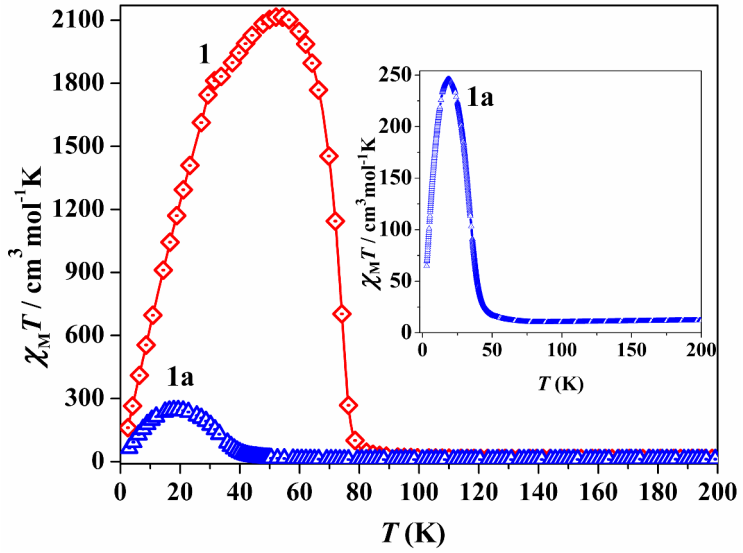

Fig. 18: Temperature dependence of the magnetic susceptibility of **1** and **1a** in an applied field of 500 Oe under zero field cooled condition. Inset shows the same for **1a** to give a clear understanding of ordering at low T.

The χ_M value for **1** at 300 K is 0.0531 cm^3 mol^{-1} ($\chi_M T$=16.17 cm^3 mol^{-1} K) which agrees well with the spin only value (0.0558 cm^3 mol^{-1}; 16.74 cm^3 mol^{-1} K) expected for magnetically isolated three Mn^{II} (S = 5/2) and two Cr^{III} (S = 3/2) ions. The $\chi_M T$ value gradually decreases with decreasing temperature to reach a minimum value of 14.96 cm^3 mol^{-1} K at 85 K, and then rapidly increases to a maximum value of 2114.96 cm^3 mol^{-1} K at 53 K and then again decreases to 161.65 cm^3 mol^{-1} K at 2.5 K. The $1/\chi_M$ vs T plot in the temperature range of 300 – 150 K obeys the Curie-Weiss law (Fig. 19) with a Weiss constant θ = -39.3 K, which suggest the antiferromagnetic interaction between the adjacent Mn^{II} and Cr^{III} ions through cyanide bridges as has already been observed.[13] The rapid increase in $\chi_M T$ value indicates a ferrimagnetic ordering, which was determined accurately as 80 K by dM/dT differential plot (Fig. 20).

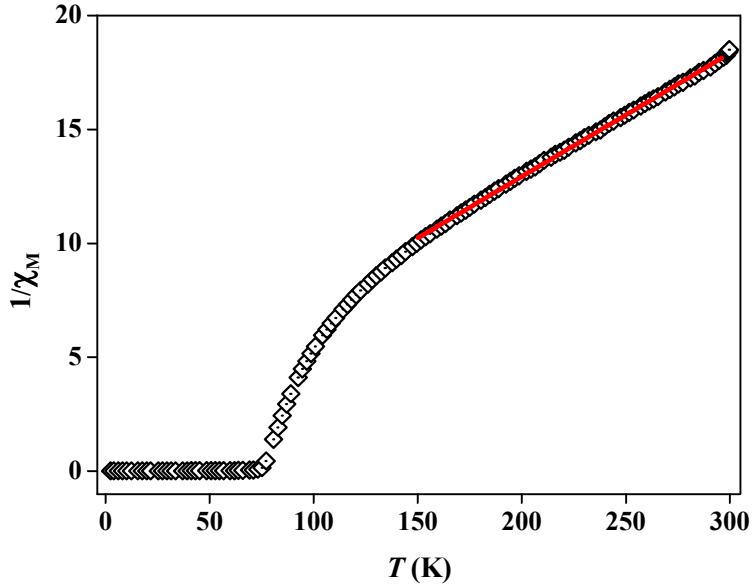

Fig. 19: Curie–Weiss fitting of **1** above 150 K with C = 18.50 $cm^3K\ mol^{-1}$, and θ = -39.3 K.

The decrease in $\chi_M T$ value after 53 K suggests further interaction between the layers through the bipy linker. The magnetic data of **1a** also shows a typical ferrimagnetic ordering below 50 K and dM/dT plot suggest the Tc is about 45.3 K (Fig. 21). The Weiss constant θ was calculated as -59.8 K (300 -150 K, Fig. S17)) suggesting stronger antiferromagnetic interaction in **1a** compared to **1** (Fig. 22). The change in Weiss constant, Tc and maxima in the $\chi_M T$ value suggest there are changes in the magnetic pathways in **1a**. The value of Tc depends on the overall magnetic interaction via covalent (cyanide or as well as bipy bridges) and noncovalent interactions (like H-bond, π-π interactions).

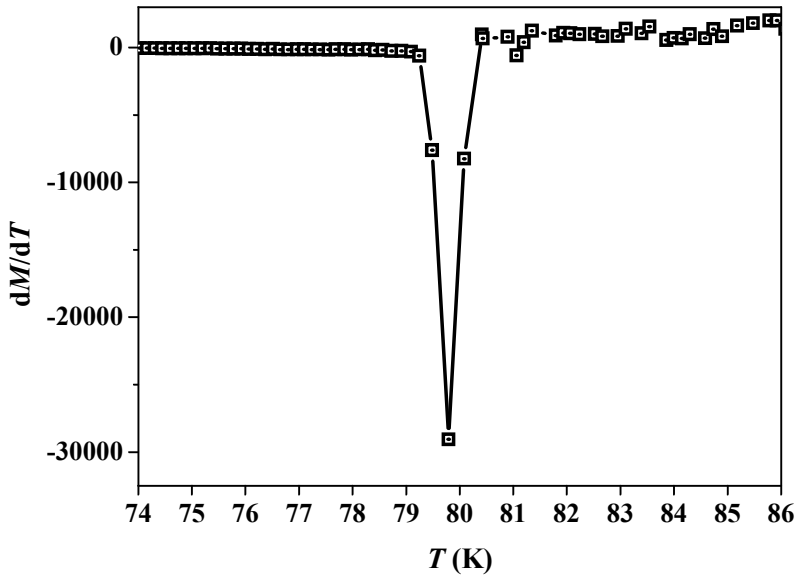

Fig. 20: dM/dT plot for **1**.

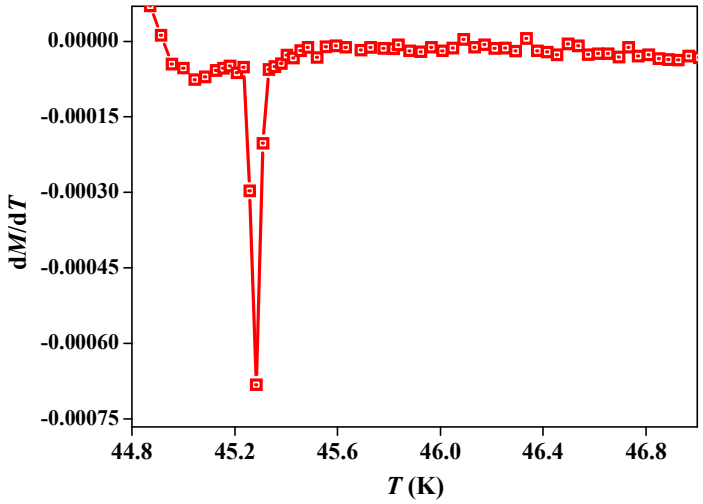

Fig. 21: d*M*/d*T* plot for **1a**.

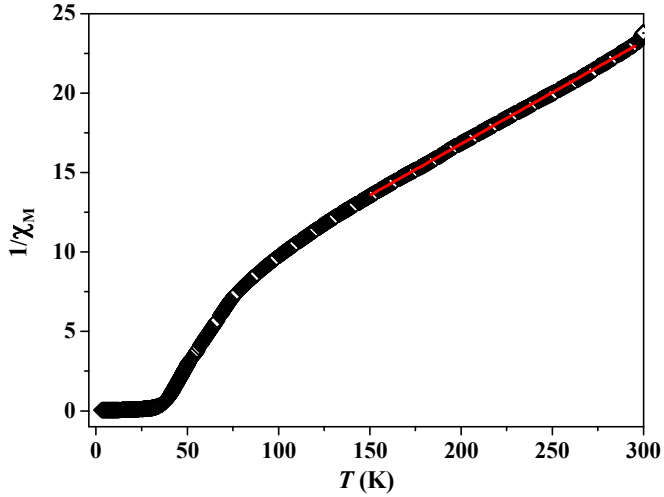

Fig. 22: Curie–Weiss fitting of **1a** above 150 K with C = 15.46 $cm^3K\ mol^{-1}$, and θ = -59.8 K.

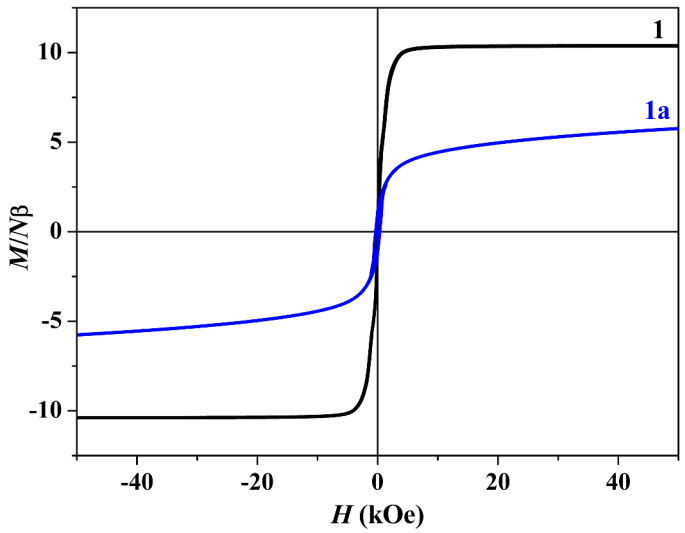

Fig. 23: Magnetization plot for **1** and **1a** measured at 2.5 K.

In **1a** upon removal of the guest water, bipy and coordinated water molecules all the H-bonding interactions (Fig. 3) (*vide supra*) between the magnetic centres are destroyed. These noncovalent interactions provide ferro-magnetic interactions in **1** and their absence in **1a** might be responsible for lowering the Curie temperature. Moreover, the structural strain in deguest phase (like bent Cr-CN-Mn pathway) also provides the negative contribution of *T*c.[3c]

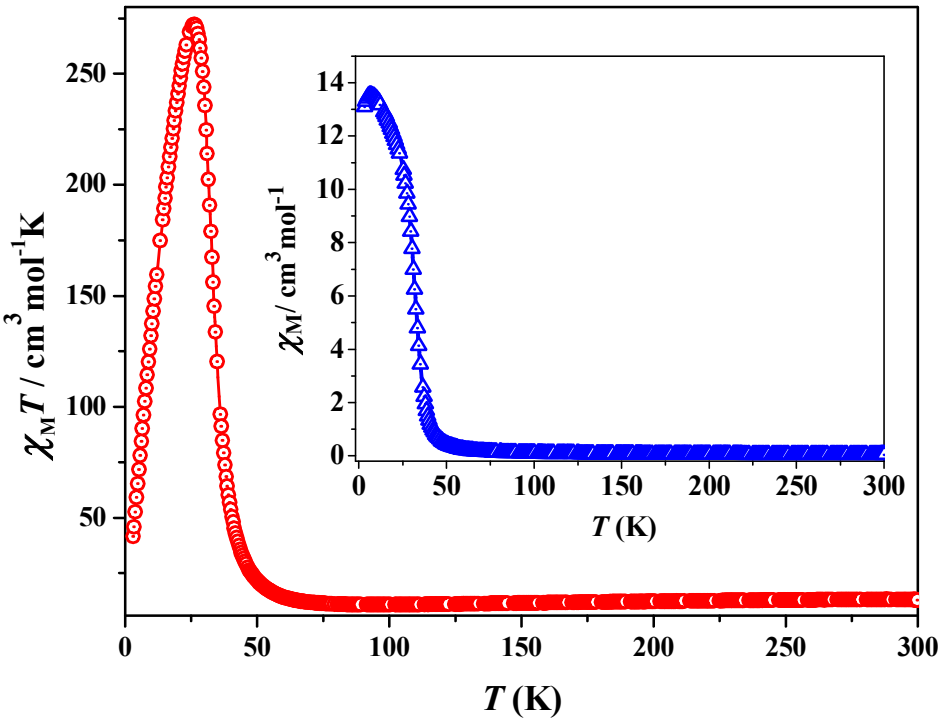

Fig. 24: Temperature dependence of the magnetic susceptibility ($\chi_M T$) of **1b** in an applied field of 500 Oe under zero field cooled condition. Inset shows the χ_M vs T plot for **1b** measured at 500 Oe under zero field cooled condition.

The increase in *T*c (59 K) in **1b** (Fig. 24 - 26) also unequivocally suggests the role of water molecules in ferromagnetic interactions as they are involved in several H-bonding interactions. The field dependence magnetization curve of **1** shows rapid increase to saturate at 8 kOe which is also the signature of magnetic ordering within the compound (Fig. 23).

The saturation magnetization value in **1** is 10 *N*β which is in good agreement with the theoretical value (9 *N*β) expected for a ferrimagnet where antiferromagnetic coupling between Cr^{III} and Mn^{II} exists. The decrease in magnetization value (6 *N*β) in **1a** at high field suggests strong antiferromagnetic interaction operating between Cr^{III} and Mn^{II} which is also in line with observed high weiss constant and low *T*c.

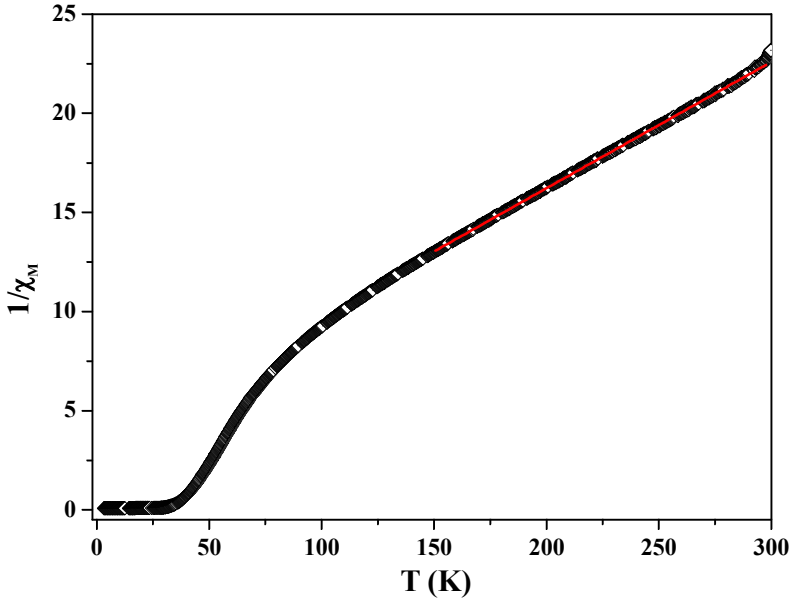

Fig. 25: Curie–Weiss fitting of **1b** above 150 K with C = 15.68 $cm^3K\ mol^{-1}$, and θ = -54.5 K.

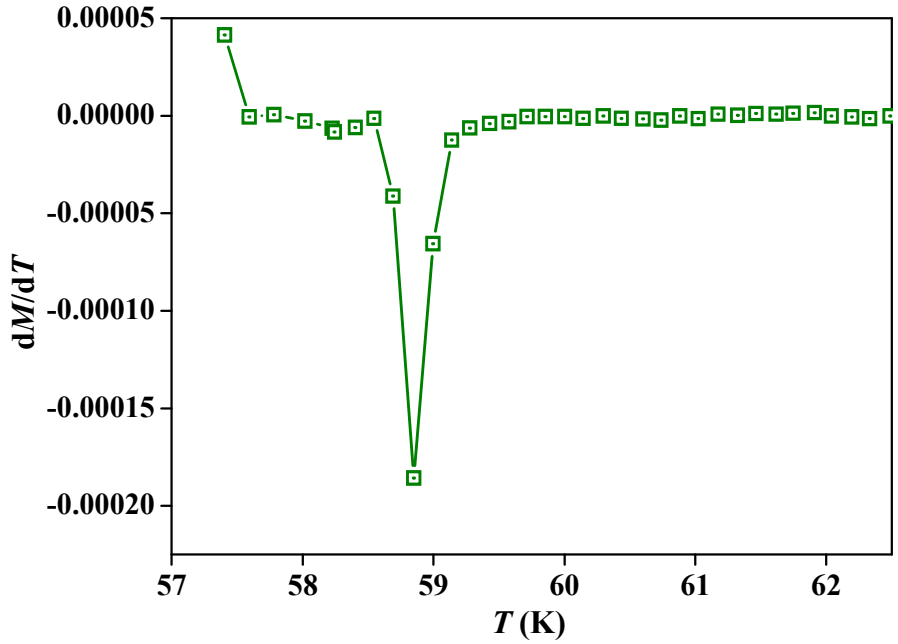

Fig. 26: dM/dT plot for **1b.**

3.5: ***Conclusion***

In conclusion, we have conceived a rational strategy to assemble 2D magnetic layers into a 3D rigid porous framework that exhibits permanent porosity and ferrimagnetic ordering at low temperature. The highly polar nature of **1a** was found to be exceedingly promising for high heat of H_2 adsorption and establishes itself to be the first member of cyanometallate

systems having heat of H_2 adsorption value of ~11.5 kJ mol^{-1}. The framework demonstrates interesting guest responsive magnetic modulation with change in *Tc* as observed from dc susceptibility measurements. Current efforts are underway to synthesize frameworks with different pillar modules and study their porosity and magnetic properties.

3.6: ***References:***

1. (*a*) L. J. Murray, M. Dincă and J. R. Long, *Chem. Soc. Rev.*, **2009**, *38*, 1294; (*b*) S. Kitagawa, R. Kitaura and S. Noro, *Angew. Chem. Int. Ed.*, **2004**, *43*, 2334; (*c*) J. R. Li, R. J. Kuppler and H. -C. Zhou, *Chem. Soc. Rev.*, **2009**, *38*, 1477; (*d*) J. Lee, O. K. Farha, J. Roberts, K. A. Scheidt, S. T. Nguyen and J. T. Hupp, *Chem. Soc. Rev.*, **2009**, *38*, 1450; (*e*) D. Maspoch, D. Ruiz-Molina and J. Veciana, *Chem. Soc. Rev.*, **2007**, *36*, 770; (*f*) S. Achmann, G. Hagen, J. Kita, I. M. Malkowsky, C. Kiener and R. Moos, *Sensors*, **2009**, *9*, 1574; (*g*) P. Horcajada, C. Serre, G. Maurin, N. A. Ramsahye, F. Balas, M. Vallet-Regi, M. Sebban, F. Taulelle and G. Férey, *J. Am. Chem. Soc.*, **2008**, *130*, 6774; (*h*) P. Kanoo, R. Matsuda, M. Higuchi, S. Ktagawa and T. K. Maji, *Chem. Mater.*, **2009**, *21*, 5860.
2. (*a*) N. R. Champness, *Dalton Trans.*, **2006**, 877; (*b*) C. J. Kepert, *Chem. Commun.*, **2006**, 695; (*c*) Z. M. Wang, B. Zhang, Y. J. Zhang, M. Kurmoo, T. Liu, S. Gao and H. Kobayashi, *Polyhedron*, **2007**, *26*, 2207; (*d*) P. Kanoo, K. L. Gurunatha and T. K. Maji, *J. Mater. Chem.* **2010**, *20*, 1322.
3. (*a*) M. Ohba, K. Yoneda and S. Kitagawa, *CrystEngComm*, **2010**, *12,* 159; (*b*) T. Mallah, S. Thiebaut, M. Verdaguer and P. Veillet, *Science*, **1993**, *262*, 1554; (*c*) W. Kaneko, M. Ohba and S. Kitagawa, *J. Am. Chem. Soc.*, **2007**, *129*, 13706.
4. (*a*) X. N. Cheng, W. X. Zhang, Y. Y. Lin, Y. Z. Zheng and X. M. Chen, *Adv. Mater.*, **2007**, *19,* 1494; (*b*) M. Kurmoo, H. Kumagai, K. W. Chapman and C. J. Kepert, *Chem. Commun.*, **2005**, 3012; (*c*) D. Maspoch, D. Ruiz-Molina, K. Wurst, N. Domingo, M. Cavallini, F. Biscarini, J. Tejada, C. Rovira and J. Veciana, *Nat. Mater.*, **2003**, *2*, 190; (*d*) G. J. Halder, C. J. Kepert, B. Moubaraki, K. S. Murray and J. D. Cashion, *Science*, **2002**, *298*, 1762.
5. (*a*) D. Maspoch, D. Ruiz-Molina and J. Veciana, *J. Mater. Chem.*, **2004**, *14*, 2713; (*b*) E. Coronado, F. Palacio and J. Veciana, *Angew. Chem. Int. Ed.*, **2003**, *42*, 2570.

6. *(a)* V. Niel, A. L. Thompson, M. C. Munoz, A. Galet, A. S. E. Goeta and J. A. Real, *Angew. Chem. Int. Ed.*, **2003**, *42*, 3760; (*b*) Z. M. Wang, B. Zhang, H. Fujiwara, H. Kobayashi and M. Kurmoo, *Chem. Commun.*, **2004**, 416; (*c*) M. Kurmoo, H. Kumagai, M. Akita-Tanaka, K. Inoue and S. Takagi, *Inorg. Chem.*, **2006**, *45*, 1627.
7. (*a*) M. H. Zeng, X. L. Feng, W. X. Zhang and X. M. Chen, *Dalton Trans.*, **2006**, 5294; (*b*) L. G. Beauvais and J. R. Long, *J. Am. Chem. Soc.*, **2002**, *124*, 12096.
8. (*a*) K. Barthelet, J. Marrot, D. Riou and G. Férey, *Angew. Chem. Int. Ed.*, **2002**, *41*, 281; (*b*) C. Livage, N. Guillou, J. Chaigneau, P. Rabu, M. Drillon and G. Férey, *Angew. Chem. Int. Ed.*, **2005**, *44*, 6488; (*c*) C. Serre, F. Millange, C. Thouvenot, M. Nogues, G. Marsolier, D. Louer and G. Férey, *J. Am. Chem. Soc.*, **2002**, *124*, 13519.
9. K. M. Thomas, *Dalton Trans.*, **2009**, 1487.
10. (*a*) S. S. Kaye and J. R. Long, *J. Am. Chem. Soc.*, **2005**, *127*, 6506; (*b*) J. G. Vitillo, L. Regli, S. Chavan, G. Ricchiardi, G. Spoto, P. D. C. Dietzel, S. Bordiga and A. Zecchina *J. Am. Chem. Soc.*, **2008**, *130*, 8386; (*c*) B. Chen, X. Zhao, A. Putkham, K. Hong, E. B. Lobkovsky, E. J. Hurtado, A. J. Fletcher and K. M. Thomas, *J. Am. Chem. Soc.*, **2008**, *130*, 6411; (*d*) S. Mohapatra, K. Hembram, U. Waghmare and T. K. Maji, *Chem. Mater.* **2009**, *21*, 5406.
11. T. K. Maji, S. Pal, K. L. Gurunatha, A. Govindaraj and C. N. R. Rao, *Dalton Trans.*, **2009**, 4426.
12. M. M. Dubinin, *Chem. Rev.*, **1960**, *60*, 235.
13. (*a*) Y. Yoshida, K. Inoue, and M. Kurmoo, *Chem*. *Lett*., **2008**, *37*, 586; (*b*) T. Glaser, M. Heidemeier, T. Weyhermüller, R. D. Hoffmann, H. Rupp and P. Müller, *Angew. Chem. Int. Ed.*, **2006**, *45*, 6033; (*c*) A. Marvilliers, S. Parsons, E. Rivière, J. P. Audière and T. Mallah, *Chem. Commun.*, **1999**, 2217.
14. SAINT+, 6.02 ed.; Bruker AXS: Madison, WI, **1999**.
15. G. M. Sheldrick, *SADABS, Empirical Absorption Correction Program*; University of Göttingen, Göttingen, Germany, **1997**.
16. Altomare, G. Cascarano, C. Giacovazzo and A. Gualaradi, *J. Appl. Crystallogr.*, **1993**, *26*, 343.
17. G. M. Sheldrick, SHELXL 97, *Program for the Solution of Crystal Structure*, University of Göttingen, Germany, **1997**.
18. A. L. Spek, *J. Appl. Crystallogr.*, **2003**, *36*, 7.
19. G. M. Sheldrick, SHELXS 97, *Program for the Solution of Crystal Structure*, University of Göttingen, Germany, 1997.

20. L. J. Farrugia, WinGX - A Windows Program for Crystal Structure Analysis, *J. Appl. Crystallogr.*, **1999**, *32*, 837.
21. R. T. Yang, *Gas Separation by Adsorption Processes*; Butterworth:Boston, 1997.
22. F. Roquerol, J. Rouquerol, K. Sing, *Adsorption by Powders and Solids:Principles, Methodology, and Applications*; Academic Press: London,**1999**.
23. (*a*) V. A. Blatov, A. P. Shevchenko and V. N. Serezhkin, *J. Appl. Crystallogr.*, **2000**, *33*, 1193; (*b*) V. A. Blatov, L. Carlucci, G. Ciani and D. M. Proserpio, *CrystEngComm***, 2004**, *6*, 377.

Chapter 4

Highly Selective CO_2 uptake in 3D Porous Frameworks of $[M(CN)_6]^{3-}$ (M = Fe, Cr) and Zn(II): Effect of Change in Pillar Modules and it's Ratio

Abstract:

In this chapter, we describe the synthesis, single crystal structural characterization and adsorption properties of four 3D metal-organic frameworks, $\{[Zn_3(bipy)_3(H_2O)_4][Fe(CN)_6]_2\cdot 2(bipy)\cdot 3H_2O\}_n$ (**1**); $\{[Zn_3(bipy)][Fe(CN)_6]_2\cdot 3H_2O\}_n$ (**2**); $\{[Zn_3(azpy)_2(H_2O)_2][Fe(CN)_6]_2\cdot 4H_2O\}_n$ (**3**) and $\{[Zn_3(bipy)_3(H_2O)_4][Cr(CN)_6]_2\cdot 2(bipy)\cdot 3H_2O\}_n$ (**4**) (bipy = 4,4′-bipyridyl and azpy = 4,4′-azobipyridyl). Compounds **1**-**4** have been successfully isolated by varying the organic linkers (bipy and azpy) and their ratios during the synthesis at RT. Compounds **1** and **4** crystallizes in orthorhombic space group, *Pbam* while **2** and **3** in monoclinic space groups, *C*2/*m* and *C*2/*c*, respectively. Frameworks **1**, **2** and **4** are structurally fascinating as they feature bi-porous networks. At 195K, compounds **1**-**4** selectively adsorb CO_2 while completely exclude other small gas molecules like N_2, Ar, O_2. High value of heat of hydrogenation at cryogenic temperatures suggest strong interaction of H_2 molecules with the unsaturated Zn(II) metal sites and as well as with the pore surface. A detail study of gas and solvent vapour adsorption of compounds **1**- **4** have been accounted in the chapter.

4.1: ***Introduction***

Infinitely extended metal–ligand networks with metal nodes and bridging organic linkers are well known as coordination polymers or metal–organic frameworks (MOFs).[1]As compared to traditional zeolites porous coordination polymers (PCPs) or MOFs have several advantages such as high surface area, feasibility of tunable pore size, modifiable pore surface which has dragged immense interest to the chemist as well as material scientist[2]. These novel functional crystalline materials shows promising applications in the area of gas storage, separation, catalysis, drug delivery, ion exchange and sensing etc[3]. The moderate coordination bond energies, variable metal coordination geometries, and flexible organic linkers have geared up themselves as a perfect material for the storage of small molecules (e.g. H_2, CH_4, CO_2 etc.) and the separation of gases from their mixture[4].

One of the greatest problem that agitates our society, concerns with the environmental friendly and economically favourable separation, capture and storage of greenhouse gases and in particular CO_2 gas which has paramount importance in the future world of economy. CO_2 is the main greenhouse gas emitted from the combustion of fossil fuels in power plants and automobiles and is considered as a threat in the context of global warming. The relationship between atmospheric CO_2 and increased temperature has been well recognized and the effect of increasing atmospheric CO_2 concentration on global warming is now regarded as one of the most crucial environmental issues. To reduce the atmospheric CO_2 level along with adjusting the world economic impact, four strategies have been proposed: (1) carbon sequestration, (2) less carbon-intensive fuels, (3) more energy-efficient methods, and finally (4) increased conservation. Under such a circumstance the development of viable carbon capture and sequestration technologies (CCSTs) is a scientific challenge of the highest prior[5,6]. Several approaches such as chemical conversion, solvent absorption, deep-sea deposition and chemisorption (using amine-based systems)[7] have been developed but have been found very costly and not efficacy.

In near future, use of less carbon intensive fuels e.g. natural gas[8] will help the environment by emitting lesser amounts CO_2 where the major component of natural gas is CH_4. On the other hand, CO_2 is often found as a major impurity in natural gas and its presence can reduce the efficiency of natural gas. The appropriate solution of this problem is to find separate storage materials for pure CO_2 and CH_4 and it is also important to separate them from their mixture.

Apart from that, separation between different gas mixtures like N_2/O_2, N_2/H_2, N_2/CH_4 is also a challenging job for material scientists.

CO_2 adsorption by metal-organic frameworks (MOFs)[9] was first reported by Yaghi and co-workers and it has been claimed that porous MOFs have great potential in CCST, as the CO_2 storage property of MOFs is greater than that of other classes of porous solids. This can be attributed to their modular nature that they can be decorated with organic and inorganic moieties which is suitable for molecular recognition of CO_2. Kitagawa et. al. have reported a coordination material which possess a chiral open channels with nitrogen rich walls which selectively adsorbs CO_2 and O_2 over N_2.[10] Further investigation by this group produced a smart porous material whose pore size and structural flexibility are suitable for CO_2 capture and it exhibits highly selective adsorption of CO_2 from a ternary gas mixture of O_2, N_2 and CO_2.[11]

4.2: ***Scope of the present study***

The emerging application of MOF in various fields makes them in the list of highly sought after material. Porous MOFs have emerged as new zeolite alternative and attracted considerable research interest in the past decade[1e]. A combination of almost all metal ions in the periodic table with variety of organic linkers can afford a wide range of crystal structures as well as chemical compositions. The properties can be easily tuned by altering the metal and of course by modifying the length and/or the functionalization of the organic linkers.

Our target was to synthesize a smart multifunctional material which can exhibit a set of well-defined properties (e.g. porosity and magnetism, porosity and optical). We have deliberately chosen $[M(CN)_6]^{3-}$ (M = Fe, Cr) as metalo-ligand which can link other metal centres to generate a 2D array. Further connection between these 2D arrays with organic pillars (e.g. 4,4′-bipyridyl, 4,4′-azobipyridyl) leads to open pillared-layer framework with permanent pore filled with guest molecules. In this present work, the metallo-ligands $[M(CN)_6]^{3-}$ have been linked to Zn(II) to build a 2D network. The capability of adopting versatile geometry of Zn(II) makes it widely adorable metal for the construction of porous framework. The 2D layers are further connected by the organic pillars to construct 3D framework. We have also carefully tuned the concentration of ligand (bipy) to enquire the change in structural topology as well as the overall porosity in the framework. To invoke greater porosity, bipy was replaced by azpy which is comparatively longer than the previous one. In this chapter I shall

discuss about the structural variety, hydrogen adsorption and selective CO_2 adsorption of four newly synthesized, metal-organic frameworks $\{[Zn_3(bipy)_3(H_2O)_2][Fe(CN)_6]_2\cdot 2(bipy)\cdot 3H_2O\}_n$, (**1**) $\{[Zn_3(bipy)][Fe(CN)_6]_2\cdot 3H_2O\}_n$ (**2**) and $\{[Zn_3(azpy)_2(H_2O)_2][Fe(CN)_6]_2.4H_2O\}_n$ (**3**), $\{[Zn_3(bipy)_3(H_2O)_2][Cr(CN)_6]_2\cdot 2(bipy)\cdot 4H_2O\}_n$ (**4**) (bipy = 4,4′-bipyridyl; azpy = 4,4′-azobipyridyl).

4.3: ***Experimental Section***

4.3.1: ***Materials***

All the reagents and solvents employed were commercially available and used as supplied without further purification. $K_3[Fe(CN)_6]$, 4,4′-bipyridyl and $ZnCl_2$ were obtained from the Aldrich Chemical Co. 4,4′-Azobipyridyl has been synthesized according to the literature procedure.[19]

4.3.2: ***Synthetic procedure***

Synthesis of $\{[Zn_3(bipy)_3(H_2O)_2][Fe(CN)_6]_2\cdot 2(bipy)\cdot 3H_2O\}_n$ (1): An aqueous solution (12.5 mL) of $K_3[Fe(CN)_6]$ (0.25 mmol) was added to an ethanolic solution (12.5 mL) of bipy (0.5 mmol) and stirred for 30 min. $ZnCl_2$ (0.25 mmol) was dissolved in 12.5 mL distilled water and 2.5 mL of this metal solution was carefully layered with the 2.5 mL of mixed bipy and $K_3[Fe(CN)_6]$ solution using an ethanol:water buffer solution (1 mL, 1:1) in a crystal tube. After 15 days, yellow coloured block crystals were appeared in the middle of the tube and separated and washed with ethanol. The bulk amount of the sample was prepared by the direct mixing of the reagents in ethanol-water solution under stirring for 24 h and the phase purity was checked with the PXRD and elemental analysis. Yield: 77%, relative to Fe. Anal. Calcd for $C_{62}H_{50}Fe_2Zn_3N_{22}O_5$: C, 50.06; H, 3.39; N, 20.73. Found: C, 49.46; H, 3.48; N, 20.48. IR (KBr, cm^{-1}): $\nu(H_2O)$ 3490, 3426; ν(ArC-H) 3064, 3054; ν(C≡N) 2162, 2098; ν(ArC=C) 1609, 1537. IR spectrum of **1** (Fig. 1) shows strong and broad bands around 3490 cm^{-1} suggesting the presence of water molecules. A strong band around 2162 cm^{-1} corroborate to free ν(C≡N) stretching frequency and a band around 1609 cm^{-1} indicates the presence bipy molecule.

Preparation of {[Zn_3(bipy)$_3$][$Fe(CN)_6$]$_2$} (1′): Compound **1′** was prepared by heating **1** at 160 ºC under vacuum (< 10^{-1} Pa) for 72 hours. This powdered sample was used for different characterizations. Anal. Calcd. for $C_{42}H_{28}Fe_2Zn_3N_{18}O_2$: C, 45.00; H, 2.51; N, 22.50. Found: C, 45.80; H, 2.53; N, 21.86.

Synthesis of {[Zn_3(bipy)][$Fe(CN)_6$]$_2$·3H_2O}$_n$ (2): An aqueous solution (12.5 mL) of $K_3[Fe(CN)_6]$ (0.25 mmol) was added to an ethanolic solution (12.5 mL) of bipy (0.25 mmol) and stirred for 30 min. $ZnCl_2$ (0.25 mmol) was dissolved in 12.5 mL distilled water and 2.5 mL of this metal solution was carefully layered with the 2.5 mL of mixed bipy and $K_3[Fe(CN)_6]$ solution using an ethanol:water buffer solution (1 mL, 1:1) in a crystal tube. After 30 days, light yellow colored block shaped crystals were appeared in the middle of the tube and separated and washed with ethanol (Yield ~ 60 %). Different procedure was employed for the preparation of the sample in bulk amount. An aqueous solution (12.5 mL) of $K_3[Fe(CN)_6]$ (0.16 mmol) was added to an ethanolic solution (1:1, 12.5 mL) of

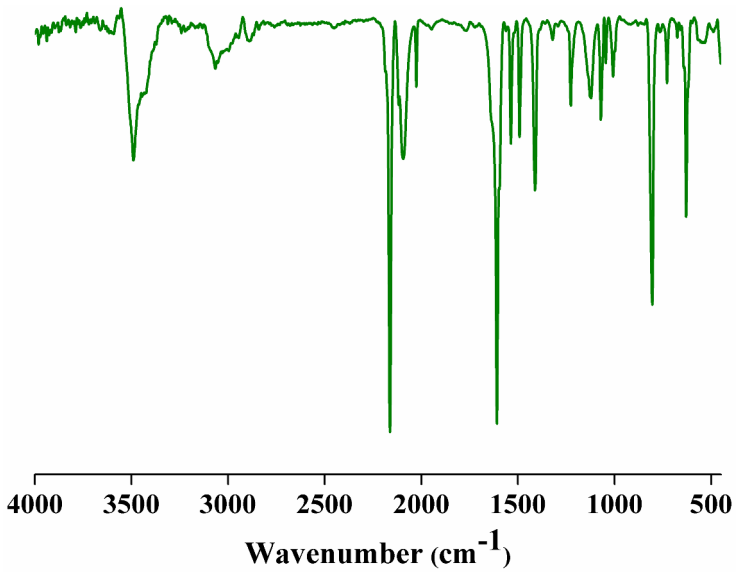

Fig.1: IR spectrum of **1**.

bipy (0.08 mmol) and stirred for 30 min. This resulting solution was added drop wise to a solution of $ZnCl_2$ (0.25 mmol) and stirred for 36 hours. The phase purity was checked with the PXRD and elemental analysis. Yield: 57%, relative to Fe. Anal. Calcd for $C_{22}H_{14}Fe_2Zn_3N_{14}O_3$: C, 31.96; H, 1.71; N, 23.74. Found: C, 33.30; H, 1.79; N, 28.87. IR (KBr, cm^{-1}): *ν*(H_2O) 3653, 3572; *ν*(ArC-H) 3107, 2982; *ν*(C≡N) 2197, 2157, 2090; *ν*(ArC=C) 1618, 1563. IR spectrum of **2** (Fig. 2) shows strong and sharp bands around 3653 cm^{-1} suggesting the presence of water molecules. A strong band around 2090 cm^{-1} corroborate to

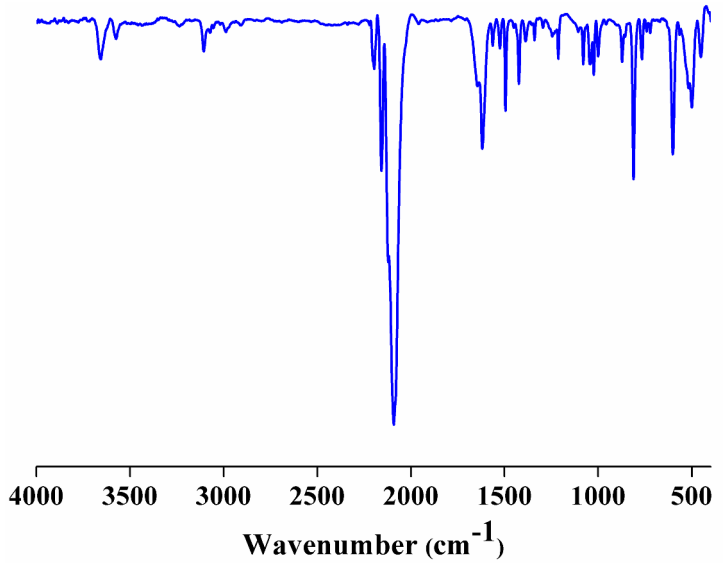

Fig.2: IR spectrum of **2**.

free ν(C≡N) stretching frequency and a band around 1618 cm^{-1} indicates the presence bipy molecule.

Preparation of {[Zn_3(bipy)][$Fe(CN)_6]_2$} (2′): Compound **2′** was prepared by heating **1** at 130 ºC under vacuum (< 10^{-1} Pa) for 72 hours. This powdered sample was used for characterization of different physical properties. Anal. Calcd for $C_{22}H_8Fe_2Zn_3N_{14}$: C, 34.21; H, 1.04; N, 25.40. Found: C, 34.82; H, 1.15; N, 24.86.

Synthesis of {[Zn_3(azpy)$_2$(H_2O)$_2$][$Fe(CN)_6]_2$.4H_2O}$_n$ (3): An aqueous solution (12.5 mL) of $K_3[Fe(CN)_6]$ (0.5 mmol) was added to an ethanolic solution (12.5 mL) of azpy (0.25 mmol) and stirred for 30 min. $ZnCl_2 \cdot 6H_2O$ (0.25 mmol) was dissolved in 12.5 ml distilled water and 2.5 mL of this metal solution was carefully layered with the 2.5 mL of mixed azpy and $K_3[Fe(CN)_6]$ solution using an ethanol : water buffer solution (1 mL, 1:1) in a crystal tube. After 15 days, orange yellow colored block crystals were appeared in the middle of the tube and separated and washed with ethanol (Yield ~ 60 %). The bulk amount of the sample was prepared by the direct mixing of the reagents in ethanol/water mixed solution with stirring for 24 h and the phase purity was checked with the PXRD and elemental analysis.

Yield: 80 %, relative to Fe. Anal. Calcd for $C_{32}H_{28}Fe_2Zn_3N_{20}O_6$: C, 35.05; H, 2.57; N, 25.54. Found: C, 35.87; H, 2.55; N, 25.37. IR (KBr, cm^{-1}): ν(H_2O) 3662, 3576, 3427 (broad) ; ν(ArC-H) 3091; ν(C≡N) 2168, 2098; ν(ArC=C) 1607, 1571. IR spectrum of **3** (Fig. 3) shows strong and sharp peak around 3662, 3576 cm^{-1} suggesting the presence of water molecules. A

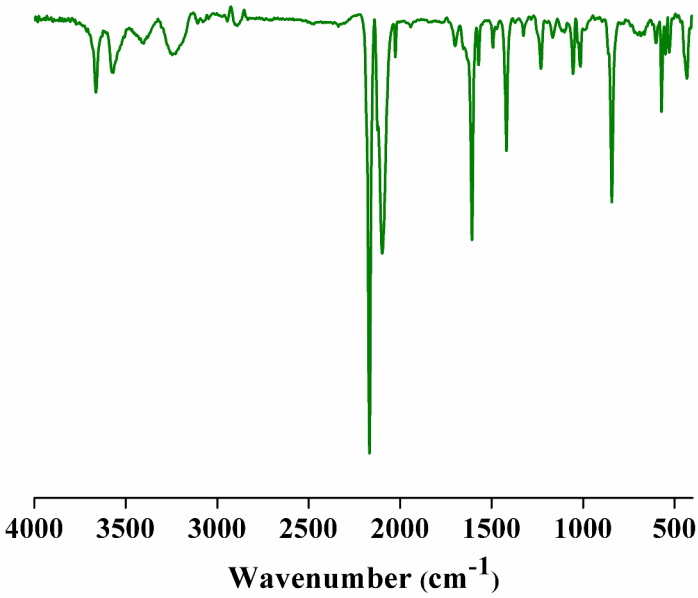

Fig.3: IR spectrum of **3**.

strong band around 2168 cm^{-1} corroborate to free ν(C≡N) stretching frequency and a band around 1607 cm^{-1} indicates the presence azpy molecule.

Preparation of {[Zn_3(azpy)$_2$][$Fe(CN)_6$]$_2$} (3′): Compound **3′** was prepared by heating **3** at 150 ºC under vacuum (< 10^{-1} Pa) for 72 hours. This powdered sample was used for characterization of different physical properties. Anal. Calcd for $C_{32}H_{14}Fe_2Zn_3N_{20}$: C, 39.11; H, 1.43; N, 28.52. Found: C, 38.91; H, 1.53; N, 28.37.

Synthesis of {[Zn_3(bipy)$_3$(H_2O)$_2$][$Cr(CN)_6$]$_2$·2(bipy)·4H_2O}$_n$ (4): An aqueous solution (12.5 mL) of $K_3[Cr(CN)_6]$ (0.25 mmol) was added to an ethanolic solution (12.5 mL) of bipy (0.25 mmol) and stirred for 30 min. $ZnCl_2$ (0.25 mmol) was dissolved in 12.5 ml distilled water and 2.5 mL of this metal solution was carefully layered with the 2.5 mL of mixed bipy and $K_3Cr(CN)_6$ solution using an ethanol : water buffer solution (1 mL, 1:1) in a crystal tube. After 15 days, transparent block crystals were appeared in the middle of the tube and separated and washed with ethanol (Yield ~ 60 %). The bulk amount of the sample was prepared by the direct mixing of the reagents in ethanol/water mixed solution with stirring for 24 h and the phase purity was checked with the PXRD and elemental analysis. This powdered sample was used for studying of different physical properties. IR (Fig. 4): ν(C≡N) 2184 and 2129 cm^{-1}; ν(C=C): 1608 cm^{-1}, 1535 cm^{-1}; ν(O-H): 3478 cm^{-1} . Anal. cald. for $C_{62}H_{52}Cr_2Zn_3N_{22}O_6$: C, 49.72; H, 3.50; N, 20.59. Found: C, 49.02; H, 3.31; N, 20.48%.

Preparation of {[Zn_3(bipy)$_3$][Cr(CN)$_6$]$_2$} (4′): Compound **4′** was prepared by heating **4** at 170 ºC under vacuum (< 10^{-1} Pa) for 72 hours. This powdered sample was used for characterization of different physical properties. Anal. cald. for $C_{42}H_{22}Cr_2Zn_3N_{18}$: C, 46.93; H, 2.06; N, 23.47. Found: C, 46.01; H, 2.18; N, 23.01%.

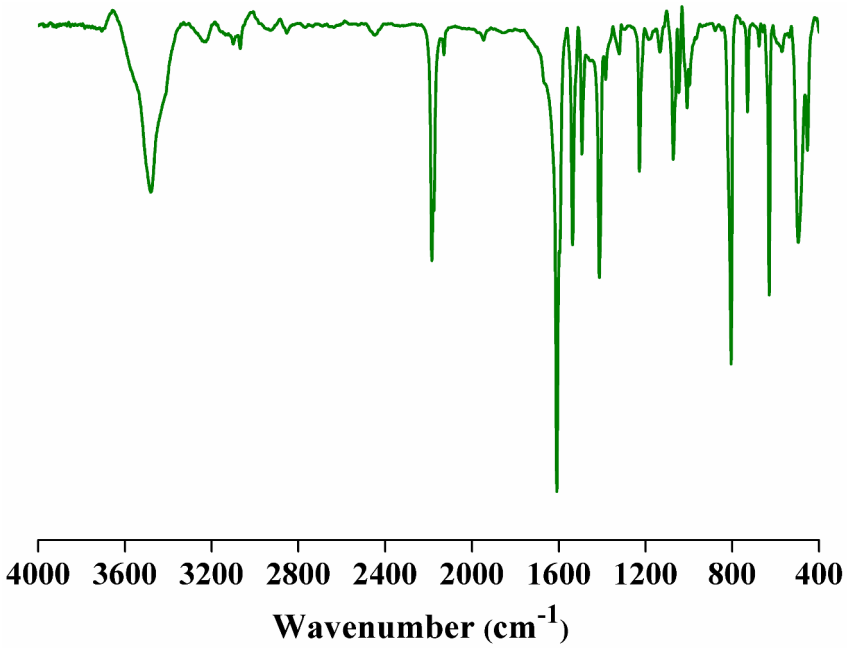

Fig. 4: IR spectra of **4**.

4.3.3: ***Physical Measurements***

The elemental analyses of each compounds and their different state were carried out on a Thermo Fisher Flash 2000 Elemental Analyser. Infra-red (IR) spectroscopic studies was carried out in the mid-IR region as KBr pellet (Bruker IFS-66v). Thermogravimetric analysis (TGA) was carried out (Metler Toledo) in nitrogen atmosphere (flow rate = 50 ml min^{-1}) in the temperature range 30 – 650 °C (heating rate = 2°C min^{-1}). Powder XRD pattern of the products were recorded by using Cu-K_α radiation (Bruker D8 Discover; 40 kV, 30 mA).

4.3.4: ***Single Crystal X-ray Diffraction***

Suitable yellow color single crystals of compound **1**, **2**, **3** and **4** were mounted on a thin glass fiber with commercially available super glue. X-ray single crystal structural data were collected on a Bruker Smart-CCD diffractometer equipped with a normal focus, 2.4 kW sealed tube X-ray source with graphite monochromated Mo-*Kα* radiation (λ = 0.71073 Å) operating at 50 kV and 30 mA. The program SAINT[12] was used for integration of diffraction

profiles and absorption correction was made with SADABS[13]program. All the structures were solved by SIR 92[14] and refined by full matrix least square method using SHELXL.[15] All the hydrogen atoms were fixed by HFIX and placed in ideal positions. Potential solvent accessible area or void space was calculated using the PLATON[16] multipurpose crystallographic software. All crystallographic and structure refinement data of **1**, **2**, **3** and **4** are summarized in Table 1. All calculations were carried out using SHELXL 97[15], PLATON[16], SHELXS 97[17] and WinGX system, Ver 1.70.01.[18]

4.3.5: ***Adsorption Study***

N_2 (77 and 195 K), H_2 (77 K) and CO_2, Ar, O_2 (77 and 195 K) adsorption studies were carried out with the desolvated samples i.e. **1′-4′**by using QUANTACHROME QUADRASORB *SI* analyzer. High-pressure hydrogen adsorption isotherm measurements at 77 and 87 K and CH_4 at 195K were carried out on a fully computer controlled volumetric BELSORP-HP, BEL JAPAN high pressure instrument. All the gases used for the high pressure measurements are of scientific/research grade with 99.999% purity. For the measurements, approximately 200 mg of degassed sample (**1′-4′**) was taken in a stainless-steel sample holder. Dead volume of the sample cell was measuredusing helium gas of 99.999% purity. Non-ideal corrections for all the gases were made by applying virial coefficients at the measurement temperature. All operations were computer controlled and automatic. The adsorption of different solvents like MeOH at 293K and H_2O, EtOH, CH_3CN at 298 K were measured in the vapor state by using BELSORP-aqua-3 analyzer. In all the measurements, in the sample tube, adsorbent samples (~100 – 150 mg) were placed which were prepared at 160 ºC (**1′**), 130 ºC (**2′**)**,** 150 ºC (**3′**) and 170 ºC (**4′**) for about 72h under high vacuum ($<10^{-1}$ Pa) prior to measurement of the isotherms. The different solvent molecules used to generate the vapour were degassed fully by repeated evacuation. Dead volume was measured with helium gas. The adsorbates were placed into the sample tubes, then the change of the pressure was monitored and the degree of adsorption was determined by the decrease in pressure at the equilibrium state.

4.4: ***Results and Discussion***

4.4.1: ***Structural description of {[$Zn_3(bipy)_3(H_2O)_4$][$Fe(CN)_6$]$_2$·2(bipy)·3H_2O}$_n$ (1)***

Single crystal X-ray Crystallographic structure determination reveals that **1** is a neutral 3D coordination architecture of Zn(II) built by $[Fe(CN)_6]^{3-}$ and bipy with the formulation of $\{[Zn_3(bipy)_3(H_2O)_4][Fe(CN)_6]_2\cdot 2(bipy)\cdot 3H_2O\}_n$.

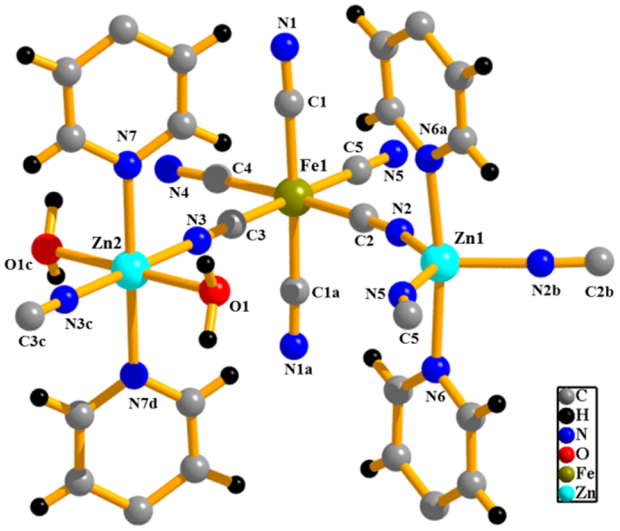

Fig. 5: Coordination environment of Zn and Fe in **1**. Symmetry codes: a = (x, y, –z); b = (0.5 – x, 0.5 + y, –z); c = (–x, –y, z) and d = (–x, –y, –z).

Compound **1** crystallizes in orthorhombic system in *Pbam* space group. There are two crystallographically independent Zn (Zn1 and Zn2) atoms in the asymmetric unit where each octahedral Zn2 is coordinated two CN groups from two $[Fe(CN)_6]^{3-}$, two bipy and two water molecules (O1, O1c). Whereas each trigonal bipyramidal Zn1 is coordinated to three CN groups from three different $[Fe(CN)_6]^{3-}$ and two bipy molecules (Fig. 5). Zn1 centre is slightly distorted from perfect octhedral which is reflected in the *cisoid* angles (105.60(14)–135.05(14)º) whereas the Zn2 centre is close to perfect octahedra. The Zn-N and Zn-O bond distances are in the range of 2.1854–2.2755 Å and 2.2125–2.2694 Å, respectively. In the 2D layer, the twelve-membered $Zn1_2Fe1_2(CN)_4$ ring is surrounded by six eighteen-membered $Zn1Zn2_2Fe1_3(CN)_{12}$ rings and each 2D layer is connected by the bipy linker through the Zn(II) centres forming a 3D pillared-layer network with two kind of channels along the *c*-axis (Fig. 6a). Examination with TOPOS[20] reveals that **1** is a tri-nodal (4-c)3(5-c)2-periodic 3D net formed by 5-connected (5-c) Zn-nodes, (4-c) Fe-nodes and (2-c) bipy and CN linkers. In a layer, the vertex symbol for Zn1, Zn2 and Fe1 points are represented by Schläfli symbols,

$\{4.6^8.8\}$, $\{6^5.8\}$ and $\{4.6^5\}$ respectively. Further examination shows that **1** adopts an unprecedented network topology with the Schläfli symbol $\{4.6^5\}_2\{4.6^8.8\}_2\{6^5.8\}$. After removing the coordinated and guest molecules (H_2O and bipy), compound **1** offers a biporous network with open channels along crystallographic *b* and *c* directions. The rectangular-shaped voids are observed along *c* (~5.8 × 3.2 $Å^2$) (Fig. 7) while another rectangular-shaped smaller channel (2.8 × 2.2 $Å^2$) is present along *b* direction. All the pores contain two water molecules and bipy molecule as guests (Fig. 6a) and both of which provide about 34% void spaces to the total crystal volume. Thus, **1** acts as a biporous host. Upon removal of the coordinated water and guest (water, bipy) molecules framework shows 37.9% void space to the total volume with coordinatively unsaturated Zn(II) centres on the pore surface (Fig 6b).

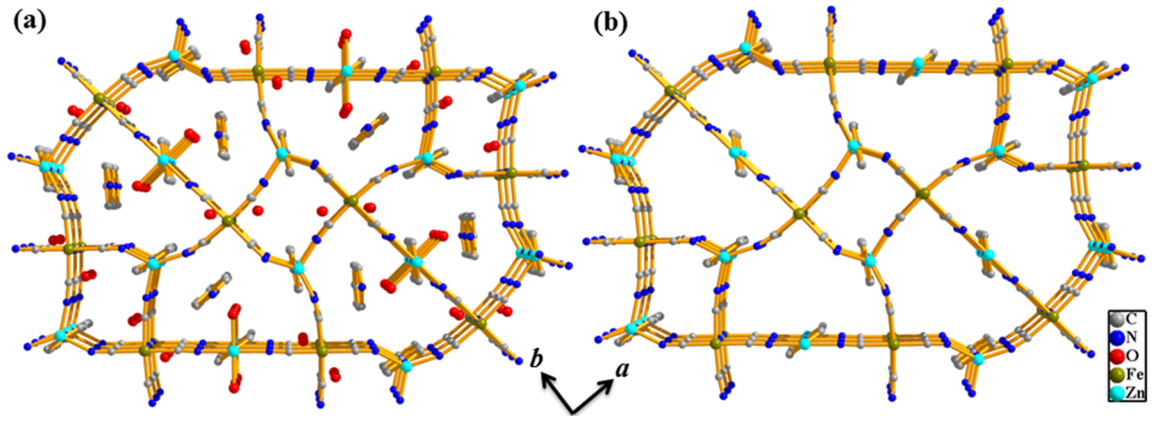

Fig. 6: (a) 3D architecture of **1**. Guest bipy and water molecules are occupying the two different type 1D channels along *c* direction. (b) Guest evacuated framework of **1** which shows unsaturated metal sites.

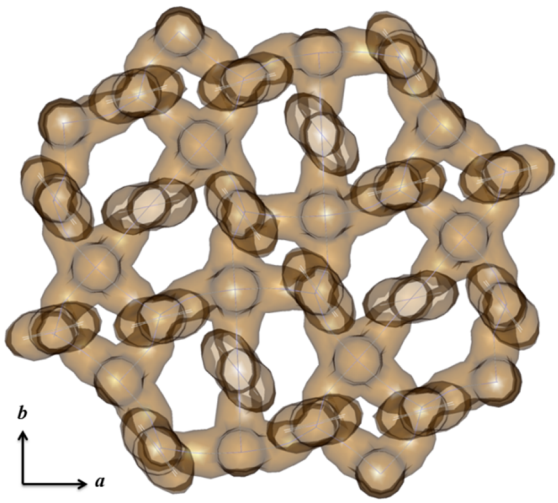

Fig. 7: View of two different kind of channels in **1** along *c* direction.

The guest water molecules O3 and O4 are H-bonded (O3···O4, 3.027Å) to each other and O3 also making a bridge between the two layers through N1 of the pendant CN group (N1···O3, 2.944 Å) (Fig. 8b). The guest bipy molecules undergoes strong face to face π···π interactions (Fig. 8a) with two different coordinated bipy (cg···cg distances are in the range of 3.631–3.905 Å) linkers connected to two Zn (Zn1 and Zn2) centres. In the 3D network, separation between the layers through Zn(II)–bipy–Zn(II) is 11.628Å while in the 2D layer, the Zn1–Fe1 and Zn2–Fe1 distances are 5.230 Å and 5.240 Å, respectively.

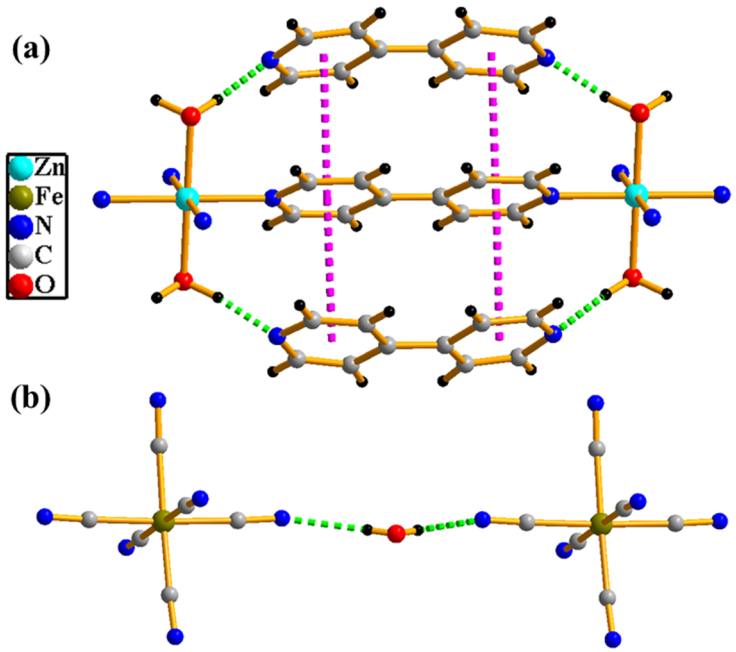

Fig. 8: The supramolecular interactions in**1**. (a) H-bonding interaction between coordinated water and guest bipy molecules leading to a connection between two Zn centres. Guest and coordinated bipy molecules are interacting with each other through strong π···π interactions. (b) Two neighbouring Fe centres interact via N···H-O hydrogen bonding of coordinated CN and guest H_2O molecule which leads to a 1D chain.

4.4.2: ***Structural description of {[Zn_3(bipy)][Fe(CN)$_6$]$_2$·3H_2O}$_n$ (2)***

Single crystal X-ray Crystallographic structure determination reveals that compound **2** crystallizes in monoclinic system in *C*2/*c* space group and is a 3D coordination framework built up by Zn(II), $[Fe(CN)_6]^{3-}$ and bipy, the later acts as a monodentate pendant ligand. There are three types of Zn(II) and two types of Fe(III) centers present in the structure and they are crystallographic independent (Fig. 9). All Fe(III) centers are distorted from ideal octahedral geometry which is clearly reflected from the Fe-C-Fe *cisoids* angles (87.3(7)º - 93.3(7)º for Fe1, 86.5(8)º – 94.2º for Fe2 and 87.4(7)º - 95.1(7)º for Fe3 centers) and Fe-C bond lengths (1.880(19) – 2.22(2)) Å). Zn1 and Zn3 centers have slightly distorted tetrahedral geometry

and connected with four nitrogen atom from four different cyanides. The degree of distortion is revealed in N-Zn-N angles (103.3(6) to 117.9(6) º). Zn-N (Zn1 and Zn3) bond lengths are in the range of 1.924(14) to 1.990(16) Å. The Zn2 center has distorted trigonal bipyramidal geometry and coordination number is fulfilled by five nitrogen atoms from four different cyanide ligands and one bipy molecule. The distorted geometry is reflected from *cisoid* (104.7(6) - 147.2(6)º) and *transoid* (84.3(6) - 100.3(6)º) angles of the Zn2 centre. Zn-N bond lengths varies from 1.944(15) - 2.430(17) Å).

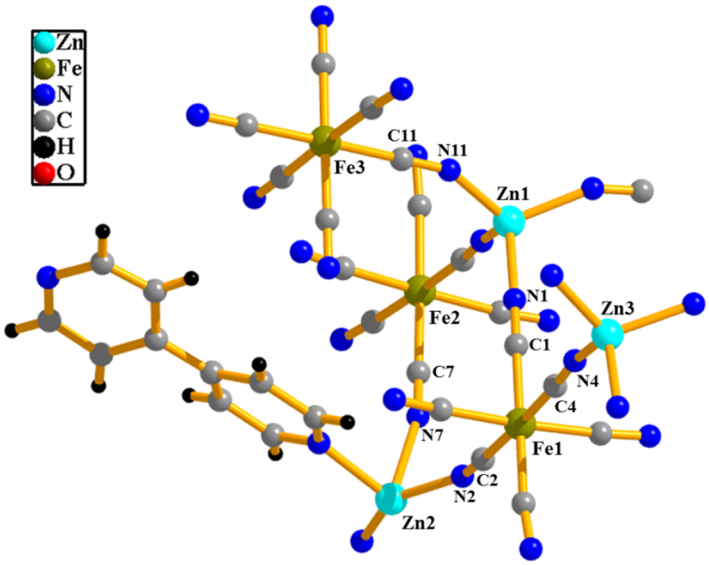

Fig. 9: Coordination environment of Zn and Fe in **2** (only those cyanide bridges are labelled which make connection between the metal centers).

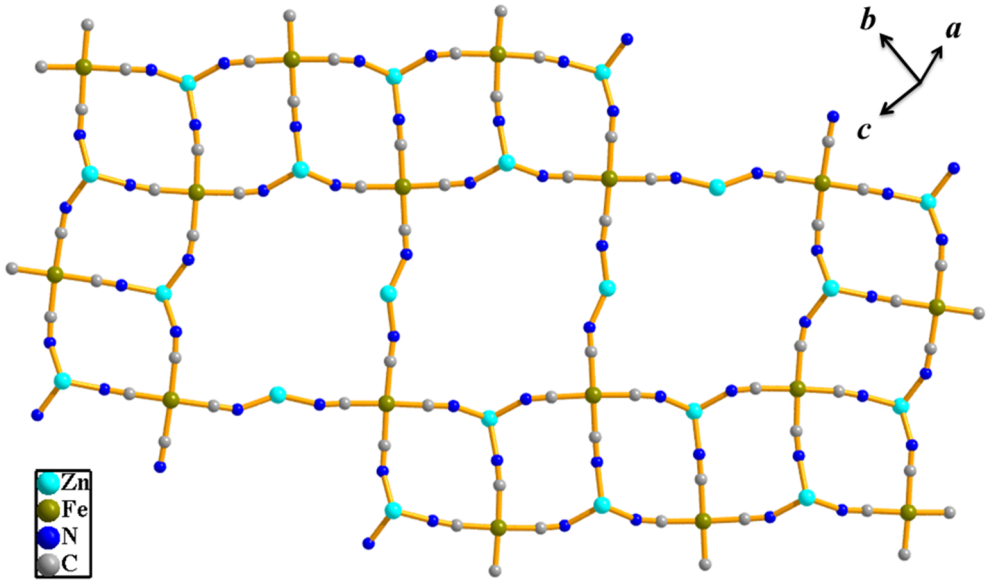

Fig. 10: Formation of 2D sheet along (101) plane which is constructed by metal and cyanide ligands.

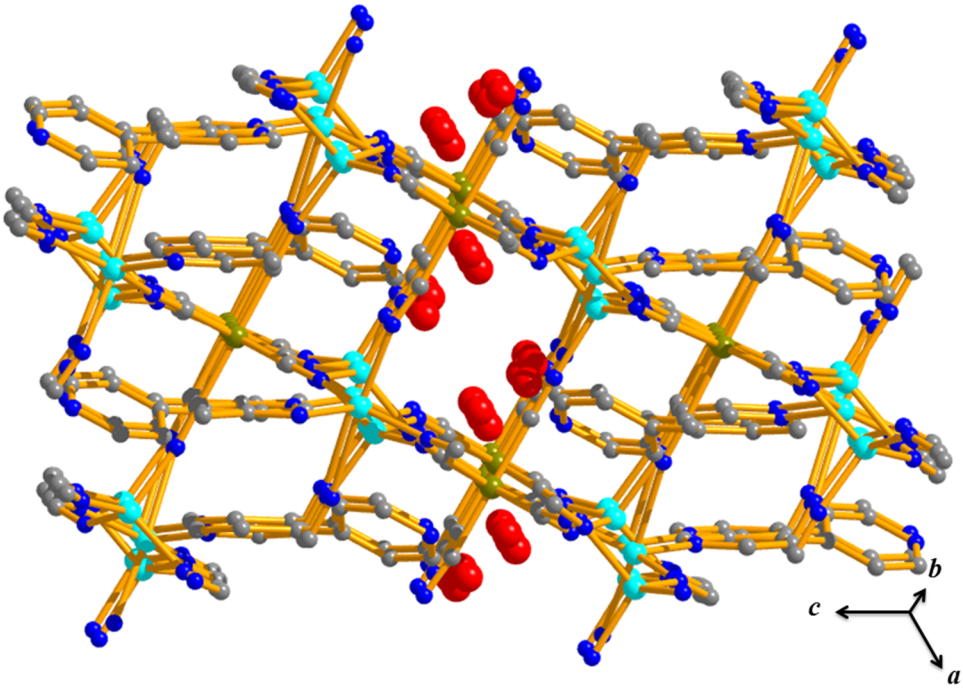

Fig. 11: View of 3D architecture of compound **2** along *b* direction. Water molecules (red colored balls) are occupying in the 1D channel.

Bipy molecule is connected with Zn2 center through the nitrogen atom where the other nitrogen end is interacting with guest H_2O molecule through H-bonding. The metal ions are connected by cyanide ligand and thus forms a 2D sheet along [101] direction (Fig. 10). These 2D sheets are further linked by cyanide ligand along the perpendicular direction of (101) plane which leads to the generation of 3D architecture (Fig. 11). Examination with TOPOS[20] reveals that **2** is a hexa-nodal (4-c)3(6-c)2 3D periodic net formed by 6-connected (6-c) Fe-nodes and 4-connected (4-c) Zn-nodes.

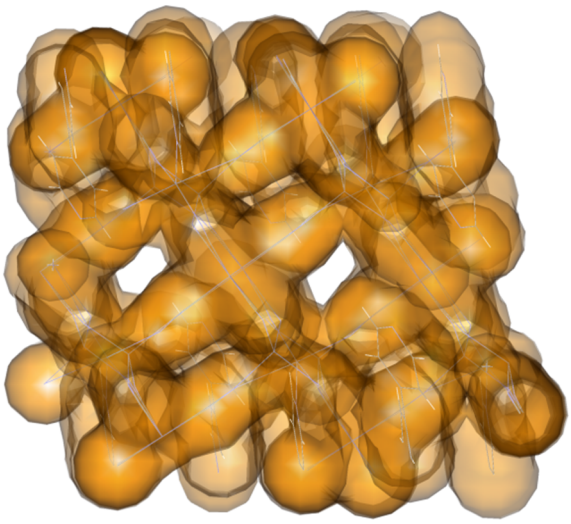

Fig. 12: View of the two different pore surfaces in **2** along *b* direction.

Among the six different nodes, the vertex symbols for Fe1, Fe2, Fe3 and Zn1, Zn2, Zn3 are represented by Schläfli symbols, $\{4^7.6^8\}$, $\{4^7.6^6.8^2\}$, $\{4^7.6^8\}$ and $\{4^5.6\}$, $\{4^5.6\}$, $\{4^4.6^2\}$ respectively. Further examination shows that **2** adopts an unprecedented network topology with the Schläfli symbol $\{4^4.6^2\}_2\{4^5.6\}_4\{4^7.6^6.8^2\}\{4^7.6^8\}_3$. The guest water molecules (O1 and O2) are linked with each other through H-bonding and placed themselves in a 1D channel along crystallographic *b* direction. Upon removal of the guest water molecules, framework shows 18% void space to the total unit cell volume (Fig. 12).

4.4.3: ***Structural description of $\{[Zn_3(azpy)_2(H_2O)_2][Fe(CN)_6]_2{\cdot}4H_2O\}_n$ (3)***

Compound **3** crystallizes in monoclinic *C*2/*m* space group and single crystal X-ray crystallographic structure determination reveals that **3** is a neutral 3D coordination architecture of Zn(II) built by $[Fe(CN)_6]^{3-}$ and azpy with the formulation $\{[Zn_3(azpy)_2(H_2O)_2][Fe(CN)_6]_2{\cdot}4H_2O\}_n$. There are two crystallographically independent Zn (octahedral Zn1 and trigonal bipyramidal Zn2) atoms in the asymmetric unit and each octahedral Zn1 is coordinated to four nitrogen atom from different $[Fe(CN)_6]^{3-}$ and another two nitrogen atoms from two azpy. Each trigonal bipyramidal Zn2 is coordinated three nitrogen atoms, one azpy and one water molecule (O1) (Fig. 13). Zn1 is slightly distorted from the perfect octahedron as reflected in the *cisoid* angles (88.5–91.5)º (Fig. 13). The Zn-N and Zn-O bond distances are in the range of 2.1854–2.2755 Å and 2.131–2.237 Å, respectively. Fe1 and Zn2 centers are connected by cyanide bridges forming a twelve membered square shaped ring. These rings are connected by cyanide ligands which lead to a 1D ladder like structure along *b* direction (Fig. 14a). With the help of cyanide linkers, Zn1 center connects these 1D ladders which leads to wavy like 2D sheet in the crystallographic *ab* plane (Fig. 14b). Along the *c* direction, these 2D sheets looks like a stair case which is further pillared by azpy linker leading to a 3D framework with 1D channels occupied by guest water molecules (14c). Examination with TOPOS[20] reveals that **3** is a tri-nodal (4-c)2(5-c)2(6-c)-periodic 3D net formed by 4-connected (4-c), 6-connected (6-c) Zn- nodes and 5-connected (5-c) Fe-nodes. In a 1D chain, the vertex symbol for Fe1, Zn1 and Zn2 are represented by Schläfli symbols, $\{4^5.6^5\}$, $\{4^4.6^{10}.8\}$ and $\{4^3.6^3\}$. Further examination shows that **3** adopts a unprecedented network topology with the Schläfli symbol $\{4^3.6^3\}_2\{4^4.6^{10}.8\}\{4^5.6^5\}_2$. Azpy molecules engage themselves in a weak π···π interaction (cg···cg distances are in the range of 4.124 Å) along the *b* direction (Fig. 14c) whereas the Fe1 and Zn2 centers are interacting with each other through O1-H···O2W and O2W-H···N4 H-bonding.

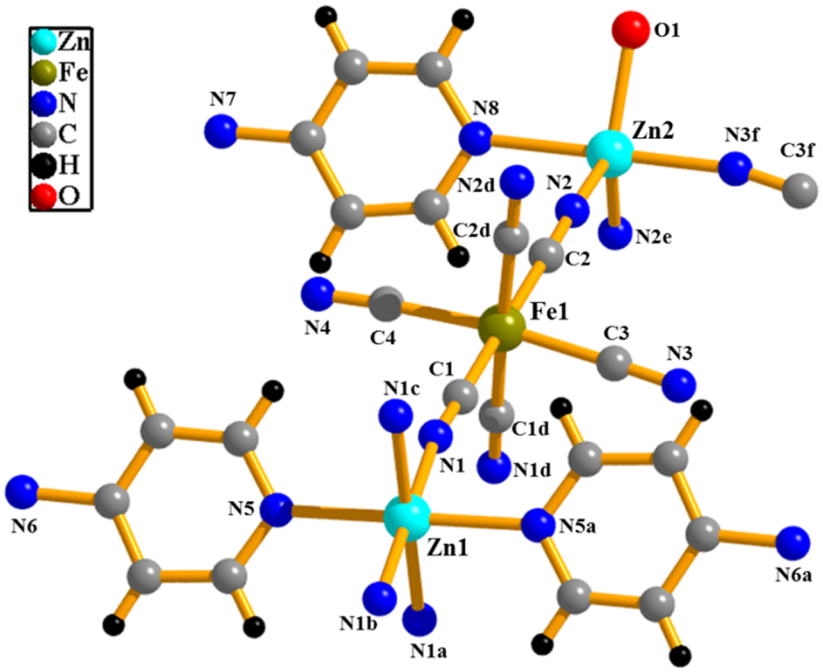

Fig. 13: Coordination environment of Zn and Fe in **3**. Symmetry code: a = (1 – x, y, –z); b = (1 – x, 1–y, –z); c = (x, 1 – y, z); d = (x, 2 – y, z); e = (x, 3 – y, z); and f = (1.5 – x, 0.5+y, –z).

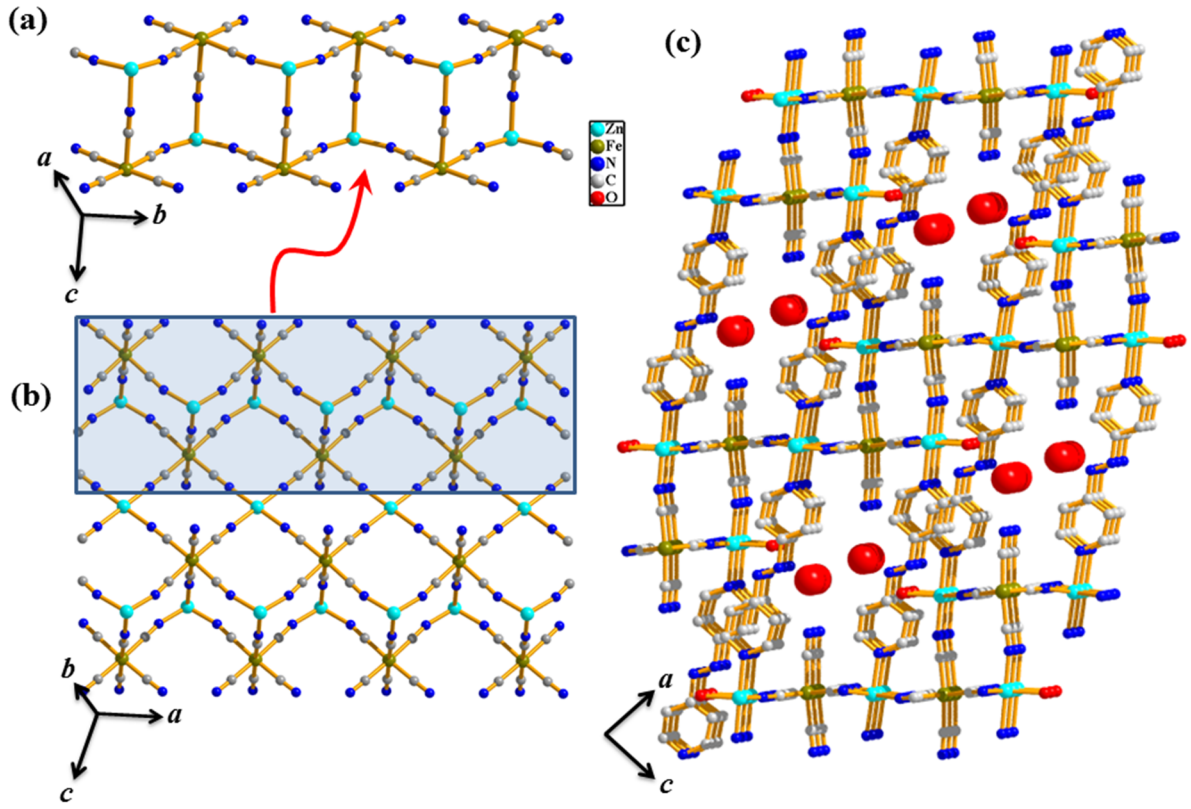

Fig. 14: 1D channels along the *b* direction (a). 1D chains are linked with each other to form 2D sheet in the *ac* plane (b) The 2D sheets are liked with each other by azby linker to generate 3D framework (c). 3D network of **3** showing the channels along the crystallographic *b*-axis occupied by water molecules.

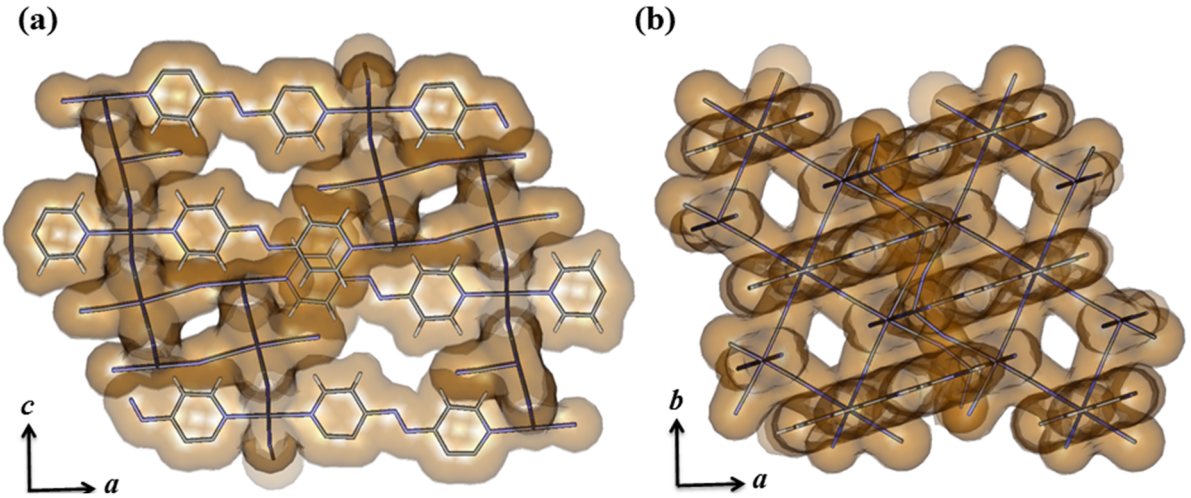

Fig. 15: Views of the pore: stick diagram of **3** showing pores along the *b* (a) and *c* (b) axis. The guest water molecules have been omitted.

The removal of guest water molecules results small rectangular channel which accounts for 27% void volume in the framework (Fig. 15).

4.4.4: ***Structural description of {[$Zn_3(bipy)_3(H_2O)_4$][$Cr(CN)_6$]$_2$·2(bipy)·3H_2O}$_n$ (4)***

Single crystal X-ray Crystallographic structure determination reveals that **4** is a neutral 3D coordination architecture of Zn(II) built by $[Cr(CN)_6]^{3-}$ and bipy with the formulation $\{[Zn_3(bipy)_3(H_2O)_2][Cr(CN)_6]_2\cdot 2(bipy)\cdot 4H_2O\}_n$. Compound **4** crystallizes in orthorhombic system in *Pbam* space group. There are two crystallographically independent Zn (Zn1 and Zn2) atoms in the asymmetric unit where each octahedral Zn2 is coordinated to two CN groups, two bipy and two water molecules (O1, O1c) and each trigonalbipyramidal Zn1 is coordinated to three CN groups from three different $[Cr(CN)_6]^{3-}$ and two bipy, (Fig. 16). Zn1 center is distorted from perfect octahedral geometry which is reflected in the *cisoid* angles (106.92(13)–134.68(13) **º)** whereas the Zn2 centre is close to perfect octahedra. The Zn-N distances are in the range of 1.990 (3)–2.204 (2) Å. In the 2D layers, the twelve-membered $Zn1_2Cr1_2(CN)_4$ ring is surrounded by six eighteen-membered $Zn1Zn2_2Cr1_3(CN)_{12}$ rings and each 2D layer is connected by the bipy linker through the Zn(II) centres which forms a 3D pillared-layer network with two kind of channels along the *c*-axis (Fig. 18b). Examination with TOPOS[23]reveals that **4** is a tri-nodal (4-c)3(5-c)2-periodic 3D net formed by 5-connected (5-c) Zn-nodes, (4-c) Cr-nodes and (2-c) bipy and CN linkers. In a layer, the vertex symbol for Zn1, Zn2 and Cr1 points are represented by Schläfli symbols, $\{4.6^8.8\}$, $\{6^5.8\}$ and $\{4.6^5\}$ respectively. Further examination shows that **4** adopts an unprecedented network topology with the Schläfli symbol $\{4.6^5\}_2\{4.6^8.8\}_2\{6^5.8\}$.

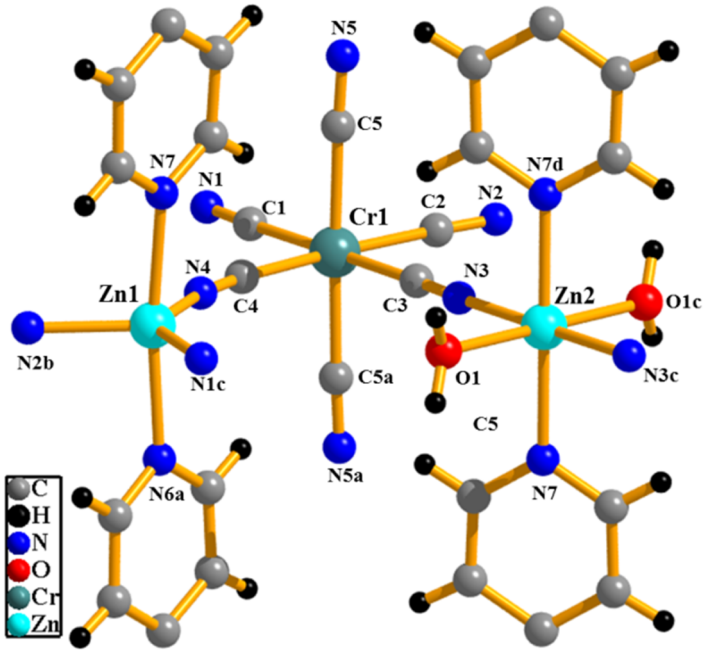

Fig. 16: View of coordination environment around Zn1, Zn2 and Cr1 in **4**. Symmetry codes: a = 2-x, 1-y, z; b = 2-x, 1-y, 1-z; c = 2.5-x, 0.5-y, 1-z; d = -0.5+x, 1.5-y, 1-z.

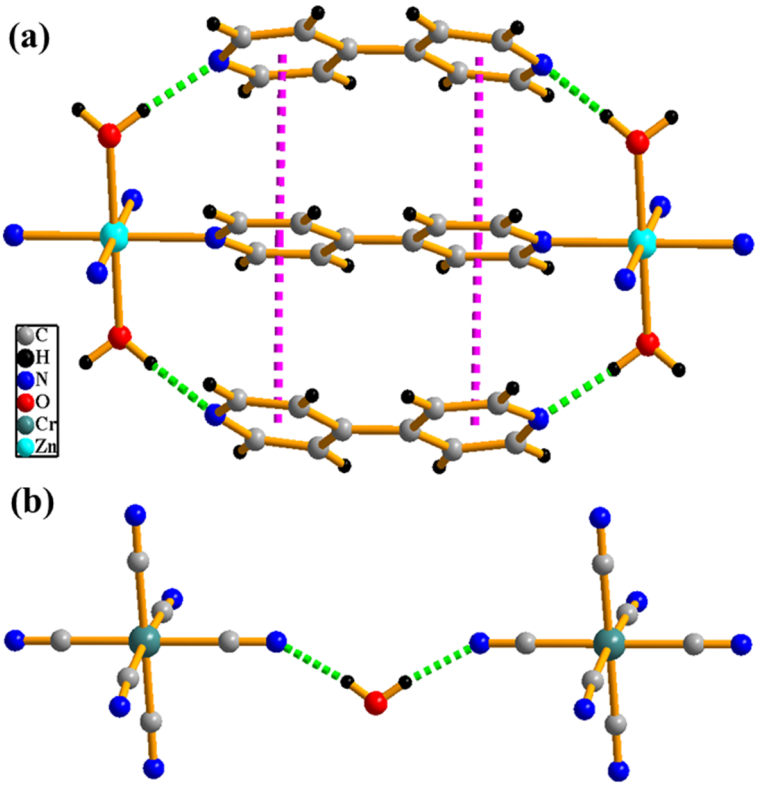

Fig. 17: The supramolecular interaction in **4**; (a) Two Zn2 centres interact via hydrogen bonding of coordinated H_2O and guest bipy molecule, (b) Two neighbouring Cr1 centres interact via N-H-O hydrogen bonding of coordinated CN and guest H_2O molecule.

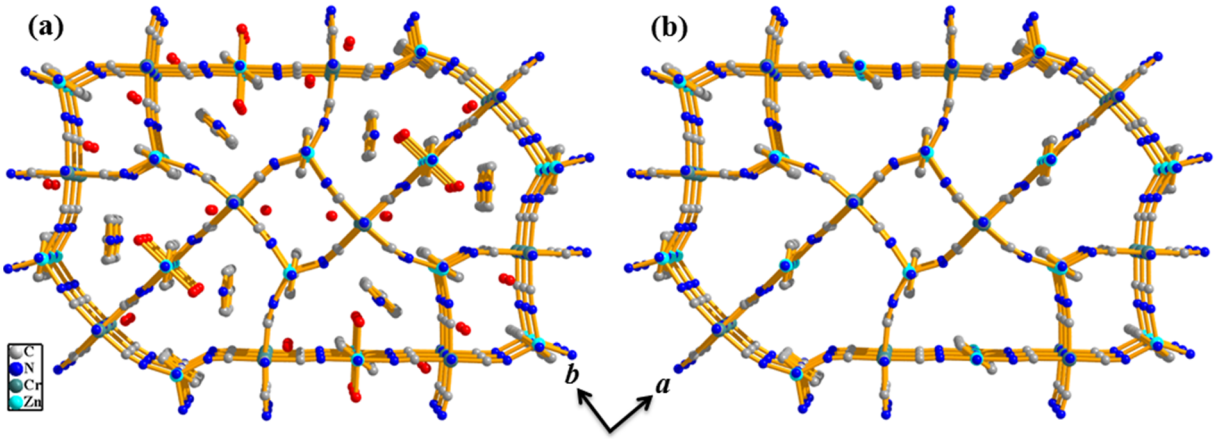

Fig. 18: (a) 3D architecture of **4**. Guest bipy and water molecules are occupying the two different type 1D channels along *c* direction. (b) Guest evacuated framework of **4** which shows unsaturated metal sites.

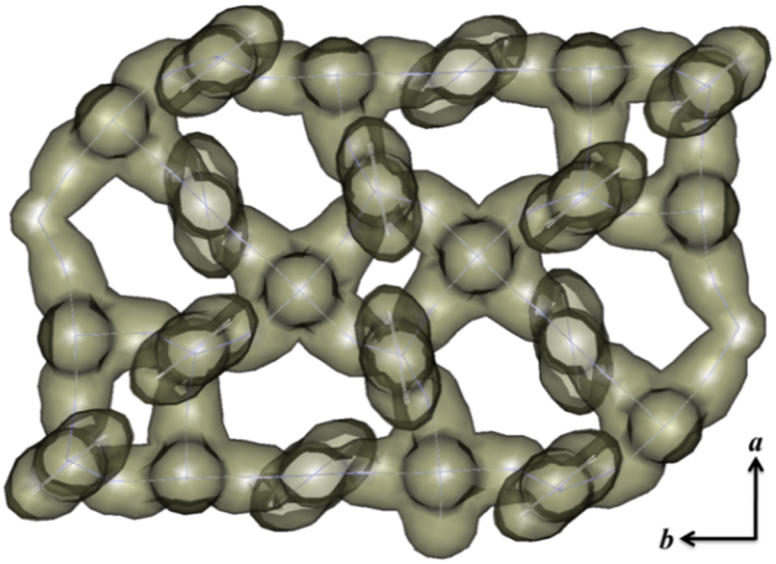

Fig. 19: View of two different kind of channels in **4** along *c* direction.

After removing the coordinated water molecules and gust molecules (H_2O and bipy) compound **4** offers a 3D porous network (Fig. 18b) with open channel along crystallographic *c* direction. The square-shaped smaller channel (2.8 ×2.2Å^2) contains two water molecules and the large channel (7.7 ×5.5 Å^2) contains one water and bipy molecule as guest (along *c* direction) both of which providing about 35% void spaces to the total crystal volume. Thus, **4** acts as a biporous host. Upon removal of the coordinated water and guest (water, bipy) molecules framework shows 38.9% void space to the total volume with coordinatively unsaturated Zn(II) centres on the pore surface (Fig 18b). The guest water molecules O1w and O2w are H-bonded (O3···O4, 3.173Å) to each other, and O1w also making a bridge between

the two layers through N1 of the pendant CN group (N1···O1w, 2.910 Å). The guest bipy undergoes strong face to face π···π interactions with two different coordinated bipy (cg···cg distances are in the range of 3.681–3.967 Å) linkers connected to two Zn (Zn1 and Zn2) centres (Fig. 17). In the 3D network, separation between the layers through Zn(II)-4,4'-bipy-Zn(II) is 11.503 Å while in the 2D layer, the Zn1–Cr1 and Zn2–Cr1 distances are 5.064 Å and 5.283 Å , respectively.

Table 1: Crystallographic table for the four compounds.

	1	**2**	**3**	**4**
Empirical formula	$C_{62}H_{50}Fe_2Zn_3N_{22}O_5$	$C_{22}H_{14}Fe_2Zn_3N_{14}O_3$	$C_{32}H_{28}Fe_2Zn_3N_{20}O_6$	$C_{62}H_{52}Cr_2Zn_3N_{22}O_6$
M	1485.06	823.97	1084.52	1497.39
Crystal system	Orthorhombic	Monoclinic	Monoclinic	Orthorhombic
space group	*Pbam* (No. 55)	*C*2/*C* (No.15)	*C*2/m (No.12)	*Pbam* (No. 55)
a (Å)	15.8354(5)	13.4237(18)	23.1680(17)	16.230(3)
b (Å)	17.5204(6)	20.496(2)	7.5344(5)	17.935(4)
c (Å)	11.4998(3)	23.570(4)	13.4973(9)	11.503(2)
α(deg)	90	90	90	90
β (deg)	90	98.472(7)	99.799(5)	90
γ (deg)	90	90	90	90
V (Å^3)	3190.53(17)	6414.1(15)	2321.7(3)	3348.4(11)
Z	2	8	2	2
T(K)	293	293	293	293
λ(Mo K$_α$)	0.71073	0.71073	0.71073	0.71073
D_c (g cm^{-3})	1.546	1.707	1.551	1.485
μ (mm^{-1})	1.623	3.142	2.199	1.440
θ_{max} (deg)	29.8	27.6	25.4	31.3
total data	44761	39796	10599	30795
unique reflection	4764	7418	2243	5348
R_{int}	0.177	0.428	0.142	0.038
data [*I*> 2σ(*I*)]	2843	2268	1174	4468
R^a	0.0528	0.1004	0.0633	0.0511
$R_w{}^b$	0.1126	0.3237	0.1845	0.1300
GOF	1.02	0.94	1.00	1.13

$^a R = \sum||Fo|-|Fc||/\sum|Fo|$; $^b R_w = [\sum\{w(Fo^2-Fc^2)^2\}/\sum\{w(Fo^2)^2\}]^{1/2}$

4.4.5: *Framework stability: Thermogravimetric (TG) and Powder X-ray diffraction (PXRD) analysis*

Thermogravimetric analysis (TGA) and powder X–ray diffraction (PXRD) measurements at different temperatures were carried out to study the stability of the framework compounds. TGA of compounds **1**-**4** were performed in the temperature range 30 – 650 ºC under nitrogen atmosphere (Fig. 20).

Compound **1** shows weight loss of ~15 % at 190 ºC which corroborate with the removal of one bipy molecule and all guest water molecules. All the water (guest and coordinated) and guest bipy molecules were removed at ~250 ºC (cal. 73.2 %, obs. 74.1%) and after that it transforms to an undetermined structure.

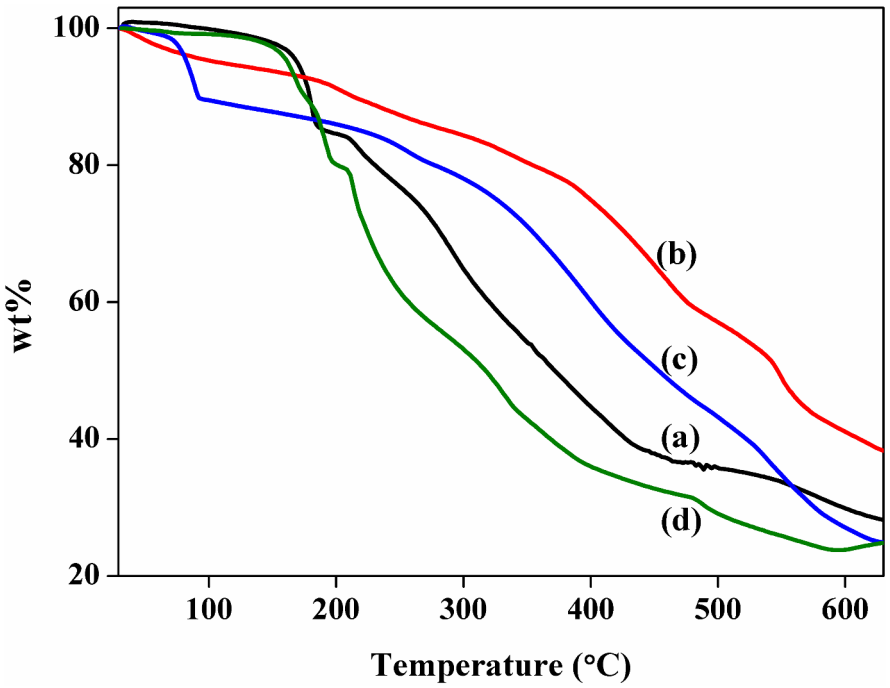

Fig. 20: TGA plot of **1** (a), **2** (b), **3** (c) and **4** (d) over the temperature range 35 to 625 ºC under nitrogen atmosphere.

Compound **2** does not show any step in TGA profile and gradually losses weight with increasing temperature. At ~150 ºC it losses all guest water molecules (cal. 92.1 %, obs. 94.40 %) and finally transforms to an undetermined structure. In case of **3**, sharp decrease in weight was observed up to 100 ºC with a total loss of ~10% (cal. 88.1 %, obs. 89.80 %) suggesting the removal of all guest water molecules. Compound **4** shows a small hump at 175 ºC and at that temperature the weight loss is ~10 % which corroborate with the removal of all

guest water molecules. Almost all the water (guest and coordinated) and guest bipy molecules are removed at ~210 ºC (cal. 75.1 %, obs. 79.80 %) and after that it transforms to an undetermined structure.

The PXRD pattern of compounds **1-4** are shown in Fig. 21-24. The position of the different peaks in simulated and as-synthesized pattern corresponds well indicating the purity of the as-synthesized compounds.

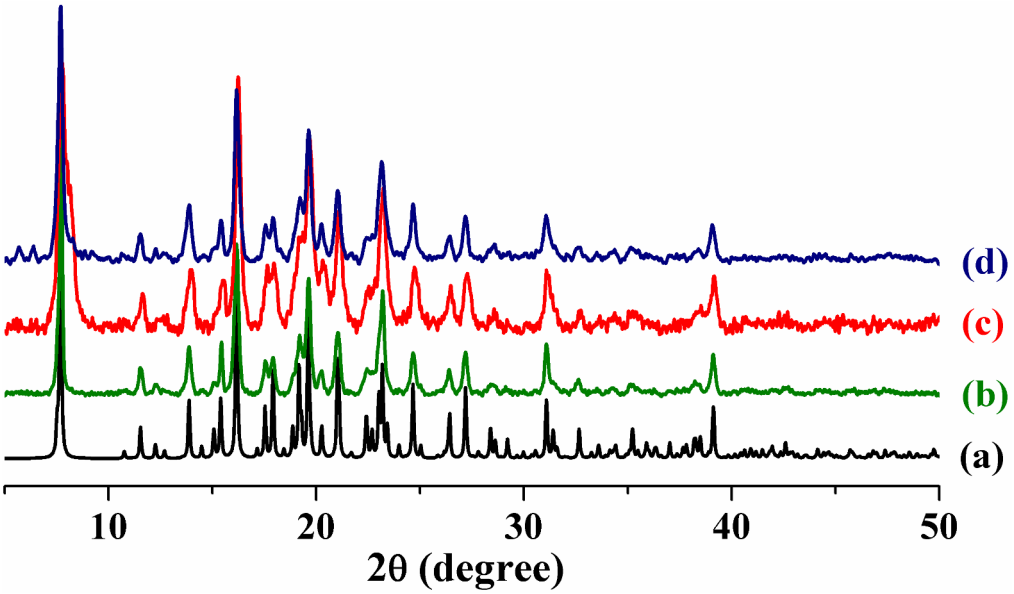

Fig. 21: PXRD Pattern of compound **1**. (a) Simulated, (b) as-synthesised, (c) heated at 160 ºC, (d) rehydrated.

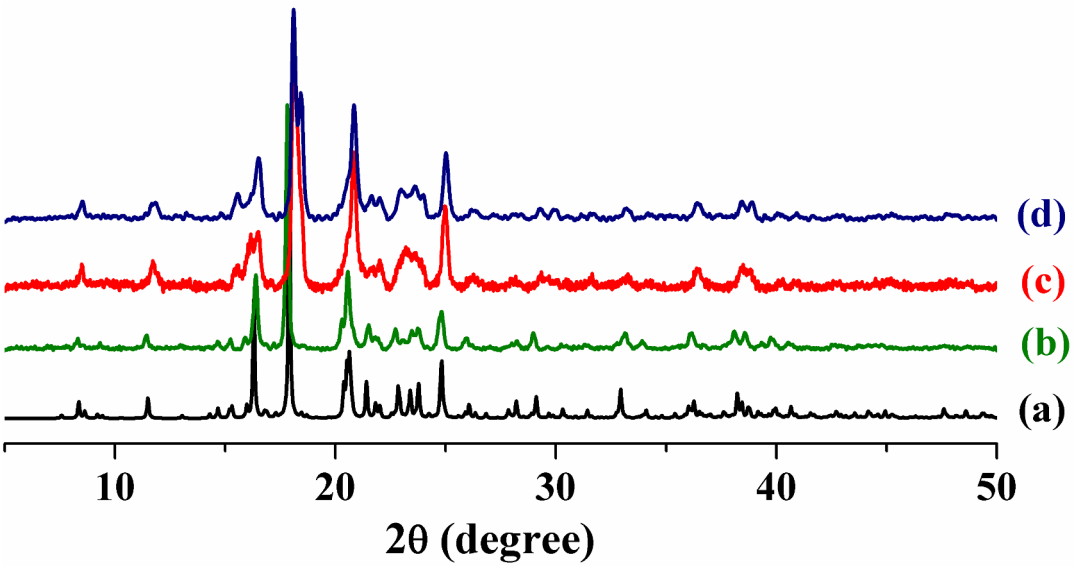

Fig. 22: PXRD Pattern of compound **2**. (a) Simulated, (b) as-synthesised, (c) heated at 130 ºC, (d) rehydrated.

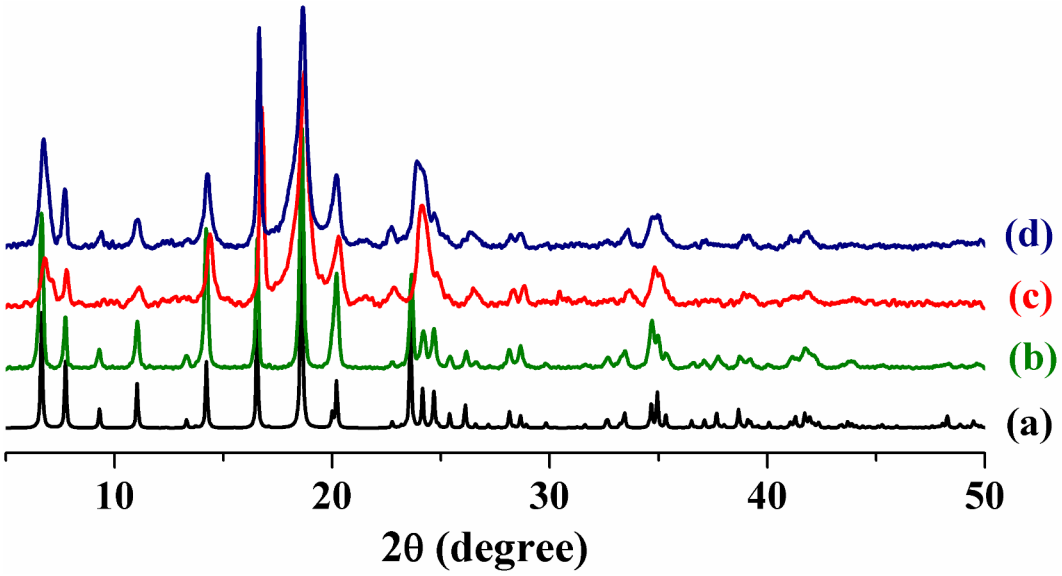

Fig. 23: PXRD Pattern of compound **3**. (a) Simulated, (b) as-synthesised, (c) heated at 150 ºC, (d) rehydrated.

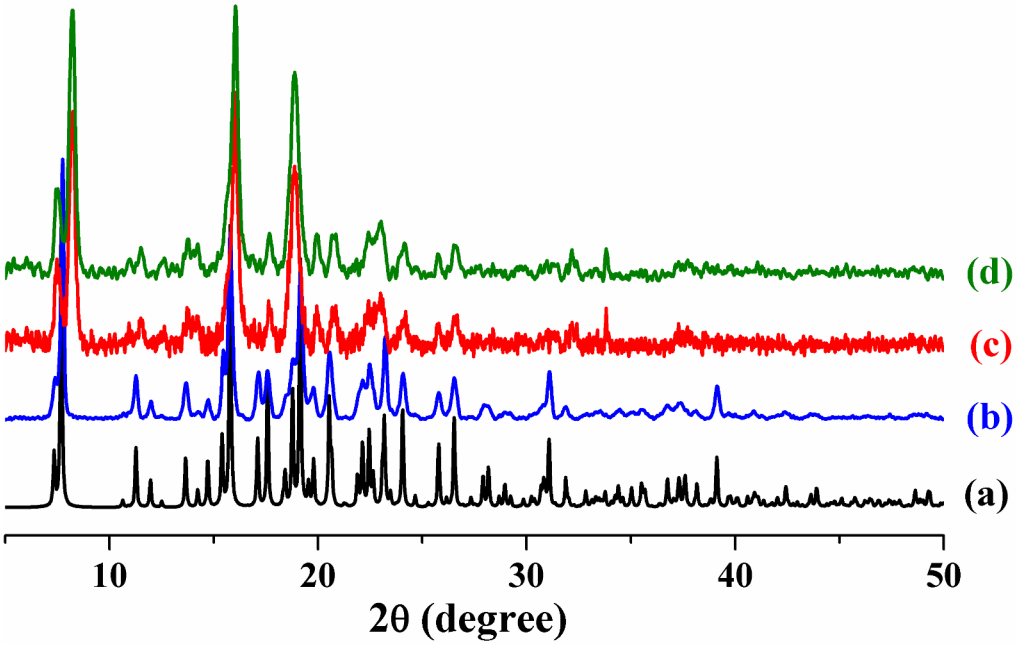

Fig. 24: PXRD plot of Compound **4** at different states: (a) simulated; (b) assynthesized; (c) heated at 170 ºC under vacuum for 72 hrs and (d) rehydrated.

In cases of **1′-4′**, the similarity between the PXRD patterns of as-synthesized and heated samples indicate that there is no significant structural change upon desolvation though there is negligible decrease in crystallinity which is reflected from the broadening of the peaks. The PXRD patterns of rehydrated samples have not changed significantly even after the rehydration of samples by exposing water vapor for 15 days.

4.4.6: ***Adsorption Study***

Selective CO_2 adsorption study: All the four compounds were subjected to N_2 adsorption at 77K and typical type-II profiles were obtained with the final uptake of 53, 35, 47 and 50 mL g^{-1} respectively. The type-II isotherm profile clearly reflects the surface adsorption of N_2 by these four compounds.

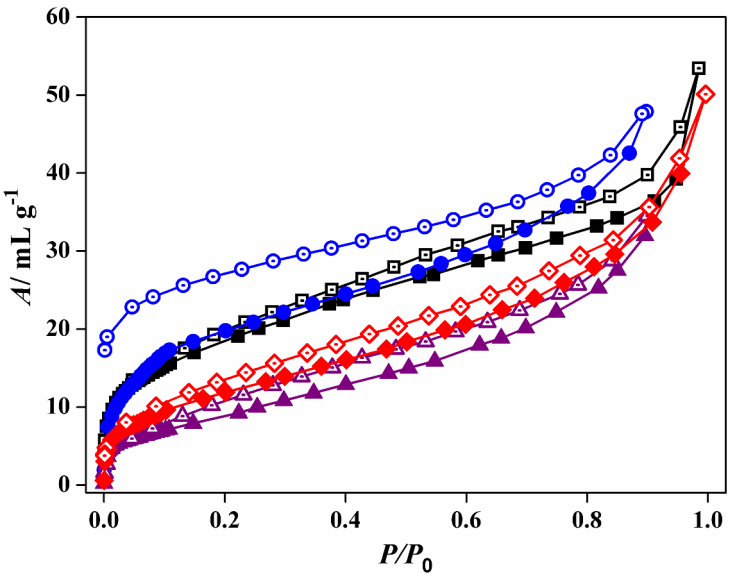

Fig. 25: N_2 adsorption isotherms of **1′**(black), **2′** (blue), **3′**(wine) and **4′** (red) at 77 K. Closed symbols and open symbols are corresponding to adsorption and desorption, respectively.

Gas (CO_2, N_2, Ar, CH_4 and O_2) adsorption studies of the four compounds at 195 K reveal a very interesting result by capturing CO_2 in a selective manner. CO_2 adsorption isotherm of **1′** shows a type-I profile with rapid uptake at low pressure. Compound **1′** adsorbs ~40 mL g^{-1} of CO_2 at very low pressure (P/P_0 = 0.05) revealing the strong interaction with pore surface. After P/P_0 = 0.05, the adsorption amount increases gradually with the final uptake of 72 mL g^{-1} (Fig. 26). The Langmuir surface area calculated from CO_2 profile turns out to be 287 m^2g^{-1}. Calculation of enthalpy of adsorption by DR equation gives a high value (41 kJ mol^{-1}) which also supports the strong affinity of CO_2 towards the pore surface of **1′**.

Compound **2′** also shows steep uptake (23 mL g^{-1} at P/P_0 = 0.1) in the low pressure region and then the adsorption isotherm gradually reaches to a final amount of 45 mL g^{-1} at P/P_0 = 0.99. Desorption curve does not follow the adsorption curve and shows a large hysteresis retaining 24 mL g^{-1} of CO_2 even at very low P/P_0 (0.001) (Fig. 27). Enthalpy of adsorption calculation gives reasonably high value (33.77 kJ mol^{-1}) which also reflects the strong

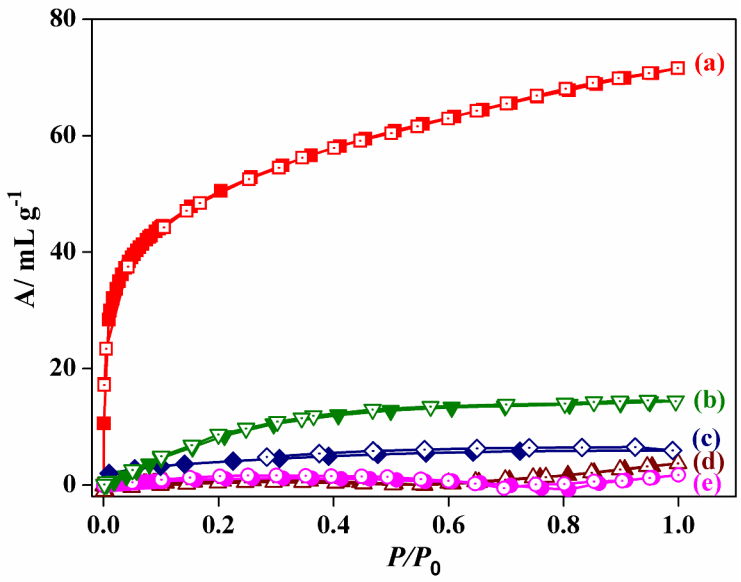

Fig. 26: Gas adsorption isotherms of **1′**at 195 K. (a) CO_2, (b) O_2, (c) CH_4, (d) Ar and (e) N_2. Closed symbols and open symbols are corresponding to adsorption and desorption, respectively.

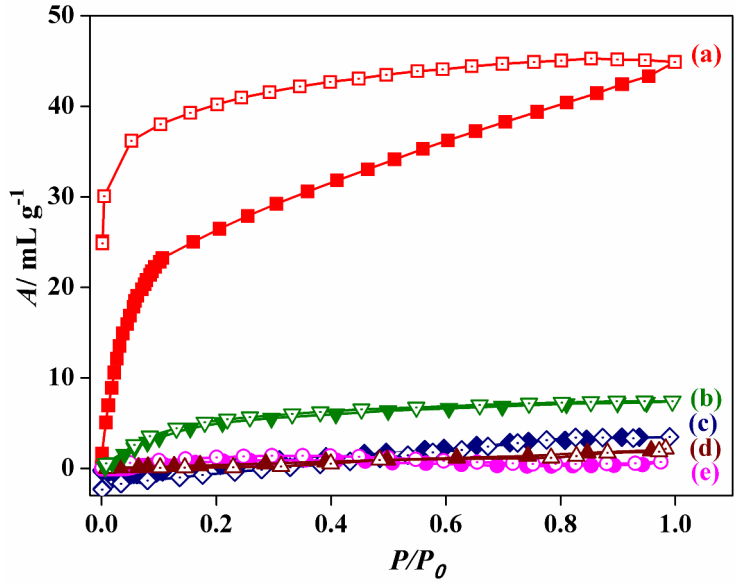

Fig. 27: Gas adsorption isotherms of **2′**at 195 K. (a) CO_2, (b) O_2, (c) CH_4, (d) Ar and (e) N_2. Closed symbols and open symbols are corresponding to adsorption and desorption respectively.

interaction between CO_2 and pore surface. The Langmuir surface area calculated from CO_2 profile gives a value of ~160 m^2 g^{-1}.

Compound **3′** reveals a strong interaction with CO_2 by showing steep uptake (50 mL g^{-1}) at low pressure (P/P_0 = 0.1). The final volume uptake is 86 mL g^{-1} at P/P_0 = 0.9 without any saturation. Desorption curve follows the same adsorption curve and retains 21 mL of adsorbent at the last point of desorption (P/P_0 = 0.001) (Fig. 28).

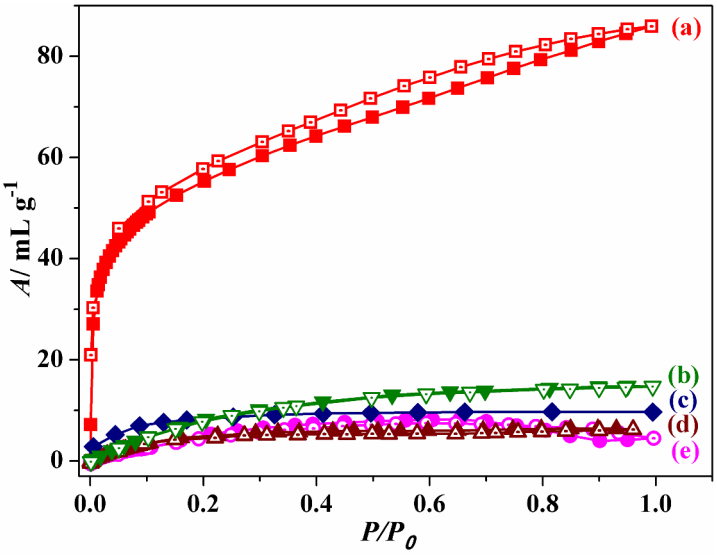

Fig. 28: Gas adsorption isotherms of **3′** at 195 K. (a) CO_2, (b) O_2, (c) CH_4, (d) Ar and (e) N_2. Closed symbols and open symbols are corresponding to adsorption and desorption, respectively.

The Langmuir surface area (273.82 m^2 g^{-1}) and high enthalpy of adsorption (40.89 kJ mol^{-1}) reveals strong interaction among CO_2 and pore surface.

Compound **4′** adsorbs ~37 mL g^{-1} of CO_2 at very low pressure (P/P_0 = 0.06) revealing the strong interaction with pore surface. After P/P_0 = 0.06 the adsorption amount increases gradually with the final uptake of 71 mL g^{-1} (Fig. 29).

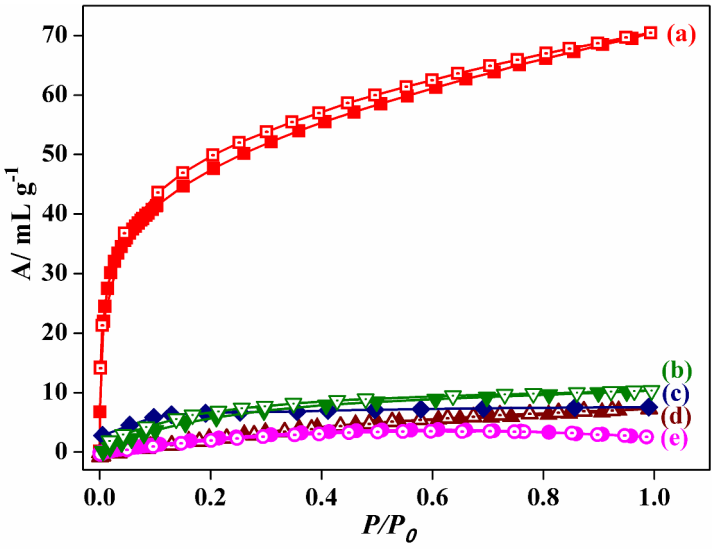

Fig. 29: Gas adsorption isotherms of **4′**at 195 K. (a) CO_2, (b) O_2, (c) CH_4, (d) Ar and (e) N_2. Closed symbols and open symbols are corresponding to adsorption and desorption, respectively.

The Langmuir surface area calculated from CO_2 profile turns out to be 310 m^2 g^{-1}. Calculation of enthalpy of adsorption from DR equation gives a high value (39 kJ mol^{-1})

which also proves the strong affinity of CO_2 towards the pore surface of **4′**. Steep uptake at low pressure and unsaturated adsorption isotherm encourage us to calculate the energy of CO_2 adsorption for **4′**. The high pressure profiles measured (Fig. 30) at 273 and 298 K were used for the calculation of enthalpy of adsorption (ΔH_{ads}) and by applying Clausius-Clapeyron equation we obtained a value of ~34 kJ mol^{-1} (fig 31-33).

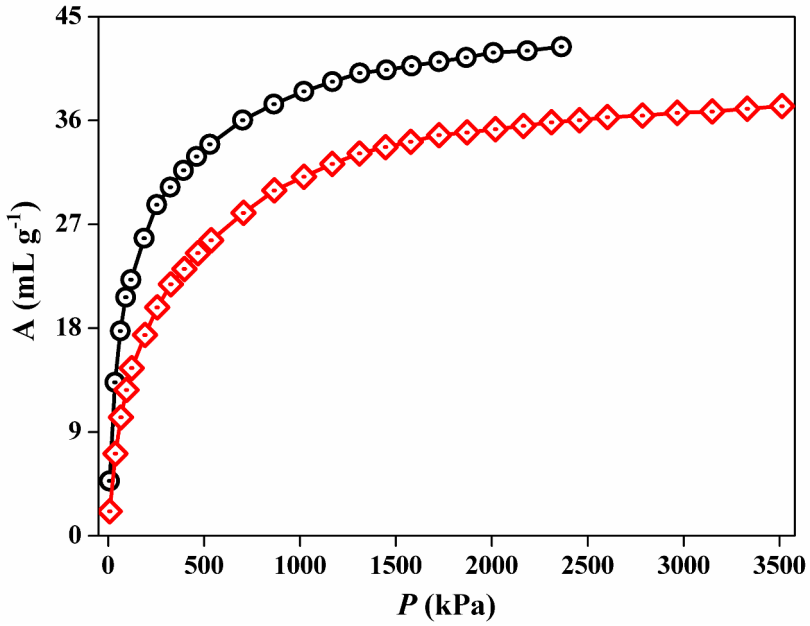

Fig. 30: High pressure CO_2 isotherms (only adsorption) of **4′** measured at 273 K (black) and 298 K (Red).

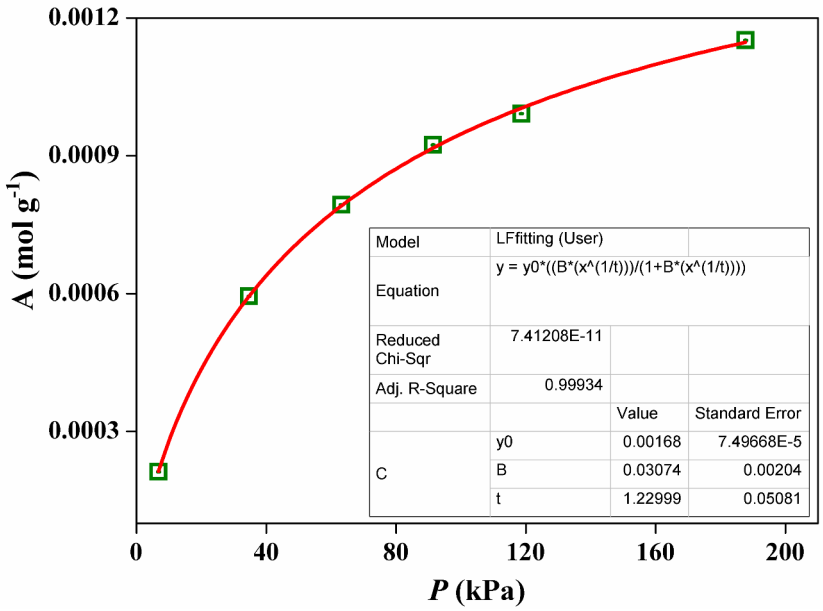

Fig. 31: CO_2 adsorption isotherm for **4′** at 273 K. The solid line represents the best fit to the data using the Langmuir-Freundlich equation, as described above.

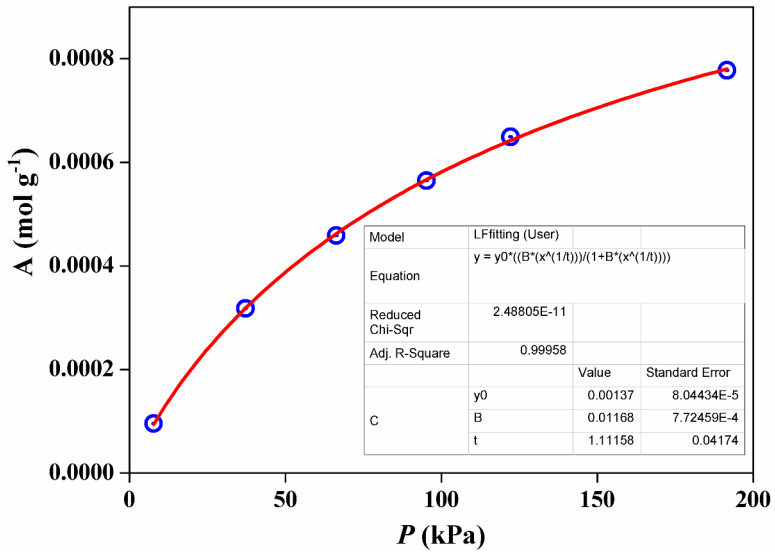

Fig. 32: CO_2 adsorption isotherm for **4′** at 298 K. The solid line represents the best fit to the data using the Langmuir-Freundlich equation, as described above.

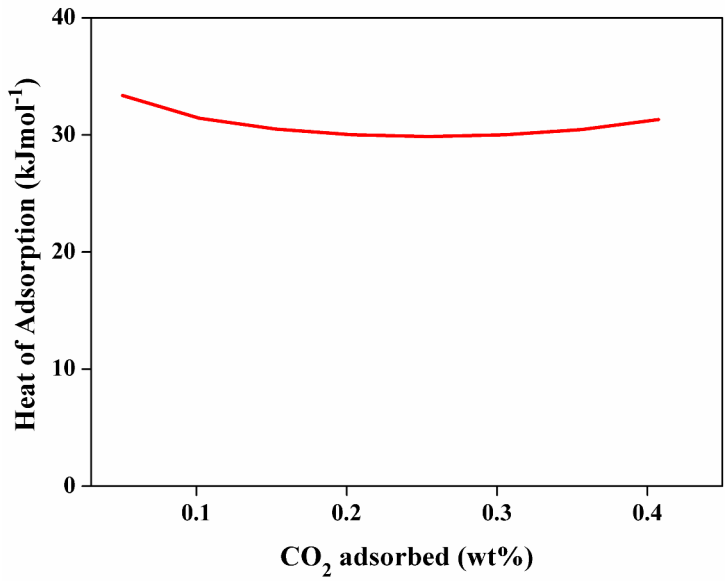

Fig.33: Enthalpy of CO_2 adsorption for **4′** calculated using Clausius-Clapeyron equation.

Ar, O_2, CH_4 and N_2 adsorption isotherms were also measured at 195 K with **1′-4′**. They show negligible amount of uptake with respect to CO_2 adsorption study (Fig. 26-29).

The selective CO_2 uptake of the four compounds can be attributed to the polar nature of the pore surface and the presence of uncoordinated metal sites (**1**, **3** and **4**) which is also supported by the high values of enthalpy of CO_2 adsorption. This could also be correlated with the well-established fact that the electric field generated in the framework by UMSs and

aromatic π-cloud interacts firmly with the quadrupole moment of CO_2 (-1.4×10^{-39} C m^2) causing a rapid uptake at low pressure.

Hydrogen storage capacity: These four compounds were also tested for its H_2-storage capacity at cryogenic temperature. Adsorption isotherms of **1′-4′**shows typical type-I curves. Compound **1′**, **3′** and **4′** reveals steep uptake at low pressure region with the final adsorption amount of 78, 56 and 63 mL g^{-1} respectively (Fig. 34).

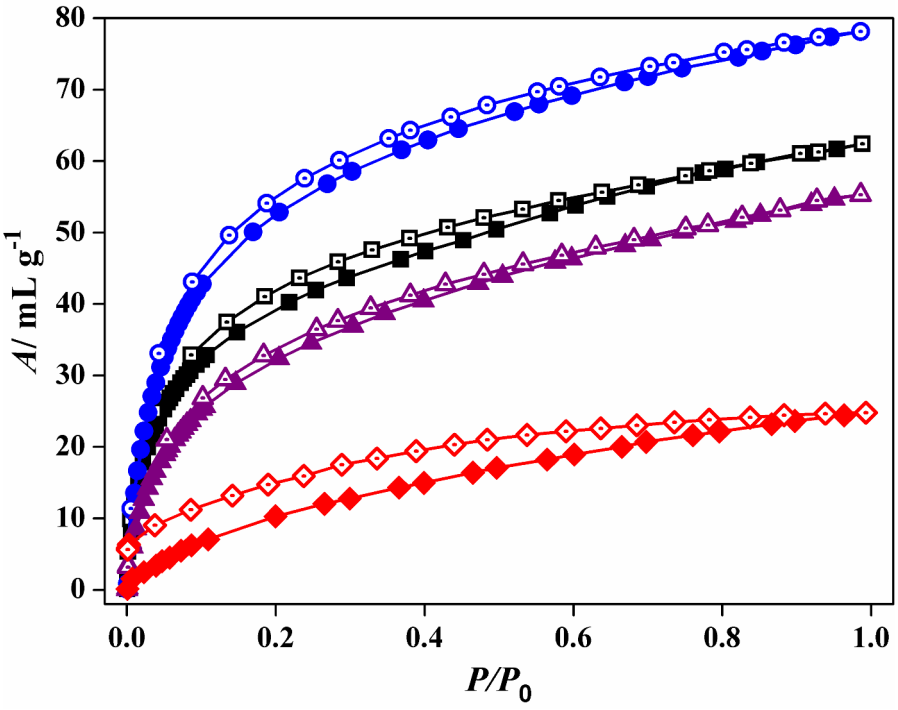

Fig. 34: H_2 adsorption isotherms of **1′**(black), **2′** (wine), **3′** (blue) and **4′** (red) at 77 K. Closed symbols and open symbols are corresponding to adsorption and desorption respectively.

In case of **2′**, the uptake amount gradually increase with increasing pressure and desorption curve does not follow the adsorption one showing a small hysteresis (Fig. 34). High affinity at low pressure region and typical unsaturated adsorption isotherms of **1′** and **3′**can be attributed to the high affinity of H_2 towards vacant Zn(II) centres and the presence of the small channels. Gravimetric H_2 adsorption data for **1′** and **3′** were recorded over the pressure range 0–50 bar at 77 K and 87 K. H_2 adsorption isotherm of **1′** gives a maximum uptake of 65 and 51 mL g^{-1} at 77 and 87 K (Fig. 35a, b) respectively while the compound **3′** takes 90 and 69 mL g^{-1} (Fig. 35a and b) at the respective temperatures.

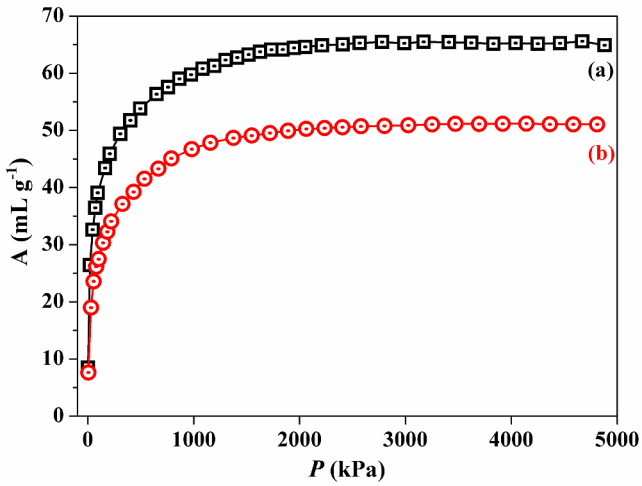

Fig. 35: The high pressure H_2 isotherm (only adsorption) of **1′** measured at 77 K (a) and 87 K (b).

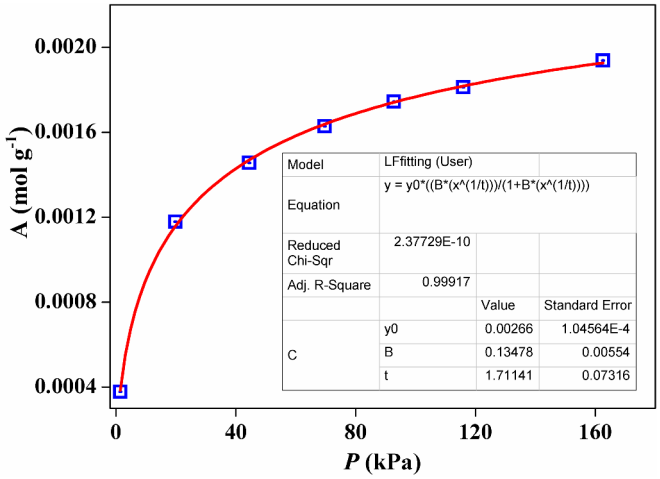

Fig. 36: H_2 adsorption isotherm for **1′** at 77 K. The solid line represents the best fit to the data using the Langmuir-Freundlich equation, as described above.

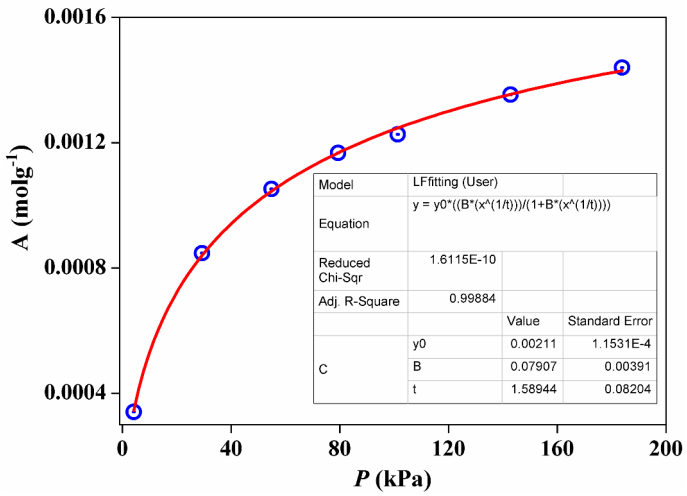

Fig. 37: H_2 adsorption isotherm for **1′** at 87 K. The solid line represents the best fit to the data using the Langmuir-Freundlich equation, as described above.

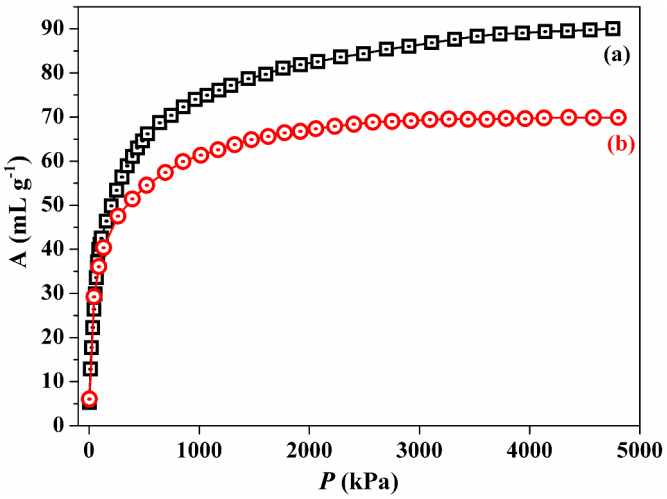

Fig. 38: The high pressure H_2 isotherm (only adsorption) of **3′** measured at 77 K (a) and 87 K (b).

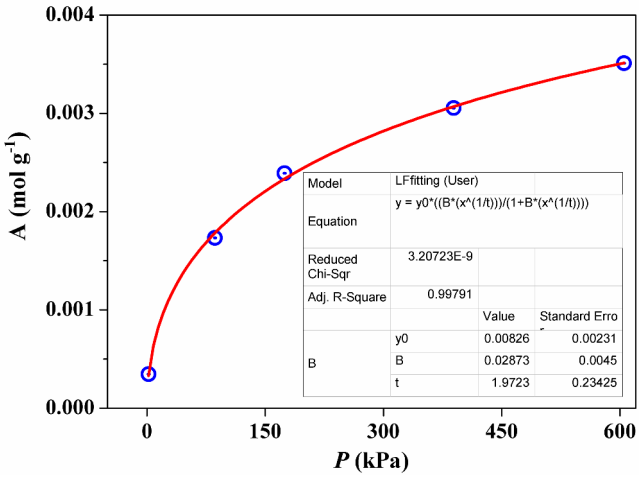

Fig. 39: H_2 adsorption isotherm for **3′** at 77 K. The solid line represents the best fit to the data using the Langmuir-Freundlich equation, as described above.

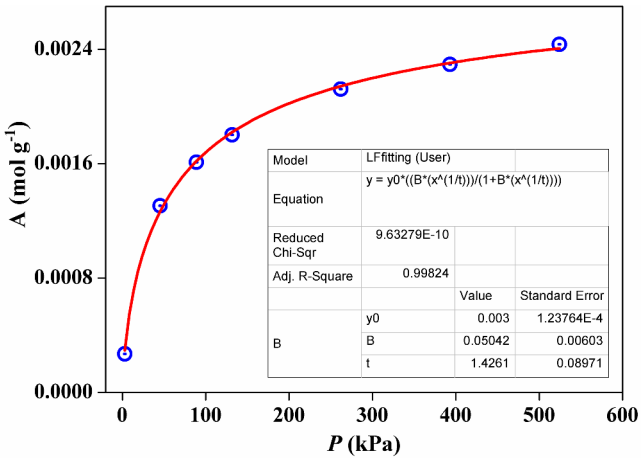

Fig. 40: H_2 adsorption isotherm for **3′** at 87 K. The solid line represents the best fit to the data using the Langmuir-Freundlich equation, as described above.

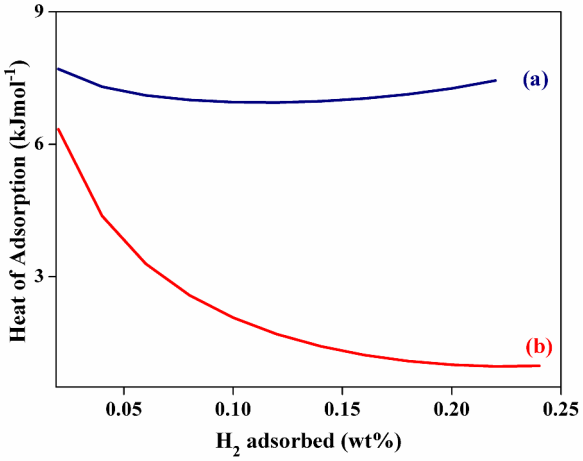

Fig. 41: Enthalpy of H_2 adsorption for **1′**(a) and **3′** (b) calculated using Clausius-Clapeyron equation.

The high pressure profiles measured at 77 and 87 K were used for the calculation of enthalpy of adsorption (ΔH_{ads}) applying Clausius–Clapeyron equation which provides a value of 7.7 and 6.34 kJ mol^{-1} (Fig. 29) for **1′** and **2′** respectively. These values are well agreed with literature value for such systems.

Solvent adsorption study: Inspired by the highly active surface with coordinatively unsaturated sites, open channel structure and presence of lattice water molecules in the cases of **1**–**4**, we anticipated that they will show interesting sorption behaviour depending upon the polarity (Lewis basicity) of guest molecules. To analyse the effect of small molecules on the pore surfaces, we have studied the adsorption properties for the dehydrated samples of **1-4** with different solvent molecules (H_2O, MeOH, EtOH, and C_6H_6).

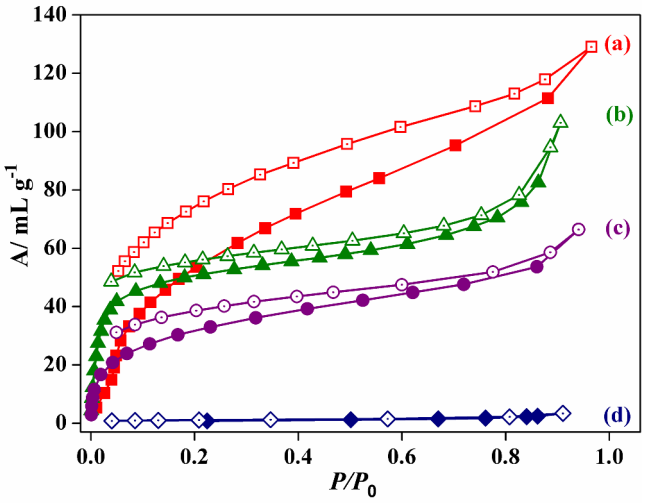

Fig. 42: Solvent adsorption isotherms of **1′**. (a) H_2O (298 K), (b) MeOH (293 K), (c) EtOH (298 K) and (d) C_6H_6 (298 K). Closed symbols and open symbols are corresponding to adsorption and desorption, respectively.

There are two types of adsorption site in compound **1**, channels along the three directions and the other one is unsaturated Zn sites. The H_2O adsorption uptake gradually increases with pressure and finally reaches an amount of ~130 mL g^{-1} at P/P_0 = 0.97. Desorption curve does not follow the adsorption one and shows large hysteresis reflecting the polar nature of the pore surface (Fig. 43a). As expected, **1′** adsorbs a large amount (130 mL g^{-1}) of H_2O which is about 6.32 molecules per formula unit of **1′**. The methanol adsorption curve of **1′**shows a steep uptake (42 mL g^{-1}) upto P/P_0 = 0.5 and then gradually reaches a final amount of 103 mL g^{-1} at P/P_0 = 0.9. The desorption curve of this type II adsorption profile almost follow the adsorption path and retains a large amount of methanol (47 mL g^{-1}) even at low pressure (P/P_0 = 0.03) (Fig. 15b). We calculate the βE_0 values for both the solvents with the help of DR equation which shows a larger value in case methanol (13.5 kJ mol^{-1}) compare to that of water (6.5 kJ mol^{-1}) adsorption. This result suggests stronger attraction of methanol with the pore surface of **1′** compare to water. The ethanol adsorption isotherm shows a gradual uptake and finally takes an amount of 66 mL at P/P_0 = 0.94 whereas **1′** completely excludes C_6H_6 molecules (Fig. 42b, 42c). The above results reflects the polar nature of the pore surface in compound **1** which may be due to the presence of free nitrogen end of cyanide ions and unsaturated metal (Zn) sites.

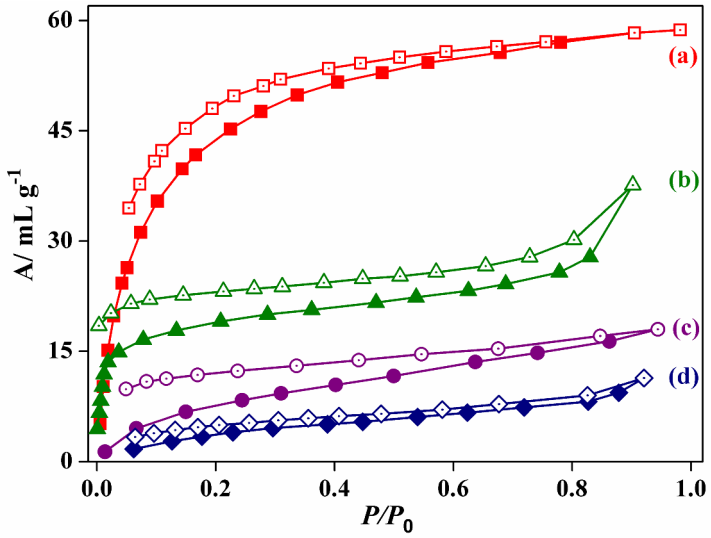

Fig. 43: Solvent adsorption isotherms of **2′**. (a) H_2O (298 K), (b) MeOH (293 K), (c) EtOH (298 K) and (d) C_6H_6 (298 K). Closed symbols and open symbols are corresponding to adsorption and desorption, respectively.

H_2O adsorption isotherm of **2** reveals a type-I isotherm with a gradual uptake. The final amount of uptake is 59 mL g^{-1} at P/P_0 = 0.98 (Fig. 43a). Like the previous compound,

methanol adsorption isotherm also shows type-II uptake with a steep increase at low pressure. The final adsorption amount is 38 mL g^{-1} at P/P_0 = 0.9. Desorption curve follows the adsorption curve and retains 19 mL g^{-1} methanol even at very low pressure (P/P_0 = 0.003) (Fig. 43b). The ethanol adsorption isotherm shows a gradual uptake and finally takes an amount of 18 mL g^{-1} at P/P_0 = 0.94 whereas **2′** completely excludes C_6H_6 molecules (Fig. 43c, 43d).

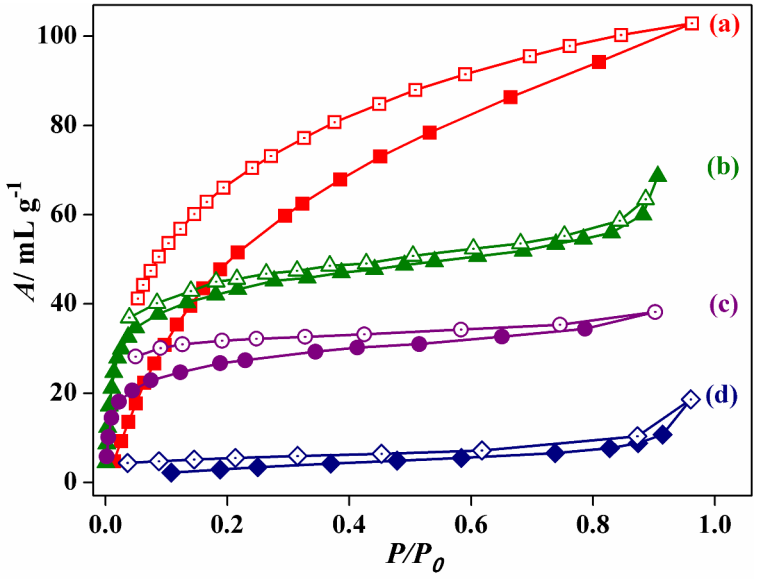

Fig. 44: Solvent adsorption isotherms of **3′**. (a) H_2O (298 K), (b) MeOH (293 K), (c) EtOH (298 K) and (d) C_6H_6 (298 K). Closed symbols and open symbols are corresponding to adsorption and desorption, respectively.

H_2O adsorption isotherm of **3′** shows a typical type-I profile with a gradual uptake. The profile reaches with a final amount of 103 mL g^{-1} (Fig. 44a) of water at P/P_0 = 0.97 which is about 4.64 molecules per formula unit of **3′**. The desorption curve does not follow the adsorption one and shows hysteresis by retaining 52 mL g^{-1} of H_2O even at very low P/P_0 = 0.05. Methanol adsorption profile shows a steep uptake upto P/P_0 = 0.04 (34 mL g^{-1}) and then gradually reaches a final amount of 69 mL g^{-1} at P/P_0 = 0.91. Desorption curve follows the same adsorption path with holding an amount of 36 mL g^{-1} at P/P_0 = 0.03 which reflects the polar nature of **3′** (Fig. 44b). Interesting results were obtained when we calculate the βE_0 values for both the solvents with the help of DR equation. βE_0 value for H_2O is 6.8 kJ mol^{-1} whereas the same for methanol is 11.39 kJ mol^{-1}, which is quite high compare to previous one. This information reveals that, methanol is interacting more with the pore surface rather than water. The final uptake of ethanol and C_6H_6 are 38 mL g^{-1} and 18 mL g^{-1} respectively.

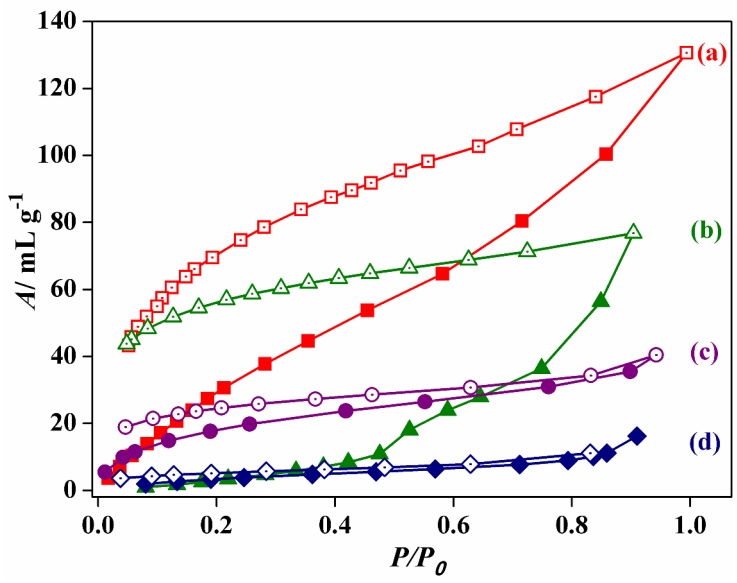

Fig. 45: Solvent adsorption isotherms of **4′**. (a) H_2O (298 K), (b) MeOH (293 K), (c) EtOH (298 K) and (d) C_6H_6 (298 K). Closed symbols and open symbols are corresponding to adsorption and desorption, respectively.

There are two types of adsorption site in compound **4**, channels along the three directions and the other one is unsaturated Zn sites. The H_2O adsorption isotherm gradually increases with pressure and finally reaches an amount of ~130 mL g^{-1} at P/P_0 = 0.99. Desorption curve does not follow the adsorption one and shows large hysteresis reflecting the polar nature of the pore surface (Fig. 45a). As expected, **4′** adsorbs a large volume (130 mL g^{-1}) of H_2O which is about 6.30 molecules per formula unit of **4′**. Methanol adsorption isotherm shows a final volume uptake of 76 mL g^{-1} at P/P_0 = 0.9. Desorption curve does not follow adsorption one and shows a large hysteresis retaining a large amount (43 mL g^{-1}) of adsorbent inside the pore (Fig. 45b). The ethanol adsorption isotherm shows a gradual uptake and finally takes an amount of 40 mL g^{-1} at P/P_0 = 0.94 whereas **4′** completely excludes C_6H_6 molecules (Fig. 45c, 45d). The above results reflects the polar nature of the pore surface present in compound **4** which may be due to the presence of free nitrogen end of cyanide ions and unsaturated metal (Zn) sites.

4.5: ***Conclusion***

We have successfully synthesized three metal-organic frameworks with the simple reactions of Zn(II), $[M(CN)_6]^{3-}$ and organic linkers (bipy, azpy). Systematic investigation was performed by changing the organic linker and as well as their concentrations. Compound **1** and **2** are fascinating from the structural point of view as they act as bi-porous host. At 195K, all the compounds selectively adsorb CO_2 while completely exclude other small molecules like N_2, Ar, O_2 etc. Heat of hydrogenation calculation at cryogenic temperature reveals strong interaction of H_2 molecules with the unsaturated Zn(II) metal site and as well as with the pore surface. We have successfully monitored the property changes with the change of organic linkers and linker concentration. Further experiments are in progress to synthesize smart MOFs with varying the metal nodes and as well as the linker length and concentration.

4.6: ***References***

1. (*a*) S. Kitagawa, R. Kitaura and S. N. Noro, *Angew. Chem., Int. Ed.,* **2004**, *43*, 2334; (*b*) R. Yang, L. Li, Y. Xiong, J. R. Li, H. C. Zhou, C.Y. Su, *Chem. Asian J.*, **2010**, *5*, 2358; (*c*) C. J. Doonan, W. Morris, H. Furukawa, and O. M. Yaghi, *J. Am. Chem. Soc.,* **2009**, *131,* 9492; (*d*) J. R. Long, O. M. Yaghi, *Chem. Soc. Rev.*, **2009**, *38*, 1213-1214; (*e*) H. Hayashi, A. P. Côté, H. Furukawa, M. O'Keeffe and O. M. Yaghi, *Nature Mater.,* **2007**, *6*, 501.
2. (*a*) M. E. Kosal, J. -H. Chou, S. R. Wilson and K. S. Suslick, *Nat. Mater.* **2002**, *1*, 118; (*b*) K. Uemura, S. Kitagawa, K. Fukui and K. Saito, *J. Am. Chem. Soc.* **2004**, *126*, 3817; (*c*) E.-Y. Choi, K. Park, C.-M. Yang, H. Kim, J.-H. Son, S.W. Lee, Y. H. Lee, D. Min and Y.-U. Kwon, *Chem. Eur. J.,* **2004**, *10*, 5535; (*d*) R. Matsuda, R. Kitaura, S. Kitagawa, Y. Kubota, R. V. Belosludov, T. C. Kobayashi, H. Sakamoto, T. Chiba, M. Takata, Y. Kawazoe and Y. Mita, *Nature*, **2005**, *436*, 238; (*e*) C. J. Kepert, *Chem. Commun*. **2006**, 695; (*f*) X. Lin, A. J. Blake, C. Wilson, X. Z. Sun, N. R. Champness, M. W. George, P. Hubberstey, R. Mokaya and M. Schröder, *J. Am. Chem. Soc.,* **2006**, *128*, 10745; (*g*) S. Ma and H.-C. Zhou, *J. Am. Chem. Soc.* **2006**, *128*, 11734; (*h*) A. C. Sudik, A. P. Côté, A. G. Wong-Foy, M. O'Keeffe and O. M. Yaghi, *Angew. Chem. Int. Ed*., **2006**, *45*, 2528; (*i*) K. L. Mulfort and J. T. Hupp, *J. Am. Chem. Soc.,* **2007**, *129*, 9604; (*j*) S. Shimomura, S. Horike, R. Matsuda and S. Kitagawa, *J. Am. Chem. Soc.,* **2007**, *129*, 10990; (*k*) Z. Wang and S. M. Cohen, *J. Am. Chem. Soc.,* **2007**, *129*, 12368.
3. (*a*) L. J. Murray, M. Dincă and J. R. Long, *Chem. Soc. Rev.*, **2009**, *38*, 1294. (*b*) S. Kitagawa, R. Kitaura and S. Noro, *Angew. Chem. Int. Ed.*, **2004**, *43*, 2334; (*c*) J. R. Li, R. J. Kuppler and H. C. Zhou, *Chem. Soc. Rev.*, **2009**, *38*, 1477; (*d*) J. Lee, O. K. Farha, J. Roberts, K. A. Scheidt, S. T. Nguyen and J. T. Hupp, *Chem. Soc. Rev.*, **2009**, *38*, 1450; (*e*) J. Lee, O. K. Farha, J. Roberts, K. A. Scheidt, S. T. Nguyen and J. T. Hupp, *Chem. Soc. Rev.*, **2009**, *38*, 1450; (*f*) D. Maspoch, D. Ruiz-Molina and J. Veciana, *Chem. Soc. Rev.*, **2007**, *36*, 770; (*g*) S. Achmann, G. Hagen, J. Kita, I. M. Malkowsky, C. Kiener and R. Moos, *Sensors*, **2009**, *9*, 1574; (*h*) P. Horcajada, C. Serre, G. Maurin, N. A. Ramsahye, F. Balas, M. Vallet-Regi, M. Sebban, F. Taulelle and G. Férey, *J. Am. Chem. Soc.*, **2008**, *130*, 6774.

4. (*a*) G. Férey, C. Mellot-Draznieks, C. Serre, F. Millange, J. Dutour, S. SurblV and I. Margiolaki, *Science*, **2005**, *309*, 2040; (*b*) X.-C. Huang, Y.-Y. Lin, J.-P. Zhang and X. -M. Chen, *Angew. Chem. Int. Ed.* **2006**, *45*, 1557; (*c*) K. S. Park, Z. Ni, A. P. Côté, J. Y. Choi, R. Huang, F. J. Uribe- Romo, H. K. Chae, M. O'Keeffe and O. M. Yaghi, *Proc. Natl. Acad. Sci. USA* **2006**, *103*, 10186; (*d*) H. Hayashi, A. P. Côté, H. Furukawa, M. O'Keeffe and O. M. Yaghi, *Nat. Mater.* **2007**, *6*, 501; (*e*) Y. -Q. Tian, Y. -M. Zhao, Z. -X. Chen, G. -N. Zhang, L. -H. Weng and D. -Y. Zhao, *Chem. Eur. J.* **2007**, *13*, 4146.
5. (*a*) S. Holloway, *Energy*, **2005**, *30*, 2318; (*b*) A. Arenillas, K. M. Smith, T. C. Drage and C. E. Snape, *Fuel*, **2005**, *84*, 2204; (*c*) K. Lackner, *Science*, **2003**, *300*, 1677.
6. C. M. White, D. H. Smith, K. L. Jones; A. L. Goodman, S. A. Jikich, R. B. LaCount, S. B. DuBose, E. Ozdemir, B. I. Morsi and K. T Schroeder, *Energy Fuels*, **2005**, *19*, 659.
7. (*a*) J. D. Figueroa, T. Fout, S. Plasynski, H. McIlvried and R. D. Srivastava, *Int. J. Greenhouse Gas Control*, **2008**, *2*, 9; (*b*) F. Li, L.-S. Fan; *Energy Environ. Sci.* **2008**, *1*, 248–267.
8. D. Singh, E. Croiset, P. L. Douglas and M. A. Douglas, *Energy ConVers. Manage.* **2003**, *44*, 3073.
9. H. Li, M. Eddaoudi, T. L. Groy and O. M. Yaghi, *J. Am. Chem. Soc.* **1998**, *120*, 8571.
10. J. R Li, Y. Tao, Q. Y., Xian-He Bu, H. Sakamoto and S. Kitagawa, *Chem. -Eur. J.,* **2008,** *14***,** 2771**.**
11. K. Nakagawa, D. Tanaka, S. Horike, S. Shimomura, M. Higuchi and S. Kitagawa, *Chem. Commun.,* **2010,** *46*, 4258**.**
12. SAINT+, 6.02 ed.; Bruker AXS: Madison, WI, **1999**.
13. G. M. Sheldrick, *SADABS, Empirical Absorption Correction Program*; University of Göttingen, Göttingen, Germany, **1997**.
14. Altomare, G. Cascarano, C. Giacovazzo and A. Gualaradi, *J. Appl. Crystallogr.*, **1993**, *26*, 343.
15. G. M. Sheldrick, SHELXL 97, *Program for the Solution of Crystal Structure*, University of Göttingen, Germany, **1997**.
16. A. L. Spek, *J. Appl. Crystallogr.*, **2003**, *36*, 7.
17. G. M. Sheldrick, SHELXS 97, *Program for the Solution of Crystal Structure*, University of Göttingen, Germany, **1997**.

18. L. J. Farrugia, WinGX - A Windows Program for Crystal Structure Analysis, *J. Appl. Crystallogr.*, **1999**, *32*, 837.
19. (*a*) E. V. Brown and G. R. Granneman *J. Am. Chem. Soc.* **1975**, *97***,** 621. (*b*) O. Theilmann, W. Saak, D. Haase, R. Beckhaus, *Organometallics,* **2009,** *28,* 2799.

Chapter-5

Synthesis, Structural Characterization, Gas Storage and Magnetic Study of a 3D Framework of Co(II) Bridged by $[Cr(CN)_6]^{3-}$ and 4,4′-Bipyridyl

Abstract:

A bimetallic pillared-layer coordination framework $\{[Co_3(bipy)_3(H_2O)_4][Cr(CN)_6]_2 \cdot 2(bipy) \cdot 4(H_2O)\}_n$ (**1**) (bipy = 4,4′-bipyridyl) has been synthesized using a cyanometallate anion ($[Cr(CN)_6]^{3-}$) and an organic linker bipy in an ethanol/water medium at RT. Indexing of the powder X-ray diffraction (PXRD) pattern of **1** suggests similar unit cell parameter to its Mn-analogue (Chapter 3). Structural robustness of the guest evacuated **1**, obtained after removal of water and guest bipy molecules, has been confirmed by variable temperature PXRD studies. The Langmuir surface area of **1** calculated from N_2 adsorption isotherm turns out to be of 226 m^2 g^{-1}. Gas adsorption studies suggests compound **1** can adsorb ~20 wt% CO_2 (low pressure) and ~1.1 wt% H_2 (50 bar) at 195 and 77 K, respectively. Moreover, solvent vapour adsorption studies indicate that the framework can incorporate small molecules such as, H_2O and EtOH while excludes large molecule like C_6H_6. Magnetic study reveals an overal ferrimagnetic interaction resulting from three Co(II) (S = 3/2) and two Cr(III) (S = 3/2) centers.

5.1: *Introduction*

The diversity of frameworks is one of the most representative features of metal-organic framework. The accomplishment of multiple functions providing interlock, coexistence or control of magnetism, optical properties, ferroelectricity and gas adsorption is an attractive topic in the field of material chemistry,[1] in which porous coordination frameworks (PCPs) are expected to perform as multifunctional materials. One can easily summarise the characteristics of PCPs as (i) the chemical versatility with the change in metal ions and ligands, (ii) a tuneable and regular framework based on the intrinsic topology of the constituents and (iii) the flexible framework based on the coordination bonds.[2,3] These characteristics enable themselves to be most desirable material in the aspect of multifunctionality.

The structural varieties in coordination polymers usually involve the corresponding changes in the compound's properties like magnetic, optical, conductivity, porosity etc.[4] For example, coordination polymer magnets, also called molecular-based magnets,[5,6] sensitively respond to the structural changes, because structural perturbations directly affect the local overlap integral of their magnetic orbitals, which is clearly reflected from their magnetic properties in bulk. Another example can be viewed in the aspect of porosity. The interaction of gases with the framework can be tuned with the change in metal ions as well as the organic linkers.[7,8] The high affinity of hydrogen toward unsaturated cobalt site is a well-established fact. The energy of adsorption value can be varied by tuning the metal centre as well as the ligands. Long and co-workers haves reported hydrogen adsorption profile of various prussian blue analogues, where they have shown the variation of final volume uptake with changing metal ions[9,10].

5.2: *Scope of the study*

Here cobalt has been introduced which links the metallocyanates to generate the magnetic platform. The variation in adsorption amount as well as high energy of adsorption clearly reflects the role of cobalt in this framework. Further work is underway to study the guest induced magnetic modulation and interesting solvent adsorption property.

5.3: *Experimental Section*

5.3.1: *Materials*

All the reagents and solvents employed were commercially available and used as supplied without further purification. $K_3[Cr(CN)_6]$, 4,4′-bipyridyl and $CoCl_2 \cdot 4H_2O$ were obtained from the Aldrich Chemical Co.

5.3.2: *Synthetic procedure*

Synthesis of $\{[Co_3(bipy)_3(H_2O)_4][Cr(CN)_6]_2 \cdot 2(bipy) \cdot 4(H_2O)\}_n$ (1): An aqueous solution (12.5 mL) of $K_3[Cr(CN)_6]$ (0.25 mmol, 0.0426 g) was added to an ethanolic solution (12.5 mL) of bipy (0.25 mmol, 0.039 g) and stirred for 30 min. $CoCl_2 \cdot 4H_2O$ (0.25 mmol, 0.0494 g) was dissolved in 12.5 mL distilled water and 2.5 mL of this metal solution was carefully layered with the 2.5 mL of mixed bipyridyl and $K_3Cr(CN)_6$ solution using an ethanol : water buffer solution (1 mL, 1:1) in a crystal tube. After 15 days, transparent block crystals appeared in the middle of the tube and separated and washed with ethanol (Yield ~ 60 %). The bulk amount of the sample was prepared by the direct mixing of the reagents in ethanol/water mixed solution with stirring for 24 h and the phase purity was checked with the PXRD and elemental analysis. This powdered sample was used for studying different physical properties. IR: ν(C≡N) 2175, 2157 and 2129 cm^{-1}; ν(C=C): 1609 cm^{-1}, 1536 cm^{-1}; ν(O-H): 3597 cm^{-1} and 3473 cm^{-1} (Fig. 1). Anal. cald. for $C_{62}H_{56}Cr_2Co_3N_{22}O_8$: C, 49.03; H, 3.72; N, 20.30. Found: C, 48.72; H, 3.52; N, 20.66%.

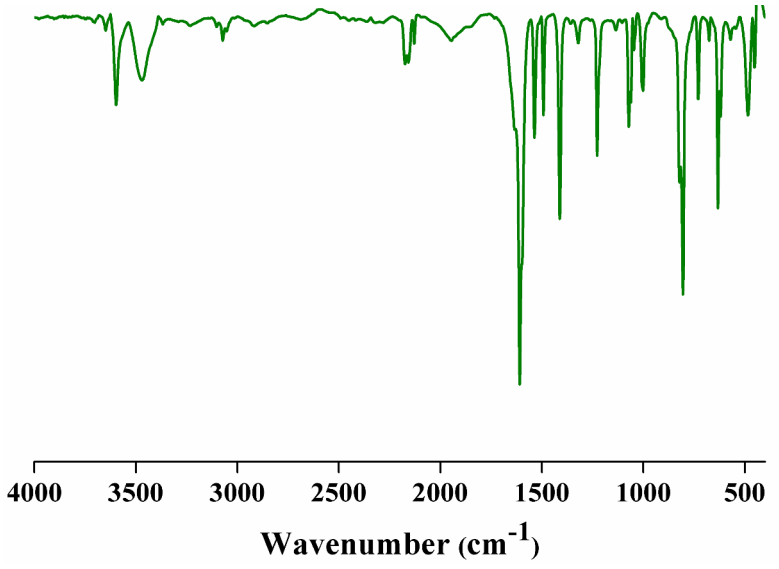

Fig. 1: IR spectrum of **1**.

Preparation of {[Co_3(bipy)$_3$][Cr(CN)$_6$]$_2$} (1′): Compound **1′** was prepared by heating **1** at 165 ºC under vacuum (< 10^{-1} Pa) for 72 hours. This powdered sample was used for characterization of different physical properties. IR: ν(C≡N) 2162 cm^{-1}; ν(C=C): 1603 cm^{-1}, 1531 cm^{-1}. Anal. cald. for $C_{42}H_{22}Cr_2Co_3N_{18}$: C, 47.59; H, 2.09; N, 23.80. Found: C, 48.84; H, 2.31; N, 23.12%.

5.3.3: ***Physical Measurements***

The elemental analyses were carried out on a Thermo Fisher Flash 2000 Elemental Analyzer. Thermogravimetric analyses (TGA) was carried out with a METTLER TOLEDO TGA850 instrument under nitrogen atmosphere. IR spectra were recorded in the region 4000-400 cm^{-1} on a Bruker IFS 66v/S spectrophotometer with samples prepared in KBr pellets. Powder X-ray diffraction (PXRD) data were collected on a Bruker D8 Discover instrument using Cu-*K*α radiation.

5.3.4: ***Adsorption Study***

N_2, H_2 and CO_2 adsorption studies were carried out with the dehydrated samples of **1** (i.e. **1a**, prepared at 175 ºC under high vacuum (<10^{-1} Pa) for 72 hours) by using QUANTACHROME QUADRASORB *SI* analyzer at 77 and 195 K, respectively. High-pressure H_2 adsorption isotherm measurements at 77 and 87 K were carried out on a fully computer controlled volumetric BELSORP-HP, BEL JAPAN high pressure instrument. The high pressure CO_2 measurements at 273 and 298 K were also carried out on a fully computer controlled volumetric BELSORP-HP, BEL JAPAN high pressure instrument. The gases used for the high pressure measurements were of scientific/research grade with 99.999% purity. For the measurements, approximately 200 mg of sample was taken in a stainless-steel sample holder and degassed at 175 ºC for about 72 hours. Dead volume of the sample cell was measured using helium gas of 99.999% purity. Non-ideal correction for hydrogen gas was made by applying virial coefficients at the measurement temperature.

5.4: *Results and Discussion*

5.4.1: *Structural description of 1*

The single crystals of **1** were very unstable in air. Hence it was very difficult to determine the structure through single crystal X-ray diffraction. We have taken a long range PXRD scan and tried to get an idea about the structure of **1**. The indexing result by DICVOL program has been given as follow which suggests an orthorhombic system with cell parameters a = 17.8274 Å, b = 16.4476 Å and c = 11.4019 Å.

From elemental analysis, PXRD patterns, IR data and above cell parameters data we have concluded the molecular formula of **1** to be $\{[Co_3(bipy)_3(H_2O)_4][Cr(CN)_6]_2 \cdot 2(bipy) \cdot 4(H_2O)\}_n$ and it may analogous with respect to the compound $\{[Mn_3(bipy)_3(H_2O)_4][Cr(CN)_6]_2 \cdot 2(bipy) \cdot 4(H_2O)\}_n$.

5.4.2: *Framework Stability: Thermogravimetric (TG) and PXRD Analysis*

Thermal studies were carried out to analyse the stability and integrity of the framework (Fig. 2). TG analysis under nitrogen flow suggests two-step release of guest and coordinated water molecules (obs. 8.8 %; calcd. 9.55 %) in the temper-ature range 40 – 180 ºC.

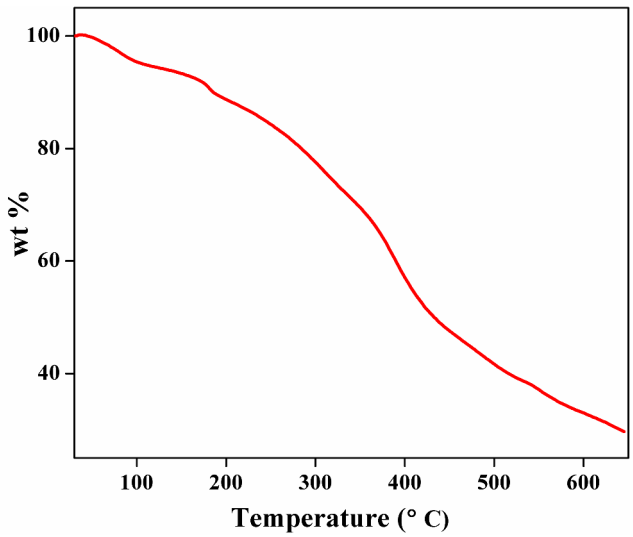

Fig.2: TGA of **1** recorded under N_2 atmosphere in the temperature range 30 – 650 ºC.

However, when **1** is heated at 175 ºC under high vacuum (to prepare **1′**) we observed loss of guest bipy together with guest and coordinated water molecules. This was confirmed by IR spetroscopy and elemental analysis.

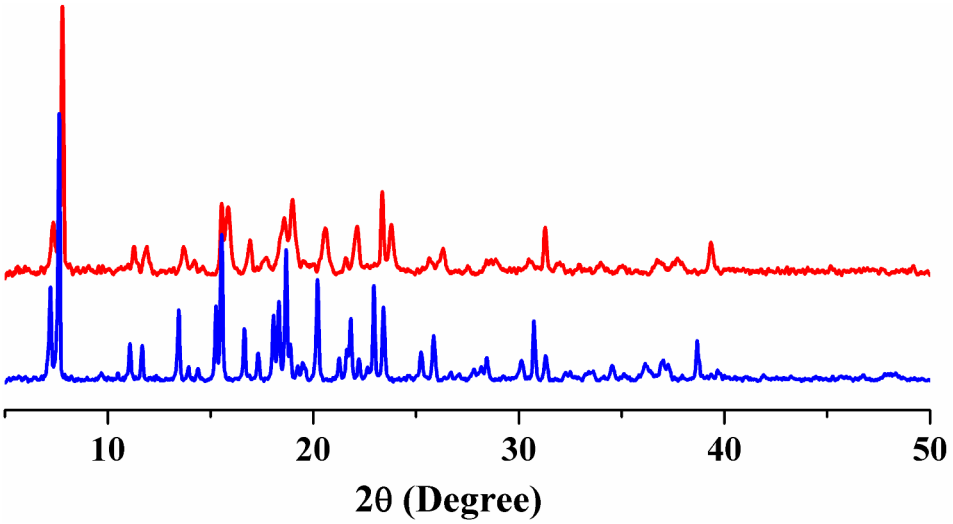

Fig. 3: PXRD patturn of **1** and $\{[Mn_3(bipy)_3(H_2O)_4][Cr(CN)_6]_2 \cdot 2(bipy) \cdot 4(H_2O)\}_n$ which suggests similar orthorhombic structure of **1**.

Powder X-ray diffraction (PXRD) (Fig. 3) pattern of **1** was given in figure 2. It was observed that it agrees well with the patturn of $\{[Mn_3(bipy)_3(H_2O)_4][Cr(CN)_6]_2 \cdot 2(bipy) \cdot 4(H_2O)\}_n$. From this data it can be concluded that both are isostructural.

5.4.3: ***Adsorption Measurement***

Gas adsorption study: The desolvated framework **1′** was used for gas adsorption studies to establish the permanent porosity of the compound.

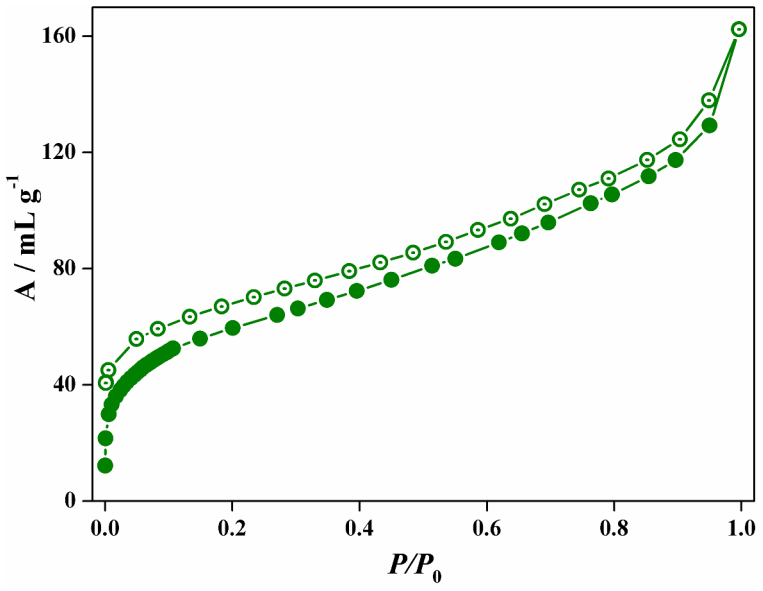

Fig. 4: N_2 adsorption isotherm of **1′** at 77 K. ((P_0 is the saturated vapour pressure of N_2 at the measurement temperature).

N_2 adsorption at 77 K reveals a type II profile with final uptake of 162 mL g^{-1} (Fig. 4). The Langmuir surface area calculated form the N_2 adsorption data was found to be 226 m^2 g^{-1}. CO_2 adsorption isotherm of **1′** shows a type I profile with rapid uptake at low pressure. Compound **1′** adsorbs ~ 44 mL g^{-1} of CO_2 at very low pressure (P/P_0 = 0.05) revealing the strong interaction with pore surface. After P/P_0 = 0.05 the adsorption amount increases gradually with the final uptake of 102 mL g^{-1} (Fig. 5). The steep uptake at low pressure motivates us to calculate the energy of adsorption for CO_2 gas.

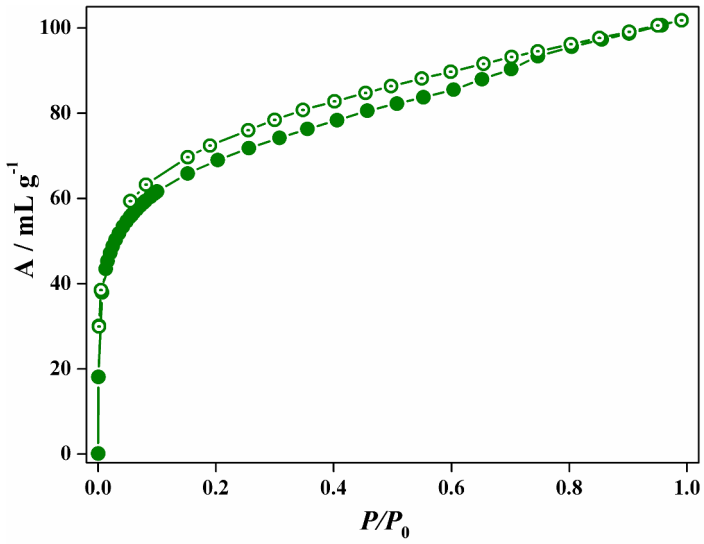

Fig. 5: CO_2 adsorption isotherms of **1′** at 195 K.

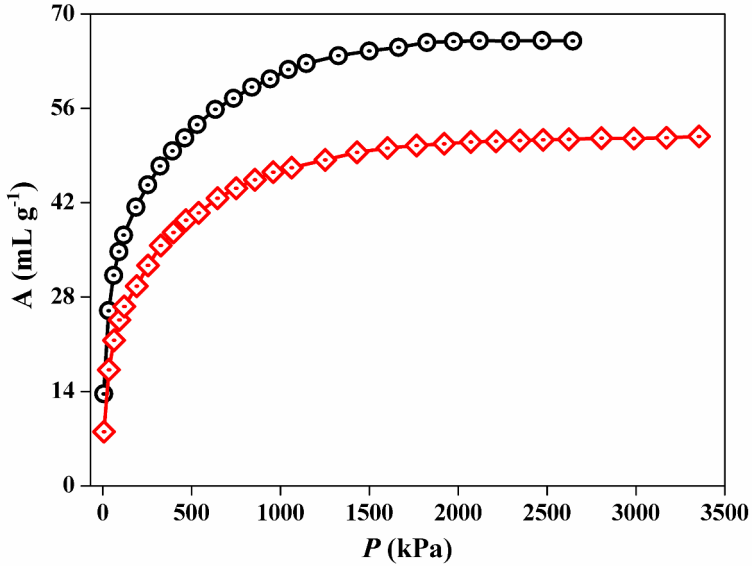

Fig. 6: High pressure CO_2 isotherms (only adsorption) of **1′** at 273 K (black) and 298 K (Red).

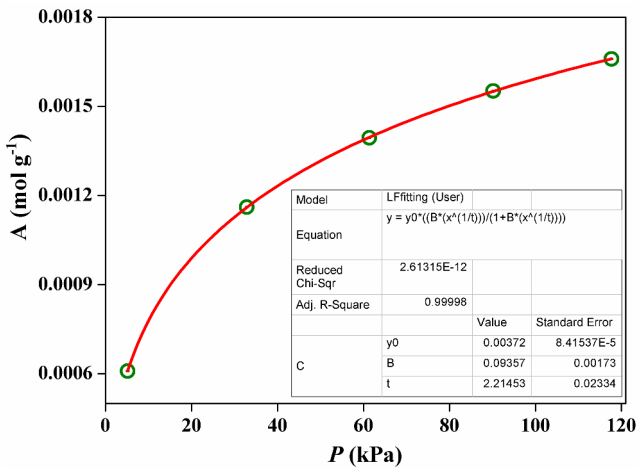

Fig. 7: CO_2 adsorption isotherm for **1′** at 273 K. The solid line represents the best fit to the data using the Langmuir-Freundlich equation, as described above.

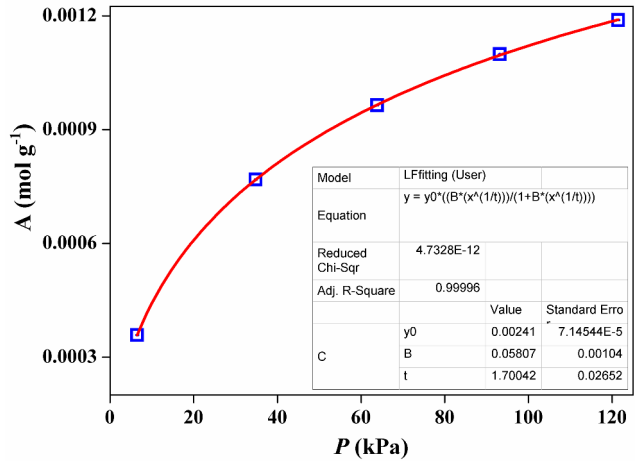

Fig. 8: CO_2 adsorption isotherm for **2a** at 298 K. The solid line represents the best fit to the data using the Langmuir-Freundlich equation, as described above.

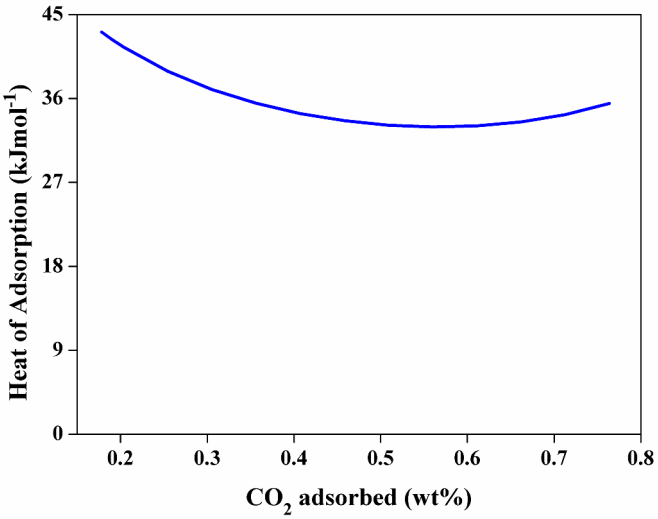

Fig. 9: Enthalpy of CO_2 adsorption for **1′** calculated using Clausius-Clapeyron equation.

The calculation was done with the help of Clausius-Clapeyron equation. High pressure CO_2 adsorption profile at 273 and 298 K was measured and the detail of calculation can be found in Chapter 3. The plots regarding the calculation are given in fig. 6-9. The energy of adsorption was turned out to be ~ 44 kJ mol^{-1}, which suggests strong interaction between the pore surface and CO_2 molecules.

Compound **1′** was also tested for its H_2-storage capacity at cryogenic temperature (Fig. 10). Adsorption isotherms of **1′** shows complete type-I curve with a steep uptake at low pressure region with the final adsorption amount of 69 mL g^{-1}. We have also calculated the energy of hydrogenation. High pressure adsorption data at 77 K and 87 K were used for calculation. The value was turned out to be 13.6 kJ mol^{-1} suggesting 1 as a promising hydrogen storage materials. The regarding plots are given in figure 10-14.

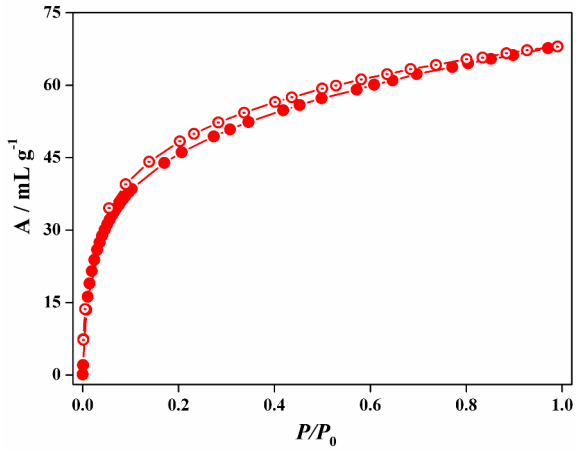

Fig. 10: H_2 adsorption isotherm of **1′.**

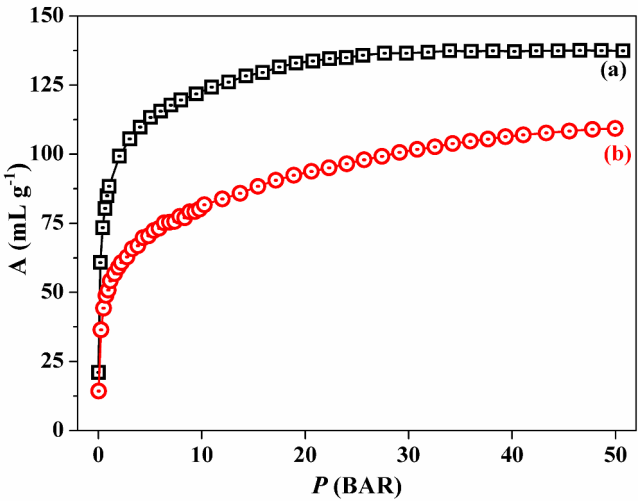

Fig. 11: The high pressure H_2 isotherms (only adsorption) of **1′** measured at 77 K (a) and 87 K (b).

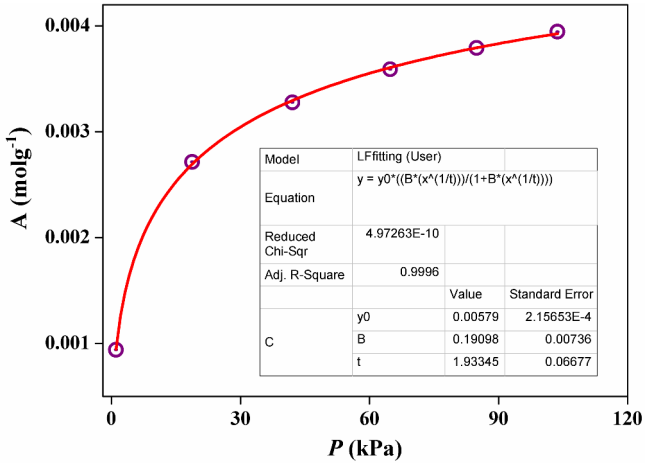

Fig. 12: H_2 adsorption isotherm for **1′** at 77 K. The solid line represents the best fit to the data using the Langmuir-Freundlich equation, as described above.

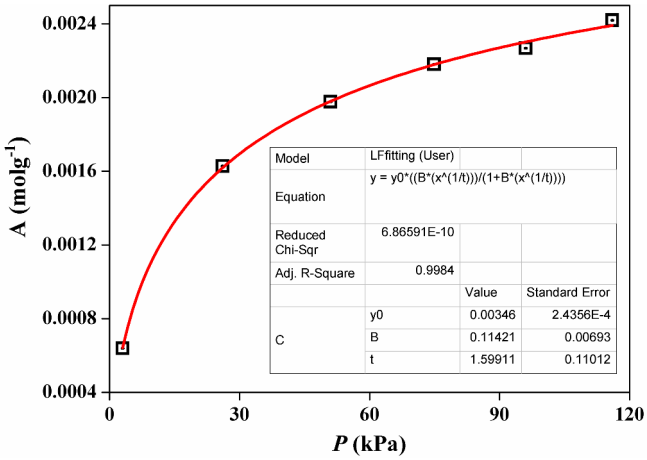

Fig. 13: H_2 adsorption isotherm for **1′** at 87 K. The solid line represents the best fit to the data using the Langmuir-Freundlich equation, as described above.

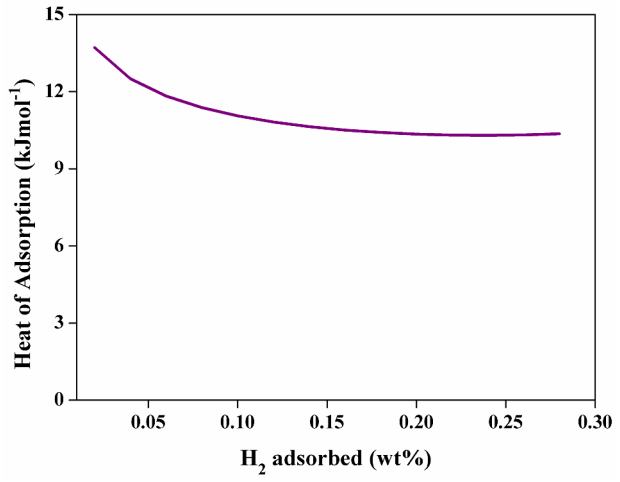

Fig. 14: Enthalpy of H_2 adsorption for **1′** calculated using Clausius-Clapeyron equation.

Solvent adsorption study: Inspired by the highly active surface with coordinatively unsaturated sites, open channel structure and presence of lattice water molecules in the case of **1**, we anticipated that they will show interesting sorption behaviour depending upon the polarity (Lewis basicity) of guest molecules. To analyze the effect of small molecules on the pore surfaces, we have studied the adsorption properties for the dehydrated samples of **1** (i.e **1′**) with different solvent molecules (H_2O, EtOH, and C_6H_6).

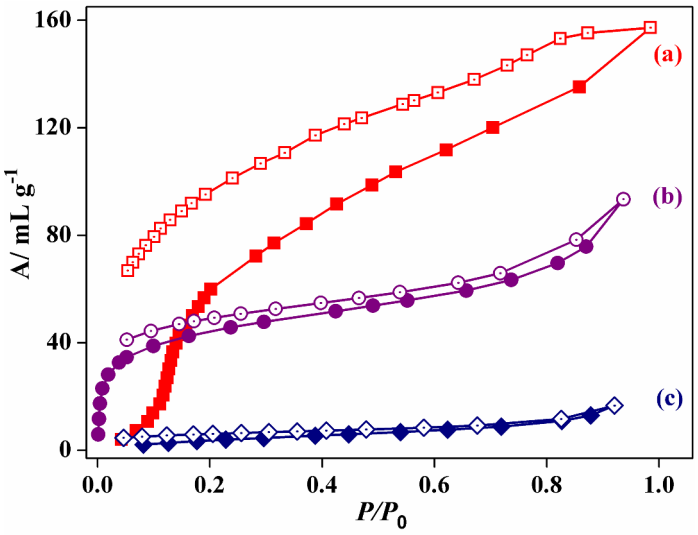

Fig. 15: Solvent adsorption isotherms of **1′**. (a) H_2O, (b) EtOH and (c) C_6H_6. Closed symbols and open symbols are corresponding to adsorption and desorption respectively.

The H_2O adsorption uptake gradually increases with pressure and finally reaches an amount of ~158 mL g^{-1} at P/P_0 = 0.98. Desorption curve does not follow the adsorption one and shows large hysteresis reflecting the polar nature of the pore surface (Fig. 15a). As expected, **1′** adsorbs a large amount (158 mL g^{-1}) of H_2O which is about ~ 7.3 molecules per formula unit of **1′**. The ethanol adsorption curve of **1′** shows a steep uptake (34 mL g^{-1}) upto P/P_0 = 0.5 and then gradually reaches a final amount of 93 mL g^{-1} at P/P_0 = 0.94. The desorption curve of this type II adsorption profile almost follow the uptaking path and retains a large amount of ethanol (41 mL g^{-1}) even at low pressure (P/P_0 = 0.03) (Fig. 15 b). Compound **1′** almost excludes benzene molecules.

5.4.4: ***Magnetic Measurement***

We have successively measured magnetic data of assynthesized **1**. The dc magnetic susceptibilities are shown in the form $\chi_M T$ vs T (**1**) in Figure 16. The χ_M value for **1** at 300 K is 0.0412 cm^3 mol^{-1}($\chi_M T$ =12.30 cm^3 mol^{-1} K) which is larger than the spin only value

(0.03117 cm^3 mol^{-1}; 9.29 cm^3 mol^{-1} K) for magnetically isolated three Co^{II} (S = 3/2) and two Cr^{III} (S = 3/2) ions. The $\chi_M T$ value gradually increases with decreasing temperature to reach a value of 17.84 cm^3 mol^{-1} K at 39 K, and then rapidly increases to a maximum value of 348.32 cm^3 mol^{-1} K at 53 K and then again decreases to 7.28 cm^3 mol^{-1} K at 3.0 K.

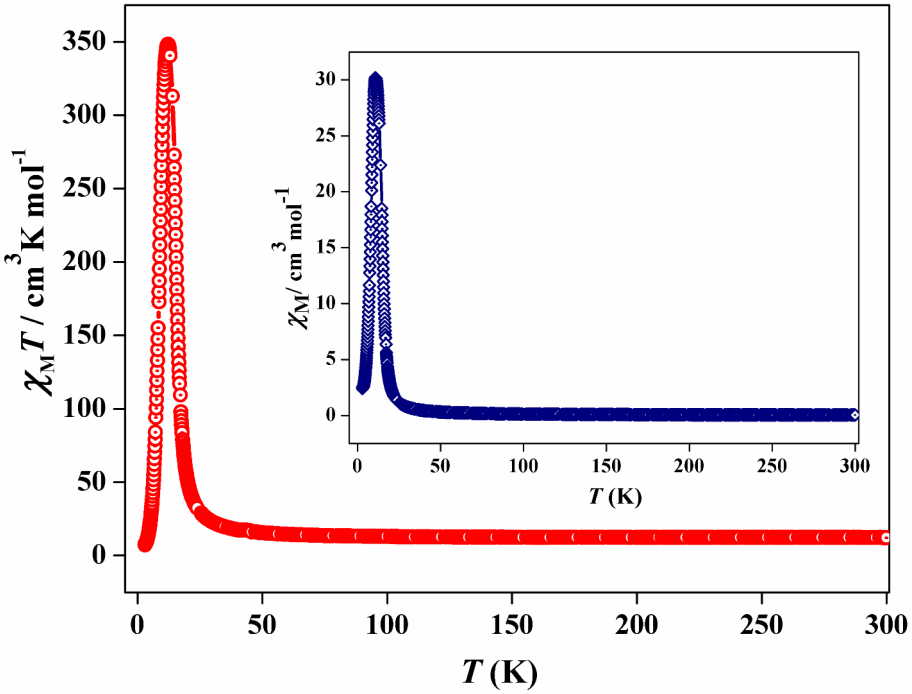

Fig. 16: Temperature dependence of the magnetic susceptibility of **1** an applied field of 500 Oe under zero field cooled condition. Inset shows the plot of χ_M vs T of **1**.

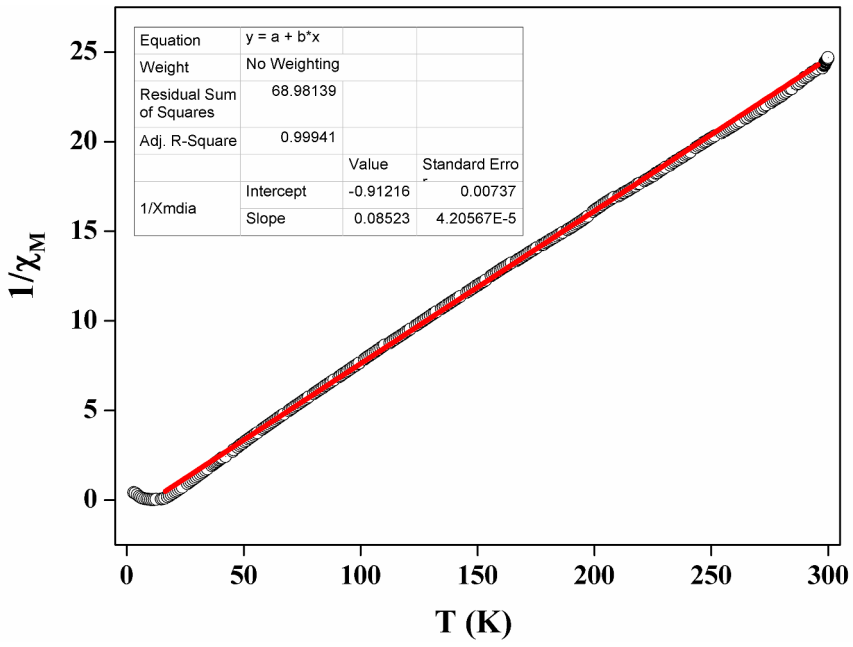

Fig. 17: Curie–Weiss fitting of **1** above 150 K with C = 11.733 cm^3 K mol^{-1}, and θ = -10.7023 K.

The $1/\chi_M$ vs T plot (Fig. 17) in the temperature range of 300 – 20 K obeys the Curie-Weiss law with a Weiss constant θ = -10.7023 K, which suggest the antiferromagnetic interaction between the adjacent Co^{II} and Cr^{III} ions through cyanide bridges. The rapid increase in $\chi_M T$ value indicates a ferrimagnetic ordering. The decrease in $\chi_M T$ value after 12 K suggests further interaction between the layers through the bipy linker. The high value of χ_M is may be due to spin-orbit coupling resulting from Co(II) ion.

The field dependence magnetization curve of **1** shows rapid increase to give highest value of 8.33 $N\beta$ at 50 kOe which is also the signature of magnetic ordering within the compound (Fig. 18).

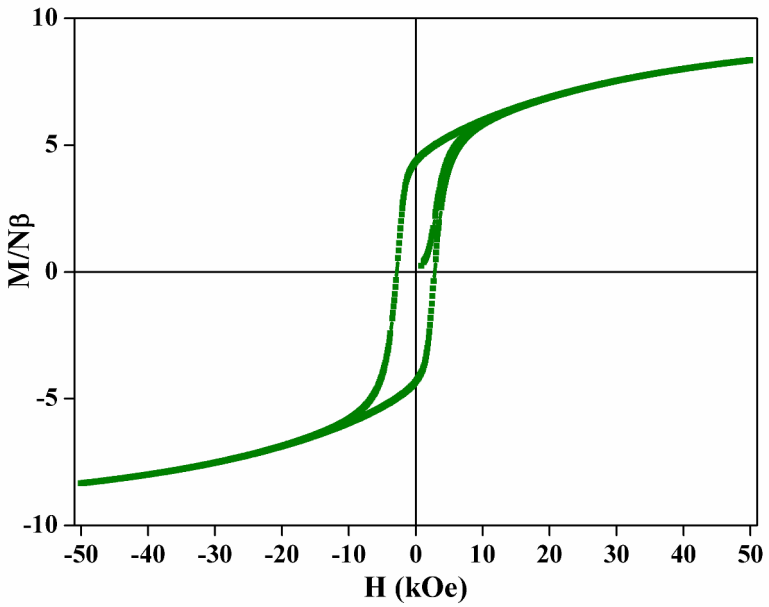

Fig. 18: Magnetization plot for **1** measured at 3 K

5.4.5: ***Conclusion***

In summary, we have adopted a simple approach to assemble 2D magnetic layers into a 3D rigid porous framework that exhibits permanent porosity and ferromagnetic ordering at low temperature. Gas adsorption studies indicate that the compound do not incorporate inert molecule N_2 into its pore but able to accommodate polar CO_2 molecules. The compound can adsorb ~20 wt% CO_2 (low pressure) and ~1.1 wt% H_2 (50 bar) at 195 and 77 K, respectively. Calculation using Clausius-Clapeyron equation suggests a high value of enthalpy of

adsorption of CO_2 (~ 44 kJ mol^{-1}) which is one among the highest values reported in literature. Magnetic study reveals an overal ferrimagnetic interaction resulting from three Co(II) (3/2) and two Cr(III) (3/2) centers.

5.4.6: ***References***

1. V. Ramamurthy and D. F. Eaton, *Chem. Mater*., **1994**, *6*, 1128.
2. (*a*) O. M. Yaghi, H. L. Li, , C. Davis, D. Richardson and T. L. Groy. *Acc. Chem. Res.* **1998**, *31*, 474; (*b*) S. Kitagawa and M. Kondo. *Bull. Chem. Soc. Jpn*. **1998**, *71***,** 1739; (*c*) A. J. Blake *et al*. *Coord. Chem. Rev.* **1999**, *183*, 117; (*d*) B. Moulton and M. J. Zaworotko. *Chem. Rev.* **2001**, *101***,** 1629; (*e*) S. L. James *Chem. Soc.* Rev. **2003**, *32*, 276.
3. (*a*) J. S. Miller, J. C. Calabrese, H. Rommelmann, S. R. Chittipeddi, J. H. Zhang, W. M. Reiff and A. J. Epstein, *J. Am. Chem. Soc.*, **1987**, *109*, 769; (*b*) J. S. Miller, A. J. Epstein, W. M. Reiff, *Chem. Rev.*, **1988**, *88*, 201.
4. F. Toda, S. Hyoda, K. Okada and K. Hirotsu, *J. Chem. Soc., Chem. Commun*., **1995**, 1531.
5. (*a*) T. Tanaka, T. Tasaki and Y Aoyama, *J. Am. Chem. Soc.* **2002**, *124*, 12453; (b) J. L. Atwood, L. J. Barbour and A Jerga. *Science*, **2002**, *296*, 2367.
6. K. Endo, T. Koike, T. Sawaki, O. Hayashida, H. Masuda and Y. Aoyama, *J. Am. Chem. Soc*., **1997**, *119*, 4117.
7. (*a*) C. L. Chen and A. M. Beatty, *J. Am. Chem. Soc.*, **2008**, *130***,** 17222; (*b*) M. B. Dewal, M. W. Lufaso, A. D. Hughes, S. A. Samuel, P. Pellechia and L. S. Shimizu, *Chem. Mater.,* **2006**, *18*, 4855; (*c*) S. A. Dalrymple and G. K. H. Shimizu, *Chem. Commun.,* **2006**, 956.
8. P. J. Langley, J. M. Rawson, J. N. B. Smith, M. Schuler, R. Bachmann, A. Schweiger, F. Palacio, G. Antorrena, G. Gescheidt, A. Quintel, P. Rechsteiner and J. Hulliger, *J. Mater. Chem.*, **1999**, *9*, 1431.
9. (*a*) A. J. Fletcher, K. M. Thomas and M. J. Rosseinsky, *J. Solid State Chem.* 2005, **178,** 2491; (*b*) K. Uemura, R. Matsuda and S. Kitagawa, *J. Solid State Chem.* 2005, *178*, 2420.
10. H. Hayashi, A. P. Côté, H. Furukawa, M. O'Keeffe, O. M. Yaghi, *Nature Materials*, **2007**, *6*, 501.

List of Publications

1. A flexible supramolecular host with a crowned chair octameric water cluster and highly selective adsorption properties. **A. Hazra**, P. Kanoo, S. Mohapatra, G. Mostafa and T. K. Maji, *CrystEnggComm*, **2010**, *12*, 2775.
2. High heat of hydrogen adsorption and guest-responsive magnetic modulation in a 3D porous pillared-layer coordination framework. **A. Hazra**, P. Kanoo and T. K. Maji, *Chem. Commun.*, **2011**, *47*, 538.
3. Soft Supramolecular Porous Framework: Supramolecular Isomerism and Effect of External Stimuli on Structural Transformation and Adsorption Properties. **A. Hazra** and T. K. Maji, *Cryst. Growth Des.* (Communicated).